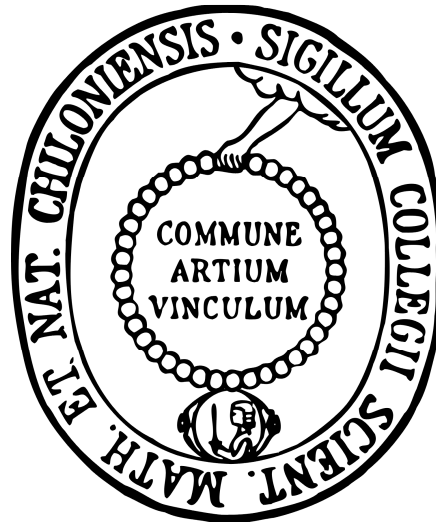


**Novel ultra-thin hydroxyapatite coatings on
medical implants used as local drug delivery
system – in-vitro and in-vivo characterization**



Doctoral thesis

submitted in fulfillment of the requirements

for the degree of

Doctor in Natural Science

at the

Christian Albrecht University, Kiel, Germany

by

Jan Henrik Sørensen

Kiel 2013

Referee: Prof. Dr. Hartwig Steckel
Co-Referee: Prof. Dr. Rainer Adlung
Date of exam: 09.12.2013
Accepted for publication: 09.12.2013
Prof. Dr. Wolfgang J. Duschl
(Decan)

The reasonable man adapts himself to the world; the unreasonable one persists in trying to adapt the world to himself. Therefore all progress depends on the unreasonable man.

(George Bernard Shaw, 1903)

Lack of a specific mark or a reference to a trademark or a patent does not imply that this work or part of it can be used or copied without copyright permission.

Publications contributing to this thesis

Lilja M, Sörensen JH, Åstrand M, Brohede U, Arnoldi J, Procter P, Steckel H, Strømme M, Drug loading and release of Tobramycin from hydroxyapatite coated fixation pins, *J Mater Sc: Mater Med*, 2013; (DOI:10.1007/s10856-013-4979-1)

Sörensen JH, Lilja M, Sörensen T, Åstrand M, Procter P, Strømme M, Steckel H, Coprecipitation of Tobramycin into biomimetic coated orthopaedic fixation pins employing sub.micron thin seed layers of hydroxyapatite, *Current Drug Delivery*, submitted

Sörensen JH, Lilja M, Sörensen T, Åstrand M, Procter P, Strømme M, Steckel H, Biomechanical and antimicrobial properties of hydroxyapatite coated fixation pins, *Journal of Biomedical Materials Research Part B: Applied Biomaterials*, submitted

Lilja M, Sörensen JH, Sörensen TC, Åstrand M, Procter P, Steckel H, Strømme M, Impact of biomechanical forces on antibiotics release kinetics from hydroxyapatite coated surgical fixation pins, *Journal of Biomaterials and Nanobiotechnology (JBNB)*, published

Conference contributions

Lilja M, Sörensen JH, Åstrand M, Brohede U, Arnoldi J, Procter P, Steckel H, Strømme M, Drug eluting hydroxyapatite coatings for biomedical applications, Oral presentation on 6th Annual meeting of the Scandinavian Society for Biomaterials, Hafjell, Norway, 13th-15th of March, 2013

Sörensen JH, Lilja M, Sörensen TS, Åstrand M, Procter P, Strømme M, Steckel H, Neuartige dünne Hydroxylapatitbeschichtungen auf medizinischen Implantaten zur lokalen Freisetzung von Arzneistoffen – in-vitro und in-vivo Charakterisierung, Oral presentation at Studierendentagung zu den Life-Sciences, Kiel, Germany, 5th of December, 2013 – first price.

Table of Contents

1	Introduction and Objectives.....	1
1.1	Introduction.....	1
1.2	Objectives	6
2	Clinical background	9
2.1	Implant stabilization	9
2.2	Hydroxyapatite and its use as functional implant coating.....	11
2.3	Implant associated infections.....	13
2.4	Prevention and infection treatment strategies.....	15
2.4.1	Tobramycin.....	17
3	Materials and Methods.....	20
3.1	Biomimetic HA coating investigations on stainless steel surfaces.....	20
3.1.1	Substrates and plasma sprayed references	20
3.1.2	Cathodic Arc deposition	20
3.1.3	Biomimetic coating of HA on stainless steel.....	20
3.1.4	Biomimetic co-precipitation process of Tobramycin-doped HA.....	21
3.1.4.1	Incorporation of Tobramycin into co-precipitated pins by adsorptive loading	23
3.1.5	Characterization of HA coatings.....	23
3.1.6	Incorporation and release of antibiotic	24
3.1.7	Antibiotic release studied by high performance liquid chromatography.....	26
3.1.8	Biomechanical insertion test in bone substitute material.....	27
3.1.9	Scratch Test	29
3.1.10	Antibacterial Test	29
3.1.11	Cell Study.....	31

Table of Contents

3.1.11.1	Isolation and Culture of Outgrowth Endothelial Cells and Primary Osteoblasts.....	31
3.1.11.2	Cell Seeding and Viability Assessment.....	32
3.1.12	Gamma Sterilization.....	32
3.2	Biomimetic HA coating investigations on titanium surfaces.....	33
3.2.1	Substrate Materials.....	33
3.2.2	Methods used for coating deposition on Titanium.....	33
3.2.3	Optimization of NaOH pretreatment.....	33
3.2.4	Biomimetic coating deposition of HA on Titanium.....	34
3.2.5	SEM evaluation.....	34
3.2.6	Tobramycin loading procedure.....	34
3.2.7	HPLC analysis.....	35
3.2.8	Antibacterial testing.....	35
3.2.9	Cell Study.....	36
3.2.9.1	Isolation and culture of outgrowth endothelial cells and primary osteoblasts.....	36
3.2.9.2	Cell seeding and viability assessment.....	36
3.2.9.3	Immunofluorescent staining.....	36
3.3	In-vivo studies.....	37
3.3.1	Animals used for in-vivo studies.....	38
3.3.2	Materials for in-vivo studies.....	38
3.3.3	HA performance study.....	41
3.3.3.1	Surgical procedure.....	41
3.3.3.2	Terminations.....	43
3.3.3.3	Biomechanical studies.....	44
3.3.3.4	Statistical evaluation.....	50

3.3.3.5	Histological preparation.....	51
3.3.3.6	Histopathological preparation	51
3.3.3.7	Histomorphometrical preparation.....	52
3.3.3.8	Micro-CT measurements	53
3.3.3.9	Micro-CT measurements after removal torque testing	54
3.3.3.10	HA performance pilot study design	55
3.3.3.11	HA performance main study design	56
3.3.3.12	Testing guidelines	57
3.3.4	HA infection study	58
3.3.4.1	Materials for microbiological preparation.....	58
3.3.4.2	Surgical procedure	58
3.3.4.3	Bacterial counts	60
3.3.4.4	Study design of infection pilot study	60
3.3.4.5	Testing Guidelines.....	61
4	Results	62
4.1	Results of investigations performed with stainless steel surfaces.....	62
4.1.1	HA coatings.....	62
4.1.2	Drug loading and release studies	65
4.1.3	Antibiotic loading and release from different HA coating thicknesses and morphologies	71
4.1.4	Biomechanical behavior of biomimetic HA coatings	74
4.1.5	Biomechanical behavior of Tobramycin loaded biomimetic HA coatings	76
4.1.6	Drug release after biomechanical treatment.....	79
4.1.7	Drug release after gamma sterilization.....	81
4.1.8	Scratch test.....	82
4.1.9	Antibacterial properties of Tobramycin loaded HA coated pins	84

Table of Contents

4.1.10	Cell study	86
4.1.11	Co-precipitation of Tobramycin into HA coatings.....	88
4.2	Results of investigations performed with titanium surfaces	95
4.2.1	NaOH pretreatment	95
4.2.2	Concentration dependent loading of HA with Tobramycin.....	96
4.2.3	Impact of different pH values during Tobramycin loading	97
4.2.4	Impact of ultrasound and vacuum during Tobramycin loading.....	98
4.2.5	Antibacterial properties of Tobramycin HA coated titanium screws	99
4.2.6	In-vitro bioassessment test	101
4.3	In-Vivo studies	104
4.3.1	HA performance pilot study	104
4.3.1.1	Screw insertion torque.....	104
4.3.1.2	Removal torque and Pull-out measurements.....	105
4.3.2	HA performance main study	105
4.3.2.1	Screw insertion torque.....	105
4.3.2.2	Biomechanical Testing	106
4.3.2.3	Histological evaluation.....	114
4.3.2.4	μ -CT evaluation	117
4.3.2.5	μ -CT evaluation after removal torque measurements.....	118
4.3.3	Infection pilot study	120
4.3.3.1	Inoculation dose 10^7 CFU inoculation dose (n=1 site per article)	121
4.3.3.2	Inoculation dose 10^5 CFU inoculation dose (n=2 sites per article).....	122
4.3.3.3	Inoculation dose 10^4 CFU inoculation dose (n=3 sites per article).....	123
4.3.3.4	X-ray evaluation	125
4.3.3.5	Microbiological analysis.....	125
4.3.3.6	Histology	127

5	Discussion.....	131
5.1	HA on stainless steel.....	131
5.1.1	HA coating comparison	131
5.1.2	Drug loading and release studies	132
5.1.3	Biomechanical behavior of biomimetic HA coatings	137
5.1.4	Drug release after biomechanical treatment.....	138
5.1.5	Scratch test.....	140
5.1.6	Antibacterial properties	142
5.1.7	Cell studies	143
5.1.8	Co-precipitation of Tobramycin into HA coatings.....	144
5.2	HA on titanium.....	148
5.2.1	NaOH pretreatment	148
5.2.2	Drug loading and release studies	149
5.2.3	Antibacterial properties	152
5.2.4	Cell studies	153
5.3	In-vivo studies.....	155
5.3.1	HA performance study	155
5.3.1.1	Development of the test set-up.....	155
5.3.1.2	Terminations	157
5.3.1.3	Findings	158
5.3.2	Infection in-vivo pilot study	163
5.3.2.1	Development of test set-up and study design.....	163
5.3.2.2	Findings	166
6	Conclusions.....	170
7	Future perspective	174
8	Summary	175

Table of Contents

9	Summary (German version)	177
10	Acknowledgment	180
11	List of figures	182
12	List of Tables.....	190
13	List of abbreviations	191
14	List of references.....	193

1 Introduction and Objectives

1.1 Introduction

The clinical treatment of trauma-related fractures with implants may result in failures at a level that is considered significant by orthopaedic surgeons. The orthopaedic implants that are in current use today are of high quality and undergo continuous improvement. Nevertheless, there are still implant related failures. This strongly suggests that there are unmet clinical needs that might be appropriately addressed by combining such implants together with new technologies.

Implant failure may occur in three main ways. One form is mechanical failure due to a fatigue process in which high levels of internal repetitive loading due to patient activity leads to breakage (>1%) [1]. A second form of failure is implant loosening and/or migration for example the “cut-out” of compression hip screws in the treatment of hip fractures. Again, as these are usually attributed to patient activity. Both of these failures usually occur within weeks or months. A third form of failure infection can occur at any time after the first moment in surgery and this is reported to be in the range of 2 to 33% [2,3]. It is thought that these implant failures through loosening/migration and implant failures through infections are closely linked under certain conditions.

The clinical problem of bone fractures is often related to poor bone quality [4] and such fractures are termed “fragility fractures”. In such an environment, the performance of standard fracture fixation implants is limited and implant fixation failures are frequent and reported to be in the range 2-40% [4,5]. The consequences of implant (screw/pin etc) loosening, migration or cut-out caused by inadequate fixation and bone ingrowth are

potentially devastating for the patient and costly in terms of healthcare resources. This has led to the development of technologies that result in osteoconductive surfaces, such as hydroxyapatite, in order to ensure both early and long term implant stabilization [6–8].

HA is frequently used today as a coating technology for orthopaedic implants because it is known to promote bony fixation of an implant to the host bone. HA coatings in both cortical and cancellous bone are now known to assure very good long term implant fixation [8]. Indeed, the fixation is often so good that it is hard to remove HA coated implants such as total hip stems at revision surgery. Furthermore, fracture devices which often incorporate screws may need to be removed so here it is necessary to have the unusual requirements of screw fixation stability whilst at the same time ensuring a low removal torque. This is to reduce the risk of damage to screw driver, screw or bone at the time of implant removal. The risk of such damage is increased by the implant surface roughening often employed by the HA coating makers with the intention of increasing the connection strength between HA and implant and subsequently implant and bone.

As noted above in addition to challenges in implant stabilization, implant related infections are becoming more and more significant over the last decade. Numerous studies have established a new field of research focusing on the development of the combination of medical devices together with pharmaceutically active ingredients such as antibiotics. Such products are intended to reduce bacterial colonization and subsequent biofilm formation [9–15].

In clinical situations it is often difficult to determine, whether implant infections lead to reduced implant stability or alternatively if reduced implant stability leads to infection.

Today's thinking is that both appear to be connected and one apparently influences the other in a "vicious circle", see Figure 1.

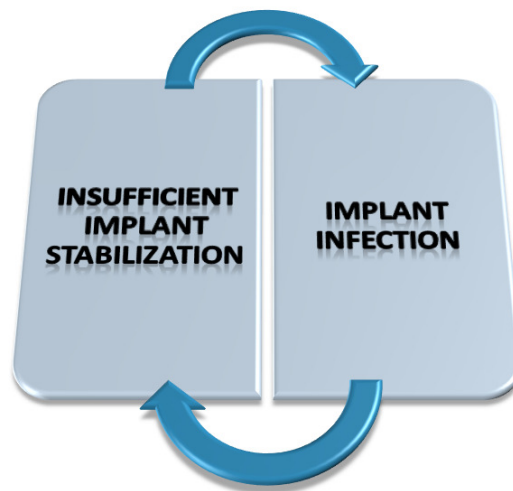


Figure 1: Schematic overview of the possible connection of insufficient implant stabilization and implant infection.

This phenomenon is further underscored by a recent meta analysis in the dental field by Ata-Ali et al. In this, it was shown that the systemic administration of antibiotics significantly lowered the implant failure rate and the "number needed to treat" to prevent one patient from having an implant failure was 48 [16]. This strongly suggests a connection between implant loosening and infection.

The idea of combining implants together with a new technology has been explored by a number of authors and a wide variety of new technologies are reported in the literature. However, there are very few that substantially address the combined needs noted above. Many implant coating technologies aim to decrease implant failure and accelerate patient recovery and these include biodegradable polymers [17–20] or calcium phosphate based materials delivering active pharmaceutical ingredients [9,10,21–23].

Moroni et al. have looked at adding an HA coating to external fixation pins and assessed the effect of a systemically administered drug on fixation strength. In this study, HA coated pins

in combination with systemic Alendronate were shown to have greater removal torque than HA coated pins on their own [24]. Others have looked at similar external fixation implants and have shown that local delivery of a bisphosphonate via a protein layer on the pin is as effective as an HA coated pin [25]. Delivering active pharmaceutical ingredients locally is reported [21,26] and is considered to have many advantages compared to systemic application [27]. Systemic delivery cannot assure high local drug concentration [28], whilst local delivery requires much lower doses and this may reduce the risk of side effects. Local delivery via an HA coating ensures that a pharmaceutically relevant dose is delivered to the intended site of treatment. This is theoretically beneficial for the patient and may enable faster recovery and prevent infections and biofilm formation at the surface of implants [10,11,29].

In summary, the technologies noted above show initial promise however, much further work is needed to prove that they can become part of a safe and effective combination treatment. Additionally, it is evident that so far no technology was able to simultaneously increase bone implant stability (as measured by pullout force), whilst at the same time allowing easy implant removal (as measured by removal torque), and additionally enabling controlled delivery of a pharmaceutically active agent over a useful time period. Accordingly, the goal of this thesis is to determine if an HA coating with these characteristics can be developed and therefore address two out of the three main causes of implant failure noted above.

Many HA deposition processes, particularly those where high temperatures are part of the deposition process, result in a very tough “glazed” surface with low interconnected porosity. It is known that biomimetic nanoporous hydroxyapatite deposition leads to much greater interconnected porosity. This will facilitate the incorporation of drugs and enable tailorable

release over time [30]. Additionally, such coatings have excellent biocompatibility, osteoinductive and osteoconductive characteristics [31,32]. Therefore, in the present study this was selected as a strong candidate that could enable local drug delivery from metal implants whilst at the same time enhancing fixation and subsequent easy release of the implant.

This thesis reports the successful development of a novel bioactive type of implant coating. By using as-finished screw implants and depositing a thin biomimetic form of HA coating (of the order of 1-5 μm) an HA coating was engineered that would have the following characteristics. It should primarily deliver enhanced implant stabilization whilst at the same time enabling the implant to be disconnected more easily from the bone upon screw removal and finally deliver an antibacterial agent over a clinically relevant time period.

1.2 Objectives

The present research aimed to develop ultra-thin forms of hydroxyapatite on metal implants with unique properties. The objectives are divided into two main sections in terms of assessing HA coating characteristics as well as antibiotic incorporation and release properties in both, in-vitro and in-vivo environments. A schematic performance overview of the HA coated antibiotic loaded screw implant is shown in Figure 2.

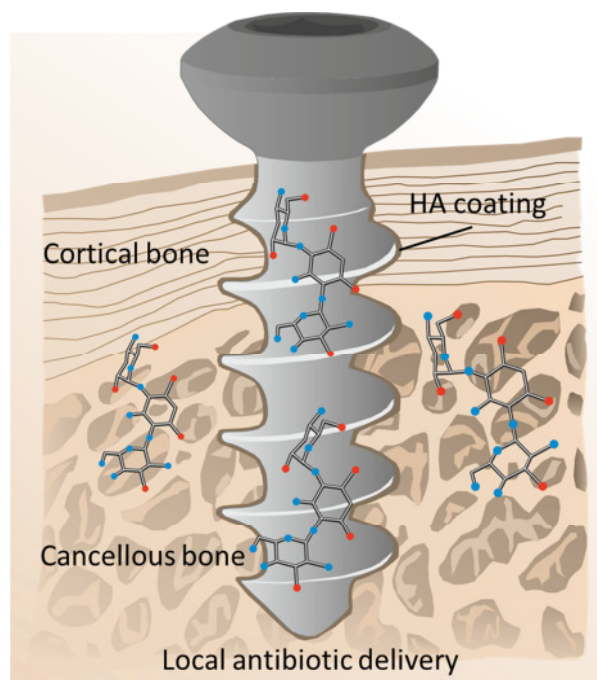


Figure 2: Schematic overview of HA coated antibiotic loaded screw in a bony environment.

Biomimetic HA coatings were manufactured on stainless steel and titanium implants with different thicknesses and morphologies. The first objective was to characterize the HA coatings by different analyzing tools to gain knowledge about the important process parameters needed to influence the HA growth. In addition it was necessary to demonstrate, that the HA coating had sufficient mechanical properties to withstand implantation into bone. Therefore, a second objective was to develop and perform a straight forward method of testing the biomechanical resistances of these different novel coatings during insertion

into synthetic bone materials to later ensure safe implantation in-vivo. As a third objective the evaluation of biocompatibility was addressed by the help of a bioassessment test using different human cell types to characterize cell attachment and differentiation in-vitro. As a fourth objective the novel HA coating was intended to provide early implant stabilization whilst at the same time ensuring implant removal with minimum trauma after full osteointegration in-vivo. This coating was intended to be functionalized on an “as finished” implant substrate (no special surface roughening or special conditioning). A lapine animal model was envisaged and further developed that would be able to discriminate and sufficiently sensitive to demonstrate differences in regards to the above mentioned characteristics. The in-vivo study was subsequently conducted to gain experience of how the HA coating influence the bone implant contact and consequently changes the biomechanical stability of the implant. This was done at both 2 and 6 week time periods (approx. equivalent to 6 and 18 weeks in a human) to assess the early implant stabilization and late degree of full osseointegration. Additionally an important aspect of this new HA interface is that it should require minimal change to current operative practice and not require either additional instruments or additional time at surgery.

Furthermore, the biomimetic nanoporous HA coating was designed to demonstrate a controlled and tailorable local antibiotic delivery to reduce bacterial contamination and consequent implant related infections. As a fifth objective, the coating should be capable of carrying pharmaceutical effective dosages of antibiotic either as sterile preload or by addition at the time of surgery. The development of a smart and simple approach for antibiotic incorporation with subsequently slow release was addressed by the use of different unique loading techniques. The novel co-precipitation approach simultaneously

combining the antibiotic and the HA coating during HA growth was established in objective six to prolong the antibiotic release period. The efficacy of this local antibiotic delivery vehicle should be assessed against the bacteria of interest in-vitro. Therefore, a modified agar diffusion test had to be developed demonstrating the efficacy against *Staph. aureus*. As a final proof of concept, a further objective was to demonstrate the in-vivo efficacy of the antibiotic carrier system in an infection model against commercially available implants. Therefore objective seven was to establish a new animal model. An infection study was conducted to gain experience on the efficacy of the Tobramycin release behavior from the ultra-thin HA coating against *Staph. aureus* in an in-vivo situation.

2 Clinical background

2.1 Implant stabilization

Implant loosening, migration and cut-out play a major role in complications that may occur post-surgery [1,33]. External fixation pins are commonly used to stabilize orthopaedic injuries and are considered to be fast and minimally invasive tools to allow for easy reduction of fractures [34,35]. Rapid implant stabilization after surgery and long term stability are main characteristics needed for this type of implant to succeed clinically. Bone screws in combination with plates are used for fixation and stabilization of a wide range of orthopaedic conditions which include osteotomies. The primary function of these implant systems is to ensure local bone fragment stability at the treatment site. The degree of stability depends upon the implant design, the implant fit, the materials used for fixation as well as the biological aspects like bone quality and the area of implantation [36,37]. Depending upon implantation site and on the implant type used, different rates of cut-out, migration and loosening are reported. For some specific areas in the skeleton the treatment with standard implants is less than satisfactory in terms of bony stabilization, e.g. in the area of the proximal humerus where implant failure rates up to 40% are reported [1,38]. In fractures of the hip, treated with internal fixation, lag-screw cut-out rates from 6 to 19% have been reported [33]. In these indications a conventional implant solution addressing the clinical complications is lacking. These examples illustrate that there are significant unmet clinical needs that might be met through innovative implants with enhanced biomechanical performance e.g. with the ability to stimulate implant integration into the bony structures and ensure early holding power. Additionally, the “race of the surface” after implantation, described by Subbiahdoss et al., should favor human bone cells attaching the implants

surface first and therefore, ensure faster implant bonding and biomechanical strength [39].

A novel bioactive surface could favor human cells rather than biofilm formation.

Independently of implant type, an early resorption phase after implantation of HA into a bony environment around the implant is already described [40,41] whilst long term stability was still reported. In general, hydroxyapatite is a common material employed in biomedical applications where enhanced implant stability is sought. HA coatings are known to be both biocompatible and enhance osteointegration of implants and therefore contribute towards more rapid and enhanced fixation [6,7,14,32,42–45]. Such coatings are frequently used in orthopaedic implants due to its excellent biocompatibility and osteoconductive properties. Plasma-sprayed HA coatings on implant surfaces in particular have already demonstrated high clinical success rates in external fixation pin applications. This is as a result of greater bone-pin contact, enhanced bone-integration and proven long term fixation [46–49].

2.2 Hydroxyapatite and its use as functional implant coating

The most widely used form of calcium phosphate is hydroxyapatite with the formula $\text{Ca}_{10}(\text{PO}_4)_6(\text{OH})_2$. HA has a close chemical and crystal resemblance to the mineral component of bones and hard tissues in humans and therefore induces a biological response similar to bone [50]. The use of HA as bone void filler is widely known and accepted. It may also be used in the form of an implant coating intended to alter the surface properties and promote bone ingrowth and ensure fast primary stabilization [6,23,51,52]. Without the HA coating the body would be in contact with a foreign body (e.g. a stainless steel or titanium implant type) and react by trying to isolate it from surrounding tissues. Dhert et al. and Slaets et al. reported early bone resorption effects around press-fit implants [53,54]. Whilst HA has been demonstrated to bind well to surgical implant materials such as stainless steel or titanium. HA was shown to increase the osteointegrative ability of screws and fixation pins resulting in increased fixation strength of up to 2.5 times non coated implants as measured by removal torque [5,48]. Most commercially available HA coatings are applied by a plasma spraying process and are designed to permanently connect the implant to the bone. These aims are particularly desirable in the field of total joint replacement. Plasma sprayed HA coatings have also found in application in the area of external fixation [5], where fast stabilization of the external pins is necessary. These coatings are generally formed at high temperature.

Hydroxyapatite and HA coatings have been extensively studied [50], demonstrating different morphologies, topographies and crystal structures depending on the manufacturing processes employed [55–57]. Implant coatings are manufactured by a number of methods: the sol-gel method, electrochemical processes, by biomimetic deposition or by plasma

spraying [6,58–61]. Each method of HA coating may result in slightly different in-vitro and in-vivo behavior although the clinical goal of enhanced fixation is the same.

The key properties of hydroxyapatite are described in the literature. In general, HA shows excellent biocompatibility due to its similarity to human bone mineral [43]. The osteoconductivity of HA encourages accelerated osteointegration and therefore it is a potential candidate for the use in patients with osteopenic and osteoporotic bone structures [6,7,62]. To date, nearly all available implants are designed for fixation in bone of normal quality and may not perform optimally in either osteopenic or osteoporotic bone [5,63].

2.3 Implant associated infections

At the present time trauma-related infections and healing of bone defects are still considered a significant clinical problem in orthopedic surgery. Infection rates reported by literature vary widely depending on the type and anatomical site of the fracture. Deep infections, which may lead to serious clinical consequences, are reported to be in the range of 1-4% for closed fractures. So called “open fractures”, where the patient’s skin has been broken by injury are almost invariably contaminated by bacteria and many open fractures are already infected by the time of initial treatment. Accordingly infection rates are much greater in open fractures and are reported to be up to 33% of patients with injuries such as an open tibia fracture [3]. Infection rates for external fixation treatments are reported in the range from 11 – 100% depending on the type of study [2]. Despite the best available standards of clinical care up to 37% of open type III tibial fractures are infected and about 14% of these infected fractures will result in amputation [64]. The long term sequelae to infection are often devastating for the patient and may include chronic osteomyelitis, multiple reoperations, prolonged antibiotic administration all of which contribute to a significant financial burden. Different bacteria types are associated with implant infections and may infiltrate the wound prior to surgery, intra or post operatively. The majority, (76%) of implant related infections are caused by *Staphylococci*, predominantly by *Staph. epidermidis* and *Staph. aureus*, see Figure 3, and these characteristically have the ability to localize and protect themselves by a biofilm that forms around the implant. A further 16% of infections are caused by combinations of different bacteria [65].

Different mechanisms and time points of bacterial attachment are described in the literature. In most cases the implant is contaminated by direct adhesion to the implant

surface and this may occur prior to implantation, during implantation or by contact with compromised tissue (sessile bacteria in the wound). In some cases planktonic bacteria deriving from blood or lymph may attach and colonize implant structures and consequently inhibit fracture repair [66,67]. Bacterial infiltration at the time of surgery accounts for the majority of early (up to 3 months) and delayed (up to two years) implant related infections [68,69].

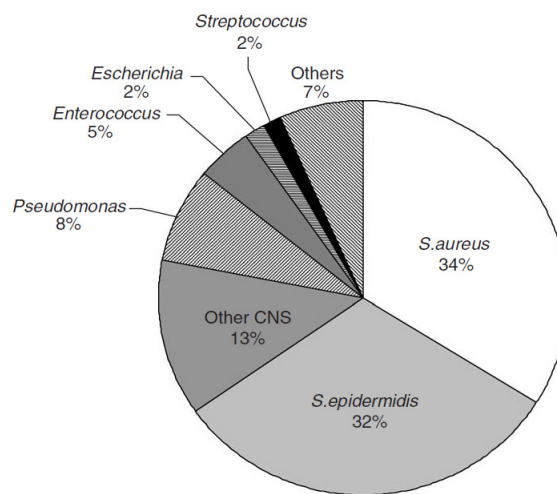


Figure 3: Frequency of main pathogenic species among orthopaedic clinical isolates of implant-associated infections [65]. (CNS=Coagulase Negative Staphylococci)

2.4 Prevention and infection treatment strategies

The conventional treatment to overcome postoperative infections is to administer high systemic doses of antibiotic [3,70,71]. This treatment is the gold standard today nevertheless infections frequently occur. Bone and associated tissues are sensitive to infections due to their poor vascularization post trauma. Systemic antibiotic treatment is frequently ineffective due to the low efficiency of drugs delivered via the circulatory pathways. The local drug concentration at the site of action is relatively low due to this poor diffusion of the antibiotic in bony regions [28]. Therefore, infections may occur even with high doses of systemically administered antibiotic treatment. Over the last few decades, researchers have been focusing on new methods for local infection control by means of functional bioactive surface modifications intending to protect the implant against bacterial colonization and consequent biofilm formation [3]. Local antibiotic release is therefore potentially an attractive strategy either to combat infections that have already occurred or as an option for prevention [3,72]. Local antibiotic delivery systems are not new to the surgical community. Septopal[®] chains (using Gentamicin) and antibiotic bone cements (e. g. Simplex[®] using Tobramycin; Palacos[®] using Gentamicin) are clinically well established products [73]. The use of antibiotic-impregnated cement is very effective and lowered the infection rate in primary hip arthroplasty by approximately 50% [74]. In revisions of previously infected hips, combinations or culture-dependent antibiotics have demonstrated that infection rates may reduce by approximately 40% [74]. This level of infection reduction is impressive and clearly demonstrates the benefits of local antibiotic release.

It would be of general interest in the implantable device field to endow implants with intrinsic antibacterial properties and that would work to combat bacterial contamination

from the moment of their implantation [27,75]. Such systems would work by passive protection of the implant surface against bacterial attachment or alternatively they could work by active diffusion protecting the both the implant surface and the surrounding tissues. Examples of surface modifications and coating technologies which act passively are polished surfaces that reduce the bacterial attachment [76] or ion releasing coatings incorporating nanoparticulate silver [77–79] or copper [13,80] ions to reduce bacterial contamination. The former has been much more studied than the latter. Local antibiotic delivery ensures active diffusion also in the vicinity of the implant, where bacteria can settle and grow as well. The effectiveness of such implants is strongly dependent on the amounts of antibacterial agent released. The release has to be above the minimal inhibitory concentration (MIC) of the bacteria of interest, for example *Staph. aureus* [81] , to ensure effective infection reduction rates. If an antimicrobial agent released is below the MIC, bacterial resistance may be induced.

To summarize, there is a strong clinical need to enable fast bone recovery after trauma. Bacterial colonization and bone recovery are clearly connected to each other in many clinical situations. Up to the present time the unmet need to protect the bone from bacterial contamination to enable bone recovery is still largely unmet and is a very valid goal for this project. Therefore effective local antibiotic delivery could be a pathway with the potential to enhance the standard of care. Accordingly an antibiotic loaded HA coating delivering effective local concentrations of antibiotic over a controllable period of time is in the focus of interest in the present study. This HA coating would ideally have the property of rapid local bone apposition as evidenced by a screw pullout test, whilst allowing ease of removal

at different time points, as evidenced by relatively low removal torques. It should also demonstrate bone healing and growth.

2.4.1 Tobramycin

Tobramycin is a bactericidal aminoglycoside antibiotic intended either for topical use or for systemic internal treatment against bacterial infections, see Figure 4. It can be derived from *Streptomyces tenebrarius* and is highly effective against gram-negative bacteria, especially useful against *Pseudomonas* infections [82].

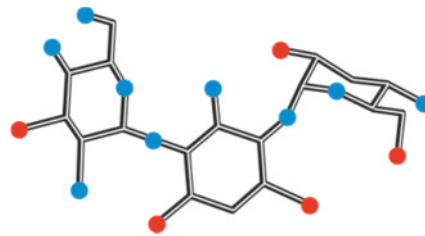


Figure 4: Molecular structure of Tobramycin $C_{18}H_{37}N_5O_9$, $M_r = 467.51$ g/mol; red dots denote NH_2 groups, blue dots denote hydrogen saturated oxygen-atoms

Due to its chemical structure and binding characteristics it is highly effective against bacteria and does not affect human cells within a high range of concentration [83]. It specifically targets the 30 S subunit of bacterial ribosomes, which is not present in human cells. Tobramycin binds irreversibly and therefore prevents the formation of the 70S complex. As a result, mRNA translation is inhibited and the proteins produced are nonfunctional. Consequently, cell death takes place. The schematic mechanism of action is illustrated in Figure 5.

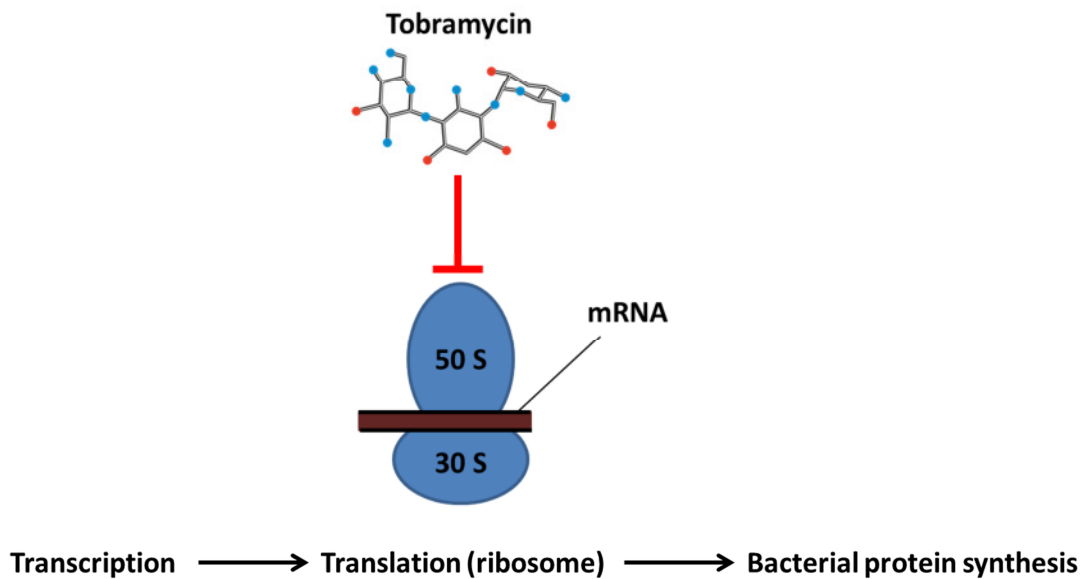


Figure 5: Schematic diagram of mechanism of action of Tobramycin during bacterial protein biosynthesis

Tobramycin is a highly hydrophilic molecule and therefore cannot pass via the gastrointestinal tract [83,85]. Systemic administration is only feasible by an injection intravenously or intramuscularly. Other methods of administration only achieve minor systemic effects. Systemic administration is always linked together with possible side effects. Tobramycin, as well as the whole group of aminoglycoside antibiotics, demonstrates ototoxicity and nephrotoxicity [85,86]. Ototoxicity can occur in genetically susceptible individuals and is generally irreversible. Patients who are so affected, show a genetic mutation that is normally harmless and allows aminoglycosides to affect cochlear cells. Due to its nephrotoxicity whilst undertaking a systemic administration regime Tobramycin needs to be carefully dosed by body weight and monitored by checking the serum concentration over time [86,87]. Accordingly, local drug release of high concentrations of Tobramycin at the needed pharmacological site of action, is potentially very beneficial in reducing the risk of systemic side effects.

Today bacteria are increasingly resistant and this has become a clinically relevant problem as some antibiotics are less and less effective against bacterial contamination and new solutions have to be found. Due to the fact that Tobramycin is a reserve antibiotic the bacterial resistance is less than for other antibiotics with broader use. Table 1 gives an overview of the resistances of both *Staph. aureus* and *Staph. epidermidis*, two bacteria of interest, against Tobramycin from 2000 to 2004 [88–90].

Year	Microorganism	Resistance to Tobramycin
2000	S. aureus	13.0%
2002	S. aureus	13.1%
2004	S. aureus	7.0 %
2000	S. epidermidis	32.9%
2002	S. epidermidis	48.6%
2004	S. epidermidis	46.1%

Table 1: Resistance of *S. aureus* and *S. epidermidis* to Tobramycin acc. [88,90].

In the present research Tobramycin was used as a model drug. In general resistance against the bacteria that frequently occur in implant related infections is acceptable and infections are relatively low compared to other antibiotics. Additionally, Gentamicin [45] and Vancomycin [91] (in the group of aminoglycoside antibiotics) are a focus of current researchers in treating implant associated infections. This is due to their high efficacy as shown by their low minimal inhibitory concentration [92]. Tobramycin represents an established antibiotic additive in bone cement since decades particularly in the US [93].

3 Materials and Methods

3.1 Biomimetic HA coating investigations on stainless steel surfaces

In order to deposit an HA coating on a stainless steel implant it was necessary to deposit a baselayer that would form the necessary nucleation sites. The TiO₂ baselayer coating of the fixation pins, as well as the pure HA coatings were manufactured at Sandvik Coromant Sverige AB, 12680 Stockholm, Sweden. Additionally, the optical coating characterization, XRD, GD-OES measurements and the scratch tests were performed by Sandvik.

3.1.1 Substrates and plasma sprayed references

Stainless steel Apex Pins (∅ 4 mm, 90 mm x 30 mm, REF 5023-3-090, LOT W11825) were used for coating deposition and plasma sprayed HA coated Apex Pins (∅ 4 mm, 90 mm x 30 mm, REF 5013-3-090S, LOT U24265) both obtained from Stryker Trauma AG (Selzach, Switzerland) served as reference samples. Stainless steel plates (20 mm x 20 mm x 1 mm) of medical grade AISI type 316L served as substrates for X-ray diffraction (XRD) measurements and glow discharge optical emission spectroscopy investigations.

3.1.2 Cathodic Arc deposition

All stainless steel samples intended for biomimetical HA deposition were coated with a crystalline TiO₂ coating through cathodic arc evaporation during a deposition time of 20 min at a temperature of 320°C resulting in a TiO₂ coating thickness of approx. 500 nm as described by Lilja et al. [94].

3.1.3 Biomimetic coating of HA on stainless steel

The HA coating was biomimetically (HA-B) precipitated on the TiO₂ coated samples using Dulbecco's Phosphate Buffered Saline (Sigma-Aldrich Laborchemikalien GmbH, Seelze,

Germany) containing CaCl_2 and MgCl_2 as ion source. Following the cathodic arc deposition of the crystalline TiO_2 , the fixation pins were ultrasonically cleaned in isopropanol and deionized water (5 min in each) and subsequently placed in plastic tubes containing 50 ml of PBS illustrated in Figure 6. The optimal soaking time and process temperature determined previously enabled the deposition of the desired HA coating thickness. To achieve a coating thickness of approx. $5 \mu\text{m}$, the tubes containing the pin were kept at 37°C for 6 days, carefully rinsed in deionized water and left to dry in air. Three different sample types, with variation in HA coating thickness and morphology, were prepared by varying the immersion time between 2.5 and 6 days at 37°C and also 6 days immersion at 60°C . The respective samples produced are denoted HA-B_37 (2 μm), HA-B_37 (5 μm) and HA-B_60 (1 μm). As will become clear from the analysis the numbers within the parenthesis of the sample names signify the sample thicknesses.

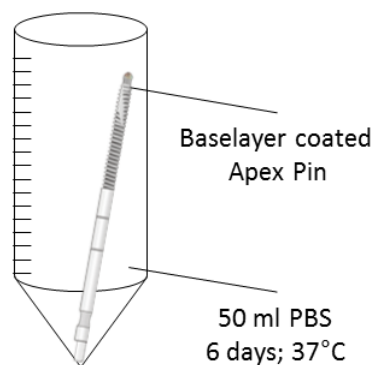


Figure 6: Positioning of the base layered fixation pin in the test tube during HA growth.

3.1.4 Biomimetic co-precipitation process of Tobramycin-doped HA

Co-precipitation of Tobramycin (Fargon GmbH & Co.KG, Barsbüttel, Germany) on the bioactive, crystalline TiO_2 coated substrates was performed by adding different amounts of Tobramycin to Dulbecco's Phosphate Buffered Saline, which served as an ion source. Following the cathodic arc deposition of the crystalline TiO_2 , the substrates were

ultrasonically cleaned in isopropanol and de-ionized water (5 min in each). Subsequently the discs and plates were placed in plastic cups containing 20 ml PBS, whereas the fixation pins were placed in plastic tubes containing 50 ml PBS, see Figure 7. Two test series were performed in order to investigate the influence of antibiotic concentration on coating growth as well as the impact of surface chemistry on the drug affinity. All samples for both test series were produced in triplicate. The first test series produced employed TiO₂ coated titanium discs. Different concentrations of Tobramycin (0.5 mg/ml; 1.0 mg/ml; 4 mg/ml; 20 mg/ml and 40 mg/ml) were added to the PBS and the samples were stored for 6 days at 37 °C and 60 °C, respectively. The affinity of Tobramycin to different surface chemistries was evaluated by covering the TiO₂ coated substrates prior to co-precipitation deposition with a sub-micron thin HA start layer in the range of 300-600 nm. The HA start layer was obtained by immersion in PBS for 3 days at 60 °C. For the second test series, discs with the HA start layer were stored for 6 days in PBS at 60 °C containing Tobramycin at concentrations of 4 mg/ml and 20 mg/ml, respectively. Co-precipitated coatings on fixation pins with the HA start layer were made by placing the pins for 6 days in PBS with Tobramycin concentrations of 4 mg/ml and 20 mg/ml at 37°C, producing samples denoted as Co-4 and Co-20, respectively. After the coating process all samples were air dried in an oven at 37 °C for 24 hours.

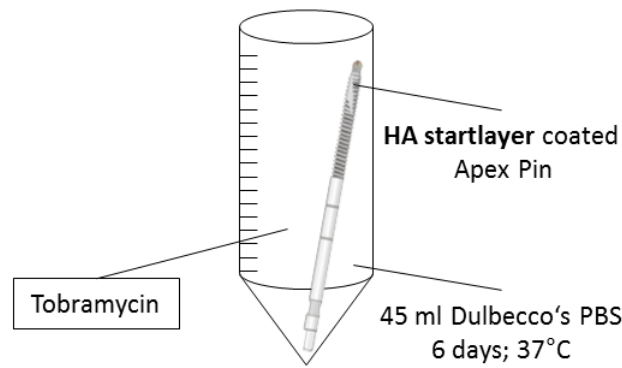


Figure 7: Positioning of the HA start layer coated fixation pin during co-precipitation process.

3.1.4.1 Incorporation of Tobramycin into co-precipitated pins by adsorptive loading

Additionally, the adsorptive loading properties of co-precipitated coating structures were evaluated. For this study Co-4 samples were placed for 5 minutes in round bottom test tubes (130 mm x 14 mm x 1 mm) containing 5 ml of room-tempered Tobramycin stock solution at a concentration of 20 mg/ml. The resulting samples were denoted Co-4/20. The coating homogeneity and thickness were evaluated by scanning electron microscopy (SEM) and the Tobramycin release from the fixation pins was assessed using high performance liquid chromatography.

3.1.5 Characterization of HA coatings

The biomimetically precipitated HA (HA-B) coatings as well as the plasma sprayed HA (HA-P) coated pins were examined using a Zeiss Supra 40 Scanning Electron Microscope (SEM). The impact of the mechanical forces on the HA-B coating performance was further investigated by 3D Optical Visualization (Alicona Infinite Focus Real 3D, Graz, Austria). XRD measurements on the TiO₂ films were performed using a Siemens D5000 diffractometer operating with 1° grazing incidence angle in parallel beam geometry using CuK α radiation (wavelength λ of

1.540598 Å). A step size of 0.1° and a scan step time of 4 s were used for the scans recorded between 20° and 60° 2θ. SEM images of the HA cross sections obtained by ion milling (E-3500, Hitachi) were recorded to evaluate the thicknesses and structures of the deposited HA coatings on the pins. The coating topography was studied by white light interferometer (Wyko NT1100, Veeco) and the surface roughness of the coatings was obtained from the Profiling Software Vision (Veeco).

3.1.6 Incorporation and release of antibiotic

For antibiotic incorporation into the HA-coatings, Tobramycin was dissolved in water of double distilled quality. Within the first investigation period five different sample types, designated as Load-RT, Load-C, Load-P, Load-HT and Load-PHT, were prepared by varying the loading time, drug concentration, pressure and temperature as described in Table 2. All samples in the Load-series were made in triplicates for both HA-coating types under study.

Table 2: Tobramycin loading parameters for both HA-B and HA-P coatings

Test	Temperature [°C]	Concentration [mg/ml]	Time [min]	Pressure [bar]
Load-C	RT	4; 20; 40	5	1
Load-RT	RT	40	5; 15; 60	1
Load-P	RT	20	5	1
Load-HT	90	20	5	6
Load-PHT	90	20	5	6

To produce samples in the Load-RT, Load-C, and Load-HT series, the HA coated pins were placed in round bottom test tubes (130 mm x 14 mm x 1 mm) containing 5 ml of Tobramycin stock solution at the concentrations specified in Table 2. During the Load-HT drug loading procedure, the test tubes were kept in a heated water quench (Heraeus) while the Load-RT and Load-C samples were produced at room temperature. The Load-P and Load-PHT samples

were prepared by placing the HA-coated pins and 30 ml of stock solution containing 20 mg/ml Tobramycin in a stainless steel tube under an applied pressure of 6 bar. The high temperature of 90 °C maintained during loading of Load-PHT was ensured by preheating the steel tube to 90 °C prior to the loading procedure. The loaded samples from all series were placed for drying in an oven at 37 °C for 24 hours.

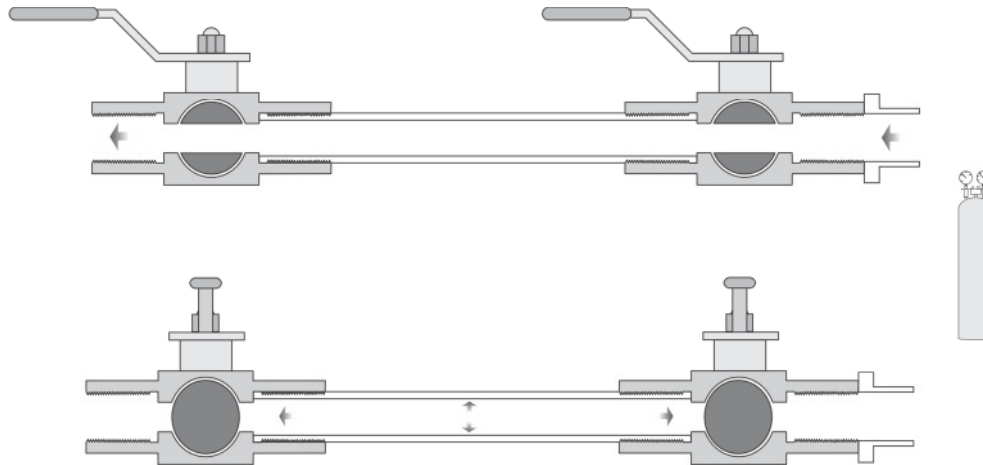


Figure 8: Schematic drawing of the chamber for loading under pressure.

For the release studies, the dried samples were placed in round bottom test tubes containing 5 ml of PBS at 37 °C. The amount of Tobramycin released from the samples was measured at different time points (typically at 5, 15, 30, and 60 min as well as 4 h, 2, 5, and 8 days) to evaluate both initial and long term slow release properties. Upon completion of the first release time point, the pin was transferred to the next test tube containing 5 ml of fresh PBS at 37°C. This procedure was carried out for each time point measured during the cumulative release testing until no Tobramycin could be measured.

The durability of the HA coatings was investigated with SEM after drug loading and also after drug release. After the last time point measured for the release in PBS, the HA coatings were dissolved by lowering the pH of the PBS to 2 through addition of hydrochloric acid in order to measure the amount of remaining drug present in the coating.

The penetration depth of the antibiotics into the different HA-B sample types was evaluated by glow discharge optical emission spectroscopy (GD-OES, GDA750-HP Spectruma Analytik GmbH, Germany). Quantitative profiles of Tobramycin characteristic elements nitrogen (N) and carbon (C) were obtained by measuring the chemical composition of drug-loaded HA-B samples from the sample surfaces towards the substrate.

3.1.7 Antibiotic release studied by high performance liquid chromatography

High performance liquid chromatography (HPLC) was used to quantify the released drug content as well as the release kinetics. The measurements were performed and modified according to the British Pharmacopoeia [95], Sekkat et al. [96] and Fabre et al. [97] using pre-column derivatization of the aminoglycoside antibiotic. A 100 ml derivatization reagent was produced by dissolving 2.47 g boric acid R (Carl Roth GmbH) in 75 ml water followed by adjusting the pH to 10.4 by using potassium hydroxide (450 g/l, Sigma-Aldrich). This mixture was diluted with water to 100 ml.

1 g ortho-phthalaldehyde R (Sigma-Aldrich) was dissolved in 5 ml methanol. This solution was mixed with 95 ml boric acid solution and 2 ml of mercaptoacetic acid (Merck). This derivatization reagent was adjusted to pH 10.4 by adding potassium hydroxide (450 g/l) and stored for a maximum of 7 days, light protected at 2-8 °C.

Pre-column derivatization was performed by mixing 1 ml sample solution containing Tobramycin with 1.1 ml methanol and 0.4 ml derivatization reagent. This solution was mixed on a magnetic stirrer at 1400 rpm for 10 minutes. A volume of 100 µl was injected.

The mobile phase consisted of 5.5 g sodium heptanesulphonate (Sigma-Aldrich) solved in a mixture of 50 ml glacial acetic acid, 700 ml methanol and 250 ml double distilled quality

water. A flow rate of 1.0 ml/min and a wavelength of 330 nm were utilized for the HPLC (Waters Corp. Milford, MA, USA) analysis. The measurements were carried out using a Hypersil ODS column (3 μm 100 x 4.6 mm; VDS Optilab Chromatographie Technik GmbH, Montabaur, Germany) as stationary phase at room temperature, a high precision pump (Waters 600E Multisolvant Delivery System), an autosampler (Waters Inline Degasser AF and a Waters 717 plus autosampler), and a Waters UV detector (Waters 996 Photodiode array detector). Data analysis was performed using the Waters Empower 1154 software.

3.1.8 Biomechanical insertion test in bone substitute material

The biomechanical properties of three HA-B coated sample types were tested by insertion tests in two different bone substitute materials. Renshape BM5166 (Vantico GmbH, Basel, Switzerland) high density bone substitute discs (\varnothing 20 mm x 4mm) were used to simulate pin insertion and low density polyurethane (PU 25) foam plates (20mm x 20 mm x 4 mm) reflected pin insertion in spongy bone. The insertion materials were hold in a fixture to simulate a bone section with single cortex. A thermocouple was placed in a \varnothing 1mm and 2 mm deep hole situated at a distance of 4 mm from the axis of the inserted pin. A heat-conductive paste ensured the heat transfer to the detector. The pin was inserted without pre-drilling through the disc or plate at a rotation speed of 10 rpm and with 100 N of axial force for Renshape BM5166 and 50 N for PU 25. The reason for not pre-drilling was to mimic the real insertion procedure of the pins during surgery. The pin performance was evaluated by determining the parameters of insertion torque, maximal temperature rise during insertion and the drilling time required for 23 mm insertion depth. After insertion the bone substitute material was carefully cut into two pieces and the HA-B surface structure of the pins as well as the bone substitute were examined by SEM.

Table 3: Overview of HA coating types tested during first biomechanical investigation series.

Sample	Bone substitute material
Stainless Steel	Renshape
TiO ₂	Renshape
HA-B_60 (1µm)	Renshape
HA-B_37 (2µm)	Renshape
HA-B_37 (5µm)	Renshape
Stainless Steel	PU25
TiO ₂	PU25
HA-B_60 (1µm)	PU25
HA-B_37 (2µm)	PU25
HA-B_37 (5µm)	PU25

During the second biomechanical test series, antibiotic loaded HA coated samples were evaluated in regards to wear and smearing effects. Subsequently antibiotic release tests were performed to gain knowledge about the change in release characteristics after biomechanical insertion. Biomechanical properties were evaluated using polyurethane (25 PU) foam blocks (20 mm x 20 mm x 4 mm) mimicking spongy bone quality. The 25 PU grade was chosen, since preliminary tests demonstrated that this induced more severe coating wear effects after insertion, compared to higher density synthetic bone reflecting cortical bone structures. Three fixation pins of each sample type were loaded with Tobramycin via adsorption at room temperature, denoted as HA-B_RT_BML, or under elevated temperature and pressure conditions, denoted as HA-B_PHT_BML followed by biomechanical insertion. Co-precipitated samples denoted as Co-4_BML were also tested in triplicate. Insertion was performed vertically, without pre-drilling to mimic real conditions of insertion, at a rotation speed of 50 rotations per minute over the full thread length of the coated pin. The pin was removed from the bone model materials by cutting two notches from both sides into the discs and plates with a distance of approximate 3 mm towards the center of the pin.

Application of an abrupt mechanical force to the weakened material resulted in two separate pieces of bone model material thus freeing the pin.

3.1.9 Scratch Test

A scratch tester (CSM Instruments Revetest) was used to determine the adhesion between the three different HA-B coating types and the underlying TiO₂ coating. A 50 µm and 500 µm spherical Rockwell C diamond indenter, respectively, was used with a progressive load from 0 to 100 N and a loading rate of 10 N/mm. Scratches of 10 mm length were carried out to define the critical normal load ($F_{N,C}$), which was taken as the normal load corresponding to continuous spalling of the HA-B coating types under study. SEM images of the scratch traces were recorded to investigate HA-B coating failure.

3.1.10 Antibacterial Test

The antibacterial efficacy of Tobramycin incorporated into HA-B_37 (5 µm) coated pins was evaluated by a modified agar diffusion test in accordance to Zarie et al. [98] and the European Pharmacopoeia [99]. Drug loading was performed as described earlier in section 3.1.6. As-deposited HA-B_37 (5 µm) pins served as references and were not loaded with Tobramycin. To assess the impact of biomechanical forces on the antimicrobial performance, RT loaded samples were inserted into PU 25 foam blocks prior testing and were denoted as HA-B_37 (5 µm), RT_BML.

The test organism, *Staphylococcus aureus* ATCC 6538 were purchased from German Collection of Microorganisms and Cell Cultures (Braunschweig, Germany). CASO agar media (Merck KGaA, Darmstadt, Germany) as dehydrated powder was rehydrated by water of double distilled quality and sterilised according to instructions of the supplier. After cooling down to approximately 50°C, the agar medium was poured into Petri dishes (Ø 9 cm) in

aliquots of 40 ml. The agar volume and consequently, the depth of agar media in the Petri dish was chosen in order to ensure vertical mechanical stability of the inserted fixation pin during incubation.

A lyophilised stock was used to culture the test organism. To prepare the germ suspension, a tube containing CASO agar media was inoculated and incubated at 37°C for 18-20 hours. The surface of the culture was floated with 2 ml sodium chloride peptone broth (SCPB) and dispersed by shaking for 5-10 seconds on a vortex device. The suspension generated was diluted by SCPB and adjusted to approx. 5×10^6 CFU/ml measuring the absorption at a wavelength of 650 nm (absorption of 1.0 = 7.3×10^8 CFU/ml). An aliquot of 0.1 ml germ suspension was mixed into 5 ml sterile agar to achieve a germ concentration of 1×10^5 CFU/ml. 5 ml germ suspended agar media was poured onto the Petri dish already containing 40 ml of gelatinized sterile agar media. After gelation of the germ suspended agar media, one fixation pin per Petri dish was vertically inserted and then inoculated for 18 hours at 35°C. The pin was mechanically stabilized during inoculation by placing a specially made stabilising device over the Petri dish. Photographs were taken of all samples tested after final inoculation and the extents of the inhibition areas were then measured.

After determination of the inhibition zones the fixation pins were rolled out over a fresh CASO agar plate followed by incubation of the Petri dish for 18 hours at 35°C to culture germs adhering directly on the implants surface. For day two the fixation pins were transferred and inserted into a fresh agar plate containing 40 ml fresh CASO agar and 5 ml germ suspended agar followed by incubation parameters as described above. This procedure was repeated until no measurable inhibition zone could be observed.

3.1.11 Cell Study

All cell studies were performed by Prof. Dr. Sabine Fuchs at Experimental Trauma Surgery, University Medical Center Schleswig-Holstein, Kiel, Germany.

3.1.11.1 Isolation and Culture of Outgrowth Endothelial Cells and Primary Osteoblasts

Outgrowth endothelial cells were isolated from buffy coats as described earlier [100,101]. In summary, blood mononuclear cells were isolated by Biocoll (Biochrom, Berlin, Germany) density centrifugation. Mononuclear cells were seeded onto collagen coated 24 well plates in density of 5×10^6 cells /well in EGM-2 (Lonza, Belgium) with full supplements from the kit, 5% FBS (PAA Laboratories, Pasching, Austria), and 1% penicillin/streptomycin (PAA Laboratories, Pasching, Austria). After one week adherent cells were collected by trypsin and reseeded on collagen coated 24 well plates in a density of 0.6×10^6 cells/ well. After 2-3 weeks colonies of endothelial cells were harvested and further expanded over several passages using EGM-2 in a splitting ratio of 1:2.

Primary osteoblasts were isolated and cultured as previously described [102,103]. In summary, bone fragments were minced and rinsed in PBS for several times followed by collagenase digestion (Type IV C-5138, Sigma, Deisenhofen, Germany) for one hour at 37°C. After the enzymatic digestion, bone fragments were rewashed and cultured in DMEM/Hams F12 including 20% FCS and Pen/Strep. When reaching confluence cells were passaged using accutase in a ratio of 1:3 and further cultured in DMEM/Hams F12 including 10% FCS. The isolation and use of primary cells from bone or blood was approved by the local ethical committees and performed according to the ethical guidelines.

3.1.11.2 Cell Seeding and Viability Assessment

TiO₂ coated stainless steel discs used for cell culture experiments were treated with 70% of methanol before cell seeding experiments. For cell seeding discs with or without HA-B_37 (5µm) coating were used and placed into 48 cell culture well plates. Endothelial cells (OEC) or primary osteoblasts were seeded in density of 100.000 cells/disc in cell culture media as described above, for the individual cell types. After 3 days of culture, cells were analysed in terms of their cellular viability and morphology using Calcein-AM. For this purpose cells were treated with 0.2 µg/ml Calcein-AM (BD, Heidelberg, Germany), in cell culture medium for 10 minutes. After medium exchange cells were visualized on a fluorescence microscope (Zeiss, Axioskop40).

3.1.12 Gamma Sterilization

Gamma Sterilization of HA-B_RT samples was carried out by Beta-Gamma-Service GmbH & Co KG, Wiehl, Germany with a minimum dose of 25.4 kGy and the sterilized samples were denoted as “HA-B_RT gamma sterilized”.

3.2 Biomimetic HA coating investigations on titanium surfaces

The NaOH optimization process, SEM analysis, HA coating manufacturing on discs as well as on cancellous bone screws were performed by BactInact AB, Uppsala, Sweden.

3.2.1 Substrate Materials

Ti₆Al₄V Ti cancellous screws (∅ 4.0 mm x 14 mm; REF 604014) obtained by Stryker AG (Selzach, Switzerland) were used as reference samples. Hydroxyapatite coated cancellous screws (same type) served as test screws. Anodized type II Ti6Al4V discs (∅ 9.0 mm x 4 mm) were used for cell adhesion and biocompatibility testing.

3.2.2 Methods used for coating deposition on Titanium

Untreated Ti cancellous bone screws (∅ 4 mm x 14 mm; REF 604014) and anodized type II Ti discs were first sonicated in acetone for 5 minutes, then sonicated in ethanol for 5 minutes, and finally sonicated for 5 minutes in deionized water.

3.2.3 Optimization of NaOH pretreatment

In order to determine the optimum NaOH pretreatment conditions, type II anodized Ti coupons (∅ 9.0mm, 4mm thick) were soaked in 5M NaOH at 70 °C for time periods ranging from 10 min to 9 h. The conditions for NaOH pretreatment are outlined in Table 4. After the pretreatment the coupons were sonicated for 5 minutes in deionized water.

Table 4: Coupon soaking conditions for optimization of NaOH pretreatment.

Number of coupons	NaOH concentration [M]	Temperature [°C]	Soaking time
3	5	70	9 h
3	5	70	6 h
3	5	70	3 h
3	5	70	1 h
3	5	70	40 min
3	5	70	20 min
3	5	70	10 min

3.2.4 Biomimetic coating deposition of HA on Titanium

Ti bone screws or discs were soaked in 1 l of phosphate buffered saline (Dulbecco's PBS, Sigma, Steinheim, Germany) for 72 h. A holder was devised that prevented coating of the screw heads and allowed for all screws to be simultaneously coated. Stirring of the PBS with a magnet stir bar was adjusted to minimize the formation of HA aggregates on the HA coating. After removal from the PBS solution, the screws were removed from the holder, rinsed in deionized water and dried with a flow of N₂. HA coated Ti screws were denoted as Ti-HA followed by a characteristic suffix.

3.2.5 SEM evaluation

Selected coated and uncoated Ti bone screws were imaged with scanning electron microscopy (FEI XL30 ESEM) using the secondary electron detector.

3.2.6 Tobramycin loading procedure

The titanium bone screws were loaded by adsorption in Tobramycin containing water of double distilled quality using different procedures. Loading at room temperature was performed by filling a test tube with 2 ml of Tobramycin stock solution, transferring the sample into the test tube for a loading time of 5 minutes. Afterwards the screw was removed by the help of an artery clamp and dried in an oven for 24 hours at 37°C in a vertical position. These samples were denoted as Ti-HA_RT. Loading at elevated temperature was performed by preheating the stock solution to 90°C. During the loading time period the test tube was stored in an oven to ensure a constant temperature of 90°C. These samples were denoted as Ti-HA_HT. Samples loaded under elevated temperature and pressure conditions were treated as described above (see section 3.1.6) and denoted as Ti-HA_PHT. For the samples loaded at pH 4 and pH 10 the stock solution was adjusted to the

desired pH by adding hydrochloric acid or sodium hydroxide. These were denoted as Ti-HA_pH 4 and Ti-HA_pH 10, respectively. Ti-HA_US was loaded under applied ultrasound, Ti-HA_USV under applied ultrasound and additional vacuum. The error bars denote the standard deviations corresponding to 3 measurements. The insets of the diagrams present enlargements of the release data following the initial burst to enable adequate visualisation at the later time points.

3.2.7 HPLC analysis

HPLC analyses were performed as described above (see section 3.1.7) to quantify the amounts of drug released after different time durations.

3.2.8 Antibacterial testing

Generally, the antibacterial tests were performed as described above (see section 3.1.10). Some modifications were incorporated in order to optimize the test setup for the geometry of the bone screws used. Accordingly a petri dish was filled with 35 ml CASO agar. After gelation 5 ml germ suspended CASO agar medium was added and inoculated for 18 hours in an incubator at 35°C according to the European Pharmacopoeia 7.0 [99]. The total volume was adequate to ensure mechanical stability of the tested screw after vertical insertion. Screws without HA coating and without antibiotic served as reference samples and were denoted as Ti-w/o. Tobramycin loaded screws by adhesion without HA coating (Ti-w/o_RT) were tested compared to HA coated screws after loading by dipping (Ti-HA_RT) and after loading at elevated temperature and pressure (Ti-HA_PHT).

Additionally, Ti-HA_RT and Ti-HA_PHT screws were tested in a Petri dish containing a *Staph. aureus* suspension in the total volume of CASO-agar and then followed by incubation. By this means the antibacterial efficacy of the whole range of the screw could be evaluated.

3.2.9 Cell Study

All cell studies were performed by Prof. Dr. Sabine Fuchs at Experimental Trauma Surgery, University Medical Center Schleswig-Holstein, Kiel, Germany.

3.2.9.1 Isolation and culture of outgrowth endothelial cells and primary osteoblasts

Outgrowth endothelial cells and primary osteoblasts were prepared as described in section 3.1.11.1.

3.2.9.2 Cell seeding and viability assessment

Titanium discs (\emptyset 10 mm x 5 mm) used for cell culture experiments were treated with 70% of methanol before cell seeding experiments. For cell seeding the titanium discs with or without hydroxyapatite coating were used and placed into 48-well cell culture plates. Cell seeding and viability assessment were performed as described for the stainless steel samples in section 3.1.11.2.

3.2.9.3 Immunofluorescent staining

After washing with PBS cells were fixed on the discs using 4% PFA. Samples were washed again with PBS and permeabilized with 0.1 % Triton-X and incubated with primary antibody mouse anti-human CD31 (Dako, Hamburg, Germany) diluted in PBS/1% BSA for one hour at room temperature. Then these samples were incubated with the corresponding secondary antibody Alexa 555 (Invitrogen, Darmstadt, Germany). Samples with primary osteoblasts were incubated after fixation and permeabilization with 5 μ g/ml Phalloidin-TRITC (Sigma, Deisenhofen, Germany) in PBS/BSA). Finally all samples were treated with Hoechst for nuclear counterstaining and, subsequently to mounting, were analysed on a fluorescence microscope (Zeiss, Axioskop40).

3.3 In-vivo studies

All animal work was performed in accordance to the ethical guidelines of NAMSA Lyon (Chasse sur Rhône, France). The studies were financially supported by the European Commission as part of the 7th Framework programme – BIODSIGN (3rd Party Funding) and additionally supported by Stryker Trauma GmbH (Schönkirchen, Germany). After screw removal the biomechanical tests and micro-CT measurements were performed at the Institute of Orthopaedic Research and Biomechanics in Ulm, Germany.

An overview of the study design can be observed in Figure 9. The studies are divided into a first HA only part, evaluating the effects of the HA coating compared to non-coated control screws in a pilot and a then subsequently a main study. A second part was then based on investigation of the in-vivo efficacy of HA coated antibiotic-loaded (HA-AB) screws compared with non-coated screws.

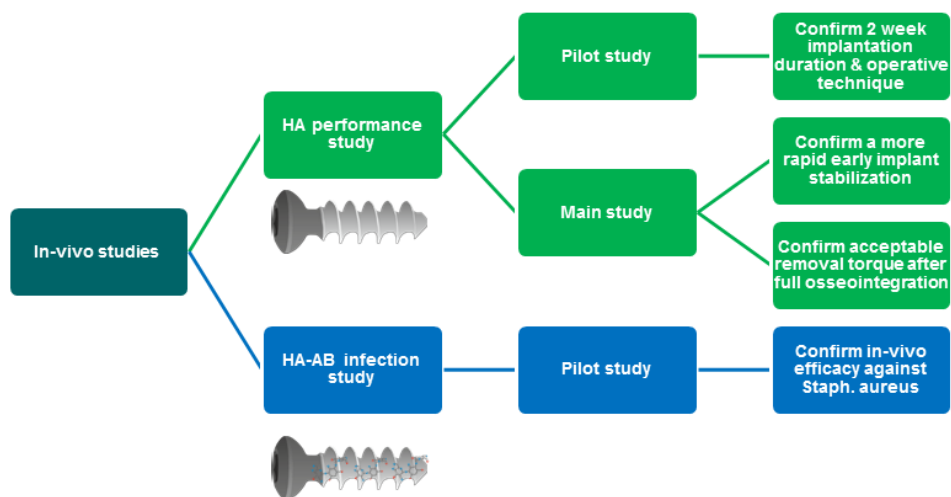


Figure 9: Overview of animal studies performed.

3.3.1 Animals used for in-vivo studies

Male New Zealand white rabbits (*Oryctolagus cuniculus*) were used as test species. For the HA performance studies the rabbits were aged to 24 weeks at implantation. For the infection pilot studies, the age lay between 15 and 16 weeks. Husbandry conditions for all studies were fully in compliance with the European requirements (2010/63/EU). Further information in regards to the husbandry conditions and treatment can be found in the study reports [104–108].

3.3.2 Materials for in-vivo studies

The following specimens were used for in-vivo evaluation in a rabbit distal femur condyle model. For all studies, cancellous titanium bone screws (\varnothing 4.0 x 14 mm; REF 604014) from Stryker Trauma AG Selzach were used as a reference. In case of the HA performance studies (pilot and main) biomimetically deposited hydroxyapatite coated cancellous bone screws were used and denoted as test screws, see Figure 10. The HA coating deposition was carried out as described in section 3.2.4 with a NaOH pretreatment time of 10 minutes. Antibiotic loaded (20mg/ml Tobramycin stock solution) HA coated screws served as test article for the infection pilot study. These screws were loaded in Tobramycin containing solution for 5 minutes under room temperature followed by drying in a vertical position at 37°C for 24 hours. All reference and test articles were packed under aseptic conditions and finally gamma sterilized at 25 kGy, see Figure 11.



Figure 10 Titanium cancellous bone screw (reference) left and HA coated cancellous bone screw (test) right.



Figure 11: Final aseptic packaging of the screws before gamma sterilization.

Further instrumentation necessary for the conduct of the animal studies (sterilized at 121°C, 21 minutes) are listed in Table 5. Figure 12 demonstrates the customized surgical equipment.

Table 5: Overview of the material used during the surgical procedure.

Description	REF Number	Supplier
Spacer 2.5 mm thick (customized)*	customized	Stryker
2.7 mm diameter cannulated drill equipped with a stop at 10 mm (customized)**	702449	Stryker
1.4 mm diameter threaded guide wire labeled using a laser marker at 10 mm (customized)***	702459S	Stryker
4.0 mm diameter cannulated screw tap	702454	Stryker



Figure 12: Picture of the customized material used for the in-vivo studies.

Insertion torque was measured with a rotating torque cell, (Type DR-2335, sensitivity, 2000 mV/V, Lorenz Messtechnik GmbH) coupled with a software (Catman®Easy, version 3.1,

Hottinger Baldwin Messtechnik GmbH), see Figure 13. This system was calibrated externally in advance of the in-vivo measurements. The tip of the measurement system was sterilized at standard conditions (121°C, 21 minutes or 134°C, 18 minutes).



Figure 13: Insertion torque measurement system used for HA performance pilot and main studies.

3.3.3 HA performance study

3.3.3.1 Surgical procedure

The surgical procedure was performed by an experienced veterinary surgeon using standard aseptic techniques. A skin incision was made on the medial side of the femur at the level of the epiphysis. The muscles were separated using blunt dissection to access the medial condyle and the periosteum was removed from the condyle surface. The entry point for drilling was localized between the distal part of the growth plate and the insertion of the collateral-lateral ligament. The direction of drilling was perpendicular to the bone surface (see Figure 14). Bone defects were made using a cordless power tool. Drilling was initiated by introducing a 1.4 mm diameter guide wire down to the opposite cortex. To avoid perforation of the lateral cortex, the guide wire was laser marked to indicate 10 mm insertion depth, see Figure 12. A 2.7 mm diameter cannulated drill was then inserted with a stop at 10 mm depth. Continuous irrigation was applied to limit the risk of the thermal impact of drilling. After removal of the drill, the defect was extensively rinsed with saline to remove bone debris. The guide wire was removed together with the drill and the guide wire was not replaced and the tapping procedure was conducted without the guide wire. The drill hole was tapped using a 4 mm diameter screw tap. The guide wire was removed and the defect was rinsed again with saline to remove bone debris. The spacer was used to create a standardized distance between bone surface and screw head. The screw was inserted until it was in contact with the spacer and was then unscrewed $\frac{1}{4}$ turn to release the spacer. The standardized gap between screw head and bone was necessary to ensure that there was access for the pull-out test jig and additionally to prevent bony overgrowth covering the screw head. These steps were taken to minimize biological variance impact on the pull-out

and removal torque measurements. The maximum insertion torque strength was recorded with a torque load cell. The contralateral femur was similarly treated. The incisions were then closed by suturing the muscle and cutaneous layers separately with absorbable suture (Vicryl or PDS™ II, Ethicon). Medio-lateral and antero-posterior radiographs were taken to locate each screw (angle and insertion depth).

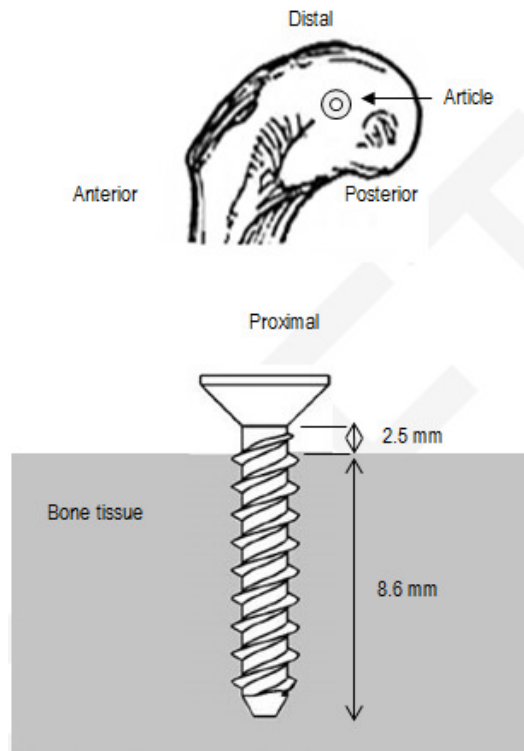


Figure 14: Target position of the screw in the distal femoral condyle of the rabbit.

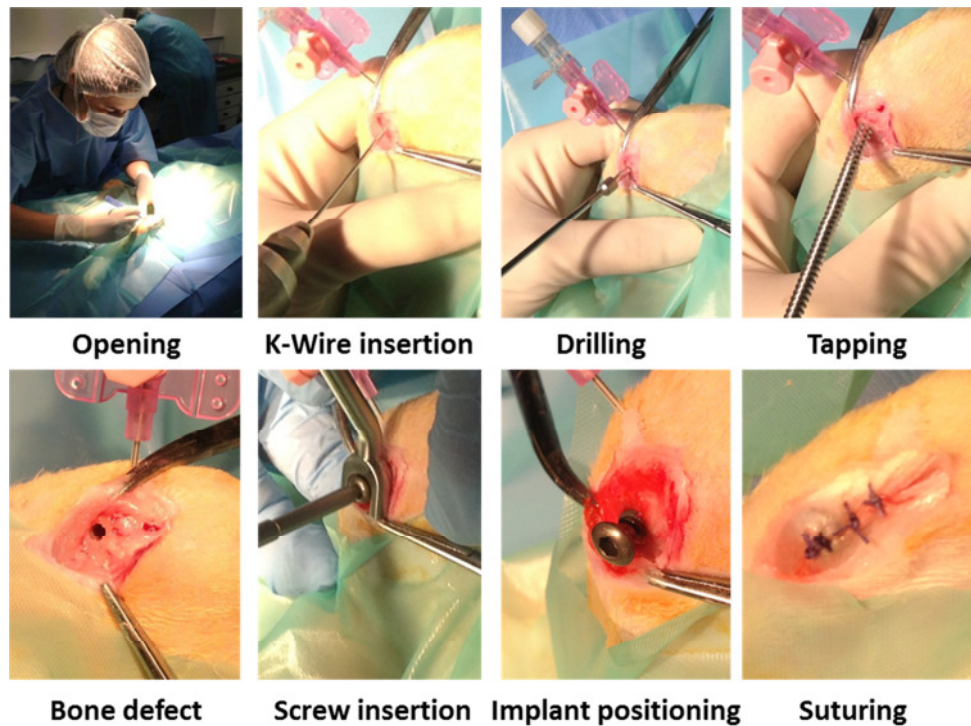


Figure 15: Pictorial overview of the surgical procedure.

3.3.3.2 Terminations

Two weeks (pilot and main study) and six weeks (main study) after implantation, the rabbits were weighed and then terminated by an intravenous injection of pentobarbital (Dolethal[®], Vetoquinol) preparation. The distal femoral condyles and the surrounding soft tissues were macroscopically observed and any abnormality was recorded using the following parameters: size, shape, color, consistency, distribution and any other observation, as appropriate. Photographs were taken of the areas of interest.

Detailed information on general animal preparation, general clinical observations and follow-up treatments can be reviewed in the corresponding reports [104–107].

3.3.3.3 Biomechanical studies

3.3.3.3.1 Removal torque measurements

To measure the removal torque of bone screws with different coatings of unknown bony ingrowth quality it is mandatory to use a standardized testing procedure. For this purpose a custom made torsion apparatus was used together with an embedding method that ensured optimal alignment of the screws with the removal tool, and further enabling the application of the removal torsion moment at a constant torsion rate.



Figure 16: Example of rabbit femur specimen with plastic storage container.

The femurs (see Figure 16) were shortened to 15-20 mm length including the distal end. Figure 17 shows the custom made torsion apparatus, which is also used for aligned embedding of the bones.

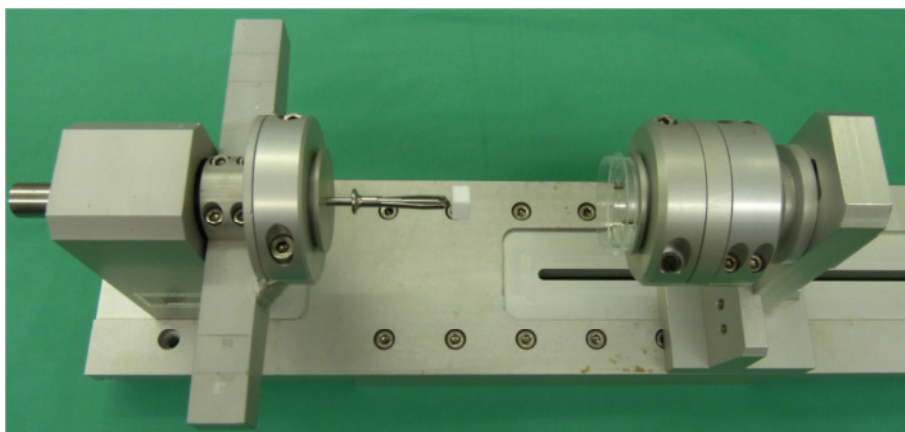


Figure 17: Custom made torsion apparatus: left side: rotatable grip holding the removal torque screw driver (here with screw, screw holder and Teflon test block); right side: grip, which cannot rotate but can translate along the screw driver axis, holding the embedding container. Both grips are mounted on a base plate.

A custom made jig was designed to enable simultaneous embedding of 8 samples, see Figure 18.

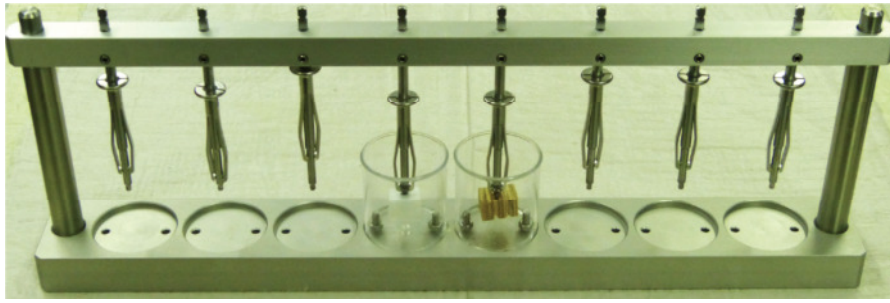


Figure 18: Embedding rig for 8 samples.

For the best possible alignment of the removal torque screw driver the screw head is retained by a special clamp, see Figure 19. Afterwards, the samples are placed inside the embedding containers, which are mounted on the base plate of the jig. Finally, the containers are filled with polymethylmethacrylate (Technovit 3040, Heraeus Kulzer, Wehrheim) to fix the specimens in the pre-aligned position. Curing of the embedding agent takes approx. 10 minutes. Embedding and all tests are carried out at room temperature.

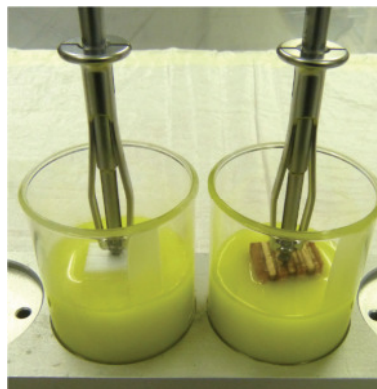


Figure 19: Embedding the dishes with polymethylmethacrylate (PMMA).

After hardening, the specimen is placed in a horizontal position in a material testing machine (Z10, Zwick, Einsingen, Germany). The clamp holding the screw head is slid backwards so that the grip holding the sample can be retracted by 0.5 mm allowing the screw to move out of the sample while applying the removal torque (screw pitch: $1.8 \text{ mm}=360^\circ$, $0.5 \text{ mm}=100^\circ$). The lever arm ($l=35 \text{ mm}$) of the rotatable grip that holds the screw driver is placed under a loading punch, see Figure 20, which can be moved downwards by the crosshead of the

material testing machine. The resulting force F is registered by a 50 N load cell (KAP-TC, A.S.T./Zwick, Einsingen). Thus, the grip holding the screw driver is rotated anticlockwise creating a removal torque acting on the screw.

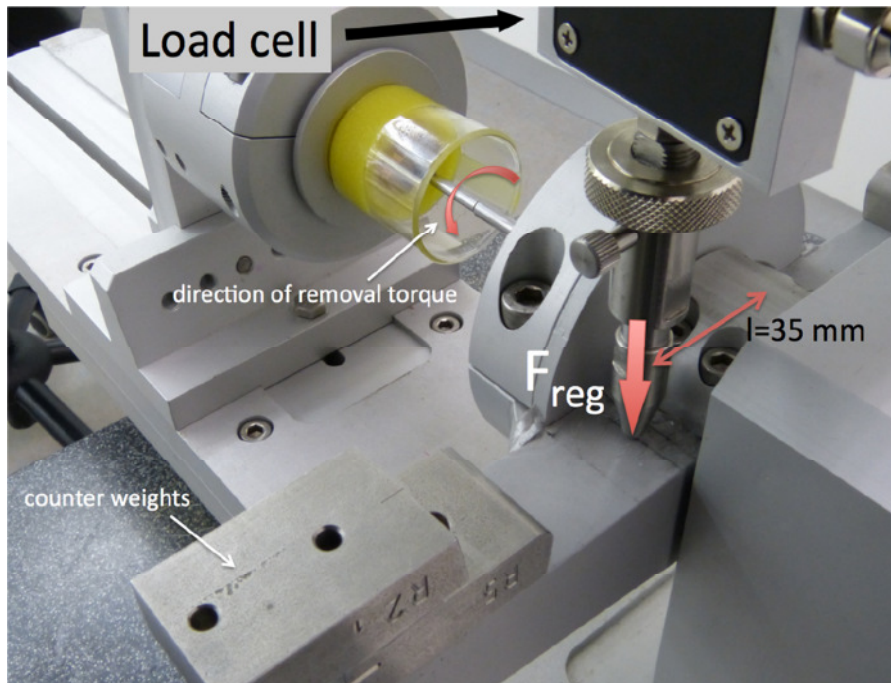


Figure 20: Test assembly placed in the material testing machine. F_{reg} : Registered force exerted to the lever arm ($l=35\text{ mm}$) of the torsion device. Load cell (range 50 N). Counter weights balance the unevenly distributed mass of the lever arm.

In the start position the loading punch is rotated to position the lever arm both horizontally and parallel to the base plate. The crosshead of the material testing machine is then moved downwards at a constant displacement rate of 3.06 mm/minute resulting in a torsion rate of 5°/minute. The torsion angle is calculated with the registered displacement of the loading punch, see Figure 21.

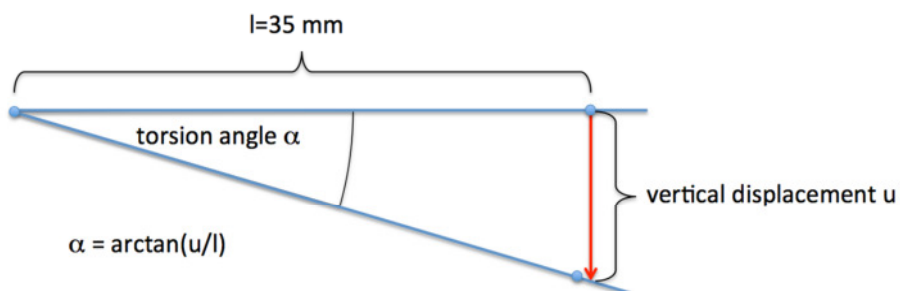


Figure 21: Calculation of the torsion angle α .

The effective torsion moment is simply the product of the registered force F_{reg} , and the lever arm l (35 mm). To avoid the need for correcting the force due to the non-axisymmetric distribution of mass of the lever counterweights were placed on both sides of the lever. This resulted in a balanced position regardless of the lever angle. Tests without sample showed that moving the lever arm needed a moment of 0.3 Ncm at maximum, which is induced by friction in the bearings.

3.3.3.3.2 Evaluation method of maximum removal torque

The maximum removal torque was evaluated as shown in Figure 22. A line parallel to the initial steep slope of the removal torque-torsion angle graph was drawn at an offset of 1°. The maximum torque occurring between the onset of the graph and the intersection of that line with the graph was then considered to be the maximum removal torque.

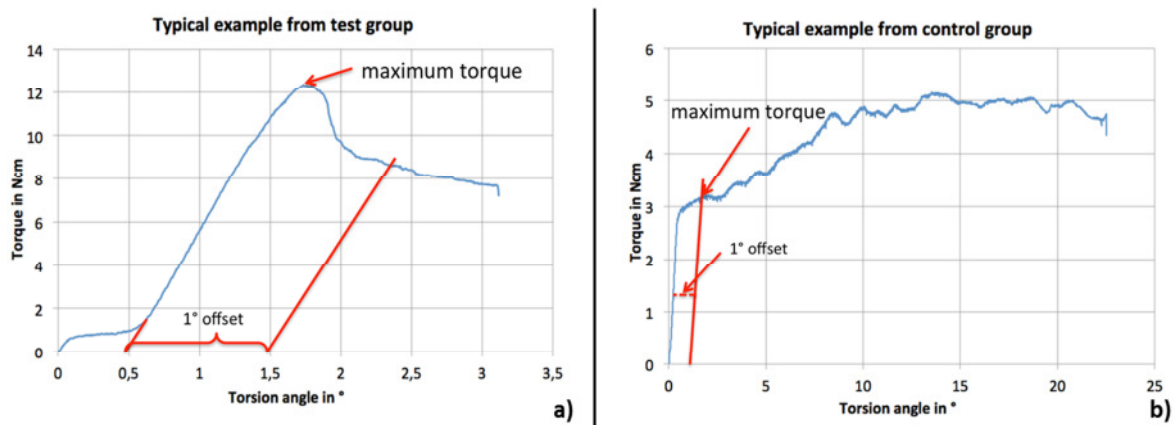


Figure 22: Evaluation method of maximum removal torque using a 1° torsion angle offset illustrated for two types of torque-torsion angle characteristics.

3.3.3.3.3 Pull-out force measurements

The evaluation of fixation strength by a pull-out test for each screw implanted in each distal femoral metaphysis is enabled by the preset 2.5 mm distance between the screw head and the bone surface.

Each bone was embedded with an alignment of the screw that enables measurement of the pull-out force with a special pull-out tool. The test was performed in a standard material testing machine at a constant pull-out rate. The femurs were shortened and embedded in PMMA as described for the removal torque measurement (see section 3.3.2.3.1). The dishes are removed from the embedding tool and placed in a materials testing machine (Z10, Zwick, Einsingen, Germany) in a special adjustable fixture, see Figure 23. The dish holding the specimen and screw was positioned under a perforated plate to enable access of the special

pull-out tool. The pullout tool is fixed to a load cell (U1, 10 KN, Hottinger Baldwin Measurements).

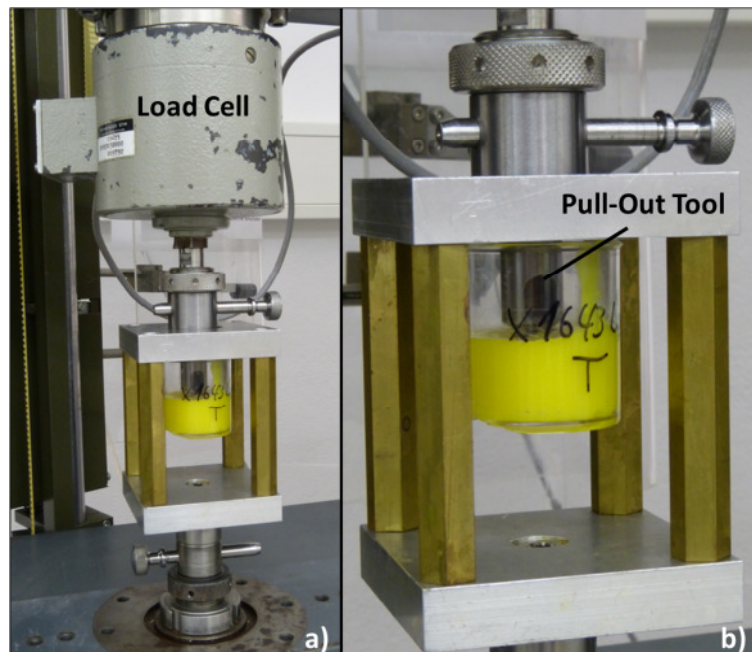


Figure 23: Test assembly in the material testing machine. Calibrated load cell (range 10 kN).

The crosshead of the material testing machine was moved upwards at a constant displacement rate of 5 mm/minute. Force and displacement are continuously registered and the test terminated after a clear drop of the force was observed. Figure 24 displays a typical force-displacement curve obtained during a preliminary test with a specimen used before removal torque testing. The maximum pull-out force F_{\max} (here 565 N) and the pull-out stiffness (here 891 N/mm) can be read from the graph.

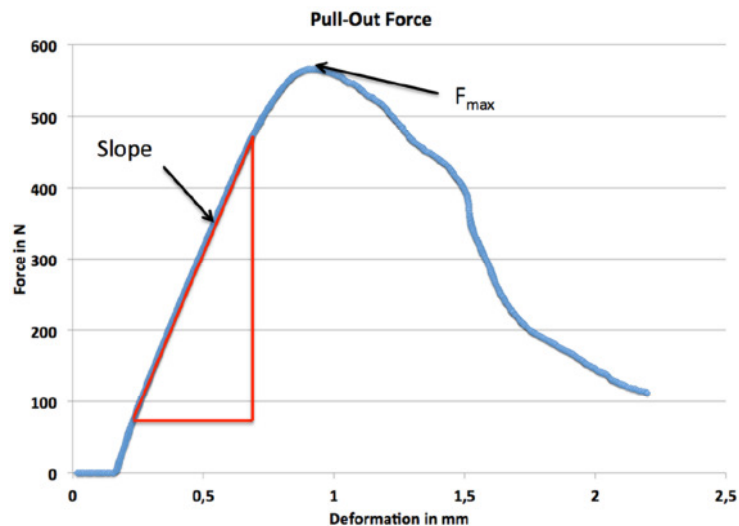


Figure 24: Pull-out test diagram: F_{max}: maximum pull-out force in N; slope: pull-out stiffness in N/mm.

3.3.3.4 Statistical evaluation

After summarizing the valid data points, all relevant descriptive parameters were identified to assess the mean and variance of the data. Normality of all continuous variables was assessed with the Shapiro-Wilk Test [109]. Due to the small sample sizes in each group ($n = 5-8$) the prediction of a normal distribution is imprecise, regardless of the Shapiro-Wilk Test outcome. Therefore, the unpaired Mann-Whitney Test was selected for comparison. Additionally, Monte Carlo Simulation was used to raise the precision of test outcome. The level of significance for all tests was set to 95% ($p < 0.05$ was significant). All calculations were performed with the software PASW Statistics Version 18.0.2 (SPSS). For graphical visualization and comparison box- and whisker plots were chosen for all variables (control and test) and time points (two or six weeks). The box corresponds to the range in which the middle half (50%) of the data are included. The median is shown as a line in the box. Furthermore, the lower quartile (25%) marks the onset of the box and the upper quartile (75%) the end of the box. The whiskers mark the minimum (0%) and the maximum data value (100%) of the data that are not outliers. Values deviating more than 1.5 times the

interquartile distance from the median were considered as outliers and marked as circles. Values shown in the graphs of $p < 0.05$ were considered significant and values of $p < 0.01$ highly significant. Statistically significant differences between the implant types (control and test) and time points (two and six weeks) are labeled in the diagram by a line and the corresponding p-value.

3.3.3.5 Histological preparation

After complete fixation, implanted sites were dehydrated in alcohol solutions of increasing concentrations, cleared in xylene and embedded in PMMA (polymethylmethacrylate) resin. After micro-CT analysis, one longitudinal central cross section of each site was obtained by a microcutting (thickness of each section between 20 to 30 μm) and grinding technique. Sections were stained with modified Paragon for qualitative, semi-quantitative and quantitative analysis.

3.3.3.6 Histopathological preparation

Qualitative and semi-quantitative histopathologic evaluation of the local tissue effects and bone healing were performed and the following parameters were graded using a semi-quantitative scoring system: inflammatory reaction (polymorphonuclear cells, lymphocytes, plasma cells, macrophages and giant cells / osteoclastic cells), necrosis, fibrosis, neovascularization, fatty infiltrate, fibrin, osteolysis, cell or tissue degeneration, osteoblastic cells, bone neoformation, osteointegration, osteoconduction, bone remodeling, coating degradation and any other relevant parameter.

3.3.3.7 Histomorphometrical preparation

A quantitative histomorphometrical analysis was conducted by scanning and examining slides with a Zeiss Axioscope microscope equipped with a color images analyzing system (Samba, version 4.27, Samba Technologies, France). The regions of interest (ROI 1 and 2) were investigated as defined in Figure 25 and Figure 26.

Quantitative analyses were performed to assess the percentages of the contact and area density parameters within the ROI's 1 and 2. The contact parameters describe the bone to implant contact as well as the soft tissue contact and the bone marrow contact. The area density was divided into bone area density (percentage of the ROI occupied by bone tissue in terms of surface area), as well as soft tissue area, bone marrow area and implant area density. The quantitative results of ROI 1 and ROI 2 were summed for analysis and the resulting average values were evaluated.

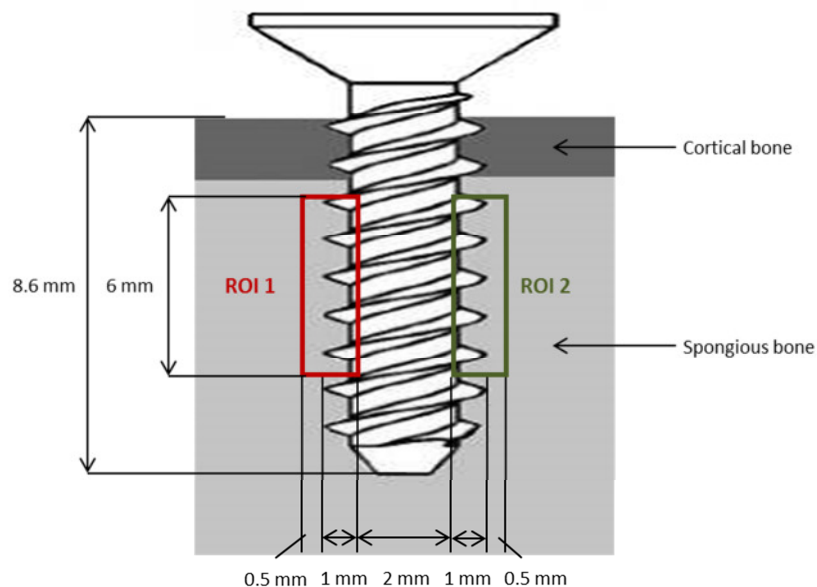


Figure 25: Scheme of the regions of interest investigated for the histomorphometrical analysis.

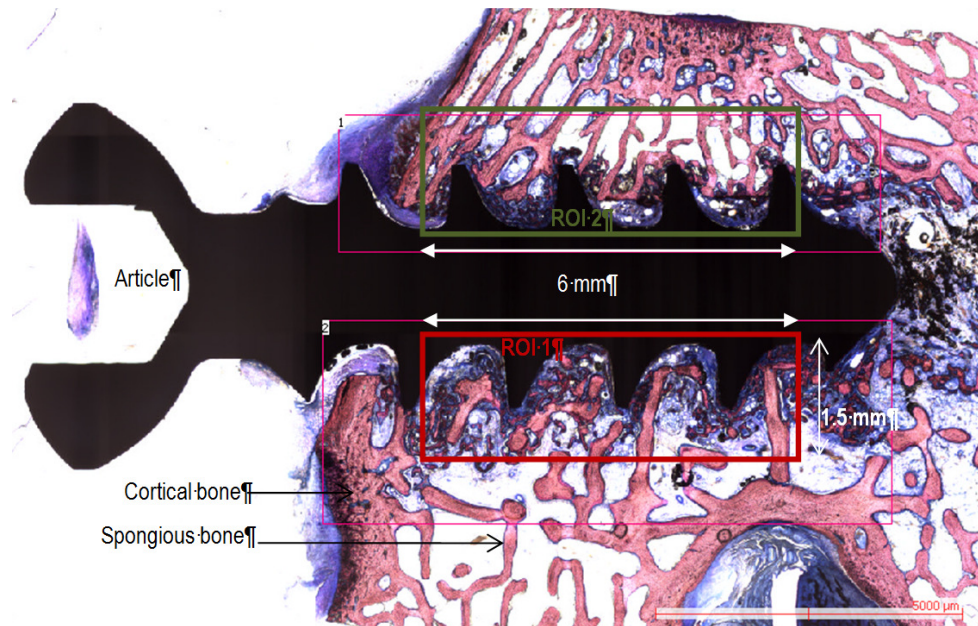


Figure 26: The rectangles 1 and 2 correspond to the area of pre-scanning before defining the ROIs

3.3.3.8 Micro-CT measurements

After fixation and resin inclusion, the sites were analyzed via micro-CT (Bruettisellen, Switzerland). The samples were scanned by micro-computed tomography (CT 100, Scanco Medical AG, Switzerland) using an energy of 90 kVp at an intensity of 89 μ A. The integration time was adjusted to 600 ms at a double fold frame average. Nominal isotropic resolution was set to 11.4 μ m. To segment bone around the implant, the measured data was filtered using a three-dimensional constrained Gaussian filter with finite filter support (1 voxel) and filter width ($\sigma = 0.5$). The outer border of the volume of interest (total volume = TV) for the bony region around the implant was defined by a defined distance from the implant (0.5 mm), see Figure 27.

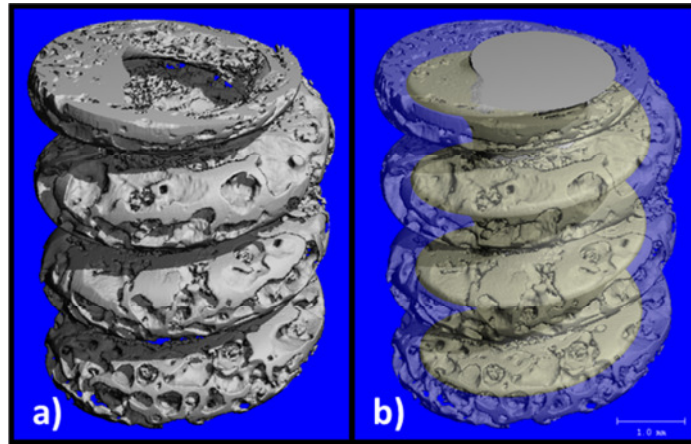


Figure 27: The defined region of interest (ROI) can be observed in the left image (a). The right image (b) demonstrates the screw (grey part) and the region of interest described by the transparent part.

Bone and implant were segmented as separate phases. As the interface of the implant to bone was blurred due to the partial volume effect, morphologic operators were used to identify the contact area of bone to the implant. The bone implant contact (BIC) was then analyzed slicewise. As part of the implant head of the screw was outside bone, the analysis region was limited to a height of 860 voxels starting 2 voxels above the tip of the implant.

3.3.3.9 Micro-CT measurements after removal torque testing

Prior to micro-CT scanning 14 screws were removed from the femurs (7 control and 7 test articles after 6 weeks in-vivo). The bones were placed with their embedding containers (including the methacrylate) in a micro-CT (Skyscan 1172) and scanned at a resolution of 30 μm . Subsequently, the cortical thickness was measured at 4 points (2 in 2 perpendicular planes) using an evaluation tool provided by the CT manufacturer (Skyscan) and averaged, see Figure 28.

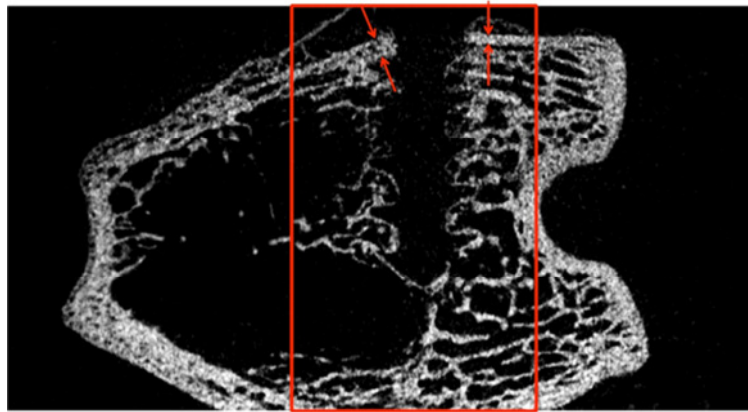


Figure 28: μ -CT image of the bone after screw removal. The arrows indicate the cortical thickness measurement (here in one plane).

3.3.3.10 HA performance pilot study design

Eight rabbits (7 + 1 reserve) were implanted bilaterally with one test or one control article in each medial femoral condyle. The articles were subdivided randomly. Torque strength at screw insertion was assessed. X-rays were taken directly after surgery. Two weeks after implantation, the rabbits were euthanized and the condyles were macroscopically evaluated. The articles were subsequently biomechanically evaluated by measuring removal torque (5 control and 5 test articles) and pull-out force (3 control and 3 test articles).

Table 6: Study design HA performance pilot study; C: Control article: cancellous screw; T: Test article: hydroxyapatite coated cancellous screw (Verum)

Time-period	2 weeks							
Rabbit number	X1427	X1441	X1465	X1429	X1469	X1569	X1595	X1630
Left femur	C	T	C	T	C	T	C	C
Right femur	T	C	T	C	T	C	T	T
Total number of control sites	8							
Total number of test sites	8							

3.3.3.11 HA performance main study design

Thirty-two rabbits (plus four reserve rabbits) were implanted with one test or one control article in each medial femoral condyle. Two or six weeks after implantation, the rabbits were euthanized. The local tissue effects and bone healing performance were evaluated by macroscopic, radiographic, histopathology and micro-computer tomography analyses. The biomechanical properties of bone/article interface were evaluated with torque removal strength measurement both during screw insertion and during removal at later time points. Alternatively a pull-out test was performed at a later timer point. All investigations performed are summarized in Table 7.

Table 7: HA-performance main study design

	Time-period	2 weeks		6 weeks	
	Group	Test group	Control group	Test group	Control group
Number of sites	Histopathology analysis	4	4	4	4
	Pull-out test	6	6	6	6
	Torque strength insertion measurement	18	18	18	18
	Torque strength removal measurement	6	6	6	6
	Reserve sites	2	2	2	2
	Total	18	18	18	18

The reserve rabbits were operated on using the same surgical procedure as the other rabbits. They were followed in exactly the same manner up to the end of the study and were planned to potentially replace rabbits removed from the study in case of unforeseen rabbit loss or any adverse event. At the end of the study, no abnormal event had occurred requiring the inclusion of these rabbits. Therefore, all reserve animal sites were sampled (control and test) and used for biomechanical testing.

3.3.3.12 Testing guidelines

The study was conducted according to an adaptation of the ISO 10993 Standard: Biological evaluation of medical devices:

- Part 2 (2006): Animal welfare requirements
- Part 6 (2007): Tests for local effects after implantation

3.3.4 HA infection study

3.3.4.1 Materials for microbiological preparation

The following materials were used for the microbiological evaluations, see Table 8. All additional surgical equipment used is recorded in section 3.3.2.

Table 8: Overview of material used for microbiological evaluation

Materials	Supplier
<i>Staphylococcus aureus</i> strain	American Type Culture Collection No. 6538
Trypcase soy agar (TSA)	bioMérieux, reference 43011
Trypcase soy broth (TSB)	bioMérieux, reference 44011
Pharmacopeia Diluent	AES CHEMUNEX, reference AEB111299
Filtration membrane 0.45µm	PALL, reference 4805
Neutralizing Pharmacopoeia Diluent (NPD)	AES CHEMUNEX, reference AEB611274

3.3.4.2 Surgical procedure

3.3.4.2.1 Defect creation and inoculation

In general, the surgical procedure was performed as described earlier in section 3.3.3.1. Within this study, the defect was inoculated by a defined method and concentration of bacteria. A total volume of 10 µl of bacterial suspension, corresponding to 10⁵ or 10⁷ CFU, was distributed onto the article (5 µl) just before implantation and into the defect (5 µl). Bacterial inoculum (5 µl) was spread into the defect by online deposition with the pipette tip moving from the bottom up to the top of the defect, see Figure 29.

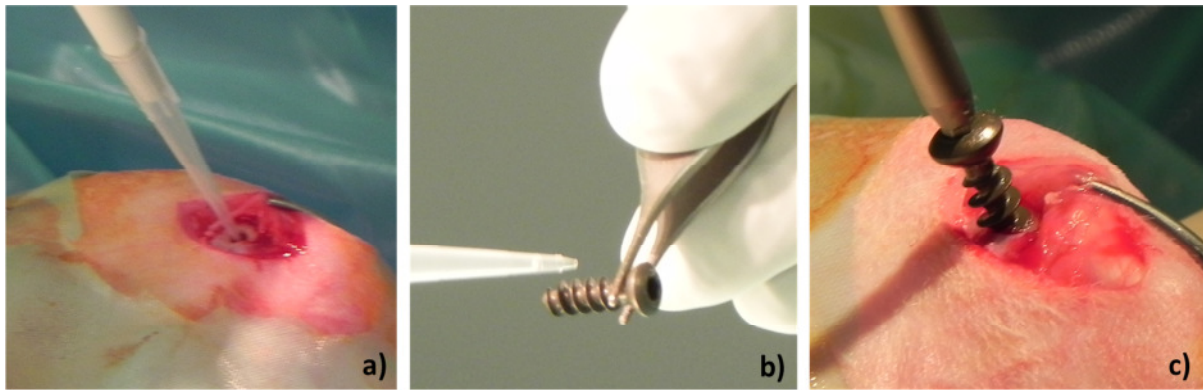


Figure 29: Inoculation method during in-vivo study – 5 µl inoculum suspended directly in the bone defect (a), 5 µl distributed directly on the screw (b) followed by insertion (c).

The inoculum was then spread by gentle scrubbing with the pipette tip. Bacterial inoculum (5 µl) was also spread between the three threads of the screw, on each side of the article, see Figure 30. The inoculation technique used was intended to ensure homogeneous distribution of the inoculum over the complete defect whilst avoiding heavy leakage of the suspension, see Figure 30. Screws were handled with sterile forceps and loss of bacterial suspension was avoided. Screws (previously inoculated) were manually screwed into the defect within minutes after their inoculation.

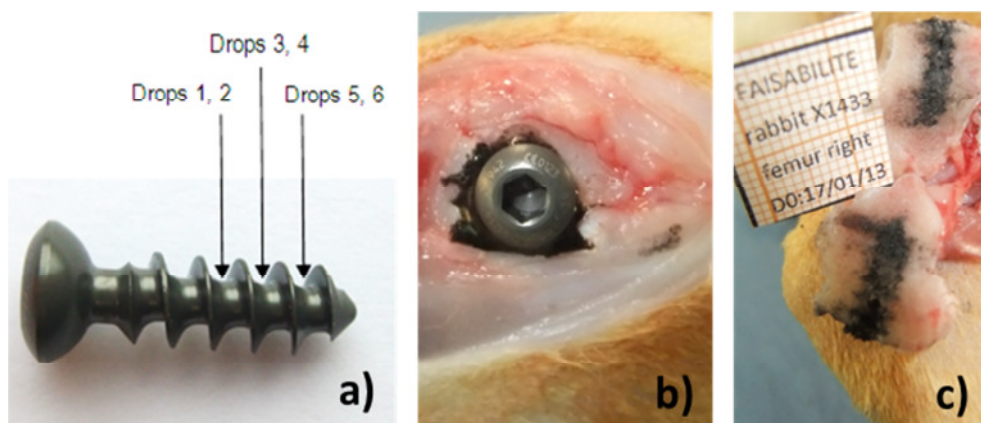


Figure 30: Distribution of 5 µl suspension directly onto the screw (a). Minimal leakage (b) and homogeneous distribution (c) of the suspension were demonstrated during a cadaveric study. The suspension mimicking the inoculum was stained with a black colorant.

The excess portion of the inoculum which came out of the defect during screwing into the bone was removed with gauze. The bone surface was cleaned with slightly moistened gauze

to remove bacteria that may induce an infection of the soft tissues. The contralateral femur was similarly treated. After inoculation the screw was inserted to full depth for all sites because it was unnecessary to leave a gap for biomechanical testing in this series. By inoculating 10^4 CFU, only the defect was inoculated with 10 μ l to again, reduce the leakage of bacterial suspension during insertion of the screw. The change of inoculation method was feasible, because the 4 rabbits treated with 10^4 CFU were operated on at a later time point after having received the results from the studies with a higher bacterial inoculation.

3.3.4.3 Bacterial counts

Bacterial suspensions prepared at implantation and extracts obtained from the explanted articles were analyzed. Accordingly, an appropriate number of dilutions were prepared with the pharmacopeia diluent (eight dilutions, from 10^{-1} to 10^{-8} fold dilutions). For each article, 1 ml of the pure extract and of each extract dilution was filtered onto 0.45 μ m membranes. These membranes were then deposited on tryptic soy agar plates and incubated in aerobic conditions at $37 \pm 2^\circ\text{C}$ for 24 ± 8 hours to determine the number of viable bacteria. Resulting colonies were counted via visual observation. The membranes that displayed 30 to 300 CFU / membrane were used to calculate the bacterial count of each article as follows:

Bacterial count (CFU) = number of colonies \times dilution factor \times fraction of the extract deposited on the membrane.

3.3.4.4 Study design of infection pilot study

Ten rabbits were implanted bilaterally in each medial femoral condyle with either one test or one control article inoculated with 10^4 , 10^5 or 10^7 CFU of *Staph. aureus* as shown in Table 9. Nine days after implantation, the surviving rabbits were euthanized and infection of the implanted sites was evaluated using macroscopical observations, x-rays at necropsy,

bacterial counts on the explanted articles and histopathological analysis of the surrounding bone tissue.

Table 9: Study design; T: Test article: Hydroxyapatite antibiotic cancellous screw; C: Control article: Cancellous screw; *: these rabbits died or were euthanized prematurely. Their sites were submitted to histopathological analysis but not to microbiology.

Time period	9 days									
Inoculation dose (CFU/site)	10⁴				10⁵			10⁷		
Rabbit number	Y575	Y594	Y653	Y576*	X1648	X1684*	X1685	X1686	X1689*	X1690*
Left femur	C	C	T	T	C	T	C	T	C	T
Right femur	T	T	C	C	T	C	T	C	T	C

3.3.4.5 Testing Guidelines

This study was based on an adaptation of ISO 10993 Standard: Biological evaluation of medical devices:

- Part 2 (2006): Animal welfare requirements
- Part 6 (2007): Tests for local effects after implantation
- Part 12 (2012): Sample preparation and reference material

As well as ISO 11737 Standard: Sterilization of medical devices – microbiological methods

- Part 1 (2006): estimation of population of microorganisms on products

4 Results

4.1 Results of investigations performed with stainless steel surfaces

4.1.1 HA coatings

Plasma-sprayed HA coatings (HA-P) were compared to biomimetic HA coatings (HA-B) in terms of microstructure as well as on antibiotic loading capacity and release characteristics after different loading parameters. Both coating types can be observed macroscopically in Figure 31.

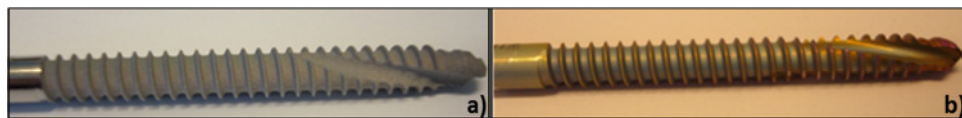


Figure 31: Photograph of a) plasma sprayed HA coating and b) biomimetically deposited HA coating on a fixation pin. As visualized by the SEM images in Figure 32 a) and b), the HA deposition process had a strong impact on the HA-coating morphology and topography.

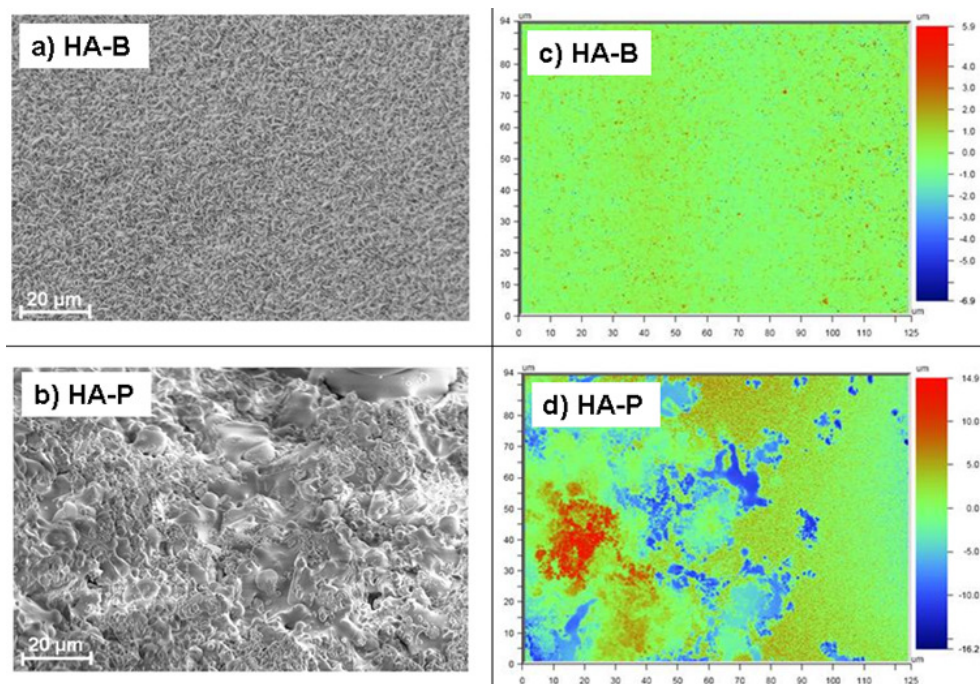


Figure 32: SEM images (left panels) and surface topography maps (right panels) of the HA-B (a, c) and HA-P (b, d) surface.

Immersion of the TiO₂ coated pins in PBS resulted in precipitation of a nano-porous, homogeneous HA-B coating with needle-like HA crystal morphology, Figure 32 b). While a rather rough morphology, consisting of droplets and variation in substrate coverage, was observed on the plasma deposited HA-P samples, Figure 32a. The surface topography maps, Figure 32 c) and d), confirmed the much rougher surface of the plasma sprayed HA coating seen in the SEM images. The surface roughness of the coatings was characterized by a profile roughness, R_a, of ~ 2.5-3.0 μm for the HA-P and ~0.5-1.0 μm for the HA-B coatings, respectively. XRD measurements of HA-B coated plates confirmed that the coating consisted of bone like mineral HA, see Figure 33.

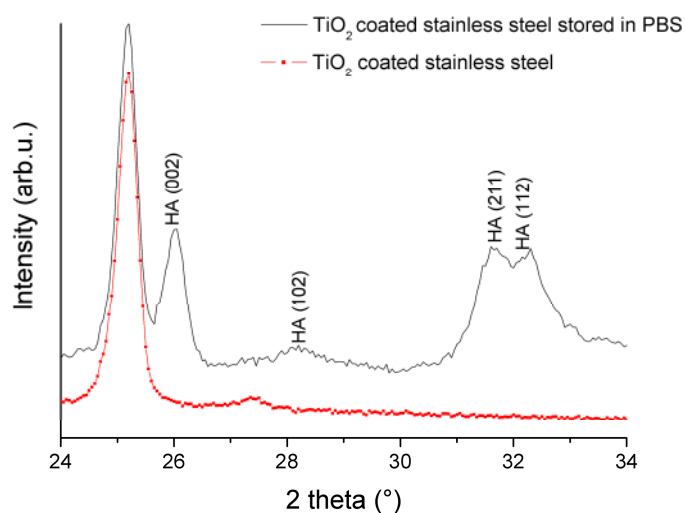


Figure 33: XRD spectra of TiO₂ and TiO₂ coated stainless steel plates stored in PBS. Diffraction peaks of crystalline HA are indicated in the figure.

SEM images of the coating cross-sections are displayed in Figure 34. The HA-P coatings have an average thickness between 20 and 40 μm, depending on the area. Cracks and micro-pores can be observed in the cross-section SEM image of these samples, Figure 34 c) and d). In comparison, the cross-section of a HA-B coating, Figure 34 a) and b), displays a denser, nanoporous, structure at the TiO₂ interface and a higher degree of porosity with a flake-like

topography towards the outer surface. The thickness of HA-B deposited coatings varied between ~ 4 and $8 \mu\text{m}$. For the HA-B coatings a higher coating thickness could be observed in the thread valleys of the pins than at the thread tops.

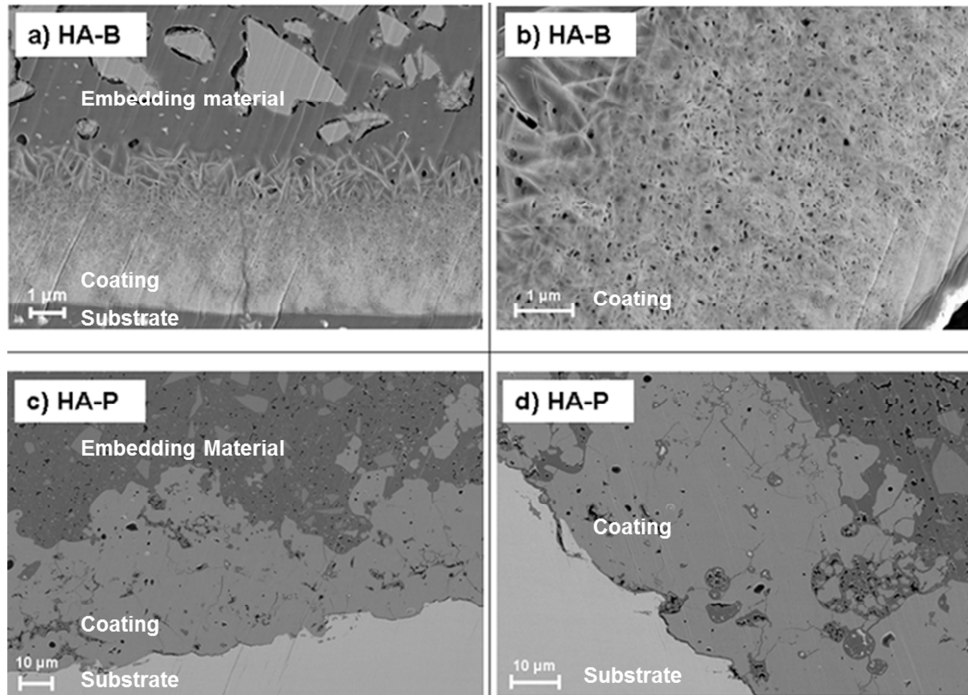


Figure 34: SEM images of ion milled cross-sections of HA-B (a, b) and HA-P (c, d) coatings deposited on fixation pins. The substrate and coating interfaces are indicated as well as the embedding material.

The incorporation of the antibiotic into the HA coatings did not cause morphological changes, as visualized by the SEM images in Figure 35. Minor cracks were seen in the HA-P coating structure for Load-P samples. These might result from the evaluated pressure during loading or occur during drying.

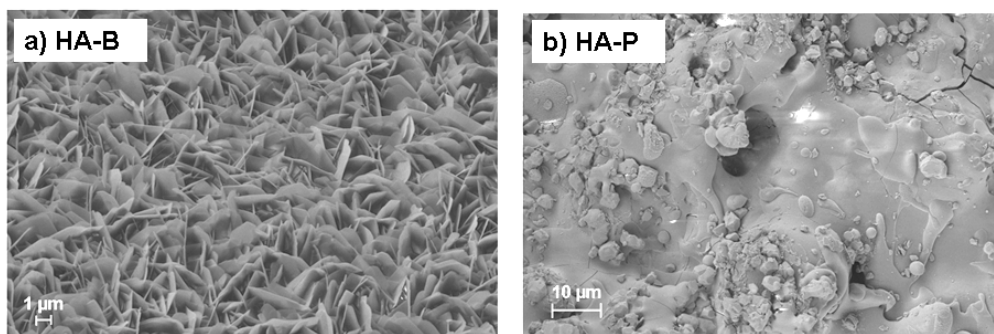


Figure 35: SEM images of HA-B (a) and HA-P (b) coatings loaded with Tobramycin under a pressure of 6 bar (Load-P).

4.1.2 Drug loading and release studies

Different loading techniques and parameters were investigated within this section. Table 2 gives an overview on the different parameters tested. Figure 36 demonstrates the drug release in PBS from Load-RT samples loaded with Tobramycin at three different soaking times. As is evident in this figure, an initial rapid release within the first 15 minutes of the studied releasing time, hereafter referred to as burst release, was seen for HA-P coatings. The amount of drug released varied slightly but did not show any clear dependence on drug loading time. In comparison, a continuous controlled release of Tobramycin for 2 days was achieved for HA-B coatings. The amount of antibiotic released from these coatings was found to lie above the MIC for *Staph. aureus*.

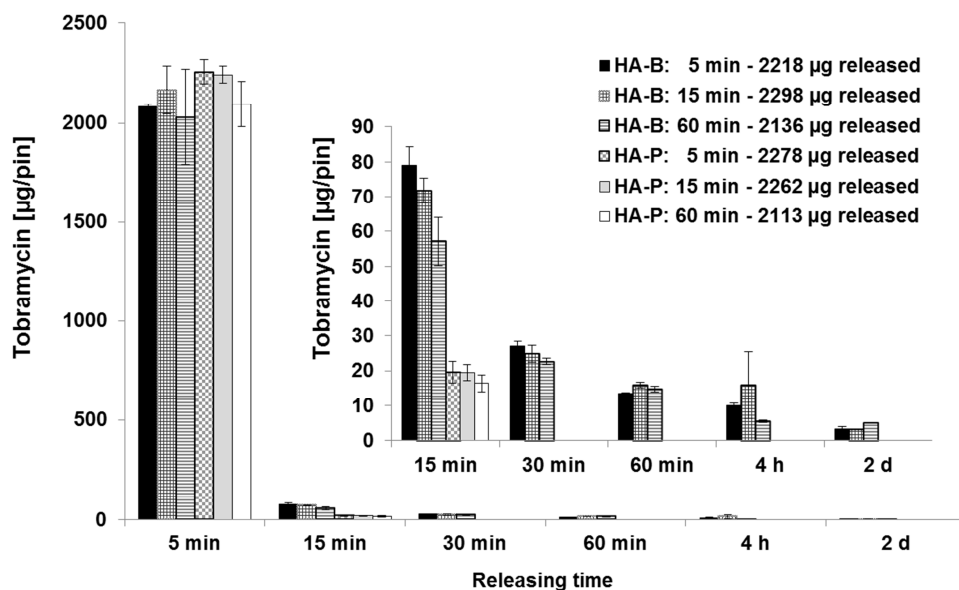


Figure 36: Non-cumulative release after loading for different time periods at room temperature in Tobramycin containing solution (20 mg/ml). The inset describes a magnification of the sustained release.

The impact of different drug loading concentrations on the release kinetics is presented in Figure 37. The Load-C samples exhibited an initial burst release, which was characterized by a linear correlation between drug loading concentration and released amount of Tobramycin. A following, continuous slow release of drug was measured from HA-B coated pins. This sustained release lasted for 2 days and was found to be independent on the antibiotic concentration during loading. These findings lead to the conclusion that a soaking time of 5 minutes is sufficient for successful drug incorporation and a drug concentration of 20 mg/ml was chosen for preparation of Load-P, Load HT and Load-PHT samples.

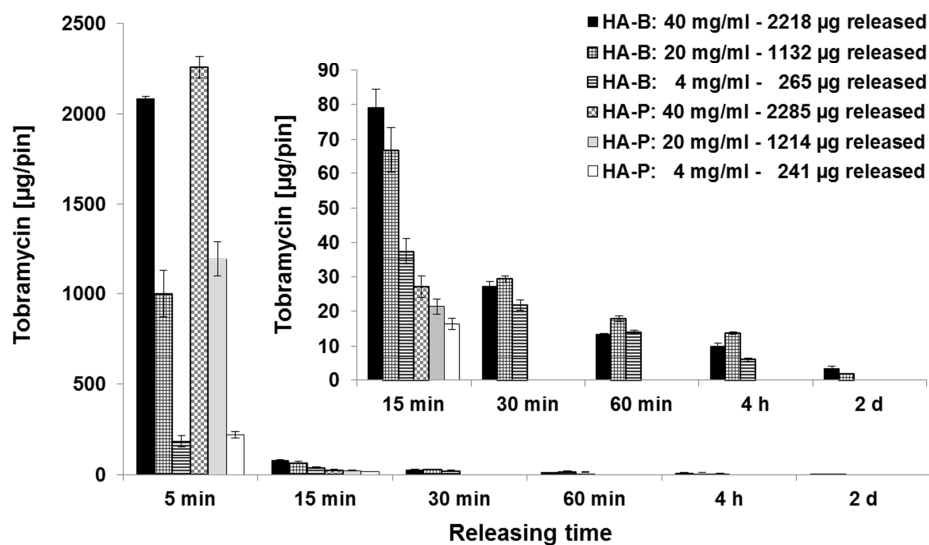


Figure 37: Non-cumulative release after loading with different concentrations of Tobramycin containing solutions. The inset describes a magnification of the sustained release.

In order to study factors enabling to tailor the sustained release process, the impact of pressure under loading by absorption on the release profile was investigated. As it is apparent from Figure 38, the evaluated pressure contributed to a prolonged release period. HA-P coatings of Load-P samples exhibited a slow release profile for up to 4 h after the initial burst and the controlled release from HA-B coatings was extended up to 5 days. In addition, a substantial increase in released amount of drug was measured for both HA coating types under these loading conditions. A sufficient dose of Tobramycin was released to ensure inhibition of *Staph. aureus* from HA-B coated pins even after 5 days.

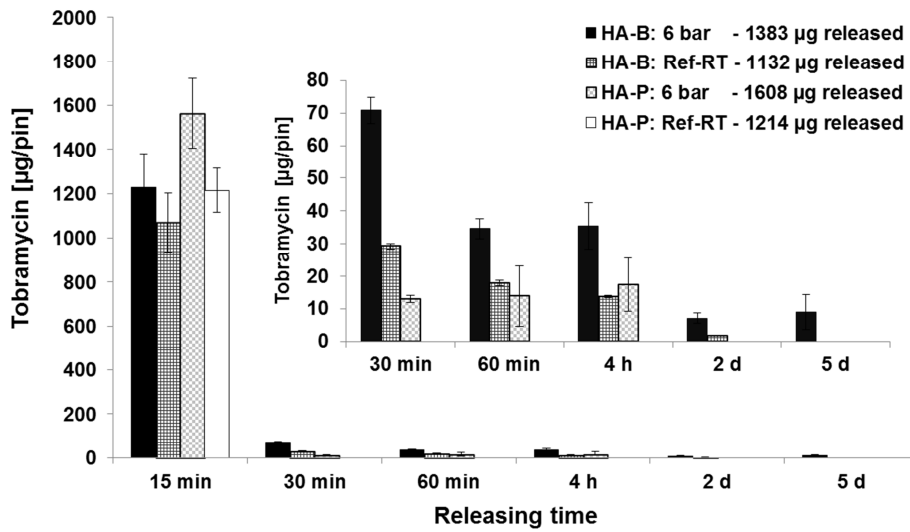


Figure 38: Non-cumulative release after loading at elevated pressure of 6 bars in a Tobramycin containing solution. The inset describes a magnification of the sustained release.

Evaluated temperature under loading was found to decrease the amount of Tobramycin incorporated into both HA coating structures compared to soaking under room temperature, as shown by lower Tobramycin values released of Load-HT samples during initial burst, Figure 39. An increased sustained release time of 60 min could be obtained for HA-P coated pins while HA-B coatings exhibited an increase in released amount of drug after 2 days.

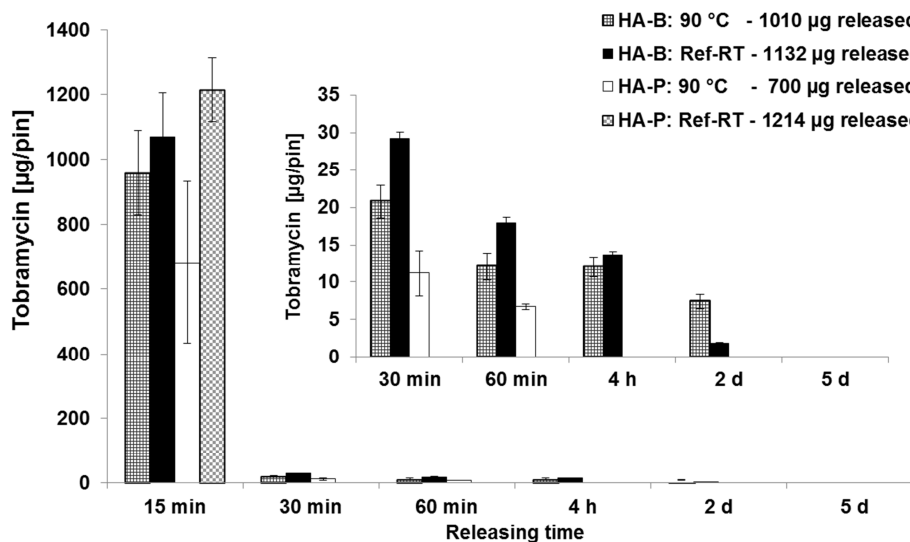


Figure 39: Non-cumulative release after loading at elevated temperature (90°C) in a Tobramycin containing solution (20 mg/ml). The inset describes a magnification of the sustained release.

Figure 40 demonstrates the combined impact of elevated temperature and pressure on the loading and release properties in comparison to the release profile of Load-RT samples. As is evident from this figure, a great improvement in releasing time and in the amount of drug incorporated into the coatings was achieved for Load-PHT samples. HA-P coatings exhibited a prolonged sustained release up to 2 days and HA-B coatings could increase the sustained releasing time by factor 4 accompanied with an released amount of Tobramycin greater than the MIC for *Staph. aureus*.

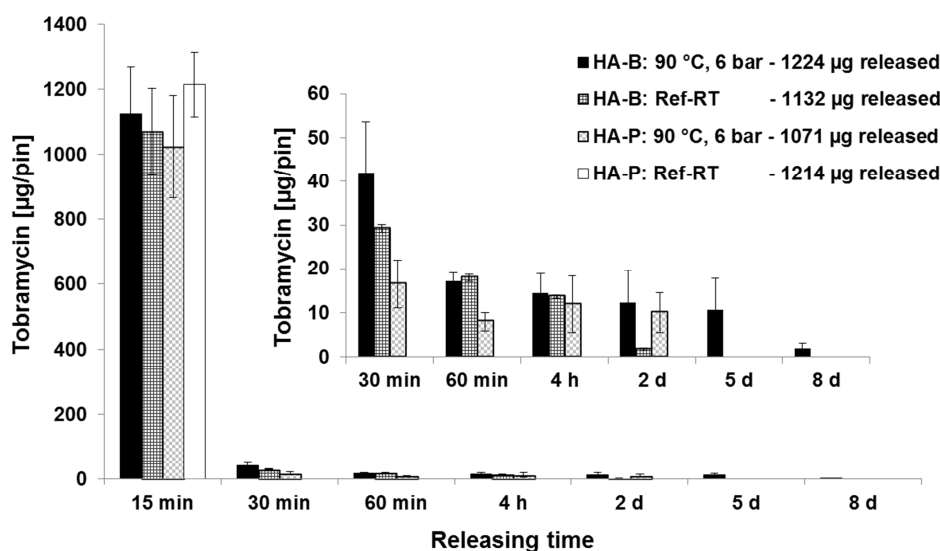


Figure 40: Non-cumulative release after loading at elevated temperature (90°C) and pressure (6 bar) in a Tobramycin containing solution (20 mg/ml). The inset describes a magnification of the sustained release.

As displayed by the SEM images of Load-P samples recorded after the performed release studies, Figure 41, no indications of dissolution or alteration of HA-B coatings could be observed. These surfaces retained their as-deposited morphology. On the other hand, needle-like HA crystals were found on HA-P surfaces after releasing for 5 days in PBS. Cracks in the coating structure have been noticed for both coating types and could be associated with either the loading method or the drying process.

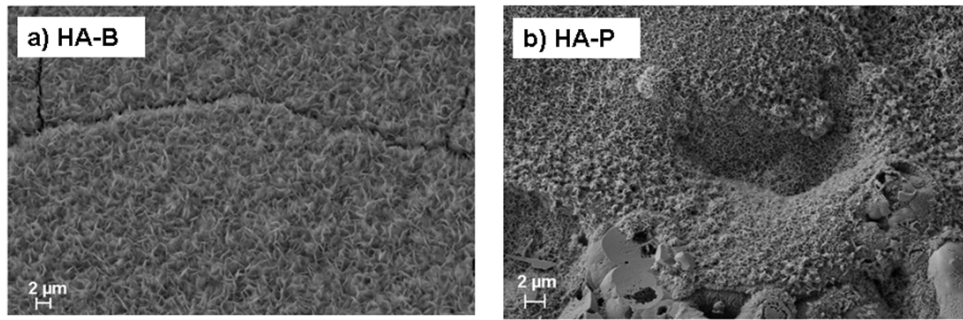


Figure 41: SEM analysis of the surface morphology after release in PBS for 5 days

Figure 42 presents the C- and N- depth profiles of loaded HA-B samples obtained from GD-OES measurements. As is evident from the profile comparisons, the drug loading parameters strongly influence the penetration depth of the antibiotic into the porous coating structure. The C- and N-profile of Load-RT samples are characterized by superficial adsorption with a peak concentration of both elements in a coating depth of about 1 μm . Elevated temperature under loading contributed towards broadening of both C- and N-profile curves for Load-HT samples with a maximum penetration depth of about 2 μm . Additionally, a slight decrease in concentration was found in the N-profile. The drug incorporation under increased temperature and pressure resulted in the highest N-concentration of all samples. A penetration depth of 3 μm was achieved for Load-PHT samples and thus allowed the drug to be incorporated into the denser structure of the HA-B coating.

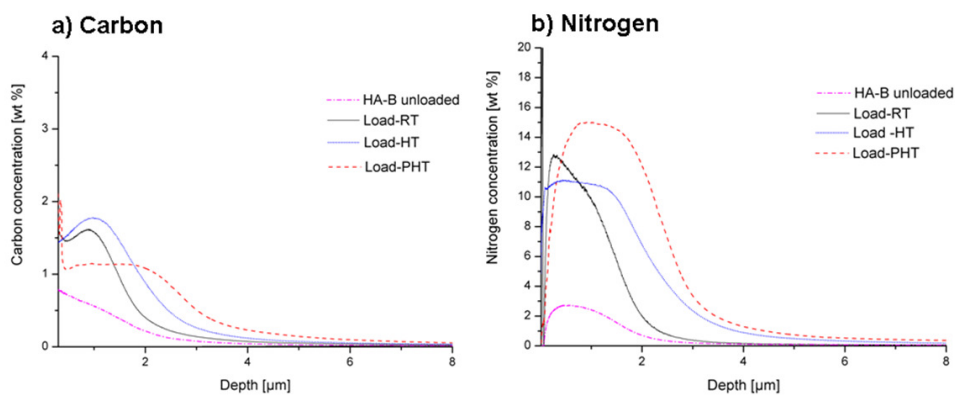


Figure 42: In-depth profiles of carbon (a) and nitrogen (b) of a HA-B sample loaded with 20mg/ml Tobramycin under the displayed loading series.

4.1.3 Antibiotic loading and release from different HA coating thicknesses and morphologies

For the next stage in the analysis, different coating thicknesses and morphologies, resulting from different coating temperatures were evaluated. SEM analysis after completed immersion in PBS showed that all sample types were continuously coated with a HA-B. Figure 43 demonstrates that the deposition temperature had strong impact on the evolution of the HA-B coating morphology. While pins immersed in 37 °C PBS were covered with large, needle-like HA crystals, see Figure 43 a), an elevated PBS temperature of 60 °C resulted in a network of small, spherical HA crystals, see Figure 43 b). The HA-B coatings for all sample types were found to be slightly thicker in the thread valleys than at the thread tops. The average thicknesses after 2.5 and 6 days in 37 °C PBS were $\sim 2 \mu\text{m}$ and $\sim 5 \mu\text{m}$, respectively, and $\sim 1 \mu\text{m}$ after 6 days in 60 °C heated PBS.

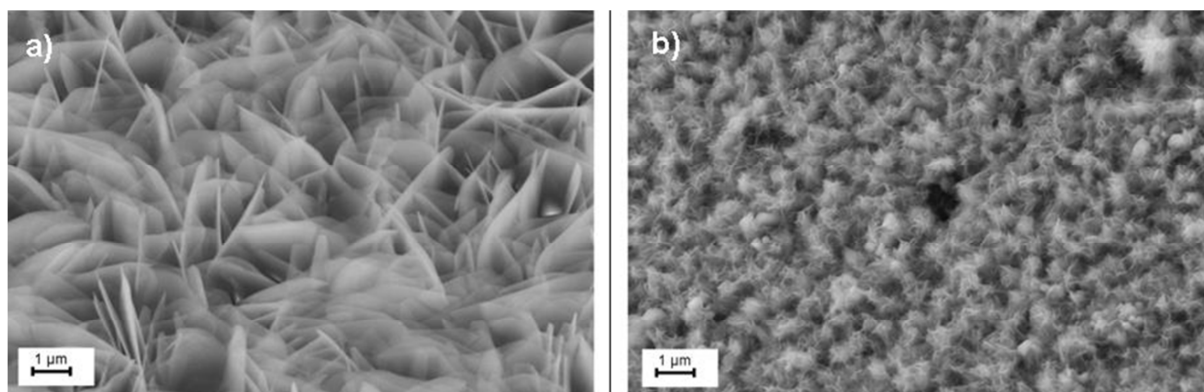


Figure 43: SEM images of HA-B coating morphology after 6 days storage of the TiO_2 covered substrates in 37°C (a) and 60°C heated PBS (b).

The release data presented in Figure 44 and Figure 45 show the total release of Tobramycin incorporated into the different sample types. After the last time point measured for the drug release in PBS, no drug remained in the coatings for any sample type, as confirmed by HPLC measurements of the HCl dissolved coatings. As can be seen from the release curves, Figure 44 and Figure 45, the amount of Tobramycin for all sample types was above the minimum inhibition concentration of $0.2 \mu\text{g/ml}$ for *Staph. aureus* [81] for all time points measured.

Therefore a minimum Tobramycin concentration of 1 μg had to be released into the PBS volume under study.

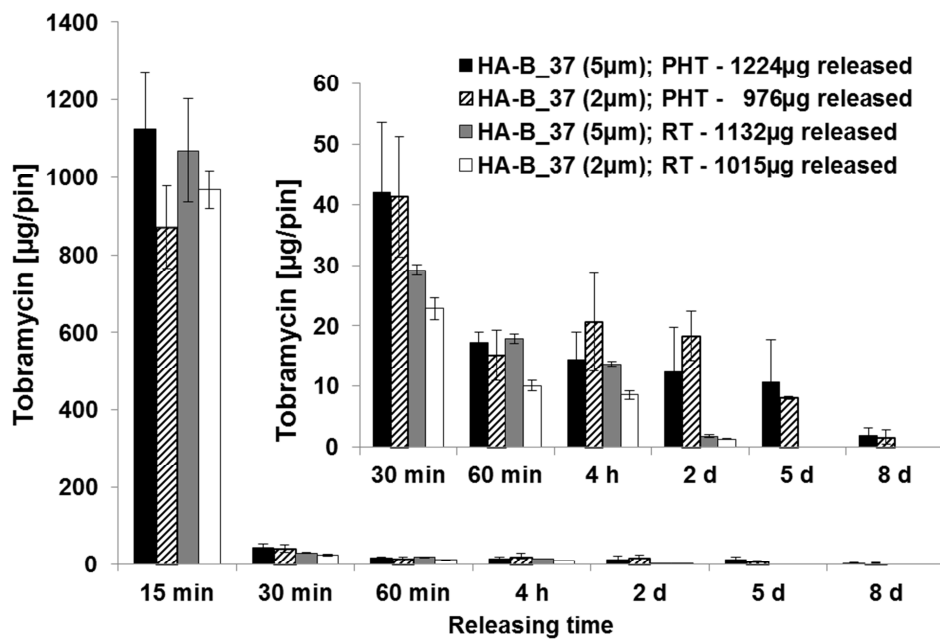


Figure 44: Non-cumulative amount of Tobramycin released in 37 °C PBS from HA-B_37 coated pins of indicated thickness after being loaded for 5 minutes in a solution containing 20 mg/ml of the antibiotics under either room temperature at atmospheric pressure (RT) or at 90 °C and 6 bar (PHT). Error bars denote the standard deviation of 3 measurements. The average total amounts of Tobramycin released from each sample type are also displayed.

The release kinetics of the different types of HA-B_37 coatings under study, Figure 44, shows an initial, burst-like release during the first 15 minutes for both HA coating thicknesses and loading methods employed. A continuously decreasing release of Tobramycin is observed for 2 days following for both sample types after RT loading, while an extended release period of 8 days was measured for PHT loaded samples. As is obvious from the comparison of burst and sustained release profiles of RT samples, pins coated with the thicker, 5 μm , HA-B coating display a slightly higher amount of drug incorporated and released compared to the 2 μm coated pins. The total amount of drug incorporated into the HA-B_37 (5 μm) samples under elevated temperature and pressure is slightly increased while the corresponding amount for the 2 μm thick samples is decreased.

The impact of HA-B coating morphology on the loading and release properties is presented in Figure 45 where the release from the thinner HA-B₃₇ coatings is compared to that from the HA-B₆₀ coatings. While the amounts of antibiotic released during initial burst are similar for both samples types after RT loading, the release period of the HA-B₆₀ (1 μ m) coated pins is only 4 hours as compared to the 2 days of release observed for HA-B₃₇ (2 μ m) coatings. Nevertheless, the PHT loading procedure was found to increase the total release time for both sample types up to 8 days. While the total amount of Tobramycin incorporated into HA-B₃₇ (2 μ m) coatings at 90 °C and 6 bar was found to be lower than the corresponding values incorporated at room temperature, a slight increase was noted for HA-B₆₀ samples.

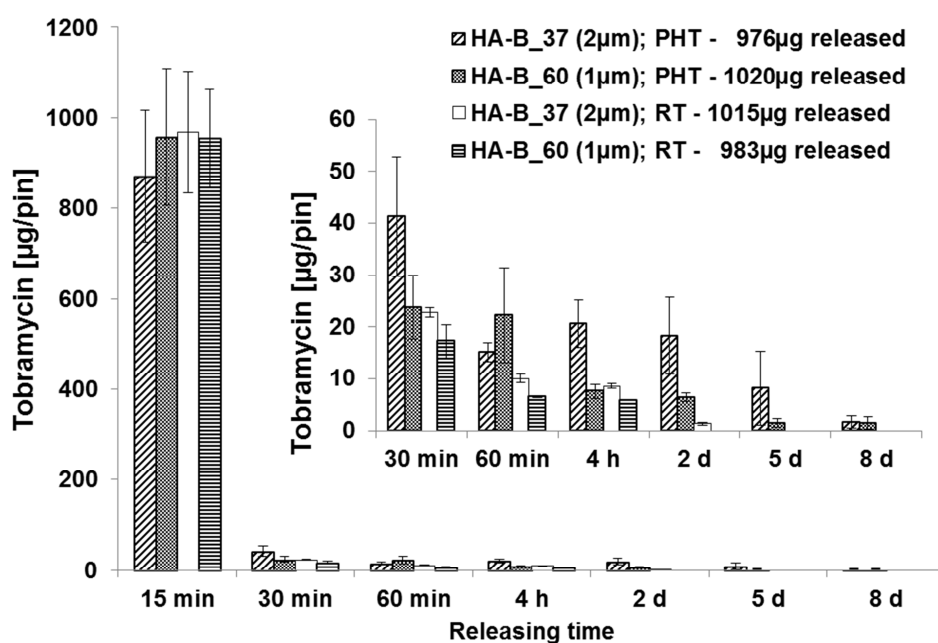


Figure 45: Non-cumulative amount of Tobramycin released in 37 °C PBS from HA-B₃₇ (2 μ m) and HA-B₆₀ (1 μ m) coated pins after being loaded for 5 minutes in a solution containing 20 mg/ml of the antibiotics under either room temperature at atmospheric pressure (RT) or at 90 °C and 6 bar (PHT). Error bars denote the standard deviation of 3 measurements. The average total amounts of Tobramycin released from each sample type are also displayed.

4.1.4 Biomechanical behavior of biomimetic HA coatings

The impact of biomechanical forces on HA-B coatings after the insertion tests is presented in the SEM images in Figure 46 and Figure 47. In general, insertion of the HA-B coated pins into PU 25 foam exposed the coatings to higher abrasive forces, as can be seen by slightly higher degree of HA-B coating deterioration in the thread valleys (Figure 46 all b) and c) panels) compared to pins inserted into Renshape (Figure 47 all b) and c) panels). For all sample types, the pin flute was identified as a region where the HA-B coating remained in its as-deposited morphology with only minor scratches (Figure 46 a) and Figure 47a)). As obvious from the SEM images in Figure 46 b) and Figure 47 b), compression and smearing of the coating could be observed in thread flanks and valleys for all samples types. Coating flake off for HA-B_37 samples was observed mainly at screw tips (Figure 46 a2) and a3) as well as Figure 47 a2) and a3)) and thread tops (Figure 46 b2) and b3) as well as Figure 47 b2) and b3)) whereas HA-B_60 samples exhibited abrasion and smearing primarily at thread flanks and valleys (Figure 46 b1) and Figure 47 b1)).

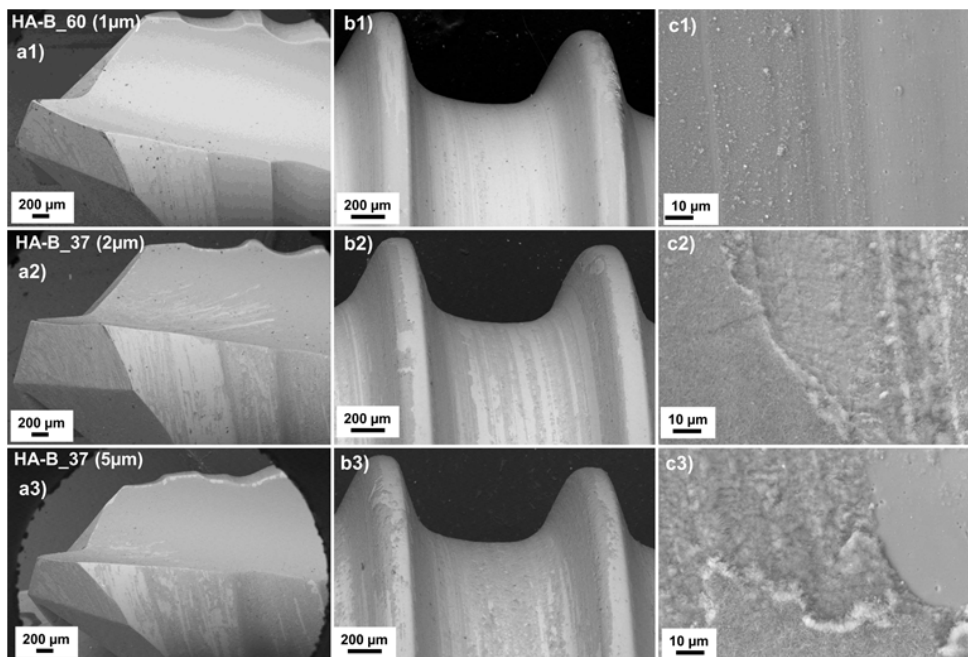


Figure 46: SEM images of HA-B coated sample types after insertion into 25 PU foam blocks.

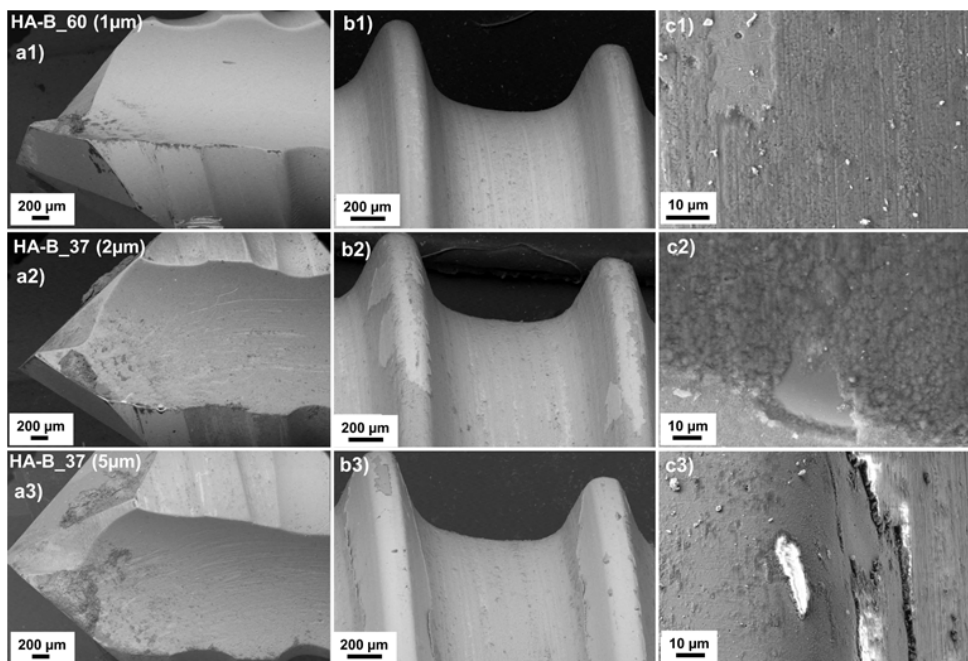


Figure 47: SEM images of HA-B coated samples after insertion into Renshape BM5166 discs.

The 3D micro visualization images taken of a HA-B_37 (5 μm) coated pin after insertion into PU 25, Figure 48, confirmed high stress areas and coating flake-off at screw tip and thread tops, as well as the presence of compressive forces in the thread valley. Insertion of TiO₂

coated pins revealed that the TiO₂ coating did not exhibit any damaged areas for any foam type.

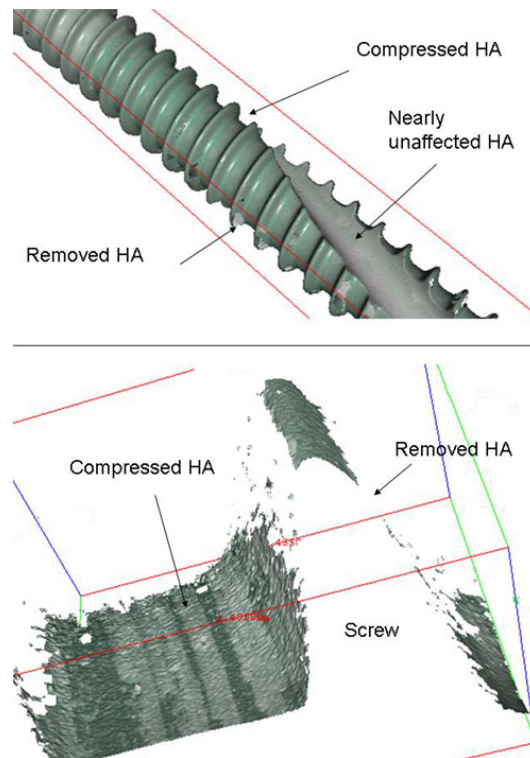


Figure 48: 3D visualization image of a HA-B_37 (5µm) sample after insertion into PU 25 foam.

4.1.5 Biomechanical behavior of Tobramycin loaded biomimetic HA coatings

SEM analysis of the HA-B coated fixation pins revealed a coating thickness of approximate 5-6 µm, whereas Co-4 samples exhibited a thickness of only 2.5-3.0 µm, as described earlier. Both sample types possessed higher thicknesses in the thread valleys while lower values were measured at the thread crests. As visualized by the SEM images in Figure 49, the coatings of all sample types under study were mechanically affected by insertion into 25 PU foam. The flute of the fixation pin maintained its “as-deposited” morphology for all samples types and showed only stochastic areas of flake off (Figure 49 b), e) and h)). Nevertheless, differences in the coating deterioration could be observed with respect to the drug loading

method applied. While RT samples showed preferential HA-B coating delamination at screw tops (Figure 49 b), c)), only minor impact of the biomechanical forces could be seen on the HA coating in screw valleys and at the screw tip (Figure 49 a)) for such samples. PHT samples exhibited coating wear patterns similar to the RT samples (Figure 49 d) – f)). However, the coating delamination within the thread valleys for the PHT samples was somewhat larger (Figure 49 f)). Drug incorporation via co-precipitation resulted in only minor coating wear after insertion. In comparison to adsorptive drug loaded samples, Co-4 samples exhibited major flake-off at the pin entry site (Figure 49 g)) and only few areas of delamination along the screw length (Figure 49 i)).

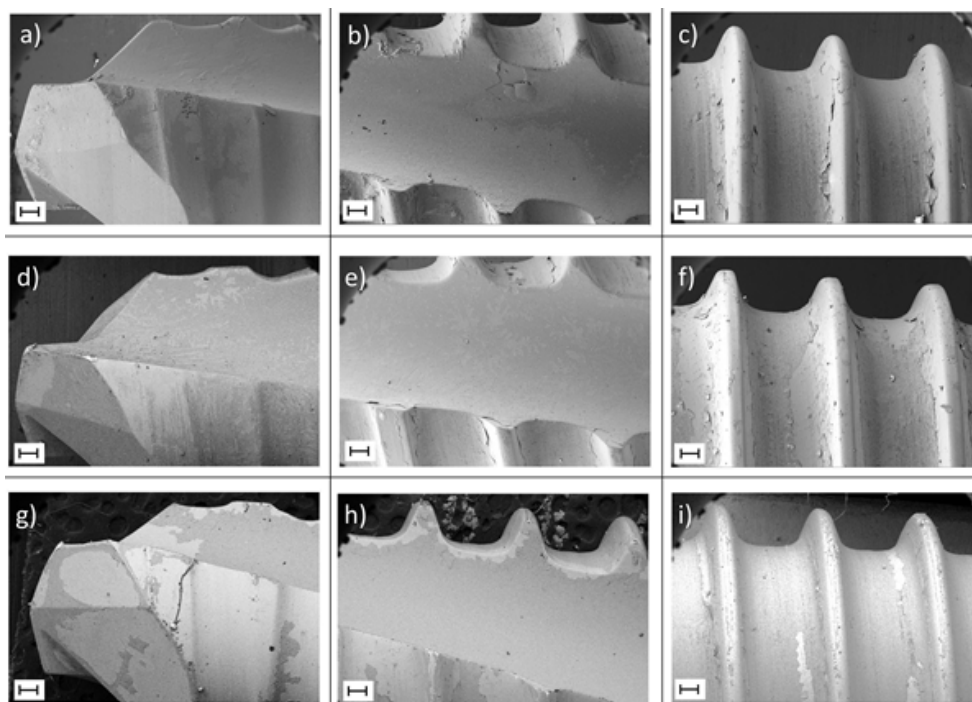


Figure 49: SEM images (scale bars 200 μm) of RT-samples (upper panels), PHT samples (middle panels) and Co-4 samples (lower panels) after insertion into 25 PU foam and subsequent drug release in PBS.

As displayed by the images in Figure 50, the HA-B coating delaminated from the TiO_2 coated pin surface seems to remain within the porous foam structure. The white discoloration of the insertion material, Figure 50 a), represents the HA-B coating delaminating from the pin during insertion. A higher concentration of HA-B coating could be observed at the pin entry

side, whereas less staining of the material could be seen with increasing insertion depth. HA-B coating flakes could be identified in the foam structure, as shown by the SEM image taken at a depth of 2 mm from the pin entry point (Figure 50 b)). Within the foam structure, the delaminated HA-B fragments showed a flake like morphology, which reflects the as-deposited coating morphology. The size of delaminated HA-B fragments, Figure 50 c), is comparable to those observed during conventional scratch testing of the $\text{TiO}_2/\text{HA-B}$ coating system.

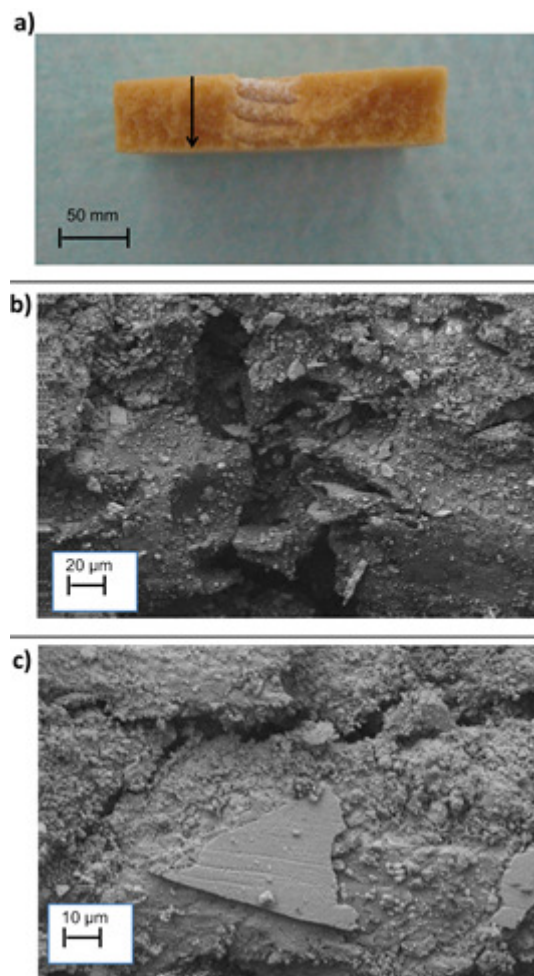


Figure 50: Macroscopical image (a) and SEM images (b, c) of 25 PU foam after insertion. The insertion direction is indicated by an arrow (a). SEM images were taken at an insertion depth of approximate 2 mm from the pin entry point. The scale bars in panels a, b and c are 50 mm, 20 μm and 10 μm , respectively.

4.1.6 Drug release after biomechanical treatment

Tobramycin release profiles were evaluated after insertion of the pins into 25 PU foam. For all samples under study, the Tobramycin release can be described by an initial burst release followed by a sustained release. The inserted samples (BML) released significantly lower amounts of drug during the initial 15 minute phase as compared to samples that had not been inserted into the bone model, see Figure 51. The sustained release, however, seemed to be less effected by the insertion into 25 PU foam. The longest release period under the prevailing conditions was detected for the PHT coated samples and lasted for 8 days, followed by PHT_BML inserted samples showing a release up to 5 days. The samples loaded at room temperature demonstrated maximum release duration of 2 days.

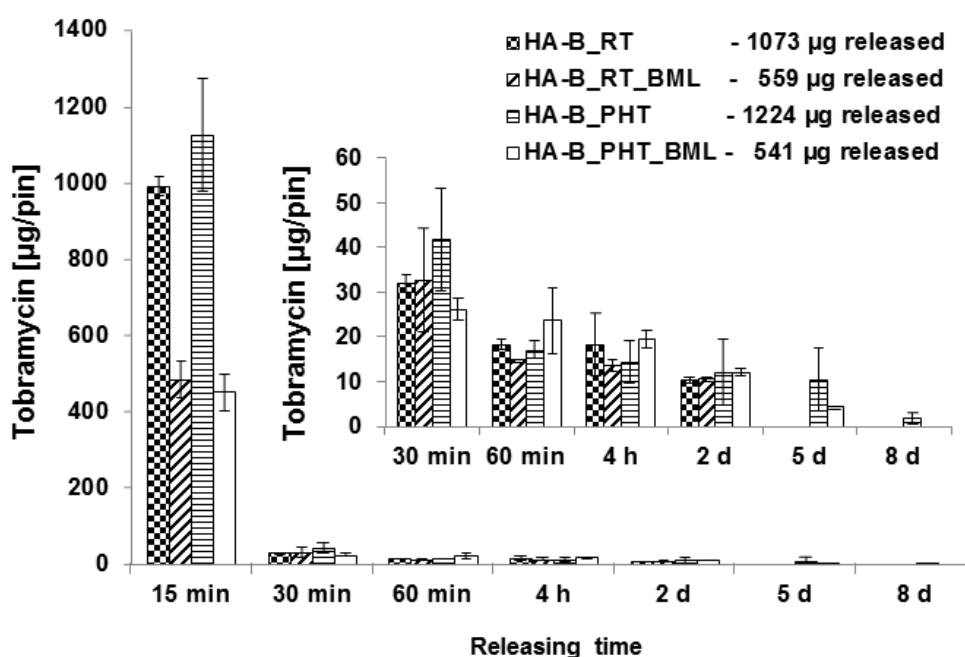


Figure 51: Non-cumulative amount of Tobramycin released in 37 °C PBS from HA-B coated pins after RT and PHT loading in a solution containing 20 mg/ml of the antibiotics and following insertion into 25 PU foam (BML samples). Release results from mechanically untreated RT and PHT samples are incorporated as reference. Error bars denote the standard deviation of 3 measurements. The average total amounts of Tobramycin released from each sample type are also displayed.

The amount of Tobramycin for all sample types was above the minimum inhibition concentration (MIC) for *Staph. aureus* for all time points measured, which corresponds to a Tobramycin concentration of 1 mg/ml in the release medium.

Figure 52 displays the effect of insertion of Co-4 coated pins into 25 PU on the drug release. The biomechanical forces significantly impacted the initial burst release and only slightly decreased the amounts of drug released at later time points. The total amount of Tobramycin released from the inserted samples was ~ 35% lower than the released amount from the Co-4 reference samples. These reference samples released a detectable amount of antibiotics for as long as 12 days, while the Co-4_BML samples demonstrated a release period of 8 days. For all time points under study the amounts of Tobramycin released was above the MIC for *S. aureus* for all time points measured.

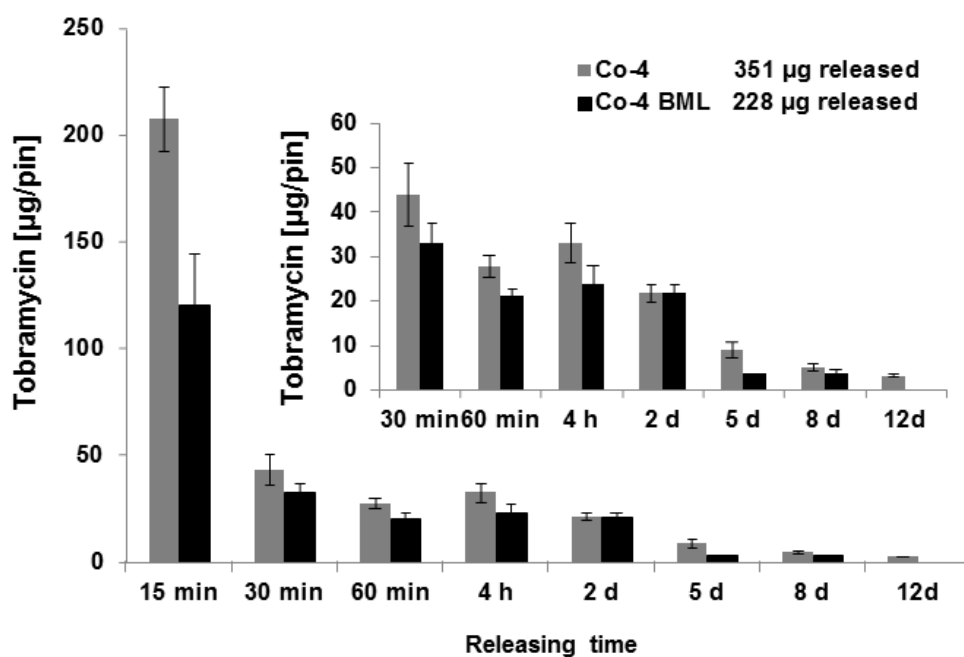


Figure 52: Non-cumulative amount of Tobramycin released in 37 °C PBS from Co-4 coated pins after insertion into 25 PU foam (BML samples). Release results from mechanically untreated Co-4 samples are incorporated as reference. Error bars denote the standard deviation of 3 measurements. The average total amounts of Tobramycin released from each sample type are also displayed.

4.1.7 Drug release after gamma sterilization

Figure 53 describes the impact of gamma sterilization on the amount of Tobramycin released from HA-B_RT coated fixation pins. No significant difference between the release kinetic from HA-B_RT and its sterilized counterpart were measured. The total release period lasted for 8 days and as for the samples tested above, the released amounts were found to be above the MIC of *Staph. aureus* for each time period under study. Furthermore, no additional peaks were identified in the HPLC analysis indicating that there is no detectable impact or inactivation of the drug molecule due to irradiation.

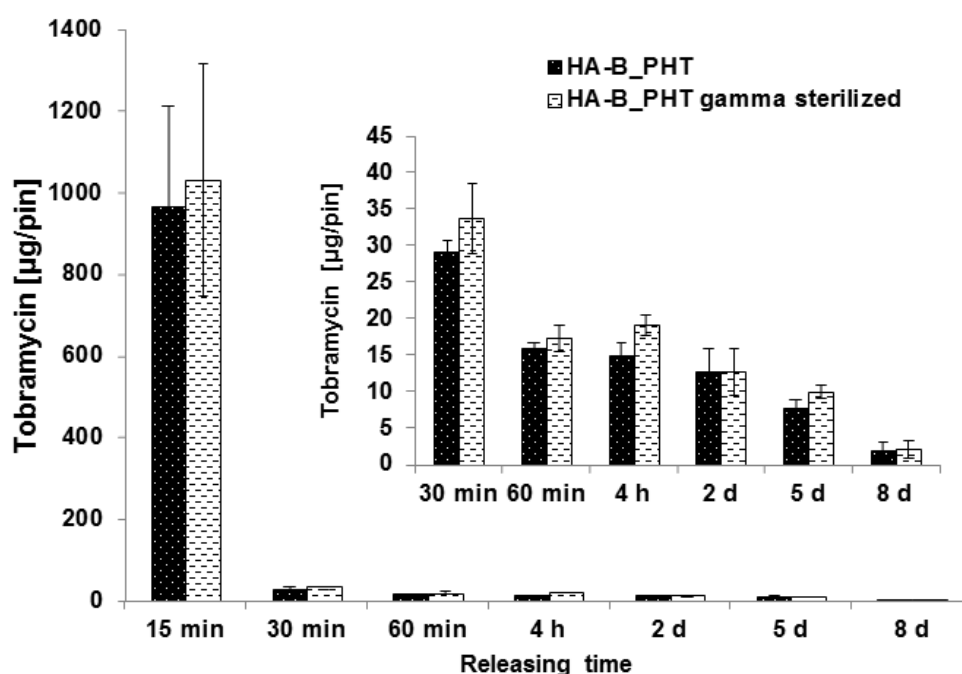


Figure 53: Non-cumulative amount of Tobramycin released in 37 °C PBS from RT loaded pins after gamma sterilization. Release results from RT samples are incorporated as reference. Error bars denote the standard deviation of 3 measurements. The average total amounts of Tobramycin released from each sample type are also displayed.

4.1.8 Scratch test

Scratch testing using the larger 500 μm radius indenter resulted in evident coating failures and critical loads, while the 50 μm radius indenter gave only very stochastic and minor failures, i.e. spalling. Hence, the results presented here refer to adhesive strength measured with the 500 μm indenter. SEM images of the single path scratch tests results are shown in Figure 54. No major failure was observed of the underlying TiO_2 layer for any of the sample types under study, thus, proving the excellent adhesion of this layer to the stainless steel substrates. HA-B_60 (1 μm) coatings exhibited preferential HA-B coating delamination at the HA-B/ TiO_2 interface, Figure 54 a), b). Small cracks could be seen in the underlying TiO_2 coating, Figure 54 b), but no spalling from the stainless steel substrate was observed. Even in the scratch track the TiO_2 coating remained, which provides an indication of good cohesive strength of this crystalline coating. As presented in Table 10, a $F_{N,C}$ value of 24 N was measured for the thinnest HA-B coating.

Just as for the HA-B_60 (1 μm) coatings, scratch test performed on HA-B_37 coatings resulted in preferential detachment from the TiO_2 surface, Figure 54 c) - f). Distinct spalling could be observed at the HA-B/ TiO_2 coating interface, Figure 54 c), e) for both the HA-B_37 coating thicknesses with the pieces detaching from the thinner coating being somewhat smaller than from the thicker coating. As presented in Table 10, normal critical loads of 56 N and 53 N were measured for the 5 μm and 2 μm thick HA-B_37 coatings, respectively.

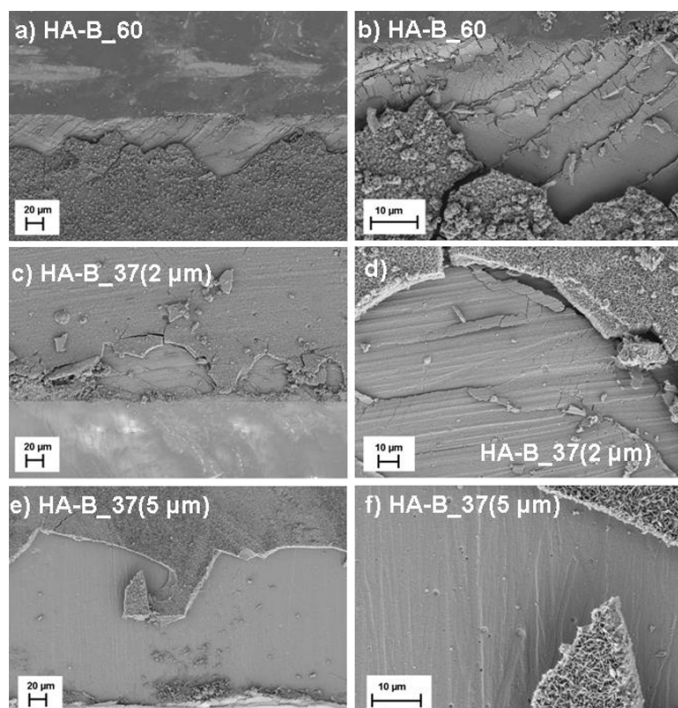


Figure 54: SEM images of scratch paths created with a 500 μm diamond indenter on HA-B₆₀ and HA-B₃₇ coated pins of indicated thickness

Table 10: Critical normal loads of HA-B coated stainless steel discs obtained from conventional single pass scratch tests.

Sample	Normal critical Load ($F_{N,C}$) [N]
HA-B ₃₇ (5 μm)	60 ± 2.4
HA-B ₃₇ (2 μm)	53 ± 2.1
HA-B ₆₀ (1 μm)	24 ± 0.9

4.1.9 Antibacterial properties of Tobramycin loaded HA coated pins

Panels a and b in Figure 55 show images of inserted fixation pins incubated for 1 day in an agar diffusion test arrangement. No inhibition zone was observed for the HA-B_37 (5 μ m) coated reference samples resulting in the observed bacterial growth after roll-out test on fresh agar, Figure 55 c1). For all other samples a clear and homogeneously distributed inhibition zone could be detected, Figure 55 a2-4) and b2-4). For all antibiotic loaded samples (RT, PHT, RT_BML) no colony forming units could be observed after roll-out test on the fresh agar plate after day 1, Figure 55 c2-4).

The inhibition zones of RT-loaded, PHT-loaded and RT_BML-loaded samples were evaluated over a time period of 6 days, Figure 55 d). In general, the inhibition zones were found to decrease with increasing test time periods. At day 1 the inhibition zones of RT- loaded samples appeared to be slightly larger compared to those of PHT-loaded samples. The RT_BML samples showed a minor reduction in inhibition zone area compared to RT or PHT loaded samples for all time points, with exception of day 4. The inhibition zones were found to slightly decrease from day 2 to day 5, whereas an antibacterial effect was measurable up to 6 days for RT-loaded and PHT-loaded samples. At day 7 no inhibition zones could be observed for any of the samples under study.

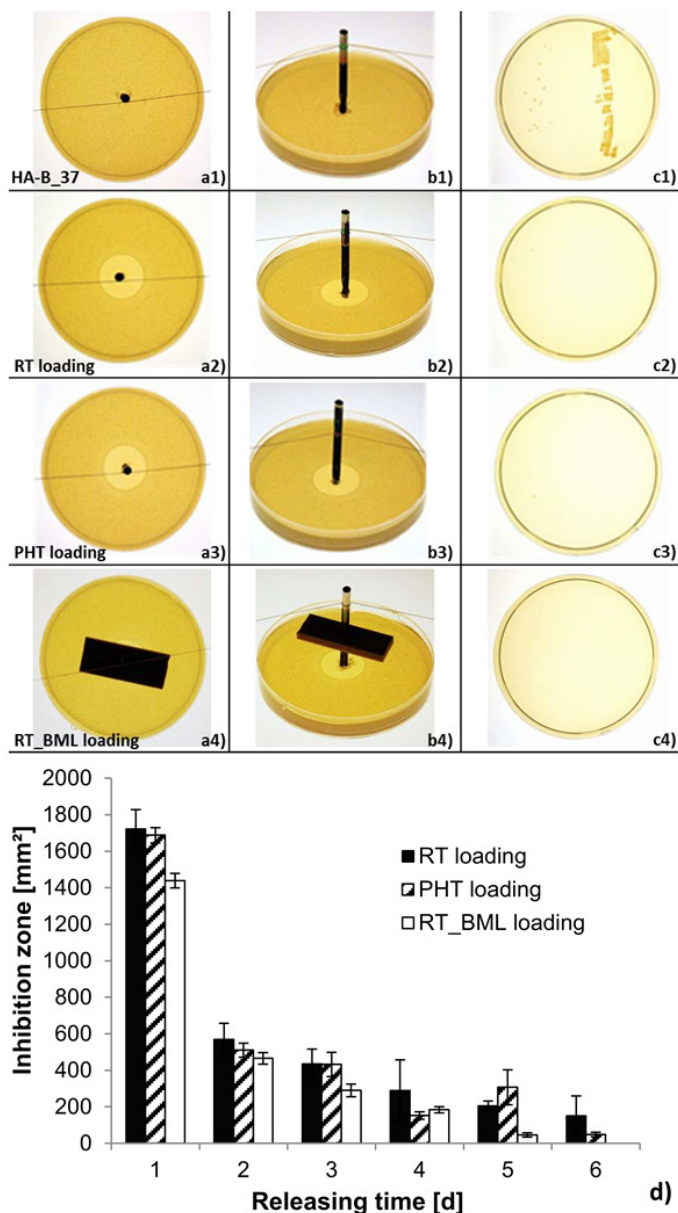


Figure 55: Images of HA-B_37 (5µm) coated, RT loaded, PHT loaded and RT_BML loaded pin after 18 hours of incubation in agar diffusion tests against *Staph. aureus*. RT_BML loaded pin was additionally inserted through a block of 25 PU foam. Panels c1-4) indicate the germs growing on fresh agar plates after roll-out test after 24 hours. Panel d) gives an overview of the inhibition zones of the different samples at each time period. The error bars indicate the standard deviations over three measurements.

4.1.10 Cell study

The biocompatibility of HA-B coated discs was evaluated in vitro using two different types of cells including primary human osteoblast and primary human endothelial cells. Both cell types would be likely to be in close contact with the coating material in-vivo. Primary human osteoblasts isolated from bone tissue and endothelial cells isolated from the peripheral blood were investigated in terms of the viability and morphology when grown on TiO₂ or HA-B₃₇ (5µm) surfaces for 3 days. Viability assessment using Calcein-AM, which is converted by viable cells to a green fluorescent substance, showed that both primary osteoblasts and primary endothelial cells were viable when grown on HA-coated or pure TiO₂ surfaces. Cells were firmly attached to the surface, see Figure 56, but with a slightly different morphology when grown on TiO₂ or HA-B₃₇ (5µm) coated samples, which might be associated with differences in the material topography. The analysis was achieved without any additional coating of the material surfaces with components of the extracellular matrix such as fibronectin or collagen.

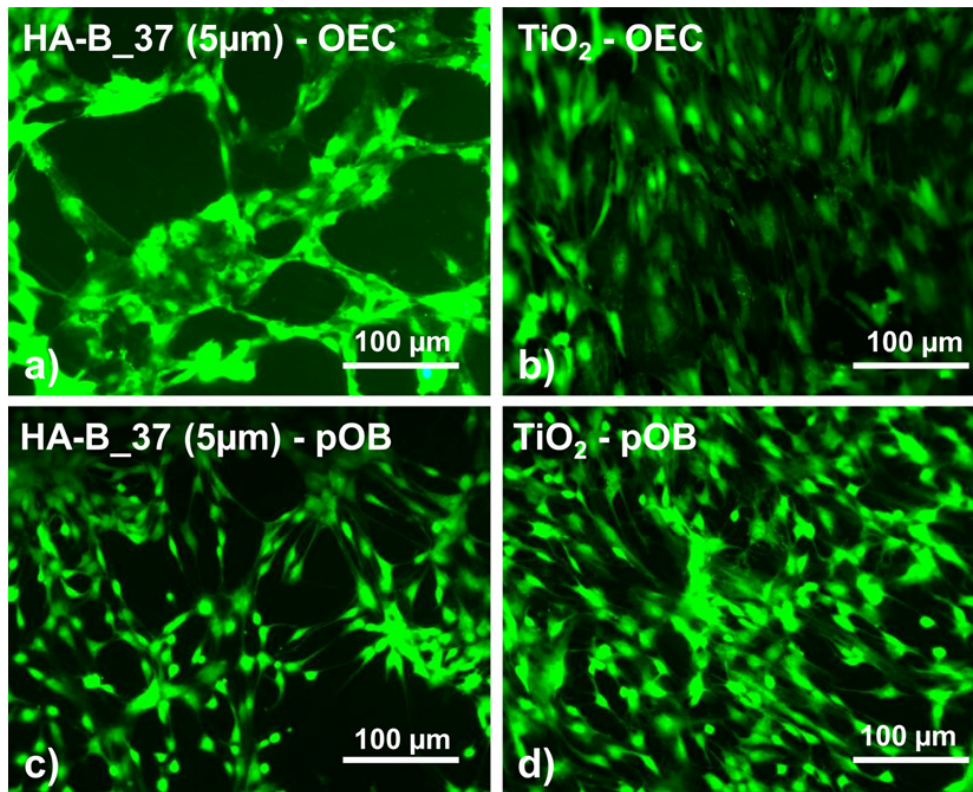


Figure 56: Calcein-AM viability assessment of outgrowth endothelial cells (a,b) and primary osteoblasts (c,d) discs with (a,c) or without HA-B_37 (5µm) (b,d) coating. On both types of substrates primary osteoblasts show a bright fluorescence after Calcein-AM staining. Similar findings can be observed for outgrowth endothelial cells which form endothelial cell layers on both types of surfaces and at both investigated time points.

4.1.11 Co-precipitation of Tobramycin into HA coatings

SEM analysis of sample surfaces from the first test series demonstrated no sign of hydroxyapatite nucleation at 37°C for Tobramycin containing PBS at any of the concentrations investigated on bioactive, crystalline TiO₂ coated discs. By decreasing the concentration to 0.5 mg/ml and 1.0 mg/ml and adjusting the temperature from 37°C to 60°C nucleation were observed for the test series with a Tobramycin concentration of 0.5 mg/ml and 1.0 mg/ml at 60°C. The samples at 37°C showed no sign of HA nucleation, see Figure 57. The HA coating thickness was measured to be approx. 1.5 µm after storage for 6 days at 60°C for both concentrations. A rough, ball-like coating morphology was observed for the 60°C samples. In addition, HA ball-like agglomerates covered the surface and these were not homogeneously distributed for either concentration tested, see Figure 57. Table 11 gives an overview of the investigations performed.

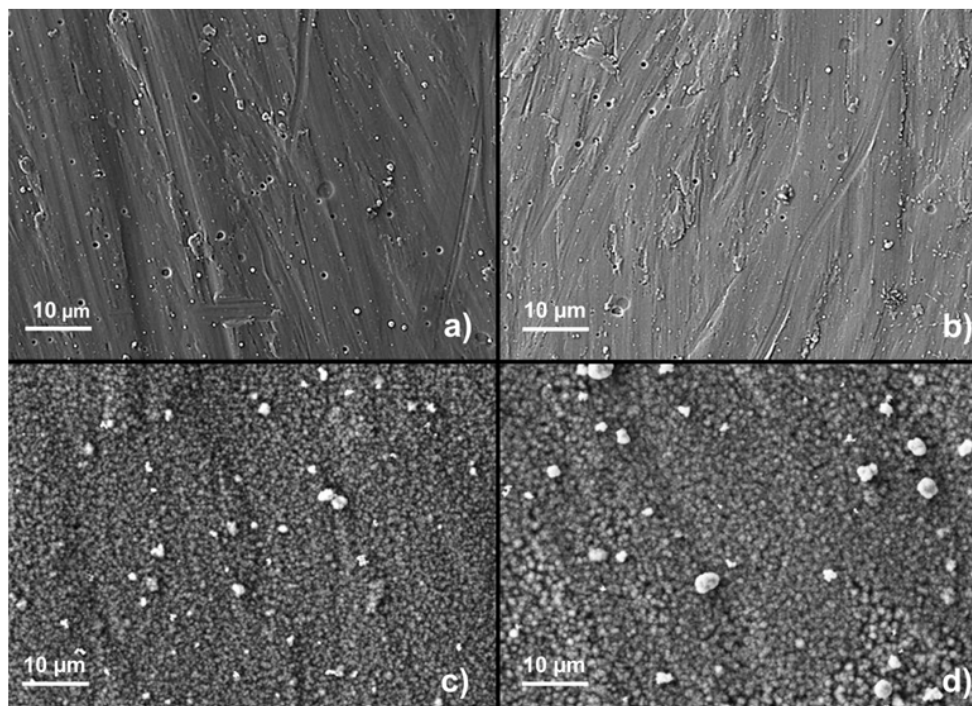


Figure 57: SEM analyses of the surface structures after immersion in Tobramycin containing PBS buffer for 6 days a) 0.5 mg/ml Tobramycin at 37 °C; b) 1.0 mg/ml Tobramycin at 37 °C; c) 0.5 mg/ml Tobramycin at 60 °C; d) 1.0 mg/ml Tobramycin at 60°C.

Table 11: Overview of all co-precipitation investigations by the given process parameters.

Sample type	Process time [d]	Process temperature [°C]	HA start layer	Tobramycin concentration [mg/ml]	Coating thickness [µm]	Coating appearance
Plate	6	37	No	40	---	---
	6	37	No	20	---	---
	6	37	No	4	---	---
Plate	6	37	No	1	---	---
	6	37	No	0.5	---	---
	6	60	No	1	~1.5	Ball-like
Plate	6	60	No	0.5	~1.5	Ball-like
	6	37	Yes	1	~5.0	Needle-like
	6	37	Yes	0.5	~5.0	Needle-like
	6	60	Yes	1	~1.5	Ball-like
	6	60	Yes	0.5	~1.5	Ball-like
Plate	6	60	No	20	---	---
	6	60	No	4	---	---
	6	60	Yes	20	~3.0	Ball-like
	6	60	Yes	4	~4.0	Needle-like
Fixation Pin	6	37	Yes	20	~2.5	Ball-like
	6	37	Yes	4	~3.5	Needle-like

The second test series was performed on bioactive, crystalline TiO₂ coated and HA start layered discs. Cross section analysis via SEM reveals a HA start layer thickness in the range of 300-600 nm, see Figure 58. Growth of Tobramycin-doped hydroxyapatite coatings were observed for both concentrations (0.5 mg/ml and 1.0 mg/ml) and both temperatures (37°C and 60°C) tested, see Figure 59. The morphology of the co-precipitated coatings was influenced by the PBS temperature. Samples immersed in PBS of 37°C appeared to be covered by a smooth and needle-like coating with an approximate coating thickness of 5 µm, whereas PBS temperatures of 60°C resulted in coating structures with rougher, ball-like morphology and appeared to have a more inhomogeneous structure, see Figure 59. SEM evaluation revealed for a coating thickness measured of approx. 1.5 µm at elevated PBS temperature.

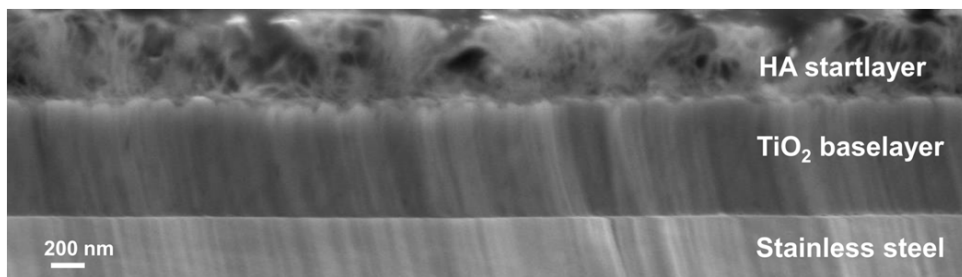


Figure 58: Cross section of the HA start layer after immersion for 3 days in PBS at 60 °C.

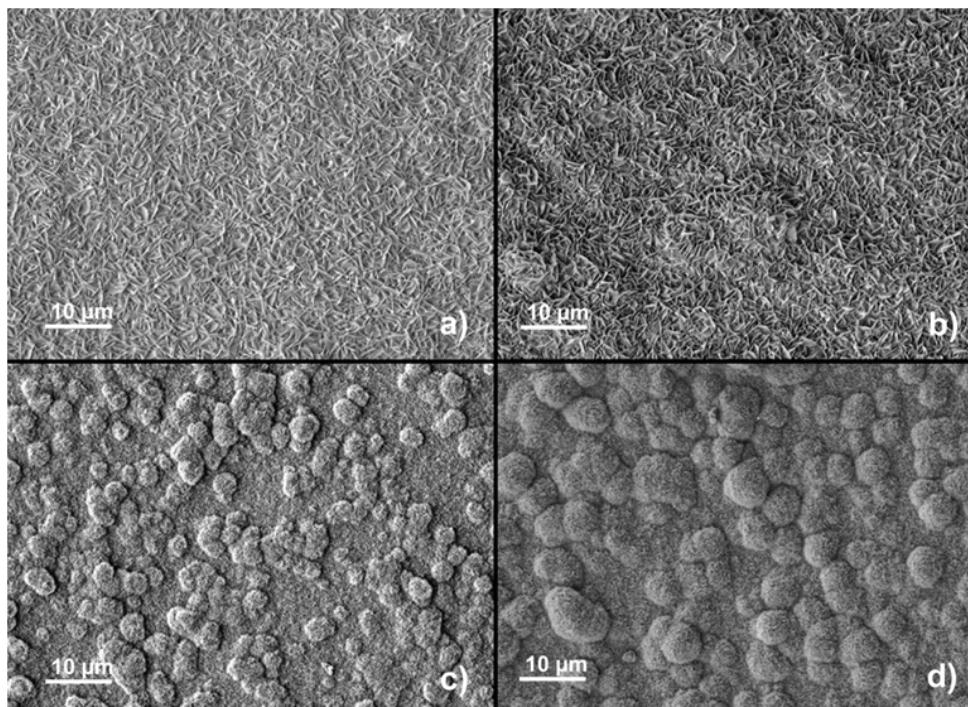


Figure 59: SEM analyses of the HA start layered surface structures after immersion in Tobramycin-containing PBS for 6 days a) 0.5 mg/ml Tobramycin at 37 °C; b) 1.0 mg/ml Tobramycin at 37 °C; c) 0.5 mg/ml Tobramycin at 60 °C; d) 1.0 mg/ml Tobramycin at 60 °C.

Figure 60 demonstrates the impact of elevated temperatures (60°C) and increased Tobramycin concentrations (4 mg/ml and 20 mg/ml) on coating growth. The reference discs without HA start layer showed no sign of nucleation at Tobramycin concentration of 4 mg/ml and 20 mg/ml at 60°C. The HA start layered discs demonstrated Tobramycin-doped hydroxyapatite growth after storage for 6 days at 60°C process temperature at a concentration of 4 mg/ml. The total coating thickness was measured to be approx. 4 μm (HA start layer thickness approx. 0.3-0.6 μm) showing a needle-like morphology. The HA start

layer coated discs tested at a concentration of 20 mg/ml confirmed Tobramycin-doped hydroxyapatite growth at 60°C, whereas the reference without HA start layer showed no sign of nucleation on the surface. The total coating thickness was measured to be approx. 3 μm with a flake-like morphology. Nucleation and growth of HA was achieved at 4 mg/ml and 20 mg/ml Tobramycin and 60°C. Different concentrations of Tobramycin in PBS showed changes in morphology of the as-deposited coatings, see Figure 60. A flake like morphology of the co-precipitated coating was observed with an increased flake density for the higher Tobramycin concentration (20 mg/ml). Additionally, ball-like agglomerates were detected on the surfaces treated with 20 mg/ml.

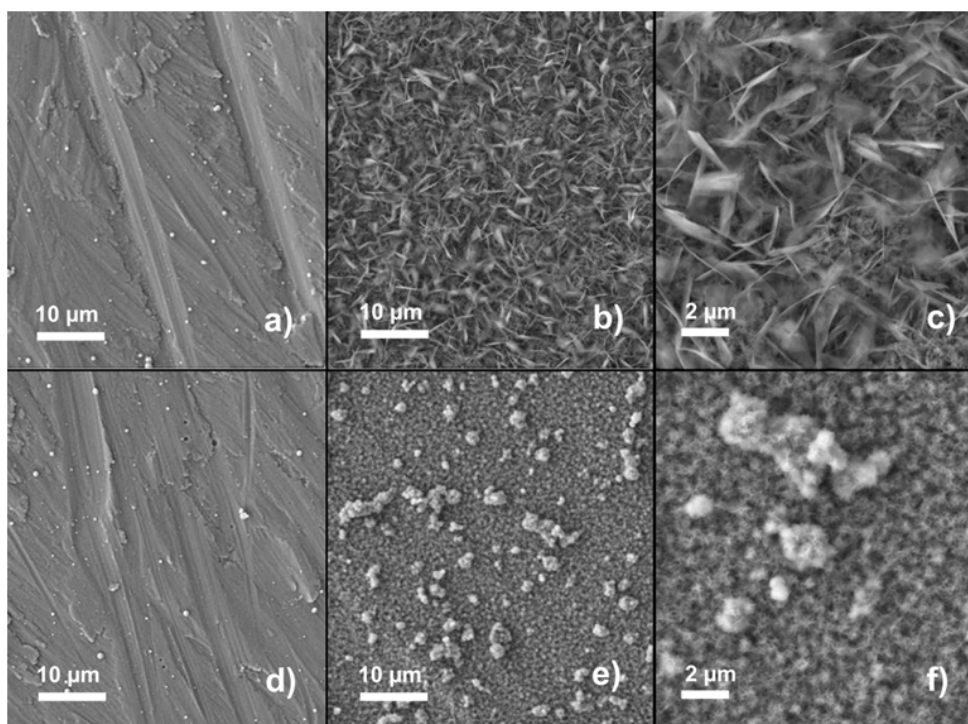


Figure 60: SEM analyses of the surface structures after immersion in Tobramycin-containing PBS for 6 days at 60 °C a) without HA start layer at 4 mg/ml; b) and c) with HA start layer at 4 mg/ml (different magnifications); d) without HA start layer at 20 mg/ml; e) and f) with HA start layer at 20 mg/ml (different magnifications).

The co-precipitation coating technique was successfully transferred from discs to fixation pins. The HA start layered fixation pins were tested at concentrations of 4 mg/ml and 20 mg/ml at with a decreased temperature of 37°C in order to achieve a homogeneous

morphology. Nucleation of Tobramycin-doped HA could be observed at both concentrations. The co-precipitated HA coating morphology changed from flake-like (4 mg/ml) towards smaller, round crystals (20 mg/ml). The total coating thickness ranged from approx. 3-3.5 μm for 4 mg/ml to 2-2.5 μm for 20 mg/ml treated fixation pins. A continuous Tobramycin-doped HA-coating was observed, fully covering the complex pin geometry, see Figure 61 a) and b).

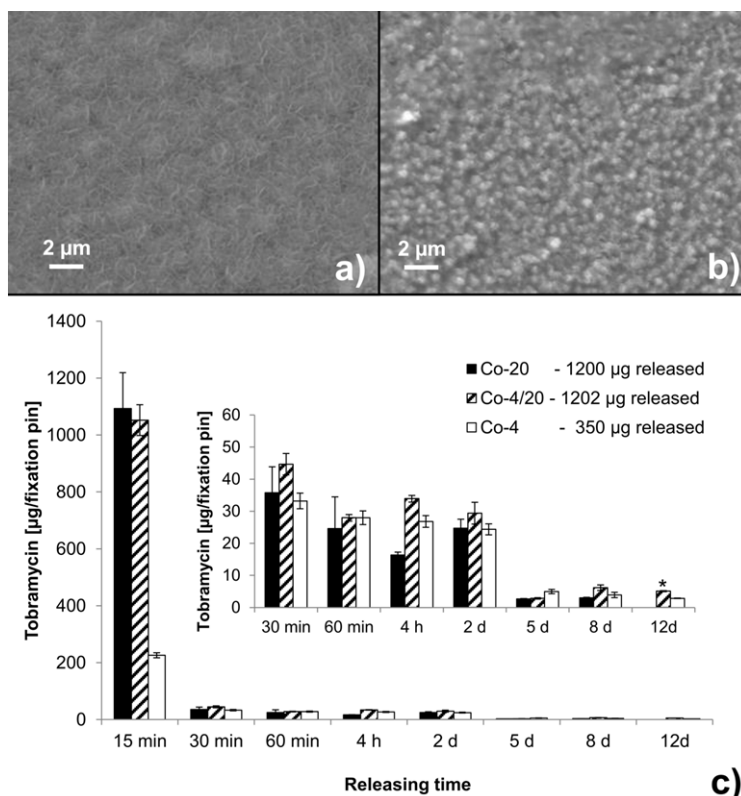


Figure 61: SEM analyses of the HA start layered surface structures after immersion in Tobramycin-containing PBS for 6 days a) 4 mg/ml Tobramycin at 37 °C; b) 20 mg/ml Tobramycin at 37 °C; c) HPLC obtained non-cumulative amount of Tobramycin released in 37 °C PBS from pins coated by co-precipitation using different concentrations of Tobramycin in PBS solution. The average total amounts of Tobramycin released from the different coatings are displayed next to the sample names. The error bars indicate the standard deviations. *calculated based on residual content.

Figure 61 c) presents the release kinetics from the co-precipitated fixation pins (Tobramycin release in $\mu\text{g}/\text{fixation pin}$) over a time period of 12 days. In general, the release profile is characterized by an initial burst and a sustained release for both sample types with concentrations released above the MIC of *Staph. aureus* [81] over the entire release period. The release of Tobramycin was greatest during the first 15 minutes and was linearly

correlated to the drug concentration within the stock solution. For both concentrations tested, the release significantly decreased after the burst release. The total amount of drug released from Co-4 samples was 350 µg/implant. A significantly higher release rate was measured for Co-20 samples with a total amount of 1200 µg/implant. The major part of the drug content in the coatings, 226 µg and 1093 µg for Co-4 and Co-20 samples, respectively, was released as an initial burst during the first 15 minutes. For both concentrations used in coating production, the amount of drug released decreased significantly during the sustained release period. Co-20 showed slightly higher release values between 15 and 30 minutes as compared to the Co-4, whereas the Co-4 samples provided higher release values at all later time points excepting the 2 day time point where the amounts released were nearly equal for both sample types. No release were detected from the Co-20 samples after 8 days while the Co-4 samples continue to provide a measurable amount of Tobramycin release up to 12 days.

Additionally, the samples Co-4/20 produced by co-precipitation at 4 mg/ml followed by fast adsorptive loading in a 20 mg/ml Tobramycin stock solution demonstrated an enhanced initial burst compared to the Co-4 samples which was comparable to the initial release seen from Co-20 samples. During the sustained release period, the Co-4/20 samples provided a higher amount of drug release overall compared to both other sample types. GD-OES measurements present the carbon- (C) and nitrogen- (N) depth profiles of co-precipitated planar plates (treated as Co-4) in comparison to a biomimetically HA-reference (HA-ref) without impact of Tobramycin during growth obtained, see Figure 62. Generally, co-precipitation enabled the integration of the drug throughout the coating thickness. SEM cross section demonstrated a sample coating thickness of approx. 3 µm whereas the HA

start-layer had a thickness of 0.3-0.6 μm . The coating morphology is characterized as a needle-like structure and appeared to be denser towards the bioactive, crystalline TiO_2 interface, see Figure 62 b). Several cracks were detected within the cross section of the measured sample. Both, C- and N- concentrations increased from the substrate interface towards the surface. The C- depth profile showed an increased weight fraction in carbon for Co-4 up to 2.5 μm penetration depth compared to the reference (HA-ref) with a total HA coating thickness of approx. 5 μm . The N-depth profile demonstrated increased nitrogen concentration for Co-4 up to 1.2 μm penetration depth compared to HA-ref.

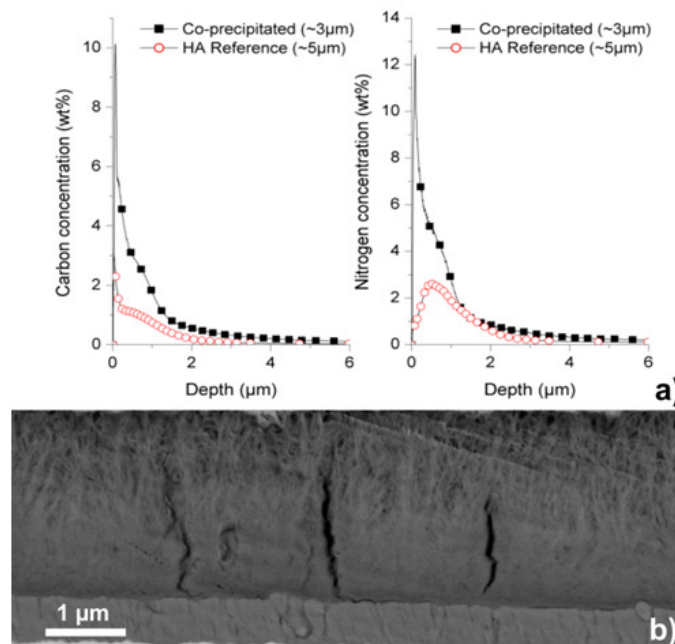


Figure 62: GD-OES analyses of the co-precipitated sample (Co-4) with an HA start layer along with a biomimetically deposited HA reference sample a) carbon depth profile (left) and nitrogen depth profile (right); b) SEM cross-section of Tobramycin-doped HA.

4.2 Results of investigations performed with titanium surfaces

4.2.1 NaOH pretreatment

In order to investigate surface morphology changes as a result of the NaOH pretreatment, the following NaOH pretreatment periods were evaluated on anodized titanium type II coupons prior to HA deposition.

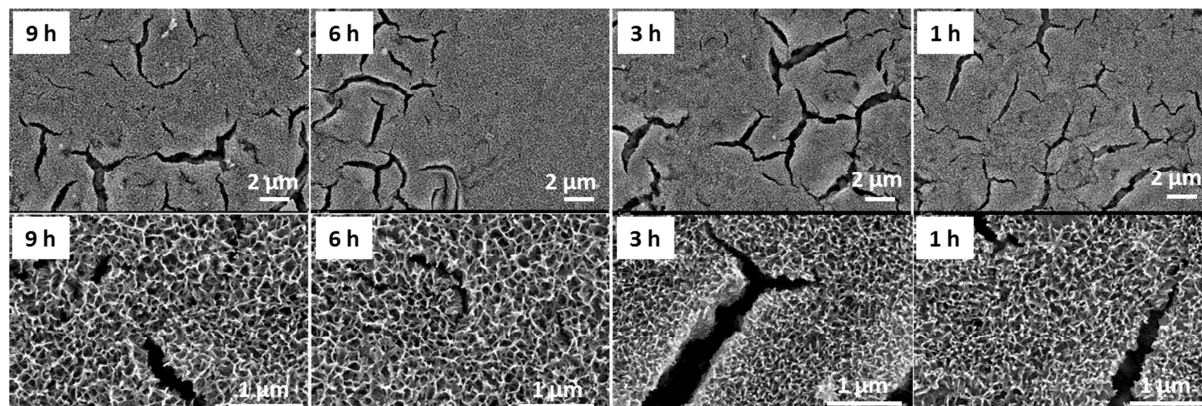


Figure 63: SEM images of 5 M NaOH pretreatment of anodized titanium type II surface after different treatment durations at 70 °C (1 – 9 hours) prior to HA deposition.

Figure 63 demonstrates extensive etching and changes of surface morphology after NaOH pretreatment of all time periods tested from 1 to 9 hours. Also heavy surface cracks were observed for all samples tested. The longer the NaOH treatment period was applied, the greater the changes in terms of surface roughness.

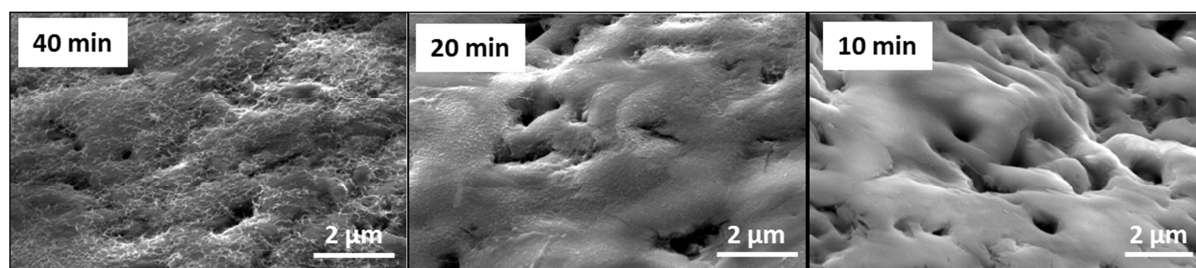


Figure 64: SEM images of 5 M NaOH pretreatment of anodized titanium type II surface after different treatment durations at 70 °C (10 – 40 minutes) prior to HA deposition.

A gradual decrease in the amount of etching was observed from 40 to 20 minutes of NaOH pretreatment (Figure 64), whereas there was no visible etching behavior observed with 10 minutes of pretreatment.

4.2.2 Concentration dependent loading of HA with Tobramycin

At first, the HA coated screws (coating deposition, see section 3.2.4) were tested with different concentrations of Tobramycin stock solution in the range of 4 mg/ml to 40 mg/ml after loading by adsorption and under elevated temperature and pressure. The amount of Tobramycin released from each implant was measured after fixed time periods, displayed in the x-axes. Additionally, the minimum inhibitory concentration of Tobramycin against *Staph. aureus* is indicated by the dotted red line, see Figure 65.

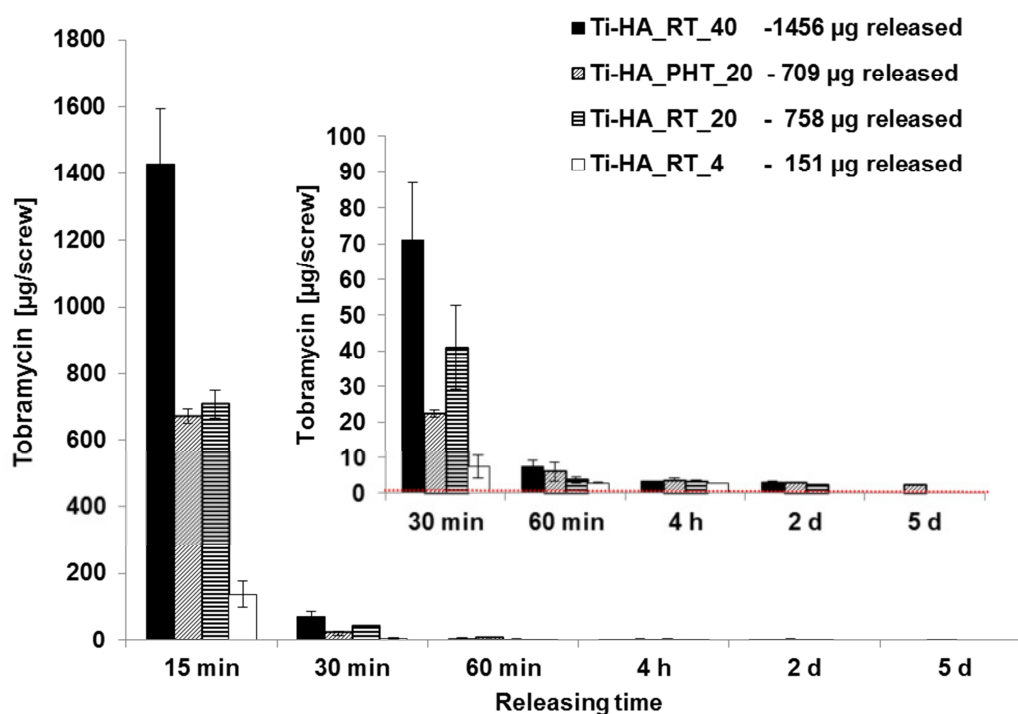


Figure 65: Non-cumulative amount of Tobramycin released in 37°C PBS from Ti-HA screws loaded in stock solution containing different concentrations of Tobramycin during the displayed loading times. Ti-HA_PHT_20 was loaded under elevated temperature and pressure.

In general, the release kinetic demonstrates an initial burst release followed by a sustained release period dependent on the concentration and loading technique. The initial burst

release shows a linear correlation to the concentration in stock solution. Loading with 40 mg/ml stock solution resulted in a burst release of approx. 1430 µg compared to loading with 4 mg/ml showing a burst release of 140 µg per implant. Loading with 20 mg/ml stock solution resulted in a burst release after 15 minutes of approx. 710 µg. The sustained release showed no linear correlation. The release after 15 minutes is greatest for the screws loaded with 40 mg/ml, followed by the RT-20 samples. A similar initial burst release was observed for PHT-20 samples compared to RT-20. PHT-20 loaded samples demonstrate the longest release period resulting in a release for 5 days, followed by RT-20 and RT-40 loaded samples showing a Tobramycin release up to 2 days. RT-4 loaded samples demonstrated a release period for 4 hours. All values measured at the given time points lay above the inhibitory concentration of *Staph. aureus*.

4.2.3 Impact of different pH values during Tobramycin loading

In the next test series, the pH dependent loading of Tobramycin was evaluated. The pH was adjusted in the range from 4 to 10. Within this pH range it could be ensured that the aminoglycoside antibiotic was stable while loading. In Figure 66 it is demonstrated that the pH value showed an impact during the initial burst release and hence, the loading capacity was in favor of the screws loaded at pH 4 and pH 10. Ti-HA_pH 4 and Ti-HA_pH 10 demonstrated a slightly higher burst release after 15 minutes compared to Ti-HA_pH 7.4. Nevertheless, this result is not significant and may be neglected due to the size of the error bars. This trend was also observed for the 30 minutes time period. For the later time points no impact of the pH values could be observed and the release stopped after 2 days.

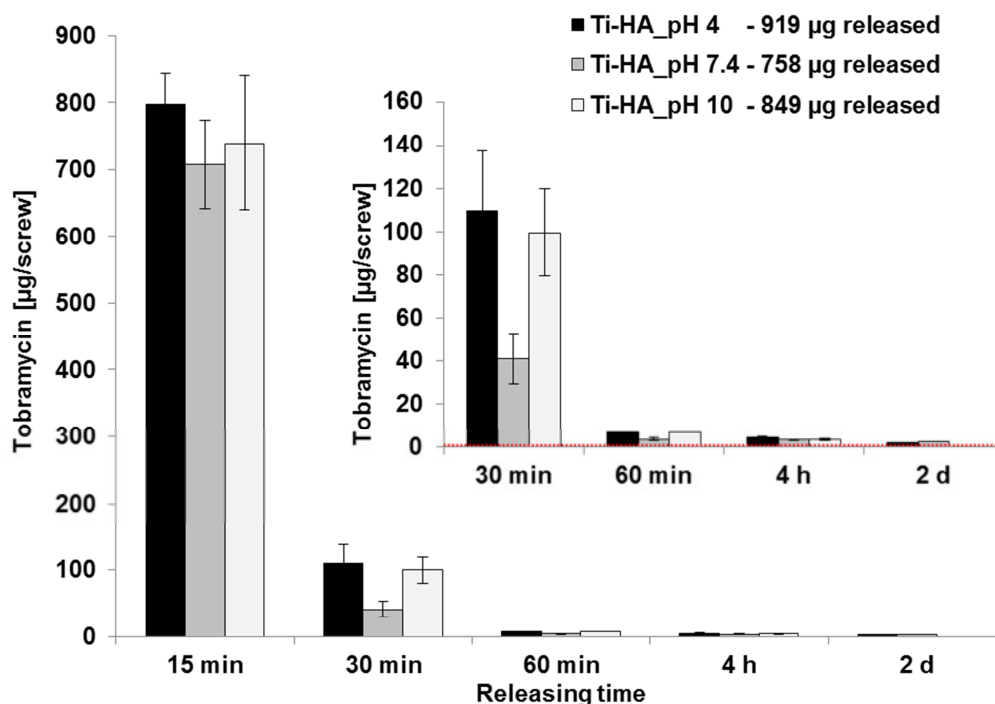


Figure 66: Non-cumulative Tobramycin release over time dependent on different pH values during loading.

4.2.4 Impact of ultrasound and vacuum during Tobramycin loading

By evaluating the release after loading under applied ultrasound and vacuum, different release values were obtained compared to Ti-HA_RT loaded samples, see Figure 67. For the initial burst release during the first 15 minutes, Ti-HA_US demonstrated the highest amounts of Tobramycin released, followed by Ti-HA_USV. After 30 and 60 minutes of release the samples loaded under ultrasound and vacuum showed the highest release values, slightly higher than loading under ultrasound conditions. For the 4 hours and 2 day time points all amounts of Tobramycin released were comparable. Overall Ti-HA_US demonstrated the highest release values with 1196 µg, followed by a release of 959 µg for Ti-HA_USV samples. Ti-HA_RT loaded screws released 758 µg Tobramycin.

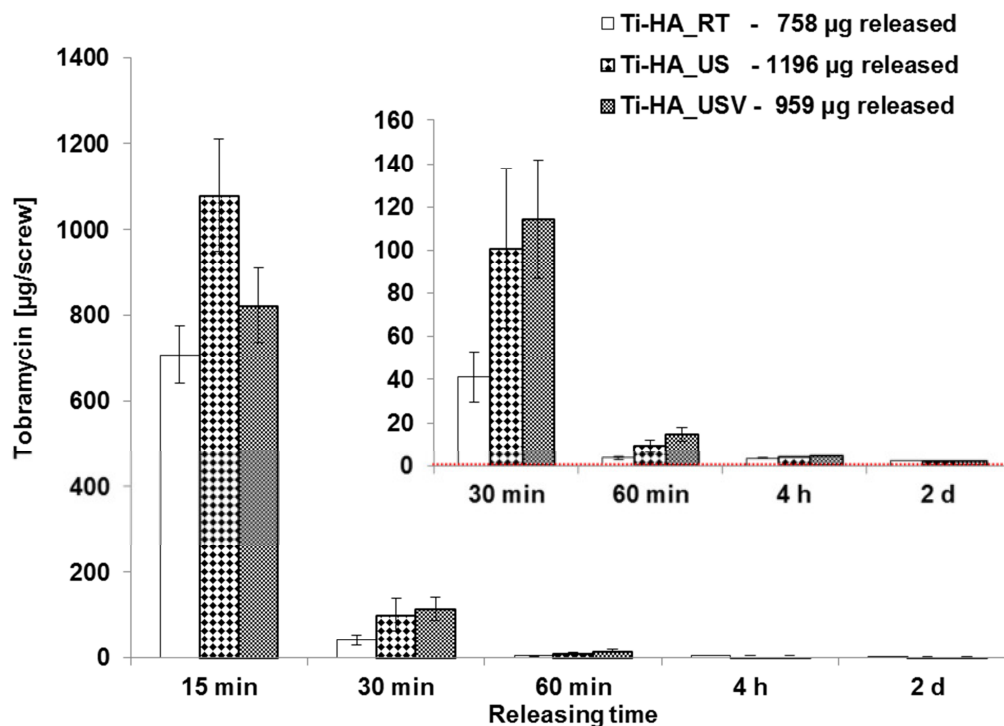


Figure 67: Non-cumulative release of Tobramycin in 37°C PBS over time from Ti-HA coated screws Tobramycin loaded in a stock solution containing 20 mg/ml for 5 minutes at room temperature, under applied ultrasound or under applied ultrasound in combination with vacuum.

4.2.5 Antibacterial properties of Tobramycin HA coated titanium screws

No inhibition zones were observed for the inserted Ti-w/o screws for any time point of incubation, as shown in Figure 68 panel a1) and b1). All other samples loaded with Tobramycin demonstrated visible and homogeneously distributed inhibition zones, denoted as a2)-a4) and b2)-b4). Ti-w/o_RT showed comparable inhibition zones at day 1 of incubation compared to Ti-HA_PHT, but no sustained antibacterial effect was observed after the first 24 hours. Ti-HA_RT showed slightly increased inhibition zone areas for day 1, 3, 4 and 5 compared to Ti-HA_PHT samples. All screws were evaluated over a time period of 5 days, Figure 68 c). The HA coated and antibiotic loaded samples Ti-HA_RT and Ti-HA_PHT demonstrated antibacterial activity over a range of 5 days. The inhibition zones were found

to slightly decrease from day 2 to day 5. At day 6 no inhibition zones were observed for any of the samples under study. Additionally, it was demonstrated that Tobramycin was still active and stable even after loading at elevated temperature and pressure.

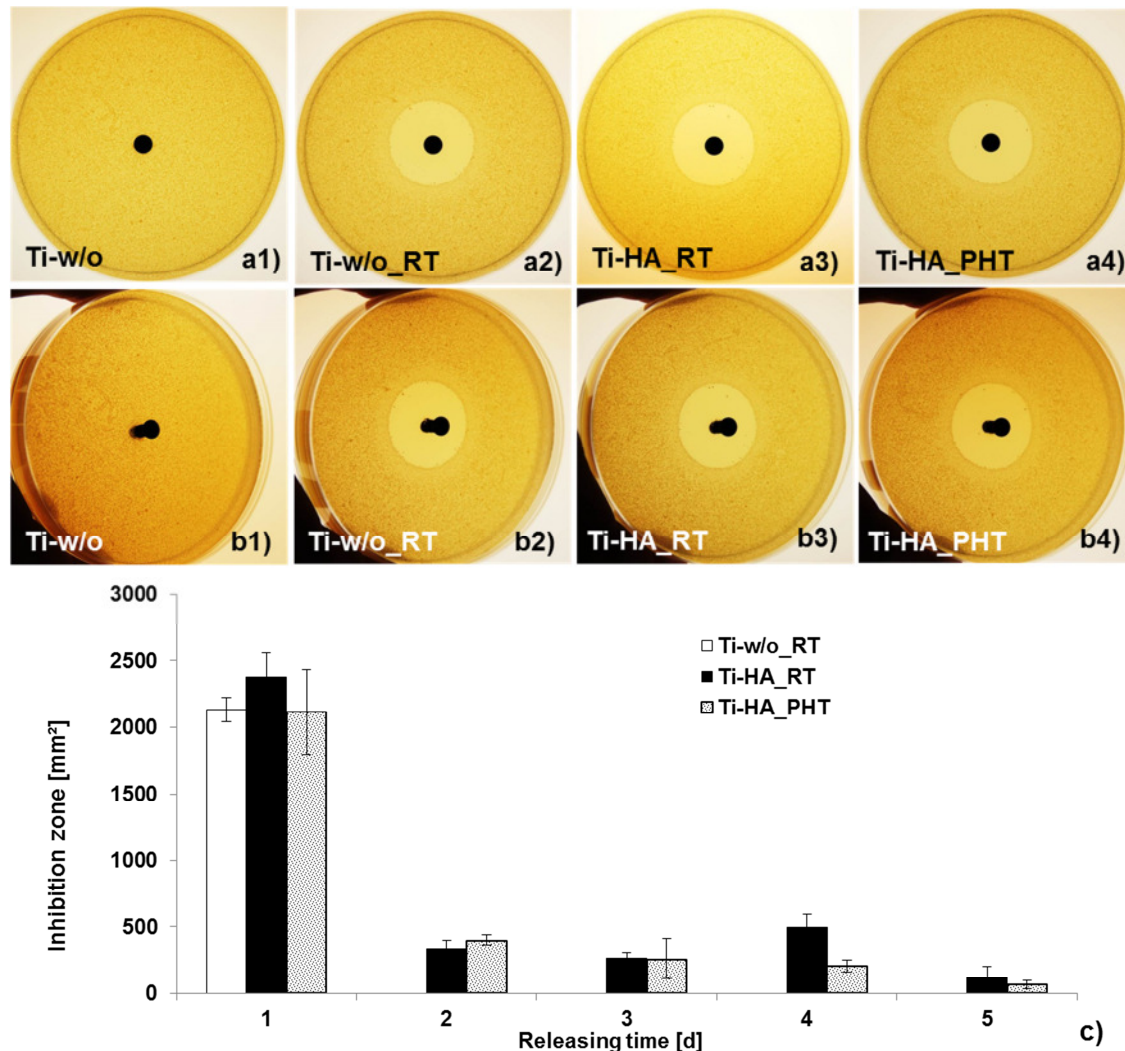


Figure 68: Images of Ti-w/o, w/o_RT loaded, HA_RT loaded and HA_PTH loaded screws inserted after 18 hours of incubation in agar diffusion tests against *Staph. aureus*. Panel c) gives an overview of the inhibition zones of the different samples in accordance to the time period. The error bars indicate the standard deviations over three measurements.

In a second test series, Ti-HA_RT and Ti-HA_PHT screws were inserted into agar plates, containing a 3-D suspension of bacteria to gain further information of the antibacterial efficacy. The screws demonstrated visibly detectable antibacterial activity over the full volume of the inserted screw, see Figure 69.

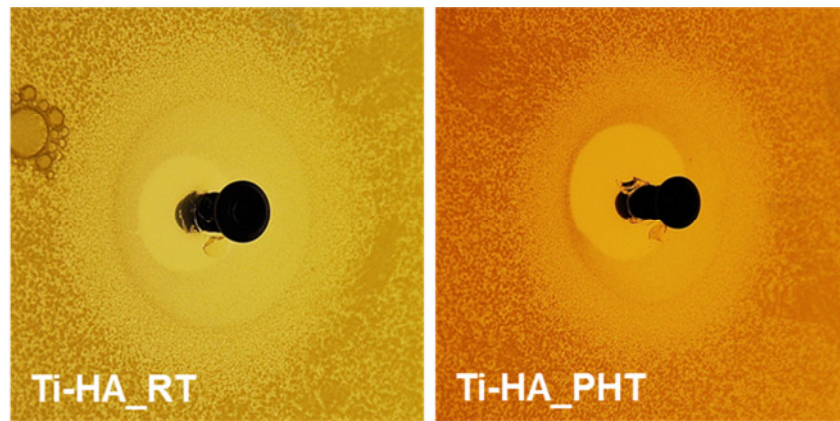


Figure 69: Antibacterial effect after 18 hours of incubation of inserted screw into fully germ suspended agar media. A 3 dimensional antibacterial effect is demonstrated over the full range of the inserted screw.

4.2.6 In-vitro bioassessment test

The biocompatibility of HA-coated titanium discs was evaluated *in vitro* using two different types of cells including primary human osteoblasts and primary human endothelial cells. Primary human osteoblasts isolated from bone tissue and endothelial cells isolated from the peripheral blood were investigated in terms of the viability and morphology when grown on anodized titanium type II or HA-coated surfaces for different time points. Viability assessment using Calcein-AM which is converted by viable cells to a green fluorescent substance showed that both primary osteoblasts and outgrowth endothelial cells were viable when grown on HA-coated or pure titanium surfaces. Cells were firmly attached to the surface and formed typical monolayers after both 7 and 14 days of culture, Figure 70. This was achieved without any additional coating of the material surfaces with components of the extracellular matrix such as fibronectin or collagen.

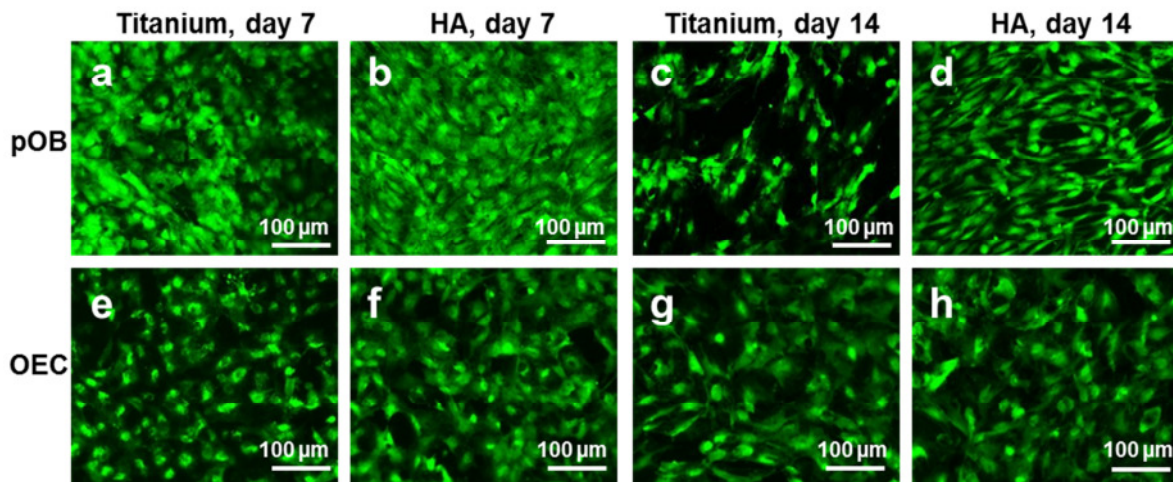


Figure 70: Calcein-AM viability assessment of primary osteoblasts (a-d) and outgrowth endothelial cells (e-h) grown on Titanium disks with (c, d, f, h) or without HA (a, c, e, g) coating. On both types of substrates consisting of either pure titanium or hydroxyapatite coated titanium primary osteoblasts show a bright fluorescence after Calcein-AM staining at both time points of investigation. Similar findings were observed for outgrowth endothelial cells which form endothelial cell layers on both types of surfaces and at both investigated time points.

In addition, immunofluorescent staining was performed for the endothelial marker CD31 in samples of OEC grown on the two types of material surfaces. In these samples CD31 staining resulted in a typical staining pattern for CD31 which is located along the intercellular borders (Figure 71 a) and b). These findings further confirm the formation of an intact endothelial cells layer on both types of material surfaces. Staining of primary osteoblasts with phalloidin-TRITC to document the actin cytoskeleton in this cell type also showed the formation of continuous cell layers by the osteogenic cells grown on the two material variants, (Figure 71 c) and d).

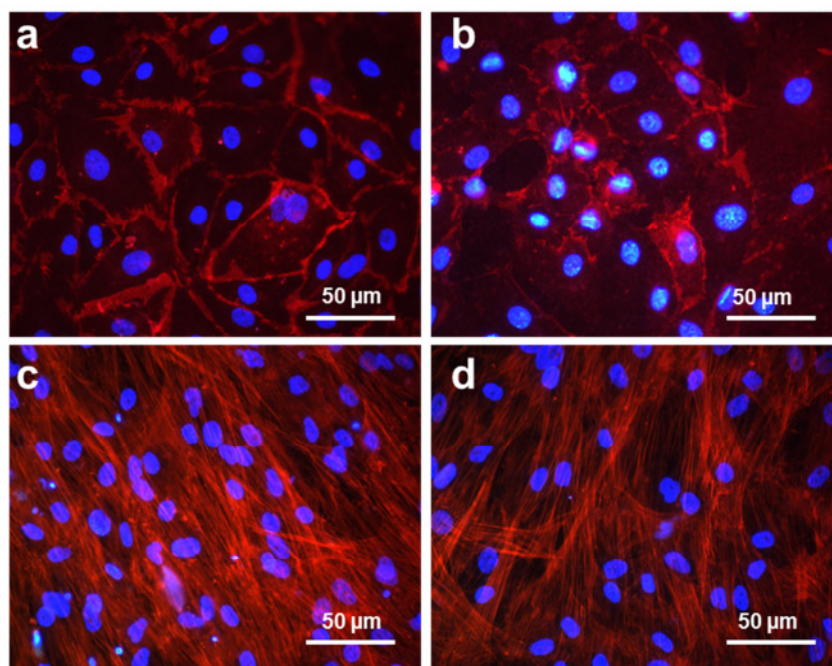


Figure 71: Morphological appearance of pOB and OEC; Staining for the endothelial marker CD31 (red) on OEC grown on pure Titanium (a) or HA-coated titanium (b). Phalloidin-TRITC (red) staining for primary osteoblasts grown for 7 days on pure Titanium (c) or HA-coated titanium (d). Nuclear counterstain in blue.

4.3 In-Vivo studies

4.3.1 HA performance pilot study

The objective of the pilot phase was to validate the implantation procedure in the femoral condyle of the rabbit, the chosen early time point of 2 weeks and the biomechanical testing of both the non-coated and the HA-coated screw. The implant procedure and biomechanical testing methods were successfully executed and optimized during this essential pilot phase. The data evaluated at 2 weeks showed that the 2 week time point was a suitable time interval to demonstrate early implant fixation when comparing the removal of non-coated and HA-coated screws.

4.3.1.1 Screw insertion torque

During implantation the insertion torques of all screws were recorded. Overall, no difference in insertion torque were detected by comparing non-coated (control) screws against HA-coated (test) screws. Figure 72 demonstrate the insertion torques of 8 control and 8 test screws. The error bars indicate the standard deviations of all screws from each group.

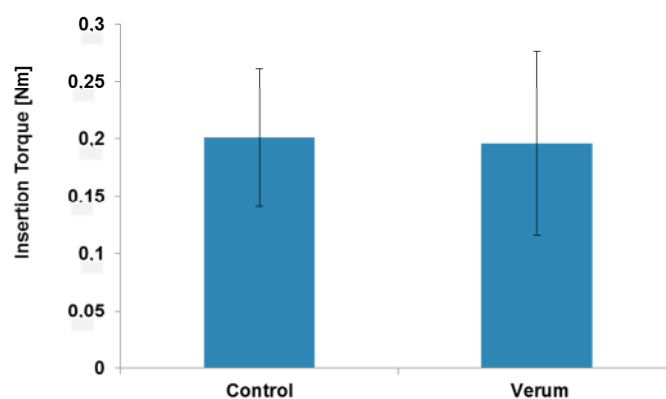


Figure 72: Summarized insertion torque measurements during implantation (n=8).

4.3.1.2 Removal torque and Pull-out measurements

Six pairs of femurs were tested for removal torque, whilst two pairs were used for pull-out force measurements. Overall a slight trend in higher removal torques was seen for the test screws compared to non-coated reference screws. Nevertheless, no significant difference was demonstrated due to the small sample size. After evaluation of the pilot phase, the removal torque and pull-out force test systems were judged to be acceptable and sensitive enough to be used as test setup for the main study.

4.3.2 HA performance main study

4.3.2.1 Screw insertion torque

The insertion torque of all screws implanted were measured during the HA performance main study. No significant difference was observed by comparing the insertion torques of control articles and HA-coated test articles. Figure 73 demonstrate the insertion torques of 35 control and 35 test screws. The error bars indicate the standard deviations of all screws from each group.

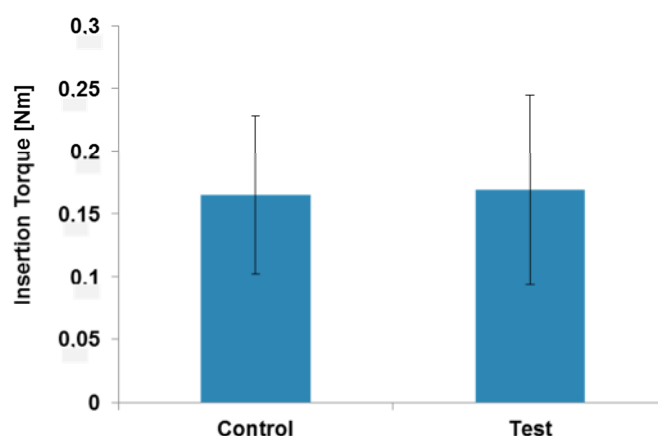


Figure 73: Summarized insertion torque measurements during implantation (n=35).

4.3.2.2 Biomechanical Testing

4.3.2.2.1 Removal torque measurements

Maximal removal torque values of both control and test articles at two and six weeks after implantation are summarized in Figure 74. At two weeks in-vivo a significant increase ($P = 0.012$) in removal torque was measured for HA coated test articles compared to control articles ($P = 0.012$). The mean maximal moment of 2.7 Ncm measured for the control group after 2 weeks strongly increased for the test group resulting in a mean value of 7.6 Ncm, see Table 12. After 6 weeks no significant difference in maximal removal torque values were observable comparing control and test articles. The mean values demonstrate a trend towards slightly increased removal torque values for the test article (mean = 12.8 Ncm) compared to the control articles (mean = 10.9 Ncm) after six weeks, see Table 13. However, when comparing control versus control group and test articles versus test articles at two and six weeks post-implantation a significant increase in removal torque were detected for both groups internally. This difference was highly significant for the control groups between two to six weeks.

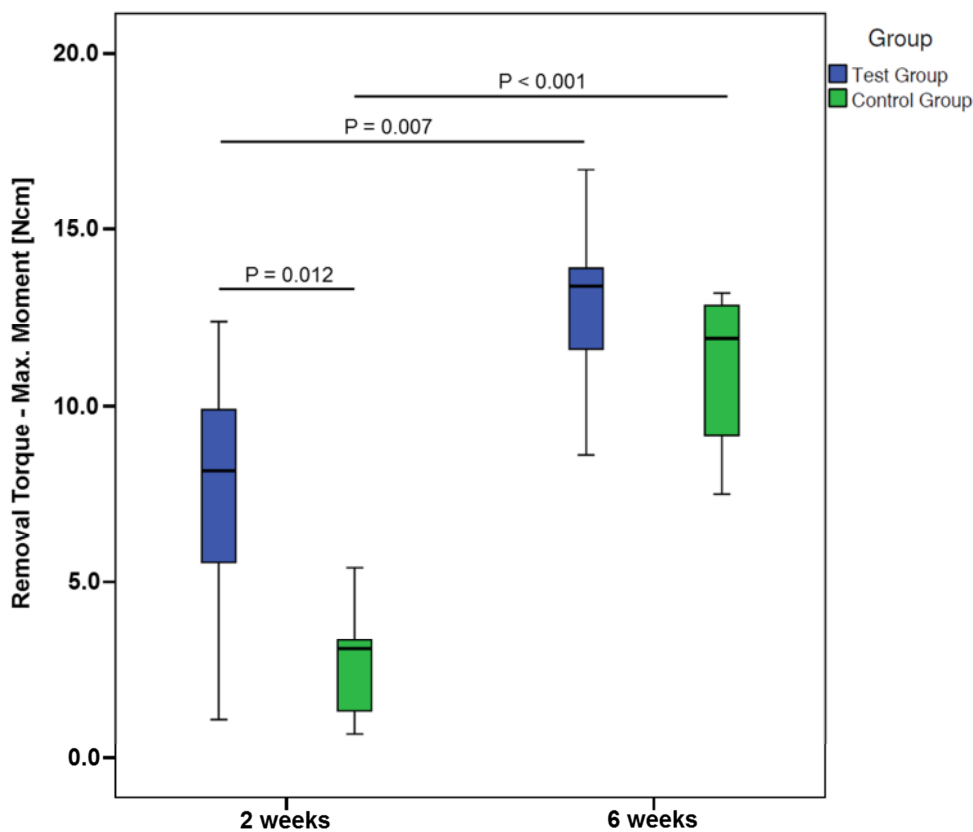


Figure 74: Maximal removal torques after 2 and 6 weeks implantation of test and control articles.

Table 12: Overview of removal torque and stiffness values after 2 weeks of implantation.

	Max. moment [Ncm]	Max. moment [Ncm]	Stiffness [Ncm/°]	Stiffness [Ncm/°]
Animal no.	Control group	Test group	Control group	Test group
X1712 (l/r)	3.1	8.8	7.0	11.5
Y3 (l/r)	3.6	8.3	9.3	8.6
Y69 (r/l)	0.7	5.0	1.5	7.4
X1658 (r/l)	5.4	12.4	9.6	11.3
X1693 (r/l)	1.3	8.0	3.2	10.4
Y632 (r/l)	1.4	11.0	3.0	9.3
X1664 (r/l)	3.1	1.1	6.8	3.0
Y34 left		6.1		10.3
Mean	2.7	7.6	5.8	9.0
SD	1.6	3.5	3.2	2.8

For the removal torque stiffness values, a similar trend is demonstrated in Figure 75. After two weeks the test group showed significant ($P = 0.048$) higher removal torque stiffness compared to the control group. One outlier was statistically detected for the test group after two weeks. After 6 weeks control and test values assimilate and no statistical difference was observed. A slight trend towards higher stiffness for the test articles (mean = 12.4 Ncm/°) compared to the control articles (mean = 10.4 Ncm/°) after six weeks is shown in Table 13. By comparing each group internally at two and six weeks in-vivo, statistically significant differences could be found between the test groups ($P = 0.008$) and control groups ($P = 0.018$).

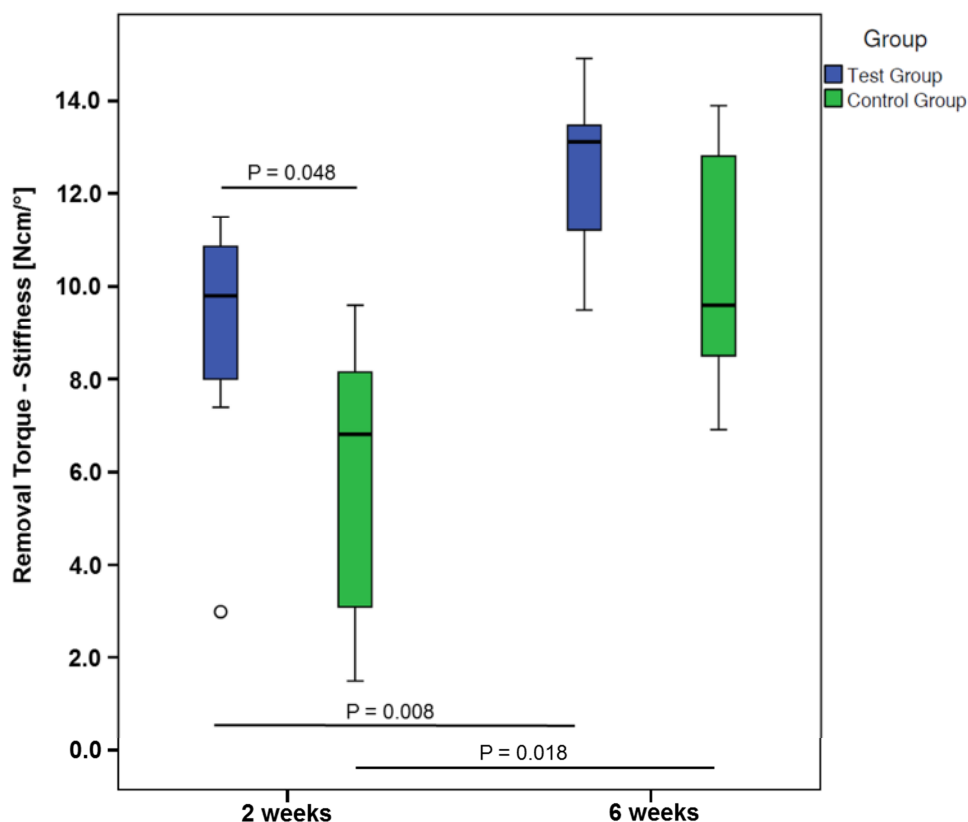


Figure 75: Removal torque stiffness after 2 and 6 weeks implantation of test and control articles.

Table 13: Overview of removal torque and stiffness values after 6 weeks of implantation.

Animal no.	Max. moment [Ncm]	Max. moment [Ncm]	Stiffness [Ncm/°]	Stiffness [Ncm/°]
	Control group	Test group	Control group	Test group
X1687 (r/l)	11.9	16.7	13.8	14.9
X1692 (r/l)	12.9	13.7	11.8	13.1
X1694 (r/l)	9.0	14.1	6.9	10.8
X1708 (r/l)	12.8	12.2	13.9	11.6
Y79 (r/l)	13.2	13.4	9.6	13.1
X1731 (r/l)	7.5	8.6	7.6	9.5
X1726 (r/l)	9.3	11.0	9.4	13.8
Mean	10.9	12.8	10.4	12.4
SD	2.3	2.6	2.8	1.9

4.3.2.2.1.1 SEM evaluation after screw removal

The following SEM images are of anodized Ti type II bone screws coated with a biomimetic HA layer as well as control screws without an HA coating after removal of the screws from the rabbit model described above. Test and control screws were removed by using the torque measurement system after 2 and 6 weeks in vivo and then analyzed.

In general at 2 weeks evidence of the HA coating was found below the point on the screw that was inserted into the bone. HA was visible just below the screw head and down to just above the first thread and some proportion was covered with some type of growth. The removed control screw demonstrated signs of cell attachment at the screw tip and between the threads after 2 weeks in-vivo, see Figure 76.

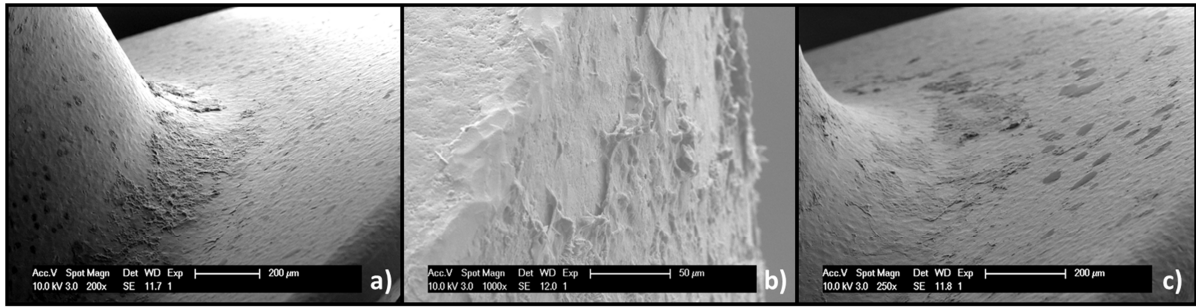


Figure 76: SEM images after screw removal of a control screw after 2 weeks implantation – a) and c) the surface between the threads and b) the surface at the tip of screw is shown.

The HA coated test screw demonstrated clean areas without residual HA coating as well as spots clearly demonstrating residual HA at the screw interface. Cell attachment was observed within these areas, see Figure 77.

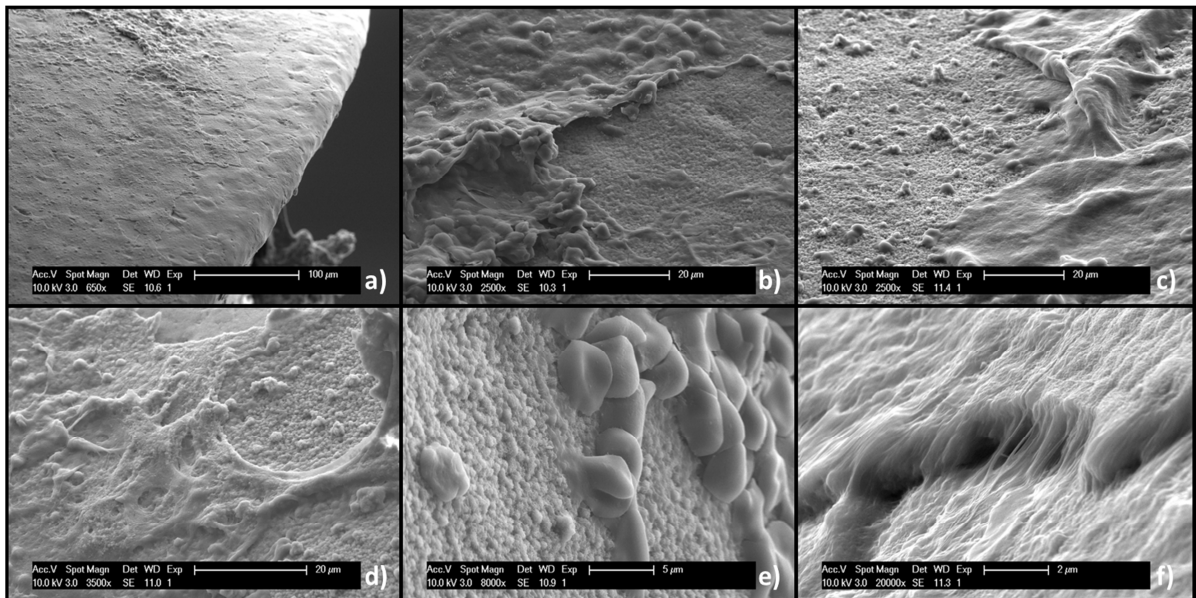


Figure 77: SEM images after screw removal of a test screw after 2 weeks implantation – a) the surface between the threads and b - f) a closer look at the surface of screw showing cell attachment and residual HA coating.

At 6 weeks in-vivo the control screws showed areas of cell attachment directly at the anodized titanium type II surface, see Figure 78.

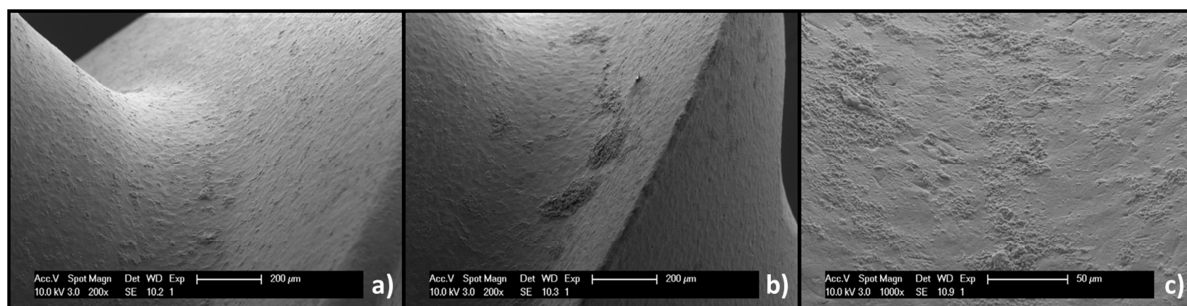


Figure 78: SEM images after screw removal of a control screw after 6 weeks implantation – a) to c) the surface between the threads of screw showing signs of cell attachment.

The test groups demonstrated only slight evidence of residual HA at 6 weeks implantation in-vivo. Cell attachment can be observed, see Figure 79.

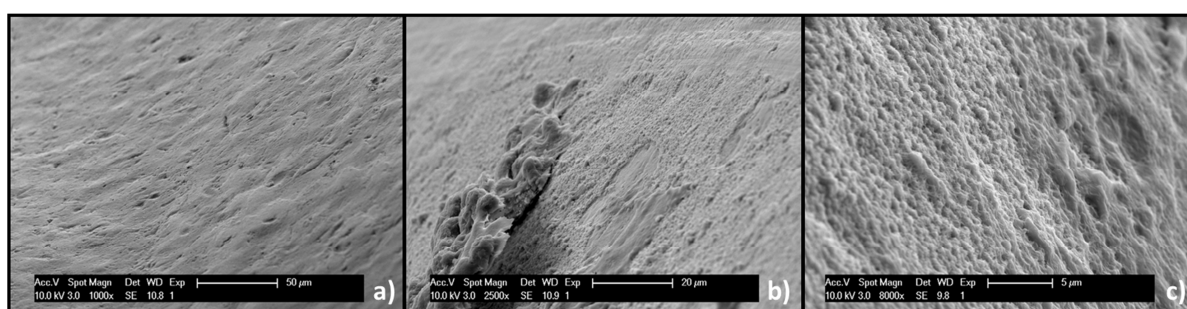


Figure 79: SEM images after screw removal of a test screw after 6 weeks implantation – a) to c) the surface between the threads of screw showing signs of cell attachment and signs of cell attachment.

4.3.2.2.2 Pull-out measurements

The maximum pull-out forces at 2 and 6 weeks implantation in-vivo are described in Figure 81. No statistical significant difference in pull-out force can be demonstrated comparing control and test articles after 2 and 6 weeks. A clear trend was observed of higher pull-out forces for the test article at 2 weeks, see Figure 80. Bilateral comparison of all 6 pairs of femurs demonstrated higher pull-out forces for every single test item compared to its respective control counterpart, see Table 14. This trend would become statistically significant, if the group size would be increased to $n = 12$ instead of $n = 6$. The internal comparison of the test and control groups between 2 weeks to 6 weeks implantation demonstrated a significant increase in pull-out forces for the control ($P = 0.008$) and for the test group ($P = 0.001$). One outlier was found for the control group at the 6 week time point.

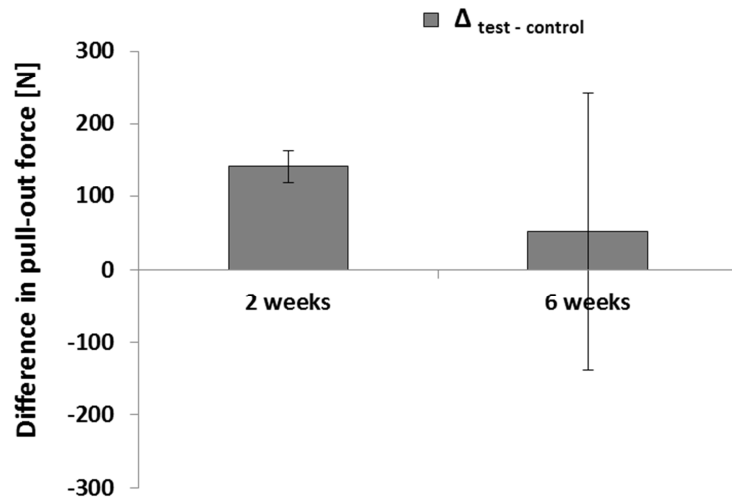


Figure 80: This image demonstrates the difference in pull-out force [N] after 2 (n=6) and 6 weeks (n = 7).

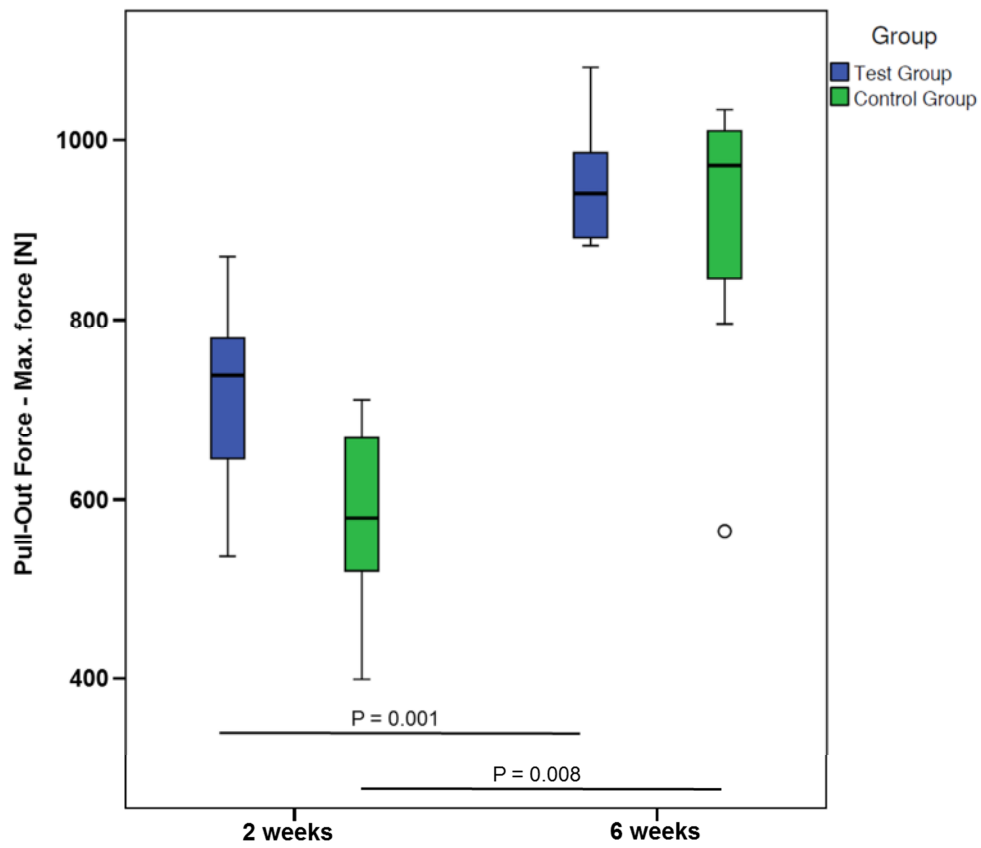


Figure 81: Maximal pull-out force after 2 and 6 weeks implantation of test and control articles.

Table 14: Overview of pull-out force and stiffness values after 2 weeks of implantation.

	Max. force [N]	Max. force [N]	Stiffness [N/mm]	Stiffness [N/mm]
Animal no.	Control group	Test group	Control group	Test group
X1643 (r/l)	627	773	1614	1169
X1674 (r/l)	668	779	1399	1646
X1666 (r/l)	532	703	1469	1316
X1705 (r/l)	520	645	1538	1412
Y46 (r/l)	399	536	1864	1653
Y75 /r/l)	711	870	2281	1875
Mean	576	718	1694	1512
SD	115	117	329	259

For the pull-out stiffness no significant difference was observed by comparing control and test group at both 2 weeks and 6 weeks, see Figure 82. The internal comparison between the control group after 2 and 6 weeks and the test group after 2 and 6 weeks showed a significant increase for both.

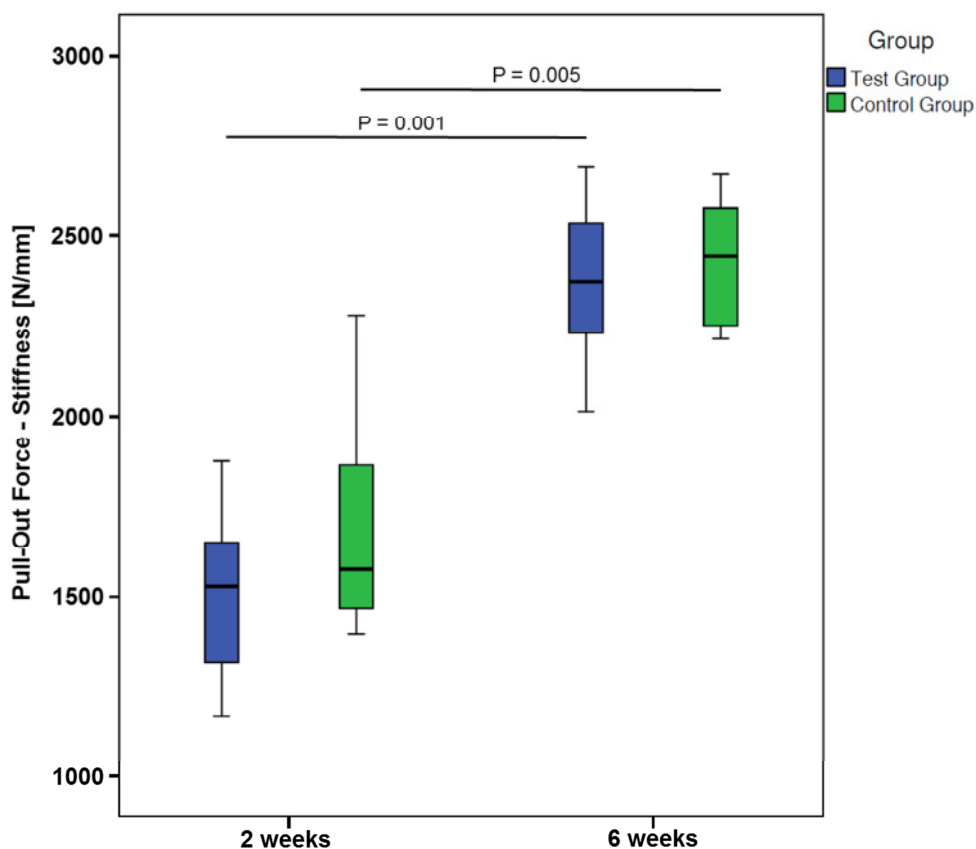


Figure 82: Pull-out force stiffness after 2 and 6 weeks implantation of test and control articles.

Results

Animal no.	Max. force [N]	Max. force [N]	Stiffness [N/mm]	Stiffness [N/mm]
	Control group	Test group	Control group	Test group
Y5 (r/l)	565	980	2224	2654
Y70 (r/l)	1000	891	2214	2374
X1695 (r/l)	796	891	2283	2285
X1730 (r/l)	896	882	2622	2177
X1660 (r/l)	972	941	2444	2425
Y7 (r/l)	1035	992	2539	2014
X1707 (r/l)	1020	1082	2674	2693
Mean	898	951	2429	2375
SD	169	73	191	245

Table 15: Overview of pull-out force and stiffness values after 6 weeks of implantation

4.3.2.3 Histological evaluation

A total of 8 sections (4 control sites and 4 test sites) were analyzed for each time point.

After 2 weeks of implantation, the histopathologic analysis showed no local adverse effects in the groups control and test. Qualitatively a higher level of osteointegration was observed with the test article, see Figure 83. This was not confirmed statistically through the histomorphometric analysis, even though a higher value of bone to implant contact was determined in the group test. However the soft tissue contact developed with control article was significantly higher than with the test article.

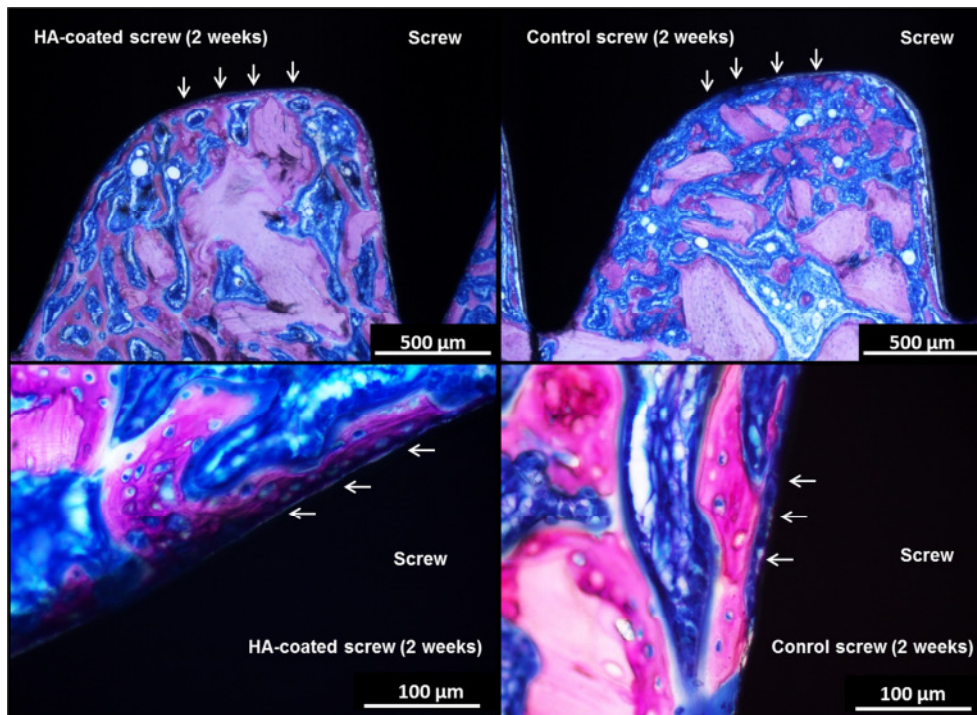


Figure 83: Histological images of HA coated screws (left) and non-coated control screws (right) after 2 weeks in-vivo. The arrows integrated on the left side demonstrating direct bone implant contact, whereas minor bone implant contact was observed for the control group (right side).

After 6 weeks, the bone tissue matured in the two groups. Although a slightly higher amount of bone tissue was qualitatively observed with the test group, quantitatively no significant difference was noted between the test and control groups, see Figure 84. However, between 2 and 6 weeks there was a significant increase of the bone density in the test group, while a steady state bone amount was noted with the group control.

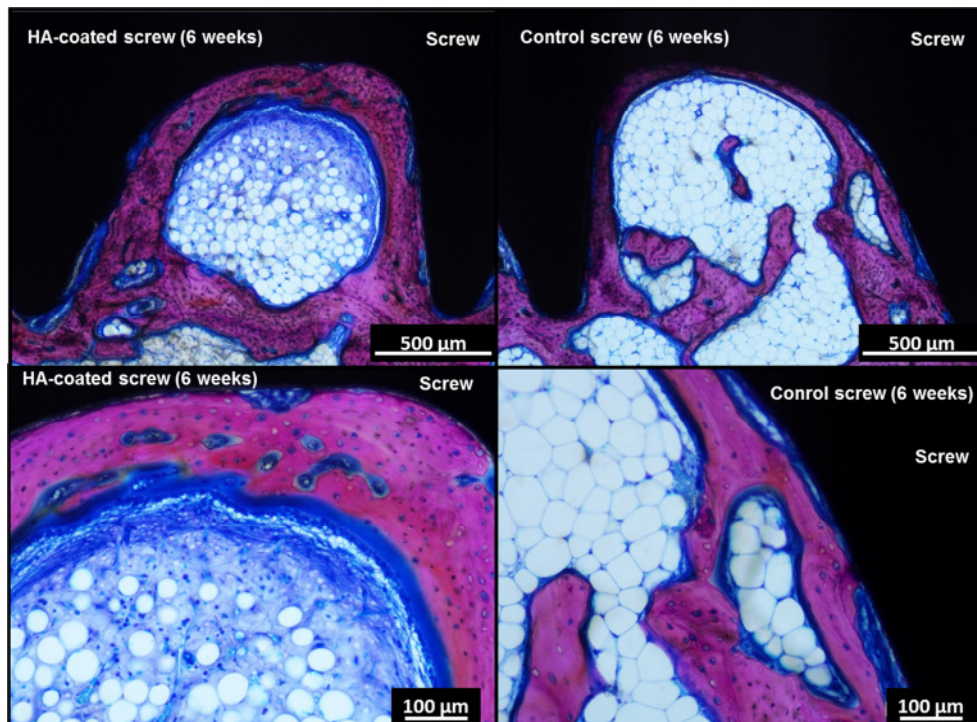


Figure 84: Histological images of HA coated screws (left) and non-coated control screws (right) after 6 weeks in-vivo. For both samples tested a good osteoconductivity were demonstrated. A greater bone thickening and a higher remodeling activity was observed for the HA-coated group.

In general, thickening of the bone trabeculae together with moderate signs of bone remodeling were evidenced around the control and the test articles after 6 weeks. A moderate grade of cancellous bone grew towards the surface of the control and test site. The signs of osteointegration and osteoconduction slightly increased compared to 2 weeks for both groups. The osteointegrated bone debris (surgery-related) were remodeled after this time period. Between 2 and 6 weeks a significant increase of bone density in the test group was noted, while a steady state bone amount was demonstrated with the control group.

In conclusion, the test article slightly outperformed the control article in terms of qualitative peri-implant bone healing however under the conditions of the study this difference did not reach statistical significance.

4.3.2.4 μ -CT evaluation

The micro CT demonstrated for the ROI which is close to the interface that there is no statistically detectable difference in bone volume density (BV/TV) comparing test and control at 2 and 6 weeks in-vivo. However, at 6 weeks a slight trend in greater bone volume density was observable for the test articles, see Figure 85. Furthermore, it was found, that trabecular elements were thicker and further separated at 6 weeks. Overall, no difference was found to be significant after evaluating a low number of specimens.

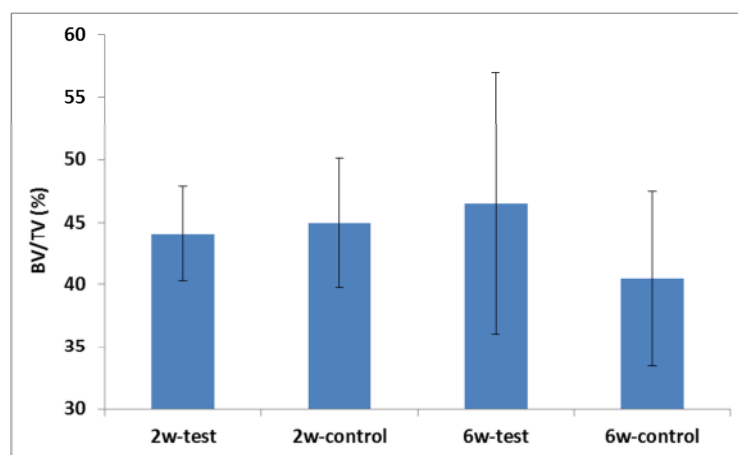


Figure 85: BV/TV (%) are demonstrated for the test and control articles at 2 and 6 weeks in-vivo.

4.3.2.5 μ -CT evaluation after removal torque measurements

The main finding during the μ -CT evaluation after removal torque was that the cortices were much thinner than the 1.5 mm that Seebeck et al. determined to be the threshold above which the pull-out force is mainly influenced by the cortical bone thickness rather than the underlying cancellous bone. This suggests that the pullout force measured in the present study is likely to represent the strength of the connection of the screw to the underlying cancellous bone. The cortical thicknesses of the femurs treated with control or test articles can be observed in Table 16. The mean values of cortical thickness of femurs treated with control (0.62 mm) and test articles (0.57 mm) were comparable.

Table 16: Cortical thickness measurement at 4 points of the control and test group.

No	side	group	Meas.1	Meas.2	Meas.3	Meas.4	Mean
x1687	right	C	0.28	0.37	0.48	0.74	0.47
x1692	right	C	0.47	0.35	0.63	0.77	0.55
x1694	right	C	0.29	0.44	0.47	0.60	0.45
x1708	left	C	0.72	0.44	0.79	0.82	0.69
x1726	left	C	0.60	0.58	0.85	0.65	0.67
x1731	right	C	0.65	0.76	0.42	0.33	0.54
y79	right	C	1.07	1.04	0.97	0.89	0.99
						Mean	0.62 mm
						SD	0.19 mm
x1687	left	T	0.51	0.35	0.62	0.16	0.41
x1692	left	T	0.55	0.68	0.34	0.44	0.50
x1694	left	T	1.08	0.45	0.79	0.66	0.74
x1708	right	T	0.79	0.61	0.46	0.41	0.57
x1726	right	T	0.79	0.42	0.86	0.61	0.67
x1731	left	T	0.51	0.33	0.84	0.45	0.53
y79	left	T	0.14	0.57	1.03	0.57	0.58
						Mean	0.57 mm
						SD	0.11 mm

Additionally, Figure 86 demonstrates that the screws were well surrounded by cancellous bone. This confirms both good implant conformity and a consistent operative technique.

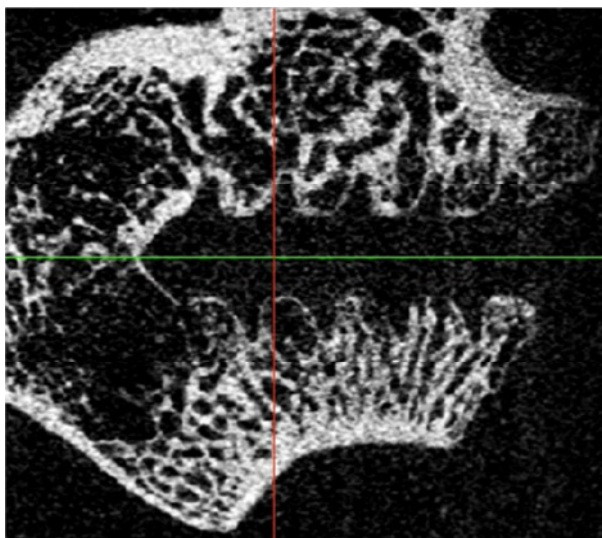


Figure 86: μ -CT image after screw removal of control group (X1708 left) after 6 weeks in-vivo.

4.3.3 Infection pilot study

For the 10^7 CFU inoculation dose study pilot, one rabbit (X1689) died on day 2 and another rabbit (X1690) died on day 7. For rabbit X1689, selected organs (spleen, heart, blood, lungs and bone marrow) were sampled for bacteriology analysis that revealed presence of *Staph. aureus* in the lungs, heart, blood and bone marrow. Moreover, this rabbit presented a body temperature increase of 2.7°C , hypertrophy of several lymph nodes but no other abnormal signs. For this reason, the death of rabbit X1689 was attributed to systemic infection by *Staph. aureus*. For rabbit X1690, hypertrophy and/or discoloration of several organs were observed. The organs seemed autolyzed (maximal duration of 20 hours between death and rabbit necropsy). Whitish deposits were also observed at the level of implantation sites and could be interpreted as pus. No hyperthermia was noted the day before rabbit death. The origin of the death of this rabbit could not be clearly identified and might be attributed to systemic infection.

For the 10^5 CFU inoculation dose pilot, one rabbit (X1684) was prostrate on day 2. This rabbit was euthanized for ethical reasons. This rabbit presented hypertrophy of the kidneys and inguinal lymph nodes, liver with a granular texture and a body temperature increase of 2.0°C . No other abnormal signs were observed. The origin of the abnormal behavior of the rabbit could not be clearly determined and it was attributed to bad recovery from the surgery and/or systemic infection.

For the 10^4 CFU inoculation dose, one rabbit (Y576) died on day 5. This rabbit had a body temperature increase of 2.0°C on day 4, hypertrophy of inguinal lymph nodes, a whitish and pasty deposit at the control implant site which could have corresponded to pus. No other

abnormal signs were observed and the cause of the death for this rabbit cannot be clearly determined but could have been attributed to systemic infection.

All other rabbits survived the 9 day implantation period. Limping from the hind legs associated with or without swelling of the implanted sites was mainly observed for the control sites. The swelling appeared later (from day 6) and was consecutive to abscess formation. Transient body temperature increase (up to 2.7°C) was observed for all rabbits. All rabbits lost body weight (up to -23%) between implantation and euthanasia. This body weight loss could be attributed to infection and post-surgical recovery.

4.3.3.1 Inoculation dose 10⁷ CFU inoculation dose (n=1 site per article)

At 9 days, before skin opening, swelling of control and test sites was observed. In the subcutaneous tissues white deposits were observed for the test and control sites. These deposits might have corresponded to pus collection which resulted in the swelling of the knee joint. The severity of these features was lower for the test site than for the control site, see Figure 87. The articular capsule was filled with the same white deposits which were more fluid for the test site. No alteration of the bone was noted for both groups.

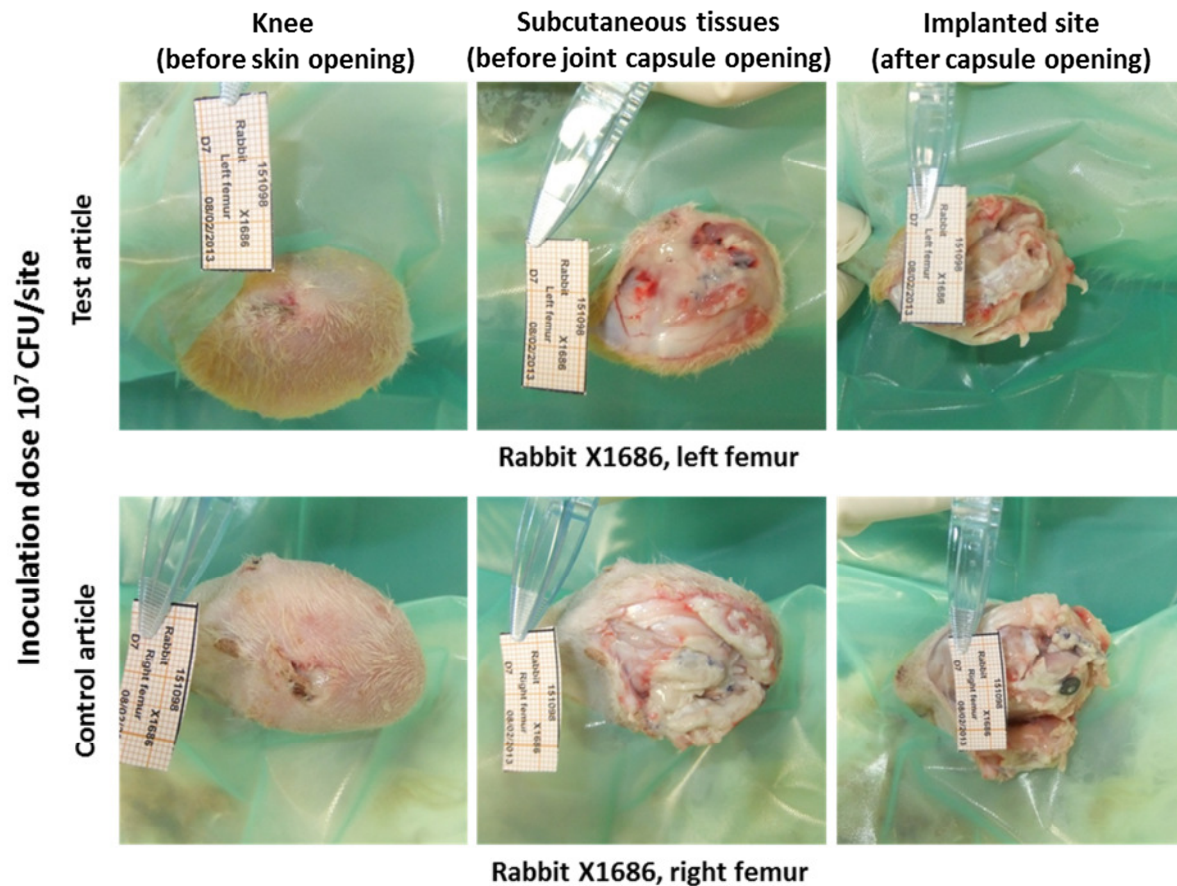


Figure 87: Macroscopic pictures at termination (day 9) – 10^7 CFU inoculation dose

4.3.3.2 *Inoculation dose 10^5 CFU inoculation dose (n=2 sites per article)*

At 9 days, before skin opening, severe swelling of one control site was observed while no swelling was observed for the test sites, see Figure 88. In the subcutaneous tissues or adjacent muscles, white and pasty deposits were observed for the two control sites but not for the test sites. These deposits might have corresponded to pus collection which resulted in the swelling of the knee joint. Articular capsule was filled with these white deposits for the control sites while clear synovial fluid was observed for the test sites. No alteration of the bone was noted for both groups.

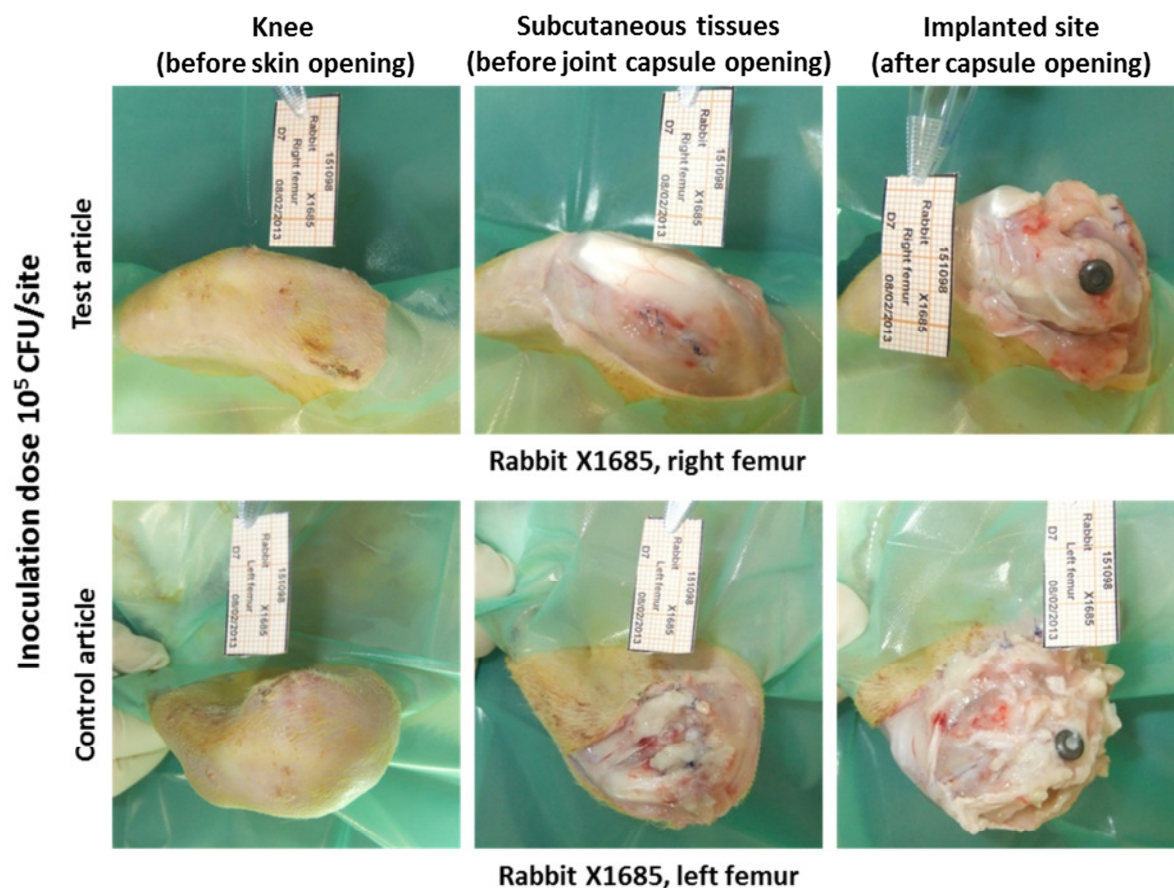


Figure 88: Macroscopic pictures at termination (day 9) – 10^5 CFU inoculation dose

4.3.3.3 Inoculation dose 10^4 CFU inoculation dose ($n=3$ sites per article)

Figure 89 shows the individual macroscopic observations at necropsy after 9 days in-vivo inoculated with 10^4 CFU per site. At 9 days and before opening of the skin, moderate to severe swelling of all control sites was observed while only slight swelling was observed at two test sites. Articular capsule was filled with white deposits at the control sites while clear synovial fluid was observed at the test sites. These deposits could have corresponded to pus collection which resulted in the swelling of the knee joint. No alterations of the bone were noted in either group.

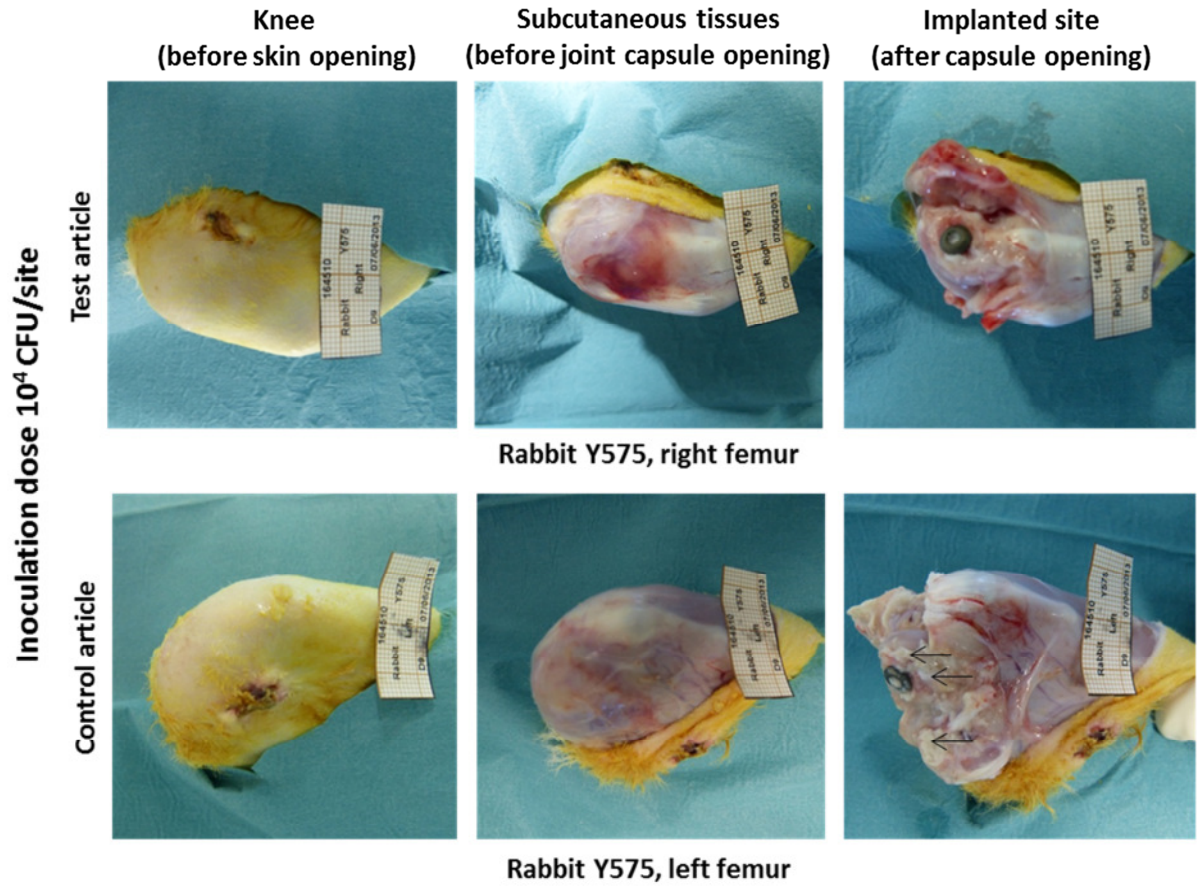


Figure 89: Macroscopic pictures at termination (day 9) – 10^4 CFU inoculation dose; --> white deposit (suspicion of pus)

4.3.3.4 X-ray evaluation

The mean radiographic score was higher for the control group than for the test group for all inoculation doses, and the score increased with inoculation dose. Osteolysis around articles was frequently observed for all inoculations doses while joint effusion and soft tissue swelling were only observed for the control group inoculated with the higher dose.

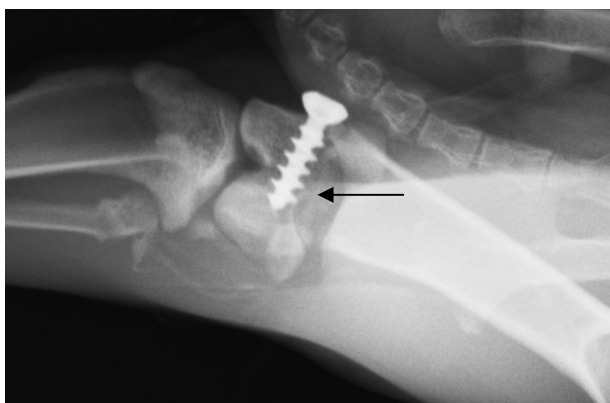


Figure 90: X-ray of the left femur of rabbit X1648 treated with control screw – 10^5 inoculation dose – day 9

————▶ Signs of osteolysis

4.3.3.5 Microbiological analysis

After removal of the test articles, the absence of an inhibitory effect during bacterial count was evidenced for two extracts. Moreover, the dosage of the antibiotic evidenced no residual Tobramycin in the extracts. This was confirmed by HPLC measurements after removal of the articles and storage in PBS buffer. The results of the microbial analysis were therefore considered as valid.

After 9 days of implantation, for the 10^7 CFU inoculation dose, a lower number of bacteria were recovered from the test article compared to the control article ($6.3E+02$ versus $1.46E+05$ CFU/article). For the 10^5 CFU inoculation dose, no bacteria could be recovered from the explanted test article while $2.85 \cdot 10^5 \pm 1.38 \cdot 10^5$ CFU were recovered from the control article, see Table 17. The group inoculated with 10^4 CFU per site demonstrated no

Results

bacterial recovery for 2 sites of the test group after 9 days of implantation. For one test site a number of 1.36E+05 CFU were determined. For all control articles in this inoculation group bacteria were recovered in the range from 1.85E+05 to 6.03E+05 CFU per implant.

Table 17: Overview of the bacterial counts on the explanted sites after 9 days.

Inoculation dose (CFU/site)	Article	Rabbit	Site	Bacterial count on the explanted article (CFU/article)
10⁴	Control	Y575	Left	1.85E+05
		Y594	Left	6.03E+05
		Y653	Right	2.42E+05
	Test	Y575	Right	<10
		Y594	Right	<10
		Y653	Left	1.36E+05
10⁵	Control	X1648	Left	1.47E+05
		X1685	Left	4.23E+05
	Test	X1648	Right	<90
		X1685	Right	<90
10⁷	Control	X1686	Right	1.46E+05
	Test	X1686	Left	6.30E+02

4.3.3.6 Histology

At days 2, 5, 7 and notably at day 9, for the inoculation dose prepared at 10^4 , 10^5 or 10^7 CFU, the test group showed in general lower level of tissue lesions related to signs of infection compared to the control group. Lower signs of infection were observed with the lower inoculation dose compared with the higher inoculation dose. Due to the low number of specimens analyzed these results can only give a hint and should be considered with caution. The infection signs were mostly observed around the tip of the screws in the two groups. Necrotizing bone debris was observed around the screws. These bone debris, presumably occurring during surgery, could have induced an additional inflammatory response linked to the necrotizing process but this did not compromise the histopathological evaluation of the antibacterial performance of the test article. After day 2 for the inoculation dose prepared at 10^5 or 10^7 CFU, the test group showed lower level of tissue lesions related to signs of infection compared to the control group. Lower signs of infection were observed with the lower inoculation dose compared with the higher inoculation dose. At day 5 for the inoculation of 10^4 CFU fewer signs of infection were observed with the test group than with the control group. At day 7 for the inoculation dose prepared at 10^5 or 10^7 CFU, the test group showed lower level of tissue lesions related to signs of infection compared to the control group. The tissue lesions were extended compared to day 2 in the two groups. After day 9 for the inoculation dose prepared at 10^5 CFU, the test group showed a noticeable lower level of tissue lesions related to signs of infection compared to the control group, see Figure 91. The tissue lesions were only observed to be extended for the day 9 control group.

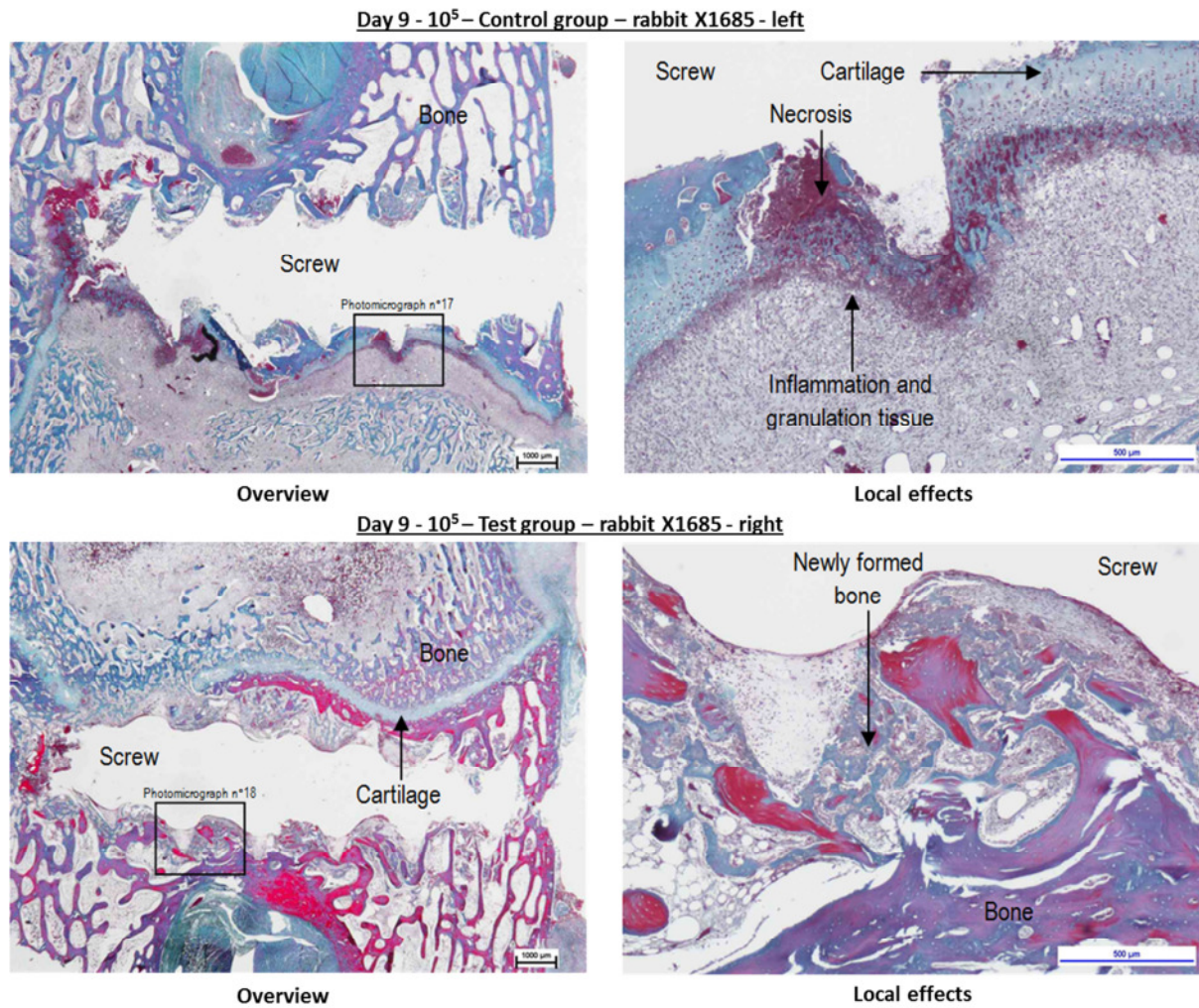


Figure 91: Histopathological photographs of non-coated screws (control group) in comparison to Tobramycin HA-coated screws (test group) after 9 days in an in-vivo infection model treated with 10⁵ CFU per defect.

For the 10⁷ CFU inoculation dose the test group showed lower level of infection related tissue lesions compared to the control group, see Figure 92.

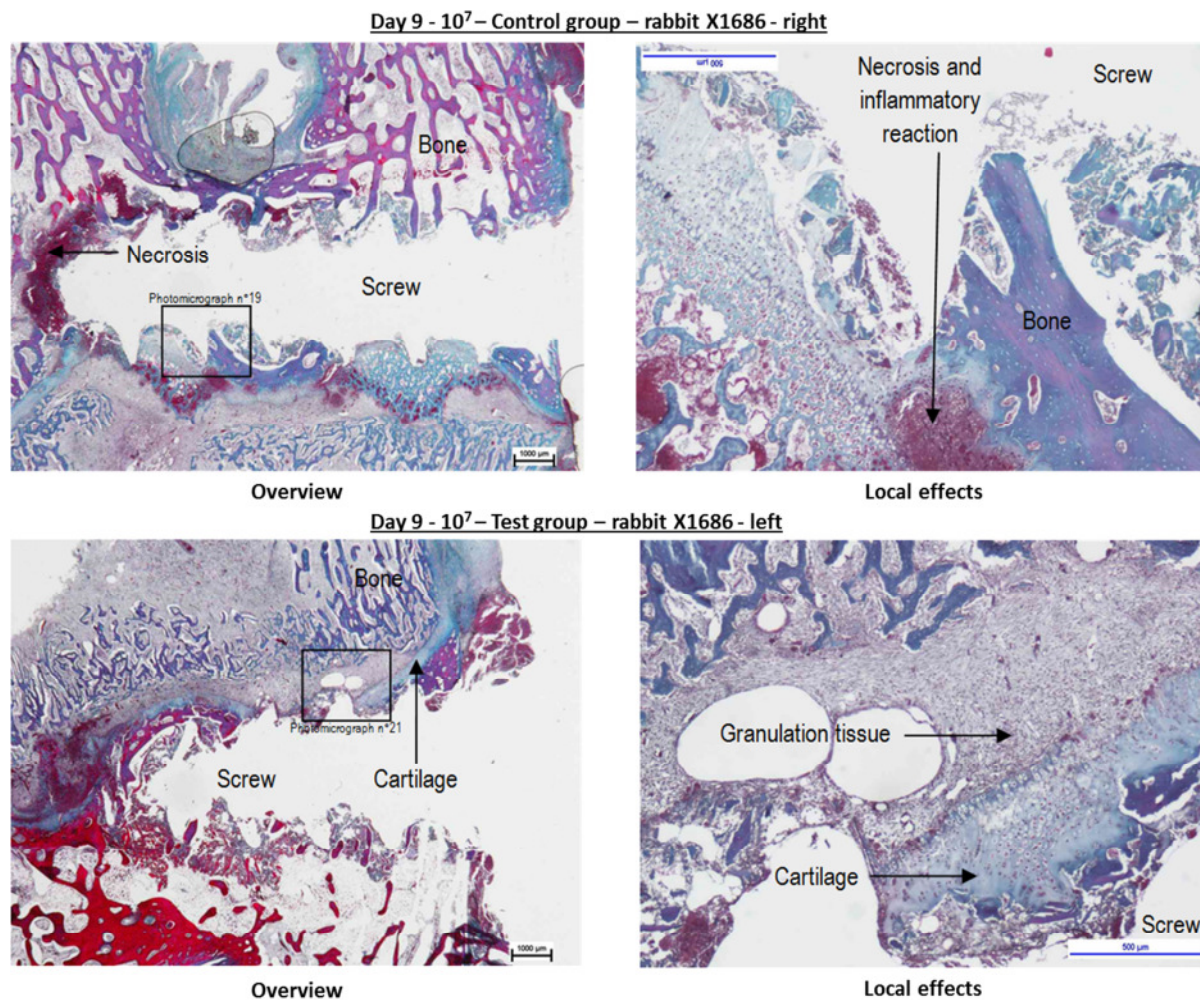


Figure 92: Histopathological photographs of non-coated screws (control group) in comparison to Tobramycin HA-coated screws (test group) after 9 days in an in-vivo infection model treated with 10⁷ CFU per defect.

For the inoculation group of 10⁴ CFU per site the test group showed a lower score of tissue lesions related to signs of infection at day 5 and day 9 as compared to the control group, see Figure 93. At day 9, one of the test sites (Y653) did not show a significant effect of the antibiotic.

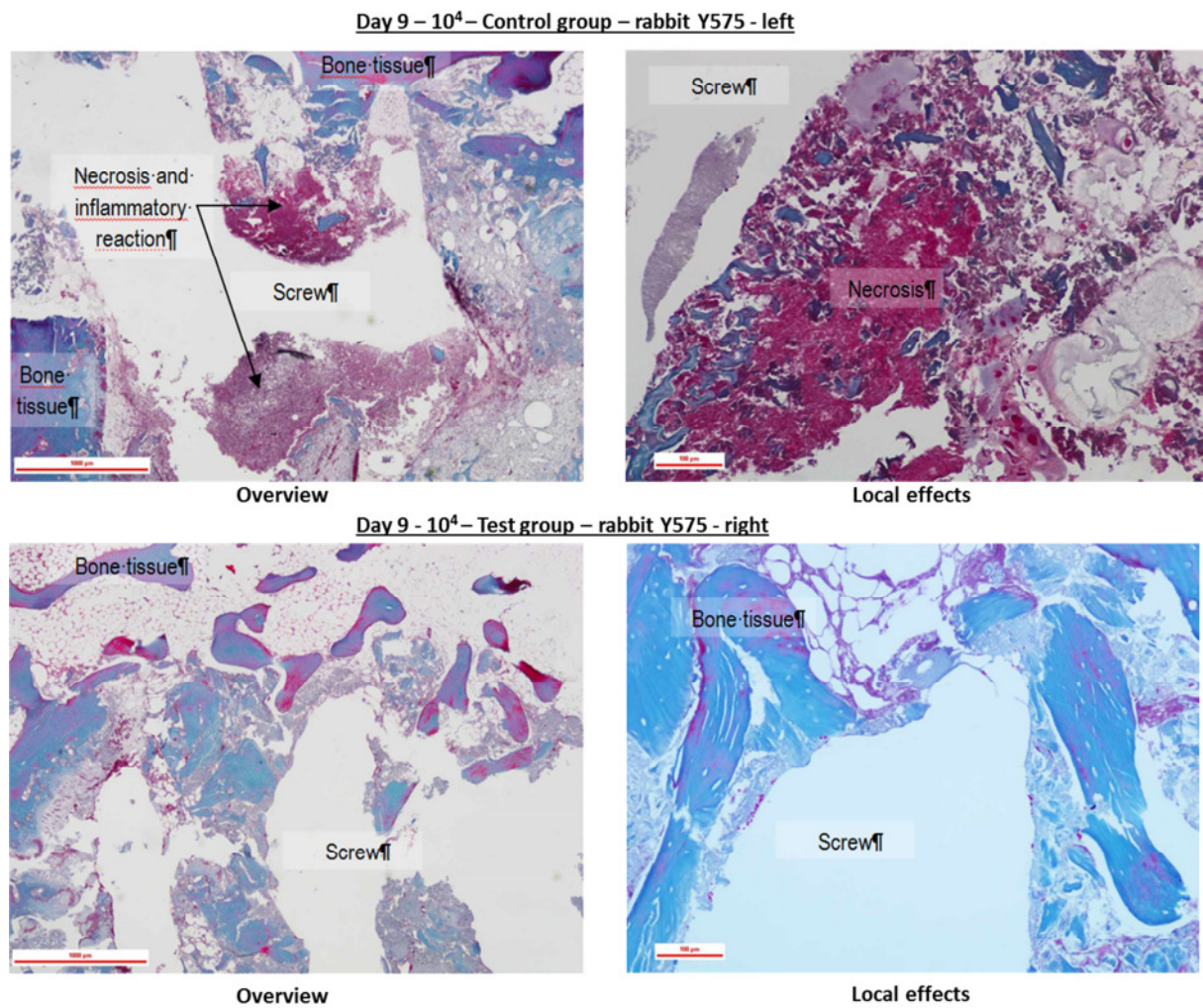


Figure 93: Histopathological photographs of non-coated screws (control group) in comparison to Tobramycin HA-coated screws (test group) after 9 days in an in-vivo infection model treated with 10⁴ CFU per defect.

5 Discussion

In keeping with the overall structure of the thesis and to guide the reader in a structured way through the present research, the discussion is divided into three main parts: the in-vitro investigations on stainless steel and on titanium followed by the in-vivo part performed with titanium screws.

5.1 HA on stainless steel

5.1.1 HA coating comparison

In the first part of the investigations dealing with HA coatings on stainless steel the different properties of biomimetic and plasma sprayed HA coatings were evaluated in terms of HA coating structure, Tobramycin loading and release parameters. Morphology, topography and microstructure showed differences comparing both types of HA coatings. Plasma sprayed HA coatings are manufactured at high process temperature resulting in a very dense “asphalt-like” structure usually demonstrating very slow degradation rates in-vivo [110]. In contrast, the biomimetic coating is a gentler process with parameters evolving over a much longer time period [9,111,112]. Therefore, the HA crystal structure can build up slowly resulting in a highly crystalline layer of HA, confirmed by Figure 33, which is expected to be adsorbed in-vivo much more rapidly. Moreover the different thicknesses of HA coating play a major role in the speed of overall resorption. The HA-P coatings demonstrated a much higher density and thickness ($\sim 50 \mu\text{m}$) compared to the thin ($\sim 5 \mu\text{m}$) and nanoporous structure of the HA-B coatings. Due to the high density and the relatively small surface area of the HA-P coating, drug loading could only be achieved by adsorption through a drying process. The Tobramycin adheres by drying on the outer surface structure resulting in a second coating. For the nanoporous biomimetic HA it is reported that drug incorporation into deeper areas of the

coating can be achieved resulting in sustained release times [113], which is also confirmed by the results obtained in this study.

5.1.2 Drug loading and release studies

Tobramycin loading and release properties of biomimetic and plasma sprayed HA coated fixation pins were systematically investigated with respect to HA coating structure and drug loading parameters. The results of this study show that coating porosity and selected physical conditions for loading, such as temperature and pressure, are important parameters for tailoring of the release profile. An initial burst like release was observed in both biomimetically deposited HA-B samples and plasma sprayed HA-P samples. No release following this initial burst could be observed for HA-P samples loaded at room temperature, while a sustained release period during 2 days was achieved from the corresponding HA-B samples. It is assumed that the nanoporous structure of the HA-B samples, facilitated drug loading into deeper pores of such coatings, thus, enabling a longer drug release period. The denser structure of HA-P samples, most likely restricts the drug penetration depth of these samples making drug deposition possible only through surface adsorption. These findings are in agreement with results obtained in previous studies [10,92,113,114]. Whilst in contrast to what has been observed in earlier studies, no clear correlation could be found between soaking time and total drug loading capacity for the room temperature loaded samples [92]. Both coating types showed the capability to absorb and release similar amounts of Tobramycin during RT loading. This observation may be related to the fact that the rough surface topography of HA-P coatings provides a particularly suitable surface favoring superficial drug adsorption. If it is assumed that the drug resides on the outermost surface of the HA-P samples, the phase composition of these coatings might additionally

influence the amount of drug able to bind to the surface. The combination of lower crystallinity and the presence of amorphous phase within the HA-P coating structure may give rise to a variation in the Ca-content of these coating types and, hence, influence the ability to bind to the drug molecule [92].

A linear correlation was observed between the drug loading concentration and the amount of Tobramycin released during the initial burst release period from HA-P and HA-B coatings for all concentrations tested. This correlation was anticipated since the initial burst, according to the above discussion, is expected to stem from Tobramycin adsorbing at the outer surface layer of the coating, and the amount present in this layer to correlate to the concentration in the loading solution.

No strong dependence was found between the antibiotic concentration used during loading and the amount released during the sustained release period from the HA-B samples. The lack of correlation may be attributed to the assumption that a concentration restricted amount of Tobramycin was present in the pore structure. As described by Stigter et al. [92], the molecular structure of Tobramycin determines the interaction with HA and may, therefore, limit the incorporation of the drug into the structure to a maximum value, as indicated for concentrations greater than 20 mg/ml.

The nanoporous structure of the HA-B coatings was further shown to play an important role in influencing the loading capacity and the sustained release profile. Drug loading at elevated pressure and temperature contributed to a significantly prolonged sustained release period, as well as to an increased amount of total drug incorporated. This was most likely due to penetration of Tobramycin into deeper regions of the coating structure which was confirmed by the C- and N-depth profile of the coatings measured by GD-OES. The increased pressure during drug loading also resulted in sustained release for the HA-P samples, however the

release period was shorter than observed in the HA-B samples. The sustained release seen in the samples loaded at higher temperatures and pressure is most probably due to the penetration of the Tobramycin solution into micropores present in the coating structure.

Increased pressure contributed to increase both the amount released during the initial burst period as well as during the sustained release period for both coating types under study.

Whilst elevated temperature had the opposite effect on the initial burst release.

The viscosity of the antibiotic loading solution decreases with increased temperature and at the same time the antibiotic diffusion coefficient would be expected to increase [115].

Hence, Tobramycin should be able to penetrate further into the coating structure whilst loading for 5 min at 90 °C when compared to loading over the same time period at room temperature. This readily explains the results showing that both Load-HT coatings under study (HA-B and HA-P) release more during the last period of detectable release than the corresponding Ref-RT samples (30 and 60 min time points for HA-P and 2 day time point for HA-B). The fact that the elevated temperature also results in a diminishing amount of drug adsorbed in the surface regions of the coating, as evidenced by the diminished burst release, shows that the temperature of 90°C is high enough to prevent some of the drug molecules from binding to sites in this surface region. A proportion of the drug that is hindered from binding diffuses into the coating, but since the total amount of drug residing in the Load-HT coatings is lower than the corresponding amount for the Ref-RT samples, one can conclude that a significant fraction is re-diffusing back into the loading solution. Additionally, the viscosity of the solution at elevated temperature is decreased. Therefore, the stock solution drops off from the implant more easily during the drying procedure resulting in a thinner Tobramycin coat compared to loading at room temperature.

The nitrogen concentration profile of the HA-B Load-HT coating gives further support to the distribution of antibiotics in the coatings described above.

The effect of temperature assumed to influence drug distribution is further supported by the release profiles observed from the Load-PHT samples. Whereas elevated pressure and temperature both increase the penetration depth of the drug during loading, these parameters counteract each other when it comes to drug incorporation in the surface regions of the coatings. The HA-B coatings show sustained Tobramycin release for as long as 8 days whereas the release from the HA-P coatings continues for 2 days instead of just 15 minutes (Ref-RT). The surface binding inhibition induced by elevated temperature results in a lower total amount of Tobramycin incorporated in the HA-P Load-PHT samples as compared to the corresponding Ref-RT samples. For the HA-B samples, on the other hand, the porous coating structure ensures pre dominance of the increased penetration depth effect over the surface binding inhibition effect. This resulted in an increased total amount of drug incorporated in the HA-B Load-PHT samples compared to the corresponding Ref-RT samples.

The HA crystal growth observed on HA-P coatings, confirmed the low overall release of Tobramycin from these surfaces and that the plasma sprayed surface is bioactive. As published in earlier work [9,92] the presence of drugs in the PBS buffer hinders the formation and growth of HA crystals on bioactive surfaces and therefore no HA formation is to be expected with Tobramycin eluting from the HA-P coating.

In summary, the presented findings emphasize the advantages of the nanoporous structure of biomimetically deposited HA over the more dense structure of plasma sprayed HA coatings in terms of antibiotic incorporation and subsequent sustained release.

In addition, the impact of HA-B coating characteristics, such as coating thickness and morphology, on the drug loading and release properties of HA coated fixation pins were assessed. Furthermore, the biomechanical properties of HA-B coatings were evaluated by means of adhesion and insertion testing. The antibiotic release showed that HA coating thickness, coating morphology and topography, as well as physical loading conditions play a major role impacting on the drug release kinetics.

The coating thickness of biomimetic coatings manufactured at 37°C (HA-B_37) samples was shown to influence the loading capacity and the sustained release profile for loading under room temperature and atmospheric pressure conditions. Greater amounts of Tobramycin were incorporated and released from 5 μm than from 2 μm coated pins, which confirms that not only the outer but also the inner part of the nanoporous structure of the HA-B plays an essential role. Deeper sections show drug incorporation that controls the drug release kinetic, which is confirmed by drug penetration measurements with GD-OES. With respect to the structural variation with coating thickness, it is most likely that the thicker HA-B coatings offer a greater surface area connected to a deeper penetration depth of drug solution compared to the 2 μm thick coatings.

Loading at increased temperature and pressure conditions greater amounts of antibiotic were released from pins with a 2 μm thick coating at the beginning of the sustained release period (time points 4h and 2d) compared to room temperature loading. This could be explained by a difference in porosity and surface area between the HA coatings of different thicknesses. Tobramycin penetration depth of about 3 μm can be expected under these conditions, which would theoretically allow incorporation of the antibiotic in pores close to the HA-B/TiO₂ interface for the thinner HA coatings. However, no GD-OES measurements were performed with this specific HA thickness to confirm this.

HA coatings with a thickness of 1 μm , which were manufactured at 60°C, showed complete release after only 4h and is confirmation of a dense HA coating structure. The incorporation of drug throughout the coating structure of these samples is therefore inhibited and further results in a physical drug adsorption process during drying. The extended release period of 8 days obtained after PHT loading can be attributed to an increased diffusion that allows the antibiotic to penetrate into denser pore structures in combination with outer pressure and higher temperature, which forces the solution in deeper pores. The thicker coating structures up to 5 μm could promote preferential penetration of the drug into the interior of the coatings instead of surface binding. This would result in an increased total amount of drug incorporated in these coatings under elevated temperature and pressure compared to the corresponding room temperature loaded samples.

5.1.3 Biomechanical behavior of biomimetic HA coatings

The biomechanical insertion tests demonstrated that all HA-B coatings studied required very similar insertion torques and generated similar temperature increases in comparison with TiO_2 covered pins and uncoated stainless steel pins. These insertion characteristics are superior to those of thicker plasma sprayed HA coated fixation pins, which have been shown to require up to 50 % higher insertion torques than uncoated implants due to the high surface roughness of such coatings [116–118]. The reduced insertion torque is expected to be beneficial during surgery, thus, external fixators are inserted into bone without predrilling. The observed HA-B coating wear pattern confirms a stress concentration at the pin entry site for all sample types and was confirmed by 3D microvisualization imaging. In accordance with literature [119], there is a reduction in stress value away from the pin entry along the pin axis. The stress distribution at the pin interface reveals build-up of stress at the

roots (curvature) of the thread in the x-direction whereas in the y-direction (loading axis) high stress is observed at the crest of the thread. In agreement with the SEM images of the HA-B coatings recorded after insertions, coating flake-off at thread tops can be attributed to high stress concentration in these areas. In contrast, shear stresses, which are concentrated around the vicinity of the roots and crests along the entire length of the thread, may contribute to the coating compression and smearing observed. Pin diameter and length, the length of the thread, and the thread shape and form are known to influence the forces experienced by the pin [120]. As seen from the comparison of insertion into synthetic materials mimicking different bone qualities, the density of the bone also influences the forces required for insertion. The 25 PU foam seemed to be more abrasive compared to denser Renshape material. The increased HA-B coating deterioration observed after insertion into 25 PU foam may be attributed to higher stress concentration at the interface between pin and synthetic bone material and thus increasing the tendency of the HA-B coating to fail.

5.1.4 Drug release after biomechanical treatment

For successful clinical implementation of antibiotic loaded HA coated implants the mechanical stability of the HA layer as well as the change in drug release profile after insertion are considered to be important criteria [121,122]. In relation to mechanical stability of HA-B coatings and local release of drugs from the same, the question arises of what would happen to the antibiotic release profile after insertion? The biomechanical forces led to HA smearing, compression and wear effects, affecting the drug release.

A decrease of the amount of Tobramycin released for all sample types investigated was observed. The most significant reduction, in the order of 50%, was seen during the initial

burst period of the release. This shows that a substantial amount of antibiotics is loaded by adsorption directly in the outer surface region in agreement with earlier findings [30]. During the sustained release period, insertion-induced wear had only minor effects on the drug release process from deeper sections of the coating.

Antibiotic release profiles of co-precipitated samples suffered less from biomechanical insertion effects than HA samples that were drug loaded after coating deposition. Reduced changes in release kinetics may be related to the coating growth conditions, which could result in different mechanical coating properties or be connected to the lower coating thickness of the co-precipitated Co-4 samples. The delaminated HA coating was found to remain within the synthetic bone material for all sample types. During *in-vivo* bone insertion, the screw design, the friction at the coating interface as well as the bone density will be factors influencing the insertion torque and coating wear properties [120]. In fact, blood and fatty substances *in-vivo* may act as lubricants and, hence, contribute to reducing the dry conditions prevailing in HA coating wear during insertion into synthetic bone [123]. Also, the delaminated HA fragments remain within the bone and will contribute positively to the local antibiotic effect. A critical area for bacterial infiltration after treatment with external fixators is the entry point of the pin [124]. It would be ideal to protect this area by high local concentrations of antibiotic. Therefore coating wear effects at the entry point can contribute to higher drug concentrations and increase local protection at the site of action. Furthermore, the rather smooth topography seen in biomimetic HA coatings could be an additional advantage in minimizing insertion torques as well as to minimizing heat generated during insertion that might lead to thermal necrosis.

5.1.5 Scratch test

Conventional scratch testing confirmed that the interface between the TiO₂ and HA-B coating is a critical factor with respect to the adhesive strength of the coating system. Poor adhesion between ceramic coatings and substrates has been discussed in earlier studies [58,125,126]. Plasma sprayed HA coatings exhibit superior adhesion compared to HA coatings deposited by biomimetic solution based methods [127], which may be explained by the highly porous structure of the HA-B coating. The critical loading forces obtained in this study were greater than those values previously reported [128,129], especially considering the rather thin HA coatings and the fact that the $F_{N,C}$ value is expected to increase with increasing coating thickness [130]. The high adhesion strength of the HA-B coatings in the present study may be attributed to the bioactive properties of the TiO₂ layer, resulting in strong chemical bonding between HA and TiO₂. Similar $F_{N,C}$ values were obtained for both biomimetic HA coating thicknesses manufactured at 37°C process temperature. Hence, increased HA-B coating thickness seems to result in an adverse effect on the adhesion strength [130]. The presence of residual stress is known to increase the tendency of HA coatings to fail [131]. The residual stresses in the coating can have a negative impact on the adhesion of the coating towards the substrate. Thus, the $F_{N,C}$ value obtained for HA-B_37 (5µm) coating may reflect the presence of structure related residual stress resulting from coating deposition [129]. Thinner HA coatings, manufactured at 60°C process temperature, on the other hand, showed promising adhesion properties, especially when considering the feature of the spalling and size of coating fragments. This strength may be attributed to the HA growth conditions at elevated temperature [132]. Smaller crystals may give rise to an increased contact area with the TiO₂ covered substrate as well as less growth-induced stress present in these coating types.

In agreement with the biomechanical insertion tests, excellent cohesive and adhesive strengths were found for the TiO₂/stainless steel interface. The cracks observed in coating structure for manufactured at higher process temperature can be attributed to the bending stresses induced by the indenter tip during scratching.

5.1.6 Antibacterial properties

The antibacterial efficacy against *Staph. aureus* was evaluated in a modified agar diffusion test arrangement. The agar plates were freshly incubated each day of the experiment with new bacteria mimicking a new infection and a high bacterial concentration present at the implant surfaces. A sizeable and circular inhibition zone, induced by radial drug from the implant into the agar medium, was detected for all antibiotic loaded samples. Thus, it may be expected that the diffusion of the antibiotics into the surroundings of the implant would not only inhibit bacterial growth at the pin surface, but also combat bacterial growth in the close proximity of the implant. This release-triggered drug diffusion could be an advantage compared to other antibacterial coatings that only protect the implant surface from bacterial attachment and biofilm formation [94,133–135]. The roll-out test confirmed protection of all investigated antibiotics loaded sample types against early bacterial attachment. In contrast, unloaded HA samples did not reveal any inhibition effects. Thus, bacterial colonization and biofilm formation would be expected for unloaded samples. The antibiotic containing samples loaded under different loading conditions (RT and PHT) showed visible inhibition zones up to 6 days, with the zones generally being large for RT loaded samples. HPLC drug release studies in PBS have revealed a Tobramycin concentration eluting from RT and PHT sample types during a time period of 2 and 8 days, respectively. Nevertheless, the present study shows that antibacterial properties are not significantly influenced by the loading method applied as confirmed by comparable inhibition zones for all sample types. The fact that no clear difference in antibacterial efficiency can be attributed to the different sample types might be explained by different diffusion behavior of the drug molecule in agar and PBS. The inhibition zone sizes are not directly comparable to the amounts of drug released. During incubation, the Tobramycin molecules are able to diffuse a

certain distance from the pin surface and inhibit growth of bacteria in the area they cover, if the amount of antibiotic released is equal to or greater than the MIC. In PBS, under sink conditions, the gradient in concentration is expected to be higher and hence give rise to a faster diffusion of Tobramycin. RT_BML samples, which were exposed to biomechanical forces prior to inhibition testing, generated a slightly smaller inhibition zone than the other samples. The zone, however, appeared to be circular and centered despite the mechanical treatment. Therefore, it might be speculated that the HA-B coating flake-off occurring during insertion in real bone would have a minor impact on the drug release profile over time. Furthermore, the coating deterioration is mainly expected to occur at the pin entry point of drilling, which would most likely result in higher Tobramycin concentrations at the bone entry site and adjacent soft tissues, where bacteria may be expected to enter during surgery.

5.1.7 Cell studies

Cell tests indicated that both investigated cell types firmly adhered to both pure TiO₂ and biomimetic HA coated surfaces with no obvious effect on the cellular viability of endothelial cells or primary osteoblasts. These findings can be considered as a first indicator for the biocompatibility of both types of materials surfaces. TiO₂ on its own allows the cell adhesion of bone forming cells. Hence, a potential delamination of the HA coating by mechanical forces would still result in cellular attachment. After introduction of the implant into bone the osteoblasts are in close contact with the implant surface and firmly fixed to the surfaces of fixation pins with osteoconductive and osteoinductive properties. Nevertheless, endothelial cells also play a major role as indicators in biocompatibility assessment [100,101]. Endothelial cells are highly sensitive to substances leaching out from scaffolding materials, or to unsuitable surface topographies of implant materials interfering with

endothelial cell attachment and bone vascularization. In addition, they are very sensitive to inflammatory stimuli with potentially severe consequences regarding the acceptance of implant materials. Although these first results are *in vitro* assessment, there are no contraindications in terms of the biocompatibility of the proposed materials and their modifications, as also recently reported for TiO₂ surfaces used for bone tissue engineering applications [136]. Overall, the excellent biocompatibility of HA was as expected, because in general, HA has an excellent history of biocompatibility [43].

5.1.8 Co-precipitation of Tobramycin into HA coatings

A further part of the present research demonstrated the feasibility of co-precipitate pharmaceutically relevant doses of Tobramycin into the biomimetic coating during coating deposition. In agreement with previous studies, the process of HA crystallization on bioactive substrates is strongly affected by the concentration of drug to be incorporated in PBS [29,92] as well as the process temperature. The presence of Tobramycin in PBS resulted in a decreased coating thickness compared to pure biomimetically deposited HA coatings [30]. An elevated PBS temperature allowed production of drug containing coatings for concentrations up to 1.0 mg/ml demonstrating rough ball-like morphology in the present investigations. As described by Lindberg et al. at higher process temperatures increased ion mobility can be expected, which can contribute to enhance HA nucleation and growth [111]. This hypothesis is supported by the current findings in which the coating growth were observed at increased temperature even in the presence of minor amounts of Tobramycin. In comparison, lower process temperatures in combination with higher concentrations of Tobramycin seemed to inhibit crystallization of HA on TiO₂ substrates. This might be explained by the fact that Tobramycin could act as an anticatalyst for the HA nucleation

process under these conditions [29,92]. The Tobramycin-induced inhibition of nucleation seems to decrease at higher temperatures and lower concentrations. At these conditions the solubility product of HA seems to be exceeded and thus, nucleation of HA seed crystals can occur. Nevertheless, a combination of higher ion mobility and changes in solubility products may affect the differences in crystallization observed. This may also explain the impact of the HA start layer on coating growth in the presence of Tobramycin. The HA coating might act like a seed crystal for all following coating growth steps and, hence, facilitate HA growth at lower process temperatures and higher concentrations of Tobramycin.

SEM analysis demonstrated needle-like morphology for Co-4 coatings grown at 37 °C. Coatings deposited at elevated temperature and in the presence of minor amounts of Tobramycin showed a change in morphology from needle- to ball-like appearance. A comparable change in morphology was observed in case of increased Tobramycin concentrations where, in addition, the formation of agglomerates on the coating surface was observed. Thus, it may be concluded that Tobramycin influences the morphology of the coating grown during co-precipitation. At a critical antibiotic concentration, nucleation and growth might be limited and even inhibited [9,92] as supported by the decrease in coating thickness and morphology with increasing drug concentrations. Elevated process temperature on the other hand improves nucleation and growth up to Tobramycin concentrations of 1 mg/ml, which may be attributed to the previously described impact of temperature on the growth kinetics. Furthermore, it may be speculated that high drug concentrations could lead to drug-drug interactions during the adsorption and crystallization processes, which minimize the chances of nucleation.

In summary, it can be concluded that Tobramycin has an effect on the development of the co-precipitated coating itself and can be classified as an impact factor for coating growth and development even in the presence of an HA start layer.

The deposition of a sub-micron thin HA start layer allowed for incorporation of higher concentrations of Tobramycin during coating growth. It is speculated that Tobramycin has a higher binding energy to HA when compared to TiO₂ which, hence, allows for co-precipitation at high drug concentrations even at low temperatures. The HA coating thickness supports the speculated preferential binding of Tobramycin to HA with increased thickness. The release profile demonstrated an enhanced release period of 12 days. The released amounts of Tobramycin were found above the MIC of *Staph. aureus* [81] which is defined as 0.2 µg/ml. These values were measured under sink conditions in PBS, which provide suitable *in vitro* conditions for evaluating the application of antibiotic releasing coatings in the fields of medical implants.

Co-precipitated samples released comparable amounts of drug during the initial burst period as did adsorptively loaded samples made using similar concentrations of drugs [30]. Nevertheless, the sustained release period showed superior amounts of drug released from co-precipitated samples. GD-OES measurements confirmed the drug incorporation throughout the entire coating thickness and, hence, an increased amount of drug released can be expected during the sustained release period deriving from drug released from deeper and denser sections of the coating.

The nanoporous structure of co-precipitated coatings revealed an ability to incorporate higher amounts of antibiotic by additional adsorptive loading. Thus, the deposition of co-

precipitated coatings allows for additional means of designing release profiles that could further enable targeted drug release in specific clinical applications.

The coating deposition method presented allows incorporation of pharmaceutically relevant amounts of drug in a single step approach. In addition, the release properties are superior to those previously reported [30,92,137] and are anticipated to provide an enhanced antibacterial effect that significantly exceeds the 3 day benchmark reported in literature [113,138].

In summary, the starting phase of crystallization presents a very important part for coating deposition using the co-precipitation approach. Surface chemistry as well as process temperature are important factors that have been shown to impact coating growth, thickness and the morphology of drug-doped HA coatings.

5.2 HA on titanium

As described earlier it was shown to be feasible to homogeneously deposit ultra-thin HA coatings on anodized Ti screws. The coating thickness in the range of 1-2 μm was judged to be the coating of choice because it resulted in less self-cracking, less agglomerates and a very homogeneous appearance overall. Additionally, the thin HA coating was designed for effective drug uptake and it was anticipated to be remodeled very rapidly in-vivo. The coating was developed to meet an unusual set of requirements i.e. to increase early holding power (as measured by screw pullout), while at the same time ensure safe removal without extensive damage to either the bone or the soft tissue, which has yet to be proven. It was shown that the nanoporous structure of the HA coating is able to load and deliver clinically relevant and effective amounts of Tobramycin in-vitro and in-vivo over a reasonable period of time.

5.2.1 NaOH pretreatment

The impact of NaOH pretreatment on the surface morphology and topography was analyzed. Extensive etching of the surface resulted in a higher roughness and incidence of cracks in the surface itself. Substrate pretreatment, in general deposition of HA on Titanium has been described earlier using biomimetic methods. But a general consensus in the literature is that the surface charge of Ti need to be negative for the HA to grow. A negative surface charge can be achieved via surface modifications, e.g. soaking the surface in NaOH, depositing a crystalline TiO_2 surface on the titanium [10,58,139,140]. Normally, the NaOH pretreatment is performed for hours, followed by the HA coating process. In this study, the aim was not to modify or change the properties of the commercially available implant surface. This surface was of the anodized titanium type II which shows excellent biocompatibility, biomechanical

properties and in-vivo performance [141]. Extensive acid etching, resulting in surface roughening, can demonstrate different in-vivo behavior compared to machined surfaces. The etching changes the initial surface properties resulting in higher osseointegration strength [142]. The goal in the present study was to take an as finished implant with the standard anodization type II surface followed by addition of the thin HA coating. Hence, optimization of the NaOH pretreatment was necessary. 10 minutes of pretreatment did not result in any morphological observable change of the surface structure as shown by SEM, while ensuring the ability of biomimetic HA growth on this specific surface. Two specific benefits were expected to result from this optimization step. Knowing of the good osteoconductive characteristics of HA in-vivo, the coating was intended to ensure fast local bone apposition and firmly connect the implant to the bone structure. After full osseointegration, the theory is, that the HA coating completely remodels in-vivo. Afterwards the screw should be well integrated within the bony structure. At the same time the surface is intended to show the removal characteristic of an untreated anodized titanium type II screw. The HA coating was designed to be very thin to achieve fast remodeling. This effect will be evaluated and analyzed in a later part of the discussion dealing with the in-vivo HA performance main study, where the two types of surfaces are compared (HA coated versus non-coated). This represents a compromise, which is hard to achieve in orthopaedic and traumatology surgery. Nevertheless, in case of infections or implant failures it is absolutely necessary to ensure a safe implant removal strategy.

5.2.2 Drug loading and release studies

Different loading concentrations of Tobramycin in stock solution and their impact on the release kinetics were tested. An initial burst was linear correlated to the Tobramycin

concentration in stock solution demonstrating a concentration dependent adsorptive loading at the interface. Without special loading techniques such as temperature and pressure to force the stock solution deeper into the coating, the absorption processes of Tobramycin dominates the loading and results in a physical drying at the interface as discussed in section 5.1.2. The loading technique of soaking the screw in a stock solution enables a simple and fast way of drug incorporation, which may be applicable for use in certain clinical applications that may allow drug loading during surgery [32]. At the same time, the simple soaking method delivers a homogeneous distribution of drug onto the surface. Tobramycin was used as a model drug in accordance to the investigations conducted by Stigter et al [92]. It could be envisaged to use alternative antibiotics or even combinations of different drugs or ions and add them into the coating structure for local delivery. In this case, the biomimetic HA could be seen as a universal carrier for drug or ion incorporation and this ability could be regarded as an added implant feature. The first successful incorporation of different antibiotics was initially tested and reported by Stigter et al [143].

Several other loading techniques were analyzed and evaluated in respect of their release kinetics. Ultrasound or ultrasound in combination with vacuum demonstrated higher release values within the initial burst. Applied ultrasound seemed to increase the wettability of the surface. Some air bubbles were seen macroscopically and were eluted from the nanoporous structure of the HA coating. Therefore, it could be speculated, that these areas were refilled with Tobramycin stock solution, thus, showing higher amounts of Tobramycin incorporated and subsequently released. Nevertheless, the release stopped after 2 days. Applied vacuum

during loading seemed to have only minor impact on this loading technique. The effect might be more pronounced when testing thicker nanoporous coatings.

Loading with stock solutions with different pH values resulted in a slightly higher initial burst release values and overall, slightly higher amounts of Tobramycin released compared to loading at pH 7.4. The pH values were adjusted from pH 4 to pH 10 to ensure molecular stability of Tobramycin during loading. At pH 4 Tobramycin, with an isoelectric point of 8.2 [92], is positively charged. Therefore an interaction with negatively charged PO_4^{2-} groups can be speculated and may result in advanced binding. At a pH of 10 the Tobramycin molecules are negatively charged. Therefore an interaction with Ca^{2+} could be postulated. During the release tests in PBS buffer at pH 7.4 these interactions will disconnect immediately. This could explain a higher drug release at the early time periods. The loading at pH 7.4 is close to the isoelectric point of Tobramycin, where the Tobramycin molecule is uncharged. Therefore, it may be speculated that reduced binding interaction to the HA coating was observed and slightly smaller amounts were released.

Loading under elevated temperature and pressure demonstrated the longest release period up to 5 days in PBS. As confirmed in the earlier investigations with the stainless steel pins (GD-OES measurements), this loading technique appears to incorporate the Tobramycin into deeper sections of the coating structure. Elevated temperature results in a lower surface tension of the solution. Therefore it is expected that smaller pores fill with stock solution, which appears to increase in combination with pressure.

To summarize, all of the loading techniques tested could potentially be utilized in tailoring a desired release kinetic from the nanoporous ultra-thin HA coatings and could be used as a basis from which to design a desired release characteristic.

5.2.3 Antibacterial properties

The antibacterial properties were assessed in a modified agar diffusion test. *Staph. aureus* was selected as a test bacteria as it is one of the main bacteria implicated in implant associated infections [65]. A clear antibacterial effect of Tobramycin was detectable for all screws loaded. The implant itself and the near vicinity of the implant were protected against bacterial colonization over a period of 5 days. The hydrophilic Tobramycin was released from the implant surface and homogeneously distributed by active diffusion into the agar media. Self-evidently an agar gel media demonstrates different structural behavior compared to a bony in-vivo environment. Nevertheless, the results demonstrate a strong trend of local efficacy of the loaded implant tested. Additionally, different loading techniques were tested according their efficacy in agar media. It was found that the HA coating presence is necessary to create a sustained antibacterial effect around the implant (colonization). When loading Tobramycin onto an implant without HA coating, the release kinetic observed was completely different. Without the HA coating the antibiotic was released immediately. Fast antibiotic loading by adsorption into HA coatings was as effective as loading under evaluated temperature and pressure with regards to the antibacterial characteristic in agar. Thus, the fast loading by adsorption was sufficient for a sustained antimicrobial effect up to 5 days. This loading technique could also be performed intra-operatively. Another clinically relevant strain of bacteria is the methicillin resistant *Staph. aureus* (MRSA). For future evaluation of the local drug delivery system antibacterial efficacy against MRSA would also be of great interest.

5.2.4 Cell studies

The attachment of primary human osteoblasts and human endothelial cells to HA-coating structure compared to their attachment behavior to uncoated anodized Ti type II surfaces was assessed over a period of 14 days. In general, HA coated cancellous bone screws or other implant types would be in close contact to both cell types in an in-vivo environment. Therefore, the attachment of these cell types is of great interest providing important information on cell biocompatibility. The cells formed characteristically typical monolayers on both surface material types without the need for any additional fibronectin coating. A firm and biocompatible attachment was achieved for both, HA coated and uncoated materials which is consistent with the findings described in the literature [144]. Also the results obtained by CD 31 staining confirmed the formation of intact endothelial cells layer on both titanium and HA-coated titanium. Overall these results suggest good biocompatibility of HA-titanium assessed *in vitro* in association with two cell types important for bone repair. In conclusion good cell compatibility of the HA coating can be expected in-vivo.

In developing the present research further it would be desirable to do an additional cell study investigating the cell attachment in the presence of Tobramycin to test any possible signs of local toxicity of antibiotic loaded HA. Intact replication of osteoblasts at a concentration of < 200 µg/ml Tobramycin is reported in the study performed by Miclau et al. [145]. During in-vitro release testing in PBS the Tobramycin concentration delivered from HA coated Tobramycin loaded screws under study was in the range of 200 µg/ml. However this was measured in a static in-vitro environment. In-vivo concentrations are expected to slow down more rapidly due to blood supply in a dynamic biological environment. Impaired cell

replication and cell death were observed at concentrations of 400 and 10,000 $\mu\text{g/ml}$ [145]. However, Duewelhenke et al. [146] reported on aminoglycoside concentrations (Tobramycin, Gentamicin) up to 400 $\mu\text{g/ml}$ and this showed no negative effects in the metabolic activity on human osteoblasts. Cell testing with Tobramycin loaded HA coated screws are recommended to assure toxicity levels of the system under study.

5.3 In-vivo studies

5.3.1 HA performance study

5.3.1.1 Development of the test set-up

During the HA performance pilot phase [104] the operative technique and the biomechanical analyses were customized, trained on and validated. Additionally, the two week time period for a first test point was assessed. A standard (Stryker Corporation developed) surgical technique was chosen that was suitable for the screw size implanted in a standardized anatomical position in the femoral condyle of the rabbit. This anatomical location was known and proven, in earlier studies, to allow good implant fit and deliver reproducible results [147,148]. In the reported studies, the same reference screw implant were used in studies of screw augmentation effects by adding either bisphosphonates [147] or injectable calcium phosphate cements [148]; see Table 18. The operative technique in these studies featured an over-drilling technique in order to weaken the bone and to a certain degree mimic the osteoporotic characteristics of the bone. This approach was not used in the present research because the aim was to demonstrate differences in early and more rapid implant stabilization in normal quality bone in a healthy rabbit. Aged rabbits were chosen (> 24 weeks) to reduce the impact of biological variation due to the growth plate which is located in the femoral condyle. The reproducibility was very important for the biomechanical testing and the presence of the active growth plate in immature rabbits could be a disturbing factor. In order to minimize the inter-biological variance in data obtained from individual rabbits a bilateral approach was performed. This enabled evaluation of both control and test values measured in the same rabbit, see Figure 80. One concern was to ensure free access to the screw heads when conducting pull-out force measurements at the

2 and 6 week time points. To avoid bony ingrowth restricting access to the screw head the screw was not fully inserted and a gap was left between the head and the bone (see Figure 15). This technique has additional advantages. For the removal torque measurements, any difference in removal torque from test to control screw could be directly attributed to the change in the screw thread to bone interface rather than to any additional fixation effect due to bone ingrowth at the screw head. This reduced the variability of the measured pull-out forces and removal torques that could affect the measurement of the effect of the HA. The pilot phase test validated that the model could detect differences in surface properties.

During removal torque measurements different curve shapes were observed for control and test articles. At both 2 and 6 week time points a steep more or less linear increase of torque with angular displacement was demonstrated at low torsional angles. The test groups at both time points showed a general characteristic of an abrupt drop after the initial steep increase and then a transition to a much less steep slope of the curve. This strongly suggests that the implants had indeed disconnected or “broken free” from the surrounding bony structure. The control groups did not in general show this abrupt transition characteristic. It may be speculated that in the control implants the bony connections were not as well established at these time points. To evaluate the results obtained reproducible standard analysis methods had to be developed as there is no standard that covers the exact experimental set up. The approach chosen was to adapt ASTM F1622 [149] in which an offset line method is used. Accordingly an offset line starting at 1° angular displacement parallel to the steep initial slope was chosen drawn on each data curve and the intersection of this line with the test curve was defined as the removal torque. At larger angular displacements the control groups often showed an increase of torsional load and this was

concluded to be an artifact. An explanation of this is as follows, friction occurs between the screw driver and the screw head while the screw is being screwed out of the bone. The frictional force increases with increasing axial translation of the screw and this in turn creates a pressure on the flanks of the screw thread, which induces additional torque. It was considered that this frictional force effect is likely to be very low, compared to other effects, in the first part of the test (steep moment increase) and would only become relevant at higher torsion angles and so could be neglected.

Table 18: Overview of published studies using cancellous bone screws in a rabbit femoral condyle model

Study	Implant	Focus	Result
Rhoshan-Ghias et al. (2011)	Cancellous bone screw + Bisphosphonate coating	Screw augmentation	Local delivery of BP's enhances stability of bone screws
Larsson et al. (2012)	Cancellous bone screw + Hydroset®	Screw augmentation	Injectable calcium phosphate cement can significantly improve screw pull out strength
Larsson et al. (2012)	Cancellous bone screw + Hydroset®	Screw augmentation	

5.3.1.2 Terminations

The 2 and 6 weeks time points after implantation were selected very carefully prior to this study. As an early time period, 2 weeks after implantation was chosen, because several studies in rabbit bones demonstrated histological and biomechanical differences at 2 weeks in-vivo. Slaets et al. [150] reported of the presence of basic remodeling units in the surrounding bone, which was already maximal after 7 days of implantation. Guo-li et al. [151,152] studied the removal torques of implants at 2, 4 and 8 weeks in rabbits. He

reported a measureable difference in removal torques after these time points. Therefore, 2 weeks after implantation were selected as the time point of choice to assess early biological and biomechanical changes associated with the thin-HA coating. This time point was additionally confirmed by the pilot phase study results.

Within the HA performance study histological and μ -CT analyses as well as biomechanical forces at 6 weeks in-vivo were evaluated and assessed. The 6 week time period was selected as an appropriate time point to look at the histological and biomechanical behavior after full osseointegration of the implant. Slaets et al. [150] published that the length of the bone remodelling cycle is 6 weeks in the rabbit compared with about 4 months in humans. Sennerby et al. [153] support this view noting that bone around the implant was mature after 6 weeks as indicated by histology and biomechanical testing. Bone formation around and adjacent to screw implant thread at this time point was clearly observed by Rhoshan-Ghias et al. [147].

5.3.1.3 Findings

A number of innovative and unique results were generated by the in-vivo HA performance study in a rabbit femoral condyle model. Overall, the insertion torque of both control and test samples showed no significant differences for any of the groups tested. No additional surgical equipment was needed to implant screws coated with HA compared to the standard operative technique for commercially available screws. No tangible impact during insertion of the HA coated screw was verbally reported by the surgeon during implantation. Thus, it may be speculated, that the thin HA coating would have little impact during surgery on human patients. Although no influence during surgery was detectable, there were very substantial differences in in-vivo behavior that were measureable via histology and

biomechanical analyses. The measured removal torque significantly increased for the HA coated test article after 2 weeks compared to control articles. The same trend was also seen for the pull-out force after 2 weeks and this is supported by histology and micro-CT measurements as well. Therefore, more rapid early implant stabilization was demonstrated by the HA coating. Zhang and Zou [154] reported better surface bioactivity and osteoconductivity of HA coatings, which could lead to the higher biomechanical forces needed for removal and pull-out of the screw seen for the test articles under study. Eom et al. [155] confirmed that HA coatings are favorable in early loading stages. "Biologically, the early phase (days) after implantation of an implantable device is considered to be critical to the long-term implant stability" [156]. The HA coating appears to encourage early implant stabilization and therefore, ensures that initial implant placement is maintained [157,158]. After implantation the HA coating was modulating the early biological response of the bone and the surrounding tissue to the screw implant. In this situation the bone was not in direct contact with the metal implant, the contact interface consists of bone-like HA in contact with bone. Consequently, the body may not immediately react to the screw as a metallic foreign body. Faster and better cell attachment is likely the result with more rapid vascularization and calcification. It is speculated, that the human cells prefer the osteoconductive surface exposed by the HA to win the "race of the surface" against bacteria infiltrating during surgery. After the rapid cell attachment phase, the thin coating is then remodelled by osteoclasts and osteoblasts. This is imaginable during the initial weeks post-implantation and is due to the high crystallinity and small coating thickness of the HA. After HA remodelling and full osteointegration, the implant provided a good ingrowth and attachment to the bone, which was seen from histology. The values measured at 6 weeks for removal torques and pull-out forces comparing test samples and control articles resulted in

no statistically observable difference. Thus, no statistical significance was observed after 6 weeks in contrast to what was demonstrated at 2 weeks. This could be explained by the adsorption of the HA coating after full osteointegration. Within the SEM evaluation of the surface after screw removal only minor residual HA coating could be found on the HA coated screws after 2 and practically none at 6 weeks in-vivo. The wear off or delamination of the HA coating during insertion can be excluded as there was evidence of significant differences in behaviour between HA coated and non-coated screws. Therefore, it could be postulated that the thin HA coating remodelled very rapidly in-vivo and that the absence of the coating at 6 weeks enabled easy and safe removal of the HA coated screws. Another potential explanation could be that the HA coating disconnected during screw removal from the bone. This would be supported by the fact that only minor areas of HA coating could be seen even at 2 weeks in-vivo. The microstructure of the anodized titanium type II underlying the HA-coating was not changed by excessive NaOH pretreatment. Thus, the implant surface showed the same characteristics as seen for the non-coated reference implant after HA remodelling and the screw was removed without damage to the bone or to the surrounding tissue. Only minor differences in biomechanical testing were observed, which could suggest HA adsorption in-vivo or disconnection of the coating while unscrewing. Additionally, no signs of immune or inflammatory response could be demonstrated for the HA coating which is consistent to the results published by Rigo et al. [159]. The results obtained in this current research demonstrated biomechanical resistance of the HA coating during insertion in-vivo. This was also tested in-vitro on external fixation pins by using different synthetic bone qualities. Nevertheless in-vivo proof was lacking. It can only be speculated if and how much coating wear was seen during insertion in-vivo, but clearly effects of the coating could be demonstrated, which supports the hypothesis of minimal coating wear effects during

insertion in-vivo. The in-vitro insertion tests were performed in a dry environment. During in-vivo insertion the fluids like blood, saline and fatty substances could behave like lubricants and take care of reduced friction coating wear effects [123].

To summarize, at 2 weeks histological evaluation, pullout and torsion tests showed effects and suggest that the coating had a measureable influence. In contrast the μ -CT showed no detectable difference for the defined ROI. This means that the coating effects observed are concentrated directly at or very close to the interface between the screw and the bone. At 6 weeks small differences between test and control for torsion and pullout tests were seen. Both test and control are significantly higher with respect to the biomechanical measures than at 2 weeks, and additionally the μ -CT showed a trend towards increased bone volume in the test group. This is also confirmed in the histology. Therefore the HA coating seems to have an early very local effect and there are some signs, although non-significant, that this early effect is seen at the later time point in the form of increased bone formation. The absence of a μ -CT difference at 2 weeks can be seen as confirmation that the coating effects seen are only at or close the implant to bone interface. An effect at some distance from the implant was reported earlier both by Peter et al. and Wermelin et al. describing increased bone density caused by zoledronic acid eluting coatings. In these studies the active pharmaceutical ingredient was shown to have a significant effect on bone remodeling for a distance of up to 400 μ m [160-161]. This remodeling effects could not be detected at 2 weeks in the HA coating under study and confirms that effect of HA on its own is more a surface or close to surface phenomenon.

Micro-CT measurements performed after removal torque evaluation [108] gave information on the cortical thickness of the bones. The cortices were measured to be far below 1.5 mm.

Seebeck et al. [162] reported that 1.5 mm is the threshold above which the pull-out force is mainly influenced by the cortical rather than the cancellous bone in a limited human cadaver bone series. In the present study the mean cortical thicknesses at 0.62 mm for test and 0.57 for control are so far below this threshold that it is likely that the pull-out force measured is mostly generated by the underlying cancellous bone. The differences in pull-out forces could therefore be attributed to the surface properties of the HA coated screws vs. non-coated screws. Micro-CT measurements additionally demonstrated good implant integration in cancellous bone.

5.3.2 Infection in-vivo pilot study

5.3.2.1 Development of test set-up and study design

Intraosseous implantation in the rabbit is generally accepted as a relevant model for orthopaedic infected implantation studies. A test set-up was developed for testing the in-vivo efficacy of a commercially available screw coated with HA and loaded with Tobramycin compared to non-coated and non-loaded ones. The bacterial strain, its inoculation size, the inoculation method, the test durations as well as the administration of systemic antibiotic were considered as key factors for success and therefore evaluated very carefully.

Inoculation with *Staph. aureus* strain was selected because orthopaedic surgical wounds are infected more frequently by *Staph. aureus* than by any other micro-organism [65]. Figure 3 gives an overview of the bacteria strains of interest associated with nosocomial implant infections. The inoculation method and size was modified and adapted to the results obtained from the study inoculated with 10^5 and 10^7 CFU/site. For these test groups the inoculation was performed by splitting the bacterial suspension in two parts. 5 μ l were directly deposited on the screw and 5 μ l directly into the bone defect. This method was selected because it allowed homogeneous distribution of bacteria into the bone defect and it was tested during a rabbit cadaveric workshop by staining the inoculation suspension. Moreover, direct deposit of a bacterial suspension on the articles before implantation was chosen because it would mimic peri-operative contamination (adhesion of microorganisms to the article during the surgical procedure). Nevertheless, a small leakage of bacterial suspension was observed which may lead to bacterial spread causing systemic infection. Single direct deposition (10 μ l) into the bone defect was chosen for the rabbits treated with 10^4 CFU/site. The proposition was to induce a local infection and at the same time lower the

risk of systemic infection. The modified technique should be sufficient to allow local bone infection while reducing infections outside of the bone defect by minimizing the leakage during screw insertion. The leakage has likely favored infection of the surrounding tissues and potential systemic infection seen for the inoculation groups 10^5 and 10^7 CFU. Single inoculation into the defect was judged to be sufficient to allow local bone infection while reducing infections outside of the bone site. Therefore, mortality of the rabbits should reduce.

The selection of the inoculation doses was based on literature of intramedullary models because only a few data on intracondylar models are available. Within these studies different inoculation sizes up to 10^8 CFU were reported in a rabbit model [91,163–165]. The inoculation doses of 10^4 , 10^5 and 10^7 CFU were estimated to be sufficient enough to induce a local osseous infection without associated morbidity. Nevertheless, a high rate of mortality (40%) was encountered during this pilot study. These mortalities were most likely due to systemic infections and occurred mainly with the higher inoculation dose (10^7 CFU/site). The inoculation dose was adjusted considering that on the one hand an excessively high dose of bacteria could induce systemic infection (leading to death of the rabbit) or very severe local infection (abscess, extended osteomyelitis and pain with consecutive adverse events). But at the same time an excessively low dose of bacteria would fail to induce local infection and no comparison between the test and the control article could be performed. In the current pilot study, 10^7 CFU inoculation dose was judged to be too high. The 10^5 CFU inoculation dose was more appropriate because signs of infection were evidenced for the control group using several analyses. However, these signs were severe enough to consider reducing the inoculation dose to 10^4 CFU / site.

The test period was defined as 9 days after implantation. Test durations from several days to weeks are described in the literature [11,91,163–165]. The aim was to create differences in local infection compared to test and control screws without causing excessive signs of osteolysis or osteomyelitis. After careful review of the first pilot test it was decided that a longer time period of 14 days could result in an unacceptably high risk of mortality.

In this study, no preventive systemic antibiotic was planned to be administered directly after surgery. Only in case of premature death or heavy infection would the antibiotic have been applied. When administering systemic antibiotic immediately after surgery, the risk of hindering also local infection was seen. In this case, no difference could have been detected. After unexpected death of rabbits due to systemic infection, immediate systemic antibiotic treatment was administered from day 2 and for 7 days to all rabbits. This administration did not prevent local bone infection. In a future main study, administering antibiotic treatment immediately post surgery should be considered to prevent systemic infection and reduce the risk of mortality. This treatment could also be appropriate as an analog of normal patient treatment because the bone penetration of the antibiotic administered systemically is usually low [28,164] and antibiotic therapy is clinically recommended following orthopaedic surgery.

5.3.2.2 Findings

The purpose of this non clinical pilot study was to evaluate antibacterial properties of titanium cancellous bone screws coated with a thin layer of hydroxyapatite and loaded with Tobramycin. Preliminary in-vitro as well as in-vivo data demonstrated initial feasibility that antibacterial agents eluting locally from functional implant coatings are an effective way to combine bacterial contamination [3,11,91,163–166]. The nanoporous structure of the HA coating should ensure efficient drug loading by simple dipping technique with the ability of subsequently slow release [137]. Alt et al. [11] also reported about the efficacy of HA coating systems loaded with Gentamicin in an intramedullary rat model improving infection prophylaxis in a rabbit model inoculated with 10^7 CFU of *Staph. aureus*.

Under the conditions of the study, for the 10^7 CFU inoculation dose, two of three rabbits died prematurely and most likely from systemic infection. The rabbit euthanized at day 9 showed excessive signs of infections at the control site, confirmed by macroscopic observations, microbiological and histological evaluation. The femur treated with the Tobramycin loaded HA coated screw showed significantly lower signs of infection. The effect of the antibiotic was macroscopically visible. The implant surfaces and the surrounding tissue seemed to be protected by the Tobramycin actively diffusing from the implants surface. Therefore, it can be expected that the concentration of Tobramycin releasing from the implant is effective in-vivo, also taking into account a very high number of bacteria inoculated. Intraoperative contamination would most likely end up in a much smaller initial bacterial concentration. Therefore, the local drug delivery system under study could not only be used as a preventive antibacterial strategy for surgeons, it could also enable local treatment of infected wounds.

For the 10^5 CFU inoculation dose, one of three rabbits showed severe signs of weakness that was likely related to poor recovery from the surgery and/or systemic infection. It was euthanized for ethical reasons. The other rabbits survived and showed enormous efficacy of the test screws compared to the control articles. No bacteria could be recovered from the surface of the screws coated with Tobramycin indicating strong in-vivo efficacy. These results confirmed the findings obtained from the higher inoculation dose. The diffusion effect seemed to inhibit bacterial growth not only at the implants surface, it additionally showed efficacy in the whole femoral condyle and completely protected this area against bacterial infection. Therefore, it may also be speculated, that the antibiotic coating leads to better bone healing, because infected bone structures often lead to insufficient bone growth [16].

Based on the results obtained with 10^7 and 10^5 CFU/site, the inoculum size was reduced to 10^4 CFU per implantation. One of four rabbits died premature at day 5. This death was likely due to infection and histology confirmed signs of infection at the control site. From the rabbits euthanized at day 9, one test article from the group inoculated with 10^4 CFU showed an unlikely result. Microbiological and histopathological analyses demonstrate signs of infection for the control as well as the test site in this rabbit. The most likely explanation is that an article without Tobramycin loading was used for implantation and denoted as test article. But nevertheless, no scientific evidence could support this hypothesis, because the implanted screw was discarded after microbiological evaluation. Contamination of the test article after explanation could be excluded, because histopathologic analysis also confirmed signs of infection. A strong inter-individual variation between the rabbits showing different antibiotic release rates or different immune responses cannot be generally excluded, but is

not likely to occur. The two other rabbits assessed, confirmed the trend seen also for the higher inoculation groups. The test articles showed significantly lower signs of infections and no bacteria could be recovered from the implants surface. Passive protection of the implants surface followed by active diffusion into the vicinity was demonstrated.

In conclusion, under the conditions of the pilot study, the test article displayed antibacterial properties after implantation in the rabbit cancellous bone. The initial burst followed by a sustained release of Tobramycin appeared to effectively combat high concentrations of bacteria in-vivo. The Tobramycin concentrations loaded into the HA coating seemed to be sufficient to eliminate very large amounts of bacteria in-vivo. Out of all the rabbits euthanized at the end of termination, 5 out of 6 sites implanted with the test article presented biologically significantly lower signs of infection based on macroscopical, microbiological, histopathological and radiological analyses. These results are in accordance with the results published by Alt et al. and Stewart et al who concluded that Gentamicin [11] and Vancomycin [167] inhibited bacterial colonization with *Staph. aureus* and therefore supported bone healing. The Tobramycin loading method used in this study was performed by soaking in a Tobramycin containing solution followed by a drying step. This technique could also be used intra-operatively during surgery and enable an optional antibiotic choice for surgeons. Adding the active pharmaceutical ingredient to the implant directly by the surgeon could also be beneficial for the development of a feasible future regulatory pathway.

Recommendations for a future study would be to conduct the analyses with a larger number of sites to reach a stronger substantiated conclusion, using a design based on the results of this pilot study. 10^4 CFU/site seemed to be appropriate for the inoculation, which should be

fully injected into in the defect. By using this method leakage was minimized and local infection could be developed. As an additional consequence of the reduction of inoculum size and changing the inoculation method was a reduction in the observed mortality. Nevertheless, to cover unforeseen animal mortality, it would be necessary to include reserve rabbits in any future main study. The immediate administration of systemic antibiotic after surgery is strongly recommended. The results demonstrated that the antibiotics did not prevent the local infection, but appeared more to protect the rabbits against systemic infection and premature death. In a future study a clinically relevant *Methicillin Resistant Staph. aureus* (MRSA) strain could be studied to assess the efficacy of Tobramycin against this bacterial strain. Joosten et al. successfully evaluated the efficacy of implants coated with Vancomycin against MRSA strains in-vivo and reported good efficacy against infections even due to MRSA [91].

6 Conclusions

The present investigation of HA coated bioactive surgical implant acting as a local drug delivery vehicle for an antibiotic has demonstrated that this is a very promising solution with the potential to meet a variety of unmet clinical needs in orthopaedic implant surgery. The novel biomimetic HA coating has demonstrated that it is both versatile yet generic enough to potentially solve a number of problems for which satisfactory clinical solutions do not exist today. The biomimetic HA coating structure itself was manufactured using relatively straightforward wet chemistry process parameters. The process was demonstrated to enable homogeneous HA deposition on both, TiO₂ layered stainless steel and anodized titanium surfaces with different morphologies and thicknesses. Controllable drug loading and release characteristics were evidenced. HA coatings intended for use in orthopaedic applications have to show excellent biomechanical resistance properties. A straight forward method of physically testing the biomechanical resistance of the HA coatings was developed. The HA coating established on TiO₂ layered stainless steel material demonstrated preferential smearing effects and deterioration on high-stress surface areas after insertion into different synthetic bone qualities resulting good biomechanical performance overall. Additionally for the HA coating on anodized Ti screws, in-vivo results confirmed that there was adequate biomechanical resistance during insertion. Cell biocompatibility tests resulted in excellent and firm attachment of human cells to the biomimetic HA coatings on both base materials (stainless steel and titanium) without any signs of incompatibility or toxicity. Unique in-vivo performance of the HA coating on titanium screws was found in terms of more rapid early stabilization of the implant which was still safely removable after osseointegration. Significantly higher removal torques and a trend of higher pull-out forces

and were measured for the HA coated implant compared to the non-coated implant after 2 weeks in-vivo. This supported the hypothesis of more early and more rapid stabilization in the presence of the HA coating. Nevertheless, after full osseointegration of the screw implants, the biomechanical tests demonstrated safe and relatively easy implant removal, which is absolutely essential requirement for such implants if they fail or require revision surgery. SEM images confirmed disconnection of the HA coating and/or HA remodeling in-vivo. Histology confirmed that the HA coating was not visible at both time points and had been replaced with newly formed bone that was intimate with the implant surface, whereas controls showed greater fibrous tissue at the implant surface. This unique “disconnection” characteristic has never been demonstrated before. Metallic implants with bioactive HA coatings are expected to enable the implant to be able to bear load at earlier time points. This was confirmed in the present study by the significantly higher biomechanical removal torques for the HA coated screws after osseointegration in-vivo. Thus the HA coating design goal of enabling more rapid fixation post-surgery was achieved.

A further part of the presented research demonstrated that functionalizing implant surfaces with nano-porous biomimetic HA coatings offer a promising method for a controlled local delivery of clinically relevant concentrations of an antibiotic. The use of antibiotic, especially the use of Tobramycin should be noted as a model drug for incorporation, release and efficacy studies in-vitro and in-vivo. Coating thickness, morphology and surface topography as well as loading parameters like temperature, pressure, ultrasound, pH were found to be important impacting the drug loading and subsequently the release profile. For the HA coating on stainless steel fixation pins a sustained drug release of 8 days was obtained, with Tobramycin concentration above the MIC value for *Staph. aureus*, after drug loading for only

5 min at high temperature and pressure. The very short loading time of 5 min suggests the possibility of developing implant kits where the implant and the drug are separate when delivered to the clinics and then combined at the time of surgery. In this case the issues associated with sterilization of implants containing drugs prior to packaging would be avoided. This approach could additionally reduce the regulatory burden to a more straight forward regulatory pathway. The fast-loading and slow-release concept offers an option to quickly add an antibiotic to an implant coating as required, thus creating a flexible antibacterial solution for the surgeon to determine. An innovative and promising co-precipitation method demonstrated on TiO₂ layered stainless steel fixation pins that it was feasible to manufacture a Tobramycin-doped HA coating capable of delivering pharmaceutically relevant amounts of Tobramycin over a 12 day period of that was above the MIC of *Staph. aureus*. The demonstrated release period is longer than all earlier presented results of biomimetic HA coatings loaded by fast-soaking techniques. In contrast to the dipping approach a co-precipitated type of implant coating would have to be delivered as a ready-to-use-implant. Antibacterial agar diffusion tests demonstrated high efficacy and local protection of the HA coating, if loaded with antibiotic. These tests displayed only minor impact of coating failure on the ability to inhibit growth of *Staph. aureus*. *In vitro* roll-out tests demonstrated effective protection of the implant surface against early bacterial attachment. As a final proof of concept the in-vivo performance of the antibiotic carrier system on titanium screws was demonstrated in an infection pilot study and achieved high bactericidal efficacy. The antibiotic not only protected the implant surface against bacterial colonization and subsequent biofilm formation but also the active diffusion of the drug ensured protection and bacterial inhibition in the near vicinity. All of biomimetic HA coatings tested fulfilled the key requirements of an implant drug delivery system. Namely

to deliver a “burst” release at high initial drug concentrations in order to eliminate bacteria introduced at surgery, followed by a continuous slow release above the MIC.

The coatings developed open up potential opportunities for the release of other antibiotics and other active pharmaceutical ingredients and combinations thereof and this might lead to numerous treatment applications in patients where local delivery could be preferred over systemic dosing. The nanoporous HA coated implants used as local drug delivery systems enable designs with the potential to minimize the risk of infections and simultaneously maximize bone ingrowth.

7 Future perspective

The nanoporous HA coatings under study were shown to be successful when used as local drug delivery systems. They are designed to minimize the risk of infections and simultaneously maximize bone ingrowth. Therefore the risk of implant failure due to infection and contrariwise should be reduced. By lowering infection rates and bacterial contamination, bone healing will be supported. A more efficient antibiotic treatment and infection prevention by local delivery using substantially less antibiotic than in systemic administration thus minimizing side effects of antibiotic use as well as positively contributing to the antibiotics resistance development problem. Local antibiotic delivery could be used as an additional precautionary treatment alongside systemic application of antibiotics post-surgery. So it could be postulated that there would be synergistic combinations of antibiotics that protect against bacteria, which are currently very difficult to treat, e.g. MRSA.

For patients who have had a traumatic bone fracture the combination of infection prevention, fast bone ingrowth and subsequent easy removal of the fixation pins/screws are all benefits potentially contributing towards faster recovery and better long term end points of the surgery.

8 Summary

This thesis reports the successful development of a novel bioactive type of implant coating. A thin biomimetic hydroxyapatite coating on metal implants with unique properties capable of delivering pharmaceutically effective dosages of Tobramycin was developed and systematically analyzed. Biomimetic, nanoporous HA coatings were demonstrated to be versatile enough to potentially solve a number of problems for which satisfactory clinical solutions do not exist today. The surface pretreatment and HA coating was designed and optimized to homogeneously distribute needle like HA crystals on TiO₂ layered stainless steel and anodized titanium type II surfaces in the range of 1 to 5 μm. The advantages of a nanoporous structure of biomimetically deposited HA over a more dense structure of plasma sprayed HA coatings in terms of antibiotic incorporation and subsequent sustained release were presented. The biomimetically deposited HA structure itself demonstrated good biomechanical resistance, excellent biocompatibility and osteoconductive surface properties in-vitro and in-vivo. The nanoporous structure allowed for controlled drug incorporation and tailorable local release. The use of Tobramycin should be noted as a model drug for incorporation, release and efficacy studies. Coating thickness, morphology and surface topography as well as loading parameters like temperature, pressure, ultrasound, pH were found to be important impacting on both drug loading and subsequent release profile. Agar diffusion tests demonstrated a sustained antibacterial effect against *Staph. aureus* over several days. A novel co-precipitation approach incorporating Tobramycin simultaneously at the time of nucleation was defined and optimized. The starting phase of crystallization represented a very important aspect for coating deposition.

Both surface chemistry as well as process temperature are important factors impacting coating growth, thickness and the morphology of the drug-doped HA coatings.

An animal test set-up was developed in order to assess the performance of the HA coating in-vivo. Overall, the insertion torques (during implantation) of the HA coated screws were comparable to uncoated, commercially available screws. After two weeks, increased early implant stabilization was demonstrated by significantly higher removal torques for HA coated screws. Furthermore, this conclusion was supported by higher pull-out forces, and histology. After 6 weeks, HA coated and non-coated screws demonstrated comparable removal-torque values as well as pull-out forces. Therefore, the HA coating resulted in more rapid early implant stabilization whilst assuring that the implant could be safely removed after full osseointegration. Furthermore, the efficacy of the Tobramycin loaded HA coating was evaluated in an in-vivo infection model. Five out of six implanted sites containing HA and Tobramycin presented biologically significant lower signs of infection based on macroscopical, microbiological, histopathological and radiological analyses.

Overall, the novel biomimetic HA coating has demonstrated delivery of enhanced implant stabilization whilst at the same time enabling the implant to be easily disconnected from the bone upon screw removal. Finally the coating is also capable of delivering clinically effective dosages of an antibacterial agent over a relevant time period.

9 Summary (German version)

Die vorliegende Doktorarbeit berichtet von der erfolgreichen Entwicklung einer neuen bioaktiven Implantatbeschichtung. Eine dünne, biomimetisch hergestellte Hydroxylapatit (HA) Beschichtung auf metallischen Implantatoberflächen mit einzigartigen Eigenschaften wurde erforscht und systematisch analysiert. Diese Schicht ist zusätzlich in der Lage, pharmazeutisch wirksame Mengen an Tobramycin gezielt freizusetzen. Die Oberflächenvorbehandlung und die HA Beschichtung wurden so entwickelt und optimiert, dass eine homogene Verteilung der nadelförmigen HA Kristalle sowohl auf dem TiO₂ beschichtetem rostfreiem Stahl, als auch auf den anodisierten Titanium Typ II Oberflächen im Schichtdickenbereich von 1 bis 5 µm erzeugt werden konnte. Die Vorteile einer biomimetisch abgeschiedenen nanoporösen HA Struktur gegenüber einer dichteren plasmagesprühten HA Beschichtungen in Bezug auf die Aufnahme und anschließender Freisetzung von Antibiotika werden untersucht und beschrieben. Die biomimetisch aufgebraute HA Beschichtung zeigt sehr gute biomechanische Widerstandsfähigkeit, ausgezeichnete Biokompatibilität und osteokonduktive Oberflächeneigenschaften in-vitro und in-vivo. Die nanoporöse Struktur erlaubt eine kontrollierte Antibiotikaaufnahme gepaart mit einer steuerbaren lokalen Freisetzung. Als Modellarzneistoff zur Testung der Aufnahme, der Freisetzung und der Wirksamkeitsstudien wurde Tobramycin ausgewählt. Schichtdicke, Morphologie und Oberflächentopographie, sowie verschiedene Beladungsparameter wie Temperatur, Druck, Ultraschall und pH-Wert wurden als wichtige Einflussfaktoren erkannt, die sowohl die Wirkstoffbeladung, als auch das anschließende Freisetzungsprofil beeinflussen. Agar-Diffusions-Tests zeigten eine anhaltende antibakterielle Wirksamkeit der mit Tobramycin beladenen Schicht gegen *Staph. aureus* über mehrere Tage. Ein neuartiger

Ansatz der gleichzeitigen Co-Kristallisation von HA und Tobramycin während der Kristallbildung wurde entdeckt und optimiert. Dabei stellte sich heraus, dass die Startphase der Kristallisation ein sehr wichtiger Schritt für die gesamte Schichtabscheidung darstellt. Oberflächenchemie und Prozesstemperatur sind zusätzlich wichtige Faktoren, die das Wachstum der Beschichtung, die Schichtdicke und die Morphologie der co-kristallisierten HA Beschichtungen beeinflussen.

Ein Tiermodell wurde entwickelt, um das Verhalten der HA Beschichtung in-vivo zu untersuchen und zu beurteilen. Zunächst waren die Eindrehmomente (während der Implantation) der HA beschichteten Schrauben vergleichbar mit den unbeschichteten kommerziell erhältlichen Kontrollschrauben. Nach zwei Wochen wurde eine verbesserte frühe Implantatstabilisierung durch signifikant höhere Drehmomente bei der Entfernung der HA beschichteten Schrauben gemessen. Diese Schlussfolgerung wurde durch höhere Auszugskräfte und histologische Untersuchungen zusätzlich unterstützt. Nach 6 Wochen zeigten die HA beschichteten Schrauben im Vergleich zu den nicht-beschichteten Schrauben sowohl vergleichbare Drehmomente bei der Entfernung, also auch ähnliche Auszugskräfte. Daher lässt sich zusammenfassen, dass die HA Beschichtung zu einer schnelleren frühen Implantatstabilisierung beiträgt, jedoch nach vollständiger Osteointegration der Schraube die wichtige Eigenschaft besitzt, sicher wieder entfernt werden zu können.

Darüber hinaus wurde die Wirksamkeit der mit Tobramycin beladenen HA-Schicht in einem in-vivo Infektionsmodell untersucht. Fünf von sechs implantierten Schrauben, die mit HA und Tobramycin beschichtet waren, zeigten biologisch signifikant geringere Anzeichen einer Infektion basierend auf makroskopischen, mikrobiologischen, histopathologischen und radiologischen Analysen.

Insgesamt zeigte die neuartige biomimetische HA Beschichtung eine verbesserte frühe Implantatstabilisierung, während es zur gleichen Zeit möglich war, das Implantat wieder sicher aus dem Knochen zu entfernen. Zusätzlich war die Beschichtung in der Lage, klinisch wirksame Mengen von Tobramycin kontrollierbar über einen sinnvollen Zeitraum freizusetzen.

10 Acknowledgment

The presented thesis has been acquired within the scope of cooperation between the Department of Pharmaceutical Technology and Biopharmacy at the Christian Albrecht University in Kiel and Stryker Trauma GmbH in Schönkirchen under the supervision of Prof. Dr. Hartwig Steckel.

I would like to express my gratitude to my supervisor Prof. Dr. Hartwig Steckel for giving me the opportunity to perform my PhD thesis in his department, for his continuous encouragement and belief in my work, and for giving me the freedom to realize my own ideas.

At this place I would like to acknowledge Stryker Trauma GmbH for financial support of this thesis. To Dr. Bernd Robioneck I wish to convey my thanks for his encouragement to realize the cooperation and make the project happen.

I gratefully acknowledge Prof. Dr. Philip Procter (aka “Lord of the Screws”) and my brother Dr. Torben Sörensen for supervising the thesis as representatives from Stryker, their guidance, valuable notes, constructive feedback and personal interest over the duration of my PhD programme. Dr. Jörg Arnoldi is much appreciated for supporting the project at the early stages.

I express my gratitude to thank Prof. Dr. Maria Strømme, Prof. Dr. Håkan Enggist, Dr. Ken Welch, Dr. Maria Astrand and Mirjam Lilja for being excellent partners in collaboration with BactInact AB and Sandvik. Prof. Dr. Sabine Fuchs is gratefully acknowledged for performing the cell tests supporting the current study.

I am grateful to Prof. Dr. Carol Toth, Nils Reimers, Claudia Beimel, Matthias Regling and the whole Medical Science group of Stryker Trauma GmbH for their helpful suggestions and stimulating comments. Claudia Beimel is acknowledged for her support with the statistical analyses.

I would like to thank the entire pharmaceutical technology working group for the kindly and positive atmosphere. I gratefully acknowledge the whole technical and analytical support, especially from Regina Krehl, Hanna Rohwer and Maren Rohlf. Rüdiger Smal, I would like to thank you not only for excellent art work, but also for many exciting conversations.

Last, but not least, I thank all those people who have provided me with help and encouragement on this way. To my parents, my brother, my girlfriend and circle of friends I wish to express my gratitude and a lot of thanks for their understanding and for so much more than I can't write down here.

11 List of figures

Figure 1: Schematic overview of the possible connection of insufficient implant stabilization and implant infection.	3
Figure 2: Schematic overview of HA coated antibiotic loaded screw in a bony environment. .	6
Figure 3: Frequency of main pathogenic species among orthopaedic clinical isolates of implant-associated infections [65]. (CNS=Coagulase Negative Staphylococci)	14
Figure 4: Molecular structure of Tobramycin $C_{18}H_{37}N_5O_9$, $M_r = 467.51$ g/mol; red dots denote NH_2 groups, blue dots denote hydrogen saturated oxygen-atoms.....	17
Figure 5: Schematic diagram of mechanism of action of Tobramycin during bacterial protein biosynthesis.....	18
Figure 6: Positioning of the base layered fixation pin in the test tube during HA growth.....	21
Figure 7: Positioning of the HA start layer coated fixation pin during co-precipitation process.	23
Figure 8: Schematic drawing of the chamber for loading under pressure.	25
Figure 9: Overview of animal studies performed.	37
Figure 10 Titanium cancellous bone screw (reference) left and HA coated cancellous bone screw (test) right.	38
Figure 11: Final aseptic packaging of the screws before gamma sterilization.	39
Figure 12: Picture of the customized material used for the in-vivo studies.....	39
Figure 13: Insertion torque measurement system used for HA performance pilot and main studies.	40
Figure 14: Target position of the screw in the distal femoral condyle of the rabbit.....	42
Figure 15: Pictorial overview of the surgical procedure.	43
Figure 16: Example of rabbit femur specimen with plastic storage container.....	44
Figure 17: Custom made torsion apparatus: left side: rotatable grip holding the removal torque screw driver (here with screw, screw holder and Teflon test block); right side: grip, which cannot rotate but can translate along the screw driver axis, holding the embedding container. Both grips are mounted on a base plate.	44
Figure 18: Embedding rig for 8 samples.....	45
Figure 19: Embedding the dishes with polymethylmethacrylate (PMMA).	45

Figure 20: Test assembly placed in the material testing machine. F_{reg} : Registered force exerted to the lever arm ($l=35$ mm) of the torsion device. Load cell (range 50 N). Counter weights balance the unevenly distributed mass of the lever arm.....	46
Figure 21: Calculation of the torsion angle α	46
Figure 22: Evaluation method of maximum removal torque using a 1° torsion angle offset illustrated for two types of torque-torsion angle characteristics.....	48
Figure 23: Test assembly in the material testing machine. Calibrated load cell (range 10 kN).	49
Figure 24: Pull-out test diagram: F_{max} : maximum pull-out force in N; slope: pull-out stiffness in N/mm.	50
Figure 25: Scheme of the regions of interest investigated for the histomorphometrical analysis.	52
Figure 26: The rectangles 1 and 2 correspond to the area of pre-scanning before defining the ROIs	53
Figure 27: The defined region of interest (ROI) can be observed in the left image (a)). The right image (b)) demonstrates the screw (grey part) and the region of interest described by the transparent part.....	54
Figure 28: μ -CT image of the bone after screw removal. The arrows indicate the cortical thickness measurement (here in one plane).	55
Figure 29: Inoculation method during in-vivo study – 5 μ l inoculum suspended directly in the bone defect (a), 5 μ l distributed directly on the screw (b) followed by insertion (c).....	59
Figure 30: Distribution of 5 μ l suspension directly onto the screw (a). Minimal leakage (b) and homogeneous distribution (c) of the suspension were demonstrated during a cadaveric study. The suspension mimicking the inoculum was stained with a black colorant.	59
Figure 31: Photograph of a) plasma sprayed HA coating and b) biomimetically deposited HA coating on a fixation pin.....	62
Figure 32: SEM images (left panels) and surface topography maps (right panels) of the HA-B (a, c) and HA-P (b, d) surface.....	62
Figure 33: XRD spectra of TiO_2 and TiO_2 coated stainless steel plates stored in PBS. Diffraction peaks of crystalline HA are indicated in the figure.....	63

Figure 34: SEM images of ion milled cross-sections of HA-B (a, b) and HA-P (c, d) coatings deposited on fixation pins. The substrate and coating interfaces are indicated as well as the embedding material..... 64

Figure 35: SEM images of HA-B (a) and HA-P (b) coatings loaded with Tobramycin under a pressure of 6 bar (Load-P)..... 65

Figure 36: Non-cumulative release after loading for different time periods at room temperature in Tobramycin containing solution (20 mg/ml). The inset describes a magnification of the sustained release. 66

Figure 37: Non-cumulative release after loading with different concentrations of Tobramycin containing solutions. The inset describes a magnification of the sustained release. 67

Figure 38: Non-cumulative release after loading at elevated pressure of 6 bars in a Tobramycin containing solution. The inset describes a magnification of the sustained release. 68

Figure 39: Non-cumulative release after loading at elevated temperature (90°C) in a Tobramycin containing solution (20 mg/ml). The inset describes a magnification of the sustained release..... 68

Figure 40: Non-cumulative release after loading at elevated temperature (90°C) and pressure (6 bar) in a Tobramycin containing solution (20 mg/ml). The inset describes a magnification of the sustained release. 69

Figure 41: SEM analysis of the surface morphology after release in PBS for 5 days..... 70

Figure 42: In-depth profiles of carbon (a) and nitrogen (b) of a HA-B sample loaded with 20mg/ml Tobramycin under the displayed loading series..... 70

Figure 43: SEM images of HA-B coating morphology after 6 days storage of the TiO₂ covered substrates in 37°C (a) and 60°C heated PBS (b). 71

Figure 44: Non-cumulative amount of Tobramycin released in 37 °C PBS from HA-B_37 coated pins of indicated thickness after being loaded for 5 minutes in a solution containing 20 mg/ml of the antibiotics under either room temperature at atmospheric pressure (RT) or at 90 °C and 6 bar (PHT). Error bars denote the standard deviation of 3 measurements. The average total amounts of Tobramycin released from each sample type are also displayed.. 72

Figure 45: Non-cumulative amount of Tobramycin released in 37 °C PBS from HA-B_37 (2µm) and HA-B_60 (1µm) coated pins after being loaded for 5 minutes in a solution containing 20

mg/ml of the antibiotics under either room temperature at atmospheric pressure (RT) or at 90 °C and 6 bar (PHT). Error bars denote the standard deviation of 3 measurements. The average total amounts of Tobramycin released from each sample type are also displayed..	73
Figure 46: SEM images of HA-B coated sample types after insertion into 25 PU foam blocks.....	75
Figure 47: SEM images of HA-B coated samples after insertion into Renshape BM5166 discs.....	75
Figure 48: 3D visualization image of a HA-B_37 (5µm) sample after insertion into PU 25 foam.....	76
Figure 49: SEM images (scale bars 200 µm) of RT-samples (upper panels), PHT samples (middle panels) and Co-4 samples (lower panels) after insertion into 25 PU foam and subsequent drug release in PBS.....	77
Figure 50: Macroscopical image (a) and SEM images (b, c) of 25 PU foam after insertion. The insertion direction is indicated by an arrow (a). SEM images were taken at an insertion depth of approximate 2 mm from the pin entry point. The scale bars in panels a, b and c are 50 mm, 20 µm and 10 µm, respectively.....	78
Figure 51: Non-cumulative amount of Tobramycin released in 37 °C PBS from HA-B coated pins after RT and PHT loading in a solution containing 20 mg/ml of the antibiotics and following insertion into 25 PU foam (BML samples). Release results from mechanically untreated RT and PHT samples are incorporated as reference. Error bars denote the standard deviation of 3 measurements. The average total amounts of Tobramycin released from each sample type are also displayed.....	79
Figure 52: Non-cumulative amount of Tobramycin released in 37 °C PBS from Co-4 coated pins after insertion into 25 PU foam (BML samples). Release results from mechanically untreated Co-4 samples are incorporated as reference. Error bars denote the standard deviation of 3 measurements. The average total amounts of Tobramycin released from each sample type are also displayed.....	80
Figure 53: Non-cumulative amount of Tobramycin released in 37 °C PBS from RT loaded pins after gamma sterilization. Release results from RT samples are incorporated as reference. Error bars denote the standard deviation of 3 measurements. The average total amounts of Tobramycin released from each sample type are also displayed.....	81

Figure 54: SEM images of scratch paths created with a 500 μm diamond indenter on HA-B_60 and HA-B_37 coated pins of indicated thickness..... 83

Figure 55: Images of HA-B_37 (5 μm) coated, RT loaded, PTH loaded and RT_BML loaded pin after 18 hours of incubation in agar diffusion tests against *Staph. aureus*. RT_BML loaded pin was additionally inserted through a block of 25 PU foam. Panels c1-4) indicate the germs growing on fresh agar plates after roll-out test after 24 hours. Panel d) gives an overview of the inhibition zones of the different samples at each time period. The error bars indicate the standard deviations over three measurements..... 85

Figure 56: Calcein-AM viability assessment of outgrowth endothelial cells (a,b) and primary osteoblasts (c,d) discs with (a,c) or without HA-B_37 (5 μm) (b,d) coating. On both types of substrates primary osteoblasts show a bright fluorescence after Calcein-AM staining. Similar findings can be observed for outgrowth endothelial cells which form endothelial cell layers on both types of surfaces and at both investigated time points. 87

Figure 57: SEM analyses of the surface structures after immersion in Tobramycin containing PBS buffer for 6 days a) 0.5 mg/ml Tobramycin at 37 °C; b) 1.0 mg/ml Tobramycin at 37 °C; c) 0.5 mg/ml Tobramycin at 60 °C; d) 1.0 mg/ml Tobramycin at 60°C. 88

Figure 58: Cross section of the HA start layer after immersion for 3 days in PBS at 60 °C. 90

Figure 59: SEM analyses of the HA start layered surface structures after immersion in Tobramycin-containing PBS for 6 days a) 0.5 mg/ml Tobramycin at 37 °C; b) 1.0 mg/ml Tobramycin at 37 °C; c) 0.5 mg/ml Tobramycin at 60 °C; d) 1.0 mg/ml Tobramycin at 60 °C. 90

Figure 60: SEM analyses of the surface structures after immersion in Tobramycin-containing PBS for 6 days at 60 °C a) without HA start layer at 4 mg/ml; b) and c) with HA start layer at 4 mg/ml (different magnifications); d) without HA start layer at 20 mg/ml; e) and f) with HA start layer at 20 mg/ml (different magnifications). 91

Figure 61: SEM analyses of the HA start layered surface structures after immersion in Tobramycin-containing PBS for 6 days a) 4 mg/ml Tobramycin at 37 °C; b) 20 mg/ml Tobramycin at 37 °C; c) HPLC obtained non-cumulative amount of Tobramycin released in 37 °C PBS from pins coated by co-precipitation using different concentrations of Tobramycin in PBS solution. The average total amounts of Tobramycin released from the different coatings are displayed next to the sample names. The error bars indicate the standard deviations. *calculated based on residual content. 92

Figure 62: GD-OES analyses of the co-precipitated sample (Co-4) with an HA start layer along with a biomimetically deposited HA reference sample a) carbon depth profile (left) and nitrogen depth profile (right); b) SEM cross-section of Tobramycin-doped HA.....	94
Figure 63: SEM images of 5 M NaOH pretreatment of anodized titanium type II surface after different treatment durations at 70 °C (1 – 9 hours) prior to HA deposition.....	95
Figure 64: SEM images of 5 M NaOH pretreatment of anodized titanium type II surface after different treatment durations at 70 °C (10 – 40 minutes) prior to HA deposition.....	95
Figure 65: Non-cumulative amount of Tobramycin released in 37°C PBS from Ti-HA screws loaded in stock solution containing different concentrations of Tobramycin during the displayed loading times. Ti-HA_PHT_20 was loaded under elevated temperature and pressure.....	96
Figure 66: Non-cumulative Tobramycin release over time dependent on different pH values during loading.....	98
Figure 67: Non-cumulative release of Tobramycin in 37°C PBS over time from Ti-HA coated screws Tobramycin loaded in a stock solution containing 20 mg/ml for 5 minutes at room temperature, under applied ultrasound or under applied ultrasound in combination with vacuum.....	99
Figure 68: Images of Ti-w/o, w/o_RT loaded, HA_RT loaded and HA_PTH loaded screws inserted after 18 hours of incubation in agar diffusion tests against <i>Staph. aureus</i> . Panel c) gives an overview of the inhibition zones of the different samples in accordance to the time period. The error bars indicate the standard deviations over three measurements.....	100
Figure 69: Antibacterial effect after 18 hours of incubation of inserted screw into fully germ suspended agar media. A 3 dimensional antibacterial effect is demonstrated over the full range of the inserted screw.	101
Figure 70: Calcein-AM viability assessment of primary osteoblasts (a-d) and outgrowth endothelial cells (e-h) grown on Titanium disks with (c, d, f, h) or without HA (a, c, e, g) coating. On both types of substrates consisting of either pure titanium or hydroxyapatite coated titanium primary osteoblasts show a bright fluorescence after Calcein-AM staining at both time points of investigation. Similar findings were observed for outgrowth endothelial cells which form endothelial cell layers on both types of surfaces and at both investigated time points.	102

Figure 71: Morphological appearance of pOB and OEC; Staining for the endothelial marker CD31 (red) on OEC grown on pure Titanium (a) or HA -coated titanium (b). Phalloidin-TRITC (red) staining for primary osteoblasts grown for 7 days on pure Titanium (c) or HA-coated titanium (d). Nuclear counterstain in blue.....	103
Figure 72: Summarized insertion torque measurements during implantation (n=8).	104
Figure 73: Summarized insertion torque measurements during implantation (n=35).	105
Figure 74: Maximal removal torques after 2 and 6 weeks implantation of test and control articles.	107
Figure 75: Removal torque stiffness after 2 and 6 weeks implantation of test and control articles.	108
Figure 76: SEM images after screw removal of a control screw after 2 weeks implantation – a) and c) the surface between the threads and b) the surface at the tip of screw is shown.	110
Figure 77: SEM images after screw removal of a test screw after 2 weeks implantation – a) the surface between the threads and b - f) a closer look at the surface of screw showing cell attachment and residual HA coating.....	110
Figure 78: SEM images after screw removal of a control screw after 6 weeks implantation – a) to c) the surface between the threads of screw showing signs of cell attachment.	111
Figure 79: SEM images after screw removal of a test screw after 6 weeks implantation – a) to c) the surface between the threads of screw showing signs of cell attachment and signs of cell attachment.....	111
Figure 80: This image demonstrates the difference in pull-out force [N] after 2 (n=6) and 6 weeks (n = 7).	112
Figure 81: Maximal pull-out force after 2 and 6 weeks implantation of test and control articles.	112
Figure 82: Pull-out force stiffness after 2 and 6 weeks implantation of test and control articles.	113
Figure 83: Histological images of HA coated screws (left) and non-coated control screws (right) after 2 weeks in-vivo. The arrows integrated on the left side demonstrating direct bone implant contact, whereas minor bone implant contact was observed for the control group (right side).....	115

Figure 84: Histological images of HA coated screws (left) and non-coated control screws (right) after 6 weeks in-vivo. For both samples tested a good osteoconductivity were demonstrated. A greater bone thickening and a higher remodeling activity was observed for the HA-coated group.....	116
Figure 85: BV/TV (%) are demonstrated for the test and control articles at 2 and 6 weeks in-vivo.	117
Figure 86: μ -CT image after screw removal of control group (X1708 left) after 6 weeks in-vivo.	119
Figure 87: Macroscopical pictures at termination (day 9) – 10^7 CFU inoculation dose	122
Figure 88: Macroscopical pictures at termination (day 9) – 10^5 CFU inoculation dose	123
Figure 89: Macroscopical pictures at termination (day 9) – 10^4 CFU inoculation dose; --> white deposit (suspicion of pus)	124
Figure 90: X-ray of the left femur of rabbit X1648 treated with control screw – 10^5 inoculation dose – day 9	125
Figure 91: Histopathological photographs of non-coated screws (control group) in comparison to Tobramycin HA-coated screws (test group) after 9 days in an in-vivo infection model treated with 10^5 CFU per defect.	128
Figure 92: Histopathological photographs of non-coated screws (control group) in comparison to Tobramycin HA-coated screws (test group) after 9 days in an in-vivo infection model treated with 10^7 CFU per defect.	129
Figure 93: Histopathological photographs of non-coated screws (control group) in comparison to Tobramycin HA-coated screws (test group) after 9 days in an in-vivo infection model treated with 10^4 CFU per defect.	130

12 List of Tables

Table 1: Resistance of <i>S. aureus</i> and <i>S. epidermidis</i> to Tobramycin acc. [88,90].....	19
Table 2: Tobramycin loading parameters for both HA-B and HA-P coatings.....	24
Table 3: Overview of HA coating types tested during first biomechanical investigation series.	28
Table 4: Coupon soaking conditions for optimization of NaOH pretreatment.	33
Table 5: Overview of the material used during the surgical procedure.	39
Table 6: Study design HA performance pilot study; C: Control article: cancellous screw; T: Test article: hydroxyapatite coated cancellous screw (Verum).....	55
Table 7: HA-performance main study design.....	56
Table 8: Overview of material used for microbiological evaluation.....	58
Table 9: Study design; T: Test article: Hydroxyapatite antibiotic cancellous screw; C: Control article: Cancellous screw; *: these rabbits died or were euthanized prematurely. Their sites were submitted to histopathological analysis but not to microbiology.....	61
Table 10: Critical normal loads of HA-B coated stainless steel discs obtained from conventional single pass scratch tests.	83
Table 11: Overview of all co-precipitation investigations by the given process parameters..	89
Table 12: Overview of removal torque and stiffness values after 2 weeks of implantation.	107
Table 13: Overview of removal torque and stiffness values after 6 weeks of implantation.	109
Table 14: Overview of pull-out force and stiffness values after 2 weeks of implantation....	113
Table 15: Overview of pull-out force and stiffness values after 6 weeks of implantation....	114
Table 16: Cortical thickness measurement at 4 points of the control and test group.	118
Table 17: Overview of the bacterial counts on the explanted sites after 9 days.	126
Table 18: Overview of published studies using cancellous bone screws in a rabbit femoral condyle model.....	157

13 List of abbreviations

∅	Diameter
°C	Degree celsius
BIC	Bone Implant Contact
CNS	Coagulase Negative Staphylococci
d	Days
g	Gram
GD-OES	Glow Discharge optical emission spectroscopy
h	Hours
HA	Hydroxyapatite
HA-B	Biomimetic hydroxyapatite
HA-P	Plasma sprayed hydroxyapatite
HPLC	High Performance Liquid Chromatography
HT	Loaded under elevated temperature (90°C)
kGy	Kilogray
mg	Milligramm (10^{-3} gram)
MIC	Minimal inhibitory concentration
μm	Micrometer (10^{-6} meter)
μg	Microgramm (10^{-6} gram)
min	Minute
ml	Milliliter (10^{-3} liter)
MRSA	Methicillin Resistant Staph. Aureus
n	Number of samples
N	Newton

List of abbreviations

nm	Nanometer (10^{-9} meter)
PBS	Phosphate buffered saline
pH	Potentia Hydrogenii
PhEur	Pharmacopoeia Europaea
PHT	Loaded under elevated pressure (6 bar) and temperature (90°C)
ROI	Region of Interest
RT	Loaded under room temperature
SEM	Scanning Electron Microscopy
Ti-HA_PHT	Ti screws with HA coating and Tobramycin after loading at elevated temperature and pressure
Ti-HA_RT	Ti screws with HA coating and Tobramycin loaded at room temperature
Ti-w/o	Ti screws without HA coating and without antibiotic
Ti-w/o_RT	Ti screws without HA coating and Tobramycin loaded at room temperature
TV	Total Volume
US	Loaded under applied ultrasound
USV	Loaded under applied ultrasound and vacuum
VOI	Volume of Interest
w	Week

14 List of references

- [1] Krappinger D, Bizzotto N, Riedmann S, Kammerlander C, Hengg C, Kralinger FS. Predicting failure after surgical fixation of proximal humerus fractures. *Injury* 2011;42:1283–8.
- [2] Schalamon J, Petnehazy T, Ainoedhofer H, Zwick EB, Singer G, Hoellwarth ME. Pin tract infection with external fixation of pediatric fractures. *Journal of Pediatric Surgery* 2007;42:1584–7.
- [3] Lucke M, Wildemann B, Sadoni S, Surke C, Schiller R, Stemberger A, Raschke M et al. Systemic versus local application of gentamicin in prophylaxis of implant-related osteomyelitis in a rat model. *Bone* 2005;36:770–8.
- [4] Palma-Carrio C, Maestre-Ferrin L, Penarrocha-Oltra D, Penarrocha-Diago MA, Penarrocha-Diago M. Risk factors associated with early failure of dental implants. A literature review. *Med Oral* 2009;514–7.
- [5] Moroni A, Faldini C, Marchetti S, Manca M, Consoli V, Giannini S. Improvement of the bone-pin interface strength in osteoporotic bone with use of hydroxyapatite-coated tapered external-fixation pins. A prospective, randomized clinical study of wrist fractures. *J Bone Joint Surg Am* 2001;83:717–21.
- [6] Moroni A, Caja V, Egger E, Trinchese L, Chao E. Histomorphometry of hydroxyapatite coated and uncoated porous titanium bone implants. *Biomaterials* 1994;15:926–30.
- [7] Kusakabe H, Sakamaki T, Nihei K, Oyama Y, Yanagimoto S, Ichimiya M, Kimura J et al. Osseointegration of a hydroxyapatite-coated multilayered mesh stem. *Biomaterials* 2004;25:2957–69.
- [8] Bidar R, Kouyoumdjian P, Munini E, Asencio G. Long-term results of the ABG-1 hydroxyapatite coated total hip arthroplasty: analysis of 111 cases with a minimum follow-up of 10 years. *Orthop Traumatol Surg Res* 2009;95:579–87.
- [9] Åberg J, Brohede U, Mihranyan A, Strømme M, Engqvist H. Bisphosphonate incorporation in surgical implant coatings by fast loading and co-precipitation at low drug concentrations. *J Mater Sci: Mater Med* 2009;20:2053–61.
- [10] Brohede U, Forsgren J, Roos S, Mihranyan A, Engqvist H, Strømme M. Multifunctional implant coatings providing possibilities for fast antibiotics loading with subsequent slow release. *J Mater Sci: Mater Med* 2009;20:1859–67.
- [11] Alt V, Bitschau A, Osterling J, Sewing A, Meyer C, Kraus R, Meissner S et al. The effects of combined gentamicin–hydroxyapatite coating for cementless joint prostheses on the reduction of infection rates in a rabbit infection prophylaxis model. *Biomaterials* 2006;27:4627–34.
- [12] Moojen DJF, Vogely HC, Fleer A, Nikkels PG, Higham PA, Verbout AJ, Castelein RM et al. Prophylaxis of infection and effects on osseointegration using a tobramycin-periapatite coating on titanium implants—An experimental study in the rabbit. *J. Orthop. Res.* 2009;27:710–6.
- [13] Chai H, Guo L, Wang X, Fu Y, Guan J, Tan L, Ren L et al. Antibacterial effect of 317L stainless steel contained copper in prevention of implant-related infection in vitro and in vivo. *J Mater Sci: Mater Med* 2011;22:2525–35.
- [14] Hasegawa M, Sudo A, Komlev VS, Barinov SM, Uchida A. High release of antibiotic from a novel hydroxyapatite with bimodal pore size distribution. *J. Biomed. Mater. Res.* 2004;70:332–9.
- [15] Emanuel N, Rosenfeld Y, Cohen O, Applbaum YH, Segal D, Barenholz Y. A lipid-and-polymer-based novel local drug delivery system—BonyPid™: From physicochemical aspects to therapy of bacterially infected bones. *Journal of Controlled Release* 2012;160:353–61.
- [16] Ata-Ali J, Ata-Ali F. Do antibiotics decrease implant failure and postoperative infections? A systematic review and meta-analysis. *International Journal of Oral and Maxillofacial Surgery* 2013;article in press.
- [17] Vester H, Wildemann B, Schmidmaier G, Stöckle U, Lucke M. Gentamycin delivered from a PDLLA coating of metallic implants. *Injury* 2010;41:1053–9.
- [18] Strobel C, Bormann N, Kadow-Romacker A, Schmidmaier G, Wildemann B. Sequential release kinetics of two (gentamicin and BMP-2) or three (gentamicin, IGF-I and BMP-2) substances from a one-component polymeric coating on implants. *Journal of Controlled Release* 2011;156:37–45.
- [19] Tamilvanan S, Venkateshan N, Ludwig A. The potential of lipid- and polymer-based drug delivery carriers for eradicating biofilm consortia on device-related nosocomial infections. *Journal of Controlled Release* 2008;128:2–22.
- [20] Schmidmaier G, Wildemann B, Bail H, Lucke M, Fuchs T, STEMBERGER A, Flyvbjerg A et al. Local application of growth factors (insulin-like growth factor-1 and transforming growth factor-β1) from a biodegradable poly(d,l-lactide) coating of osteosynthetic implants accelerates fracture healing in rats. *Bone* 2001;28:341–50.
- [21] Peter B, Pioletti D, Laib S, Bujoli B, Pilet P, Janvier P, Guicheux J et al. Calcium phosphate drug delivery system: influence of local zoledronate release on bone implant osteointegration. *Bone* 2005;36:52–60.

- [22] Abtahi J, Tengvall P, Aspenberg P. A bisphosphonate-coating improves the fixation of metal implants in human bone. A randomized trial of dental implants. *Bone* 2012;50:1148–51.
- [23] Sörensen TC, Arnoldi J, Procter P, Robionek B, Steckel H. Bone substitute materials delivering zoledronic acid: Physicochemical characterization, drug load, and release properties. *Journal of Biomaterials Applications* 2011;27:727–38.
- [24] Moroni A, Faldini C, Hoang-Kim A, Pegreff F, Giannini S. Alendronate improves screw fixation in osteoporotic bone. *J Bone Joint Surg Am* 2007;89:96–101.
- [25] Toksvig-Larsen S, Aspenberg P. Bisphosphonate-coated external fixation pins appear similar to hydroxyapatite-coated pins in the tibial metaphysis and to uncoated pins in the shaft. *Acta Orthop* 2013;84:314–8.
- [26] Trajkovski B, Petersen A, Strube P, Mehta M, Duda GN. Intra-operatively customized implant coating strategies for local and controlled drug delivery to bone. *Advanced Drug Delivery Reviews* 2012;64:1142–51.
- [27] Schmidmaier G, Lucke M, Wildemann B, Haas NP, Raschke M. Prophylaxis and treatment of implant-related infections by antibiotic-coated implants: a review. *Injury* 2006;37:S105.
- [28] Papat KC, Eltgroth M, LaTempa TJ, Grimes CA, Desai TA. Titania Nanotubes: A Novel Platform for Drug-Eluting Coatings for Medical Implants? *Small* 2007;3:1878–81.
- [29] Hickok NJ, Shapiro IM. Immobilized antibiotics to prevent orthopaedic implant infections. *Advanced Drug Delivery Reviews* 2012;64:1165–76.
- [30] Lilja M, Sörensen JH, Brohede U, Åstrand M, Procter P, Arnoldi J, Steckel H et al. Drug loading and release of Tobramycin from hydroxyapatite coated fixation pins. *J Mater Sci: Mater Med* 2013;24:2265–74.
- [31] Roveri N, Foresti E, Lelli M, Lesci I, Marchetti M. Microscopic investigations of Synthetic Biomimetic Hydroxyapatite. *Microscopy: Science, Technology, Applications and Education* 2010:1868–79.
- [32] Forsgren J. In Vivo Evaluation of Functionalized Biomimetic Hydroxyapatite for Local Delivery of Active Agents. *JBNB* 2011;02:149–54.
- [33] Adams CI, Robinson CM, Court-Brown CM, McQueen MM. Prospective randomized controlled trial of an intramedullary nail versus dynamic screw and plate for intertrochanteric fractures of the femur. *J Orthop Trauma* 2001;15:394–400.
- [34] Chao EY, Hein TJ. Mechanical performance of the standard Orthofix external fixator. *Orthopedics* 1988;11:1057–69.
- [35] Huiskes R, Chao EY, Crippen TE. Parametric analyses of pin-bone stresses in external fracture fixation devices. *J Orthop Res* 1985;3:341–9.
- [36] Basler SE, Traxler J, Müller R, van Lenthe GH. Peri-implant bone microstructure determines dynamic implant cut-out. *Medical Engineering & Physics* 2013;35:1442–9.
- [37] Windolf M, Braunstein V, Dutoit C, Schwiieger K. Is a helical shaped implant a superior alternative to the Dynamic Hip Screw for unstable femoral neck fractures? A biomechanical investigation. *Clinical Biomechanics* 2009;24:59–64.
- [38] Fakler JKM, Hogan C, Heyde CE, John T. Current concepts in the treatment of proximal humeral fractures. *Orthopedics* 2008;31:42–51.
- [39] Subbiahdoss G, Kuijjer R, Grijpma DW, van der Mei HC, Busscher HJ. Microbial biofilm growth vs. tissue integration: “The race for the surface” experimentally studied. *Acta Biomaterialia* 2009;5:1399–404.
- [40] Hadi SA, Ashfaq N, Bey A, Khan S. Biological factors responsible for failure of osseointegration in oral implants. *Biology and Medicine* 2011;3:164–70.
- [41] Dhert WJ, Thomsen P, Blomgren AK, Esposito M, Ericson LE, Verbout AJ. Integration of press-fit implants in cortical bone: a study on interface kinetics. *J Biomed Mater Res* 1998;41:574–83.
- [42] Larsson S, Procter P. Optimising implant anchorage (augmentation) during fixation of osteoporotic fractures: Is there a role for bone-graft substitutes? *Injury* 2011;42:S72.
- [43] Baker K, Anderson M, Oehlke S, Astashkina A, Haikio D, Drelich J, Donahue S. Growth, characterization and biocompatibility of bone-like calcium phosphate layers biomimetically deposited on metallic substrata. *Materials Science and Engineering: C* 2006;26:1351–60.
- [44] Allegrini S, Rumpel E, Kauschke E, Fanghänel J, König B. Hydroxyapatite grafting promotes new bone formation and osseointegration of smooth titanium implants. *Annals of Anatomy - Anatomischer Anzeiger* 2006;188:143–51.
- [45] Alt V, Bitschnau A, Böhner F, Heerich KE, Magesin E, Sewing A, Pavlidis T et al. Effects of gentamicin and gentamicin–RGD coatings on bone ingrowth and biocompatibility of cementless joint prostheses: An experimental study in rabbits. *Acta Biomaterialia* 2011;7:1274–80.
- [46] Shepperd J, Apthorp H. A contemporary snapshot of the use of hydroxyapatite coating in orthopaedic surgery. *J Bone Joint Surg Br* 2005;87:1046–9.

-
- [47] Piza G, Caja VL, Gonzalez-Viejo MA, Navarro A. Hydroxyapatite-coated external-fixation pins. The effect on pin loosening and pin-track infection in leg lengthening for short stature. *J Bone Joint Surg Br* 2004;86:892–7.
- [48] Caja VL, Moroni A. Hydroxyapatite coated external fixation pins: an experimental study. *Clin Orthop Relat Res* 1996:269–75.
- [49] Magyar G, Toksvig-Larsen S, Moroni A. Hydroxyapatite coating of threaded pins enhances fixation. *J Bone Joint Surg Br* 1997;79:487–9.
- [50] Heimann RB. Structure, properties, and biomedical performance of osteoconductive bioceramic coatings. *Surface and Coatings Technology* 2012.
- [51] Cao N, Dong J, Wang Q, Ma Q, Xue C, Li M. An experimental bone defect healing with hydroxyapatite coating plasma sprayed on carbon/carbon composite implants. *Surface and Coatings Technology* 2010;205:1150–6.
- [52] Sörensen TC, Arnoldi J, Procter P, Beigel C, Jönsson A, Lennerås M, Emanuelsson L et al. Locally enhanced early bone formation of zoledronic acid incorporated into a bone cement plug in vivo. *J Pharm Pharmacol* 2012;65:201–12.
- [53] Dhert WJA, Thomsen P, A. K. Blomgren. Integration of press-fit implants in cortical bone: A study on interface kinetics.
- [54] Slaets E, Carmeliet G, Naert I, Duyck J. Early Cellular Responses in Cortical Bone Healing Around Unloaded Titanium Implants: An Animal Study. *Journal of Periodontology* 2006;77:1015–24.
- [55] Xue W, Tao S, Liu X, Zheng X, Ding C. In vivo evaluation of plasma sprayed hydroxyapatite coatings having different crystallinity. *Biomaterials* 2004;25:415–21.
- [56] Zhang H, Darvell BW. Morphology and structural characteristics of hydroxyapatite whiskers: Effect of the initial Ca concentration, Ca/P ratio and pH. *Acta Biomaterialia* 2011;7:2960–8.
- [57] Wang P, Li C, Gong H, Jiang X, Wang H, Li K. Effects of synthesis conditions on the morphology of hydroxyapatite nanoparticles produced by wet chemical process. *Powder Technology* 2010;203:315–21.
- [58] Forsgren J, Svahn F, Jarmar T, Engqvist H. Formation and adhesion of biomimetic hydroxyapatite deposited on titanium substrates. *Acta Biomaterialia* 2007;3:980–4.
- [59] Ma J, Wang C, Peng K. Electrophoretic deposition of porous hydroxyapatite scaffold. *Biomaterials* 2003;24:3505–10.
- [60] Liu DM, Troczynski T, Tseng WJ. Water-based sol-gel synthesis of hydroxyapatite: process development. *Biomaterials* 2001;22:1721–30.
- [61] Mihryan A, Forsgren J, Strømme M, Engqvist H. Assessing Surface Area Evolution during Biomimetic Growth of Hydroxyapatite Coatings. *Langmuir* 2009;25:1292–5.
- [62] Ginebra M, Traykova T, Planell J. Calcium phosphate cements as bone drug delivery systems: A review. *Journal of Controlled Release* 2006;113:102–10.
- [63] Moroni A, Faldini C, Pegreff F, Giannini S. HA-coated screws decrease the incidence of fixation failure in osteoporotic trochanteric fractures. *Clin Orthop Relat Res* 2004:87–92.
- [64] Johnson EN, Burns TC, Hayda RA, Hospenthal DR, Murray CK. Infectious Complications of Open Type III Tibial Fractures among Combat Casualties. *Clinical Infectious Diseases* 2007;45:409–15.
- [65] Campoccia D, Montanaro L, Arciola CR. The significance of infection related to orthopedic devices and issues of antibiotic resistance. *Biomaterials* 2006;27:2331–9.
- [66] Knobben BAS, Engelsma Y, Neut D, van der Mei HC, Busscher HJ, van Horn JR. Intraoperative contamination influences wound discharge and periprosthetic infection. *Clin Orthop Relat Res* 2006;452:236–41.
- [67] Knobben BAS, van Horn JR, van der Mei HC, Busscher HJ. Evaluation of measures to decrease intraoperative bacterial contamination in orthopaedic implant surgery. *J Hosp Infect* 2006;62:174–80.
- [68] Trampuz A, Widmer AF. Infections associated with orthopedic implants. *Curr Opin Infect Dis* 2006;19:349–56.
- [69] Osmon DR, Berbari EF, Berendt AR, Lew D, Zimmerli W, Steckelberg JM, Rao N et al. Diagnosis and Management of Prosthetic Joint Infection: Clinical Practice Guidelines by the Infectious Diseases Society of America. *Clinical Infectious Diseases* 2012;56:e1.
- [70] Lord CF, Gebhardt MC, Tomford WW, Mankin HJ. Infection in bone allografts. Incidence, nature, and treatment. *J Bone Joint Surg Am* 1988;70:369–76.
- [71] Mankin HJ, Doppelt S, Tomford W. Clinical experience with allograft implantation. The first ten years. *Clin Orthop Relat Res* 1983:69–86.
- [72] Praveen S, Rohaizak M. Local antibiotics are equivalent to intravenous antibiotics in the prevention of superficial wound infection in inguinal hernioplasty. *Asian J Surg* 2009;32:59–63.
- [73] Diefenbeck M, Mückley T, Hofmann GO. Prophylaxis and treatment of implant-related infections by local application of antibiotics. *Injury* 2006;37:S95.
-

- [74] Parvizi J, Saleh KJ, Ragland PS, Pour AE, Mont MA. Efficacy of antibiotic-impregnated cement in total hip replacement. *Acta Orthop* 2008;79:335–41.
- [75] Lucke M, Schmidmaier G, Sadoni S, Wildemann B, Schiller R, Haas N, Raschke M. Gentamicin coating of metallic implants reduces implant-related osteomyelitis in rats. *Bone* 2003;32:521–31.
- [76] Belcarz A, Bieniaś J, Surowska B, Ginalska G. Studies of bacterial adhesion on TiN, SiO₂–TiO₂ and hydroxyapatite thin layers deposited on titanium and Ti6Al4V alloy for medical applications. *Thin Solid Films* 2010;519:797–803.
- [77] DeVasConCellos P, Bose S, Beyenal H, Bandyopadhyay A, Zirkle LG. Antimicrobial particulate silver coatings on stainless steel implants for fracture management. *Materials Science and Engineering: C* 2012;32:1112–20.
- [78] Secinti KD, Özalp H, Attar A, Sargon MF. Nanoparticle silver ion coatings inhibit biofilm formation on titanium implants. *Journal of Clinical Neuroscience* 2011;18:391–5.
- [79] Santillán M, Quaranta N, Boccaccini A. Titania and titania–silver nanocomposite coatings grown by electrophoretic deposition from aqueous suspensions. *Surface and Coatings Technology* 2010;205:2562–71.
- [80] Hoene A, Prinz C, Walschus U, Lucke S, Patrzyk M, Wilhelm L, Neumann H et al. In vivo evaluation of copper release and acute local tissue reactions after implantation of copper-coated titanium implants in rats. *Biomed Mater* 2013;8:35009.
- [81] D'Arrigo M, Ginestra G, Mandalari G, Furneri P, Bisignano G. Synergism and postantibiotic effect of tobramycin and *Melaleuca alternifolia* (tea tree) oil against *Staphylococcus aureus* and *Escherichia coli*. *Phytomedicine* 2010;17:317–22.
- [82] Pignatello R, Mangiafico A, Basile L, Ruozi B, Furneri PM. Amphiphilic ion pairs of tobramycin with lipoamino acids. *European Journal of Medicinal Chemistry* 2011;46:1665–71.
- [83] Li B, van Schepdael A, Hoogmartens J, Adams E. Characterization of impurities in tobramycin by liquid chromatography–mass spectrometry. *Journal of Chromatography A* 2009;1216:3941–5.
- [84] Pacifici GM. Clinical pharmacokinetics of aminoglycosides in the neonate: a review. *Eur J Clin Pharmacol* 2009;65:419–27.
- [85] Motozono H, Mizuno N, Morita E, Fujioka Y, Takahashi K. Effect of age on gastrointestinal absorption of tobramycin in rats. *International Journal of Pharmaceutics* 1994;108:39–48.
- [86] Lin L, Grenier L, Thériault G, Gourde P, Yoshiyama Y, Bergeron MG, Labrecque G et al. Nephrotoxicity of low doses of tobramycin in rats: Effect of the time of administration. *Life Sciences* 1994;55:169–77.
- [87] Xuan D, Lu J, Nicolau DP, Nightingale CH. Population pharmacokinetics of tobramycin in hospitalized patients receiving once-daily dosing regimen. *International Journal of Antimicrobial Agents* 2000;15:185–91.
- [88] Robert Koch-Institut: *Epidemiologisches Bulletin* 26 2011;26:233–41.
- [89] Mingeot-Leclercq MP, Glupczynski Y, Tulkens PM. Aminoglycosides: activity and resistance. *Antimicrob Agents Chemother* 1999;43:727–37.
- [90] Huppertz K. *GERNARS Resistenzstatistik*;2004.
- [91] Joosten U, Joist A, Gosheger G, Liljenqvist U, Brandt B, Eiff C von. Effectiveness of hydroxyapatite–vancomycin bone cement in the treatment of *Staphylococcus aureus* induced chronic osteomyelitis. *Biomaterials* 2005;26:5251–8.
- [92] Stigter M, Groot K de, Layrolle P. Incorporation of tobramycin into biomimetic hydroxyapatite coating on titanium. *Biomaterials* 2002;23:4143–53.
- [93] Frommelt L., Schnettler R. *Lokale Antibiotikatherapie - Weshalb lokale Antibiotika bei der Behandlung von Infektionen am Bewegungsapparat? Septische Knochenchirurgie*, Georg Thieme Verlag 2004:89.
- [94] Lilja M, Welch K, Åstrand M, Engqvist H, Strømme M. Effect of deposition parameters on the photocatalytic activity and bioactivity of TiO₂ thin films deposited by vacuum arc on Ti-6Al-4V substrates. *J. Biomed. Mater. Res.* 2012;100:1078–85.
- [95] HPLC detection of Gentimcin sulphate. *British Pharmacopoeia* 1999, I:695–7.
- [96] Sekkat M, Fabre H, Simeon de Buochberg M, Mandrou B. Determination of aminoglycosides in pharmaceutical formulations--I. Thin-layer chromatography. *J Pharm Biomed Anal* 1989;7:883–92.
- [97] Fabre H, Sekkat M, Blanchin MD, Mandrou B. Determination of aminoglycosides in pharmaceutical formulations--II. High-performance liquid chromatography. *J Pharm Biomed Anal* 1989;7:1711–8.
- [98] Zarie ES, Kaidas V, Gedamu D, Mishra YK, Adelung R, Furkert FH, Scherliess R et al. Solvent free fabrication of micro and nanostructured drug coatings by thermal evaporation for controlled release and increased effects. *PLoS One* 2012;7:e40746.
- [99] *Mikrobiologische Wertbestimmung von Antibiotika*. *European Pharmacopoeia* 7.0 2011:287–90.
- [100] Fuchs S, Hermanns MI, Kirkpatrick CJ. Retention of a differentiated endothelial phenotype by outgrowth endothelial cells isolated from human peripheral blood and expanded in long-term cultures. *Cell Tissue Res* 2006;326:79–92.

-
- [101] Kolbe M, Dohle E, Katerla D, Kirkpatrick CJ, Fuchs S. Enrichment of outgrowth endothelial cells in high and low colony-forming cultures from peripheral blood progenitors. *Tissue Eng Part C Methods* 2010;16:877–86.
- [102] Fuchs S, Ghanaati S, Orth C, Barbeck M, Kolbe M, Hofmann A, Eblenkamp M et al. Contribution of outgrowth endothelial cells from human peripheral blood on in vivo vascularization of bone tissue engineered constructs based on starch polycaprolactone scaffolds. *Biomaterials* 2009;30:526–34.
- [103] Hofmann A, Konrad L, Gotzen L, Printz H, Ramaswamy A, Hofmann C. Bioengineered human bone tissue using autogenous osteoblasts cultured on different biomatrices. *J Biomed Mater Res A* 2003;67:191–9.
- [104] 160074 RA Stryker Osteosynthesis.
- [105] 164256 RA Stryker Osteosynthesis.
- [106] 151098 RA Stryker Osteosynthesis.
- [107] 164510 RA Stryker Osteosynthesis.
- [108] Test report 5.1 micro CT 12072013.
- [109] S. S. Shapiro uMBW. An Analysis of Variance Test for Normality Complete Samples. *Biometrika* 1965;3:591–611.
- [110] Darimont GL, Cloots R, Heinen E, Seidel L, Legrand R. In vivo behaviour of hydroxyapatite coatings on titanium implants: a quantitative study in the rabbit. *Biomaterials* 2002;23:2569–75.
- [111] Fredrik Lindberg, Jannica Heinrichs, Fredric Ericson, Peter Thomsen, Håkan Engqvist. Hydroxylapatite growth on single-crystal rutile substrates. *Biomaterials* 2008;29:3317–23.
- [112] Ulrika Brohede, Shuxi Zhao, Fredrik Lindberg, Albert Mihranyan, Johan Forsgren, Maria Strømme, Håkan Engqvist. A novel graded bioactive high adhesion implant coating. *Applied Surface Science* 2009;255:7723–8.
- [113] Chai F, Hornez J, Blanchemain N, Neut C, Descamps M, Hildebrand H. Antibacterial activation of hydroxyapatite (HA) with controlled porosity by different antibiotics. *Biomolecular Engineering* 2007;24:510–4.
- [114] Yamamura K, Iwata H, Yotsuyanagi T. Synthesis of antibiotic-loaded hydroxyapatite beads and in vitro drug release testing. *J Biomed Mater Res* 1992;26:1053–64.
- [115] Society of Petroleum Engineers. *The Viscosity of Air, Water, Natural Gas, Crude Oil and Its Associated Gases at Oil Field Temperatures and Pressures* 1946.
- [116] Moroni A, Aspenberg P, Toksvig-Larsen S, Falzarano G, Giannini S. Enhanced Fixation With Hydroxyapatite Coated Pins 1998;346:171–7.
- [117] Sanden B, Olerud C, Johansson C, Larsson S. Improved extraction torque of hydroxyapatite-coated pedicle screws. *Eur Spine J* 2000;9:534–7.
- [118] Orienti L, Fini M, Rocca M, Giavaresi G, Guzzardella M, Moroni A, Giardino R. Measurement of insertion torque of tapered external fixation pins: A comparison between two experimental models. *Journal of Biomedical Materials Research* 1999;48:216–9.
- [119] Capper M, Soutis C, Oni OO. Comparison of the stresses generated at the pin-bone interface by standard and conical external fixator pins. *Biomaterials* 1994;15:471–3.
- [120] Koistinen A, Santavirta SS, Kroger H, Lappalainen R. Effect of bone mineral density and amorphous diamond coatings on insertion torque of bone screws. *Biomaterials* 2005;26:5687–94.
- [121] Jae Hyup Lee, Hyun-Seung Ryu, Dong-Soo Lee, Kug Sun Hong, Bong-Soon Chang, Choon-Ki Lee. Biomechanical and histomorphometric study on the bone–screw interface of bioactive ceramic-coated titanium screws. *Biomaterials* 2005;26:3249–57.
- [122] Ulrika Brohede, Shuxi Zhao, Fredrik Lindberg, Albert Mihranyan, Johan Forsgren, Maria Strømme, Håkan Engqvist. A novel graded bioactive high adhesion implant coating. *Applied Surface Science* 2009;255:7723–8.
- [123] Chan S, Neu C, Komvopoulos K, Reddi A. The role of lubricant entrapment at biological interfaces: Reduction of friction and adhesion in articular cartilage. *Journal of Biomechanics* 2011;44:2015–20.
- [124] Mahan J, Seligson D, Henry SL, Hynes P, Dobbins J. Factors in pin tract infections. *Orthopedics* 1991;14:305–8.
- [125] Morscher EW, Hefti A, Aebi U. Severe osteolysis after third-body wear due to hydroxyapatite particles from acetabular cup coating. *Journal of Bone & Joint Surgery, British Volume* 1998;80:267–72.
- [126] Yang Y, Ong JL. Bond strength, compositional, and structural properties of hydroxyapatite coating on Ti, ZrO₂-coated Ti, and TPS-coated Ti substrate. *Journal of Biomedical Materials Research Part A* 2003;64:509–16.
- [127] Kui Cheng, Gaorong Han, Wenjian Weng, Haibo Qu, Piyi Du, Ge Shen, Juan Yang et al. Sol–gel derived fluoridated hydroxyapatite films. *Materials Research Bulletin* 2003;38:89–97.
- [128] Wang J, Layrolle P, Stigter M, Groot K de. Biomimetic and electrolytic calcium phosphate coatings on titanium alloy: physicochemical characteristics and cell attachment. *Biomaterials* 2004;25:583–92.
-

- [129] Sam Zhang, Zeng Xianting, Wang Yongsheng, Cheng Kui, Weng Wenjian. Adhesion strength of sol-gel derived fluoridated hydroxyapatite coatings. *Surface and Coatings Technology* 2006;200:6350–4.
- [130] Matthews A. Methods for assessing coating adhesion. *Le Vide, les Couches Minces* 1988;1:7–15. 1988:7–15.
- [131] Yang YC, Chang E. Influence of residual stress on bonding strength and fracture of plasma-sprayed hydroxyapatite coatings on Ti-6Al-4V substrate. *Biomaterials* 2001;22:1827–36.
- [132] Lindgren M, Astrand M, Wiklund U, Engqvist H. Investigation of boundary conditions for biomimetic HA deposition on titanium oxide surfaces. *J Mater Sci Mater Med* 2009;20:1401–8.
- [133] Lilja M, Forsgren J, Welch K, Astrand M, Engqvist H, Stromme M. Photocatalytic and antimicrobial properties of surgical implant coatings of titanium dioxide deposited through cathodic arc evaporation. *Biotechnol Lett* 2012;34:2299–305.
- [134] Cai Y, Strømme M, Melhus Å, Engqvist H, Welch K. Photocatalytic inactivation of biofilms on bioactive dental adhesives. *Journal of Biomedical Materials Research. Part B - Applied biomaterials* 2013.
- [135] Welch K, Cai Y, Engqvist H, Stromme M. Dental adhesives with bioactive and on-demand bactericidal properties. *Dent Mater* 2010;26:491–9.
- [136] Piskounova S, Forsgren J, Brohede U, Engqvist H, Stromme M. In vitro characterization of bioactive titanium dioxide/hydroxyapatite surfaces functionalized with BMP-2. *J Biomed Mater Res B Appl Biomater* 2009;91:780–7.
- [137] Forsgren J, Brohede U, Mihranyan A, Engqvist H, Strømme M. Fast loading, slow release a new strategy for incorporating antibiotics to hydroxyapatite: *Key Engineering Materials* 2009; 396-398: 523–526. In: *Key Engineering Materials* 2009; 396-398: 523–526.
- [138] Simchi A, Tamjid E, Pishbin F, Boccaccini AR. Recent progress in inorganic and composite coatings with bactericidal capability for orthopaedic applications. *Nanomedicine* 2011;7:22–39.
- [139] Xia W, Lindahl C, Lausmaa J, Engqvist H. Biomimetic Hydroxyapatite Deposition on Titanium Oxide Surfaces for Biomedical Application: ISBN: 978-953-307-191-6, InTech, DOI: 10.5772/14900. Available from: <http://www.intechopen.com/books/advances-in-biomimetics/biomimetic-hydroxyapatite-deposition-on-titanium-oxide-surfaces-for-biomedical-application>. *Advances in Biomimetics* 2011:ISBN: 978-953-307-191-6, InTech, DOI: 10.5772/14900. Available from: <http://www.intechopen.com/books/advances-in-biomimetics/biomimetic-hydroxyapatite-deposition-on-titanium-oxide-surfaces-for-biomedical-application>.
- [140] Lindahl C, Borchardt P, Lausmaa J, Xia W, Engqvist H. Studies of early growth mechanisms of hydroxyapatite on single crystalline rutile: a model system for bioactive surfaces. *J Mater Sci Mater Med* 2010;21:2743–9.
- [141] Yao C, Perla V, McKenzie JL, Slamovich EB, Webster TJ. Anodized Ti and Ti6Al4V Possessing Nanometer Surface Features Enhances Osteoblast Adhesion. *Journal of Biomedical Nanotechnology* 1;2005:68–73.
- [142] Cho S, Park K. The removal torque of titanium screw inserted in rabbit tibia treated by dual acid etching. *Biomaterials* 2003;24:3611–7.
- [143] Stigter M, Bezemer J, Groot K de, Layrolle P. Incorporation of different antibiotics into carbonated hydroxyapatite coatings on titanium implants, release and antibiotic efficacy. *Journal of Controlled Release* 2004;99:127–37.
- [144] Zhang E, Zou C, Yu G. Surface microstructure and cell biocompatibility of silicon-substituted hydroxyapatite coating on titanium substrate prepared by a biomimetic process. *Materials Science and Engineering: C* 2009;29:298–305.
- [145] Miclau T, Edin ML, Lester GE, Lindsey RW, Dahners LE. Bone toxicity of locally applied aminoglycosides. *J Orthop Trauma* 1995;9:401–6.
- [146] Duewelhenke N, Krut O, Eysel P. Influence on Mitochondria and Cytotoxicity of Different Antibiotics Administered in High Concentrations on Primary Human Osteoblasts and Cell Lines. *Antimicrobial Agents and Chemotherapy* 2006;51:54–63.
- [147] Roshan-Ghias A, Arnoldi J, Procter P, Pioletti DP. In vivo assessment of local effects after application of bone screws delivering bisphosphonates into a compromised cancellous bone site. *Clinical Biomechanics* 2011;26:1039–43.
- [148] Larsson S, Stadelmann V, Arnoldi J, Behrens M, Hess B, Procter P, Murphy M et al. Injectable calcium phosphate cement for augmentation around cancellous bone screws. In vivo biomechanical studies. *Journal of Biomechanics* 2012;45:1156–60.
- [149] ASTM F1622. Standard test method for measuring the torsional properties of metallic bone screws.
- [150] Slaets E, Naert I, Carmeliet G, Duyck J. Early cortical bone healing around loaded titanium implants: a histological study in the rabbit. *Clinical Oral Implants Research* 2009;20:126–34.

-
- [151] Yang G, He F, Yang X, Wang X, Zhao S. Bone responses to titanium implants surface-roughened by sandblasted and double etched treatments in a rabbit model. *Oral Surgery, Oral Medicine, Oral Pathology, Oral Radiology, and Endodontology* 2008;106:516–24.
- [152] Yang G, He F, Hu J, Wang X, Zhao S. Effects of biomimetically and electrochemically deposited nano-hydroxyapatite coatings on osseointegration of porous titanium implants. *Oral Surgery, Oral Medicine, Oral Pathology, Oral Radiology, and Endodontology* 2009;107:782–9.
- [153] Sennerby L, Thomsen P, Ericson LE. Early tissue response to titanium implants inserted in rabbit cortical bone. *Journal of Material Science: Materials in Medicine* 1993;240–50.
- [154] Zhang E, Zou C. Porous titanium and silicon-substituted hydroxyapatite biomodification prepared by a biomimetic process: Characterization and in vivo evaluation. *Acta Biomaterialia* 2009;5:1732–41.
- [155] Eom T, Jeon G, Jeong C, Kim Y, Kim S, Cho I, Cho Y et al. Experimental study of bone response to hydroxyapatite coating implants: bone-implant contact and removal torque test. *Oral Surgery, Oral Medicine, Oral Pathology and Oral Radiology* 2012;114:411–8.
- [156] Esposito M, Hirsch JM, Lekholm U, Thomsen P. Biological factors contributing to failures of osseointegrated oral implants. (I). Success criteria and epidemiology. *Eur J Oral Sci* 1998;106:527–51.
- [157] Yildirim O, Aksakal B, Celik H, Vangolu Y, Okur A. An investigation of the effects of hydroxyapatite coatings on the fixation strength of cortical screws. *Medical Engineering & Physics* 2005;27:221–8.
- [158] Pieske O, Kaltenhauser F, Pichlmaier L, Schramm N, Trentzsch H, Löffler T, Greiner A et al. Clinical benefit of hydroxyapatite-coated pins compared with stainless steel pins in external fixation at the wrist: A randomised prospective study. *Injury* 2010;41:1031–6.
- [159] Rigo E, Boschi A, Yoshimoto M, Allegrini M, Konig B, Carbonari MJ. Evaluation in vitro and in vivo of biomimetic hydroxyapatite coated on titanium dental implants. *Materials Science and Engineering: C* 2004;24:647–51.
- [160] Peter B, Pioletti DP, Laib S, Bujoli B, Pilet P, Janvier P, Guicheux J, Zambelli PY, Bouler JM and Gauthier O. Calcium phosphate drug delivery system: influence of local zoledronate release on bone implant osteointegration. *Bone* 2005;36:52–60.
- [161] Wermelin K, Suska F, Tengvall P, Thomsen P. Stainless steel screw coated with bisphosphonates gave stronger fixation and more surrounding bone. *Histomorphometry in rats. Bone* 2008;42:365–371.
- [162] Seebeck J, Goldhahn J, Morlock MM, Schneider E. Mechanical behavior of screws in normal and osteoporotic bone. *Osteoporos Int* 2005;16 Suppl 2:S107–11.
- [163] Gursel I, Korkusuz F, Turesin F, Alaeddinoglu NG, Hasirci V. In vivo application of biodegradable controlled antibiotic release systems for the treatment of implant-related osteomyelitis. *Biomaterials* 2001;22:73–80.
- [164] Meulemans L, Hermans K, Duchateau L, Haesebrouck F. High and low virulence *Staphylococcus aureus* strains in a rabbit skin infection model. *Vet Microbiol* 2007;125:333–40.
- [165] Xie Z, Liu X, Jia W, Zhang C, Huang W, Wang J. Treatment of osteomyelitis and repair of bone defect by degradable bioactive borate glass releasing vancomycin. *J Control Release* 2009;139:118–26.
- [166] Emanuel N, Rosenfeld Y, Cohen O, Applbaum YH, Segal D, Barenholz Y. A lipid-and-polymer-based novel local drug delivery system--BonyPid: from physicochemical aspects to therapy of bacterially infected bones. *J Control Release* 2012;160:353–61.
- [167] Stewart S, Barr S, Engiles J, Hickok NJ, Shapiro IM, Richardson D, Parvizi J et al. Vancomycin-Modified Implant Surface Inhibits Biofilm Formation and Supports Bone-Healing in an Infected Osteotomy Model in Sheep A Proof-of-Concept Study. *J Bone Joint Surg Am* 2012;94:1406.

Curriculum Vitae (CV)

Personal Data

Surname	Sörensen
Forename	Jan Henrik
Date of Birth	February 2 nd , 1985
Place of Birth	Kiel
Citizenship	German

Education

1991 – 1995	Primary School, Schönkirchen
1995 – 2004	Heinrich-Heine High School, Heikendorf
06/2004	University Entrance Diploma
10/2004 – 05/2009	Studies of Pharmacy, CAU Kiel
07/2009 – 12/2009	Postgraduate Studies for "Diplom-Pharmazeut" at the Department of Pharmaceutical Technology and Biopharmacy, CAU Kiel
01/2010 – 06/2010	Trainee for Approbation, Belvedere Apotheke in Kiel
07/2010 – 09/2010	Apotheke am Rathaus, Schwentinental
08/2010	Approbation as Pharmacist
Since 10/2010	PhD-student at the Department of Pharmaceutical Technology and Biopharmacy, CAU Kiel

Erklärung

Hiermit erkläre ich gemäß § 8 der Promotionsordnung der Mathematisch-Naturwissenschaftliche Fakultät der Christian-Albrechts-Universität zu Kiel, dass ich die vorliegende Arbeit, abgesehen von der Beratung durch meine Betreuer, selbstständig und ohne fremde Hilfe verfasst habe. Ich habe keine anderen als die angegebenen Quellen oder Hilfsmittel benutzt und die den benutzen Werken wörtlich oder inhaltlich entnommenen Stellen als solche kenntlich gemacht. Die vorliegende Arbeit ist unter Einhaltung guter wissenschaftlicher Praxis entstanden und wurde bei keiner anderen Universität zur Begutachtung eingereicht.

Jan Henrik Sörensen